Regio- und stereoselektive Thianthrenierung von Olefinen zum Zugang zu vielseitigen Alkenylelektrophilen und Fluorierung von Arylthianthreniumsalzen

Von der Fakultät für Mathematik, Informatik und Naturwissenschaften der RWTH Aachen University zur Erlangung des akademischen Grades eines Doktors der Naturwissenschaften genehmigte Dissertation

vorgelegt von

Junting Chen

Bachelor of Science

aus

Hunan, China

Berichter: Professor Dr. Tobias Ritter

Universitätsprofessor Dr. Franziska Schoenebeck

Universitätsprofessor Dr. Carsten Bolm

Tag der mündlichen Prüfung: 17. September 2020

Regio- and Stereoselective Thianthrenation of Olefins to Access Versatile Alkenyl Electrophiles and Fluorination of Aryl Thianthrenium Salts

Inaugural dissertation submitted to the
Faculty of Mathematics, Computer Science, and Natural Science
of the RWTH Aachen University
For the degree of Doctor of Natural Science

presented by

Junting Chen

Bachelor of Science

from

Hunan, China

Examiner:	Prof. Dr. Tobias Ritter
Co-examiners:	Univ.-Prof. Dr. Franziska Schoenebeck
	Univ.-Prof. Dr. rer. nat. Carsten Bolm
Chairman:	Univ.-Prof. Dr. rer. nat. Jun Okuda
Extra auditor:	Univ.-Prof. Dr. rer. nat. Jürgen Klankermayer

Defense date: September 17th, 2020

Mülheim an der Ruhr, 2020

Dissertation Advisor: Prof. Dr. Tobias Ritter Junting Chen

Regio- and Stereoselective Thianthrenation of Olefins to Access Versatile Alkenyl Electrophiles and Fluorination of Aryl Thianthrenium Salts

ABSTRACT

Direct C–H functionalization is one of the most straightforward yet challenging strategies to quickly build up functionalities from existing organic compounds. Considering the ubiquitous existence of multiple C–H bonds in one molecule, such as the coexistence of alkyl (sp^3), aryl/alkenyl (sp^2) and alkynyl (sp) C–H bonds or several with the same hybridization (aryl sp^2 and alkenyl sp^2), functionalization with high positional selectivity is a challenge. Typically, direct C–H functionalization protocols can differentiate C–H bonds with different hybridization (sp^3 vs. sp^2), yet there remains challenges for site-selectivity especially when the target C–H bonds have a similar chemical environment (e.g. *ortho*, *meta*, *para* C–H bonds in one arene). In 2019, the Ritter group reported a highly positional-selective C–H thianthrenation of arenes with a broad substrate scope and high functional group tolerance, and the resulting aryl thianthrenium salts provide access to versatile functional groups via Pa catalysis or photoredox chemistry. The work summarized in this thesis describes one site-selective functionalization of alkenes and one two-step site-selective fluorination of arenes, both of which benefit from the site-selective C–H thianthrenation reaction.

Part I describes the development of a method for regio- and stereoselective C–H thianthrenation of alkenes. The reaction can be carried out under ambient atmosphere without exclusion of air and moisture and can be performed on a gram scale. For terminal olefins, the reaction provides alkenyl thianthrenium products with high stereoselectivity; the *E* isomers are often the only isolable products. For internal olefins, the double bond geometry maintains unchanged throughout the thianthrenation reaction. Terminal olefins containing structurally complex and highly functionalized moieties are functionalized well. We isolated thianthrenium dicationic bicycloadducts, which afforded the desired alkenyl thianthrenium salts upon treatment with base; most likely via an $E1cB_{irr}$ deprotonation mechanism.

The resulting alkenyl thianthrenium salts are good alkenyl electrophiles in conventional palladium-catalyzed cross-coupling reactions such as Negishi, Sonogashira and Heck reactions and ruthenium-catalyzed (pseudo)halogenation.

Part II describes the development of a photoredox catalyzed fluorination method for aryl thianthrenium (ArTT) salts, obtained from site-selective C–H thianthrenation of arenes. The substitution of aryl C–H bonds by thianthrene creates a precursor, which readily engages in photoredox chemistry. The C–H thianthrenation reaction tolerates a variety of functional groups and was applied to the synthesis of natural product derivatives. The photoredox properties of aryl thianthrenium salts were established by cyclic voltammetry, density functional theory studies, Hammett analysis, and fluorescence quenching experiments. Subsequent fluorination of ArTT species with fluoride under copper mediation and photoredox catalysis (also termed as metallophotoredox catalysis) provides pharmaceutically relevant aryl fluorides as a single constitutional isomer in a two-step sequence from the corresponding unfunctionalized arenes.

Keywords: C–H functionalization; alkenes; arenes; site-selectivity; stereoselectivity; late-stage fluorination; (metallo)photoredox catalysis; thianthrenation.

Dissertation Advisor: Prof. Dr. Tobias Ritter Junting Chen

Regio- und stereoselektive Thianthrenierung von Olefinen zum Zugang zu vielseitigen Alkenylelektrophilen und Fluorierung von Arylthianthreniumsalzen

ZUSAMMENFASSUNG

Die direkte C–H Funktionalisierung ist eine der einfachsten und dennoch herausforderndsten Strategien, um aus vorhandenen, organischen Verbindungen schnell Funktionalitäten aufzubauen. In Anbetracht der allgegenwärtigen Existenz mehrerer C–H Bindungen in einem Molekül, wie der Koexistenz von Alkyl(sp^3)-, Aryl/Alkenyl(sp^2)-, und Alkinyl(sp) C–H Bindungen oder mehreren mit derselben Hybridisierung (Aryl sp^2 und Alkenyl sp^2) ist die Funktionalisierung mit hoher Positionsselektivität eine Herausforderung. In der Regel können direkte Funktionalisierungsprotokolle C–H Bindungen mit unterschiedlicher Hybridisierung (sp^3 und sp^2) unterscheiden. Die Regioselektivität bleibt jedoch weiterhin eine Herausforderung, insbesondere wenn die Ziel C–H Bindungen eine ähnliche chemische Umgebung aufweisen (z. B. ortho-, meta-, para-C–H Bindungen in einem Aren). Im Jahre 2019 berichtete die Ritter-Gruppe über eine höchst positionsselektive C–H Thianthrenierung von Arenen mit einem breiten Substratspektrum und einer hohen Toleranz gegenüber funktionellen Gruppen. Die resultierenden Arylthianthreniumsalze erlauben Zugang zu vielseitigen funktionellen Gruppen mittels Palladium-Katalyse order Fotoredoxchemie. Die in dieser Arbeit zusammengefasste Methodik beschreibt eine regioselektive Funktionalisierung von Alkenen und eine zweistufige regioselektive Fluorierung von Arenen, die beide von der spezifischen C–H Thianthrenierungsreaktion profitieren.

Teil I beschreibt die Entwicklung einer Methode zur regio- und stereoselektiven C–H Thianthrenierung von Alkenen. Die Reaktion kann unter Standardbedingungen und im Gramm-Maßstab durchgeführt werden. Für terminale Olefine liefert die Reaktion Alkenylthianthreniumsalze mit hoher Stereoselektivität; die *E*-Isomere sind oft die einzigen isolierbaren Produkte. Bei internen Olefinen blieb die Doppelbindungsgeometrie während der gesamten

Thianthrenierungsreaktion erhalten. Terminale Olefine, die strukturell komplexe und hoch funktionalisierte Einheiten enthalten, werden erfolgreich thianthreniert. Wir isolieren dikationische Bicycloaddukte mit Thianthren, die bei Behandlung mit Base die gewünschten Alkenylthianthreniumsalze liefern; höchstwahrscheinlich über einen E1cB$_{irr}$-Deprotonierungsmechanismus. Die resultierenden Alkenylthianthreniumsalze ähneln (Pseudo-)halogeniden in herkömmlichen Palladium-katalysierten Kreuzkupplungsreaktionen, wie Negishi-, Sonogashira-, und Heck-Reaktionen und Ruthenium-katalysierten (Pseudo-)Halogenierungen.

Teil II beschreibt die Entwicklung einer fotoredox-katalysierten Fluorierungsmethode für Arylthianthrenium(ArTT)-Salze, die durch regioselektive Thianthrenierung von Arenen erhalten wird. Durch die Substitution von Aryl-C–H Bindungen durch Thianthren entsteht eine Vorstufe, die sich leicht fotoredoxchemisch umsetzen lässt. Die C–H Thianthrenierungsreaktion toleriert eine Vielzahl von funktionellen Gruppen und wurde zur Synthese von Naturstoffderivaten angewendet. Die Fotoredoxeigenschaften von Arylthianthreniumsalzen wurden durch Cyclovoltammetrie, Studien zur Dichtefunktionaltheorie, Hammett-Analyse und Fluoreszenzlöschungsexperimente ermittelt. Die anschließende Fluorierung von ArTT-Spezies mit Fluorid unter kupfervermittelter Fotoredoxkalalyse (auch als Metallophotoredoxkatalyse bezeichnet) liefert pharmazeutisch relevante Arylfluoride als einziges Isomer in einer zweistufigen Sequenz aus den entsprechenden nicht funktionalisierten Arenen.

Schlüsselwörter: C–H Funktionalisierung; Alkene; Arene; Regioselektivität; Stereoselektivität; Fluorierung; (Metallo)Fotoredoxkatalyse; Thianthrenierung.

“Keep Ithaka always in your mind.
Arriving there is what you’re destined for.
But don’t hurry the journey at all.”

—“Ithaka” by Constantine P. Cavafy
Translated by Edmund Keeley

DECLARATION

I, *Junting Chen*

declare that this thesis and the work presented herein are my own and has been generated by me as the result of my own original research.

Hiermit erkläre ich an Eides statt/ I do solemnly swear that:

1. This work was done wholly or mainly while in candidature for the doctoral degree program at this faculty and university;
2. Where any part of this thesis has previously been submitted for a degree or any other qualification at this university or any other institution, this has been clearly stated;
3. Where I have consulted the published work of others or myself, this is always clearly attributed;
4. Where I have quoted from the work of others or myself, the source is always given. This thesis is entirely my own work, with the exception of such quotations;
5. I have acknowledged all major sources of assistance;
6. Where the thesis is based on work done by myself jointly with others, I have made clear exactly what was done by others and what I have contributed myself;
7. Portions of part I and III have been taken, with permission, from **Chen, J.**; Li, J.; Plutschack, M. B.; Berger, F.; Ritter, T.* *Angew. Chem. Int. Ed.* **2020**, *132*, 5665–5669.
8. Portions of part II and III have been taken, with permission, from Li, J.; **Chen, J.**; Sang, R.; Ham, W.; Plutschack, M. B.; Berger, F.; Chabbra, S.; Schnegg, A.; Genicot, C.; Ritter, T.* *Nat. Chem.* **2020**, *12*, 56–62.
9. Additional work performed during my doctoral studies that does not appear in this thesis has been published in:
    - **Chen, J.**; Ritter, T.* *Org. Synth.* **2019**, *96*, 16–35.
    - Sun, X.; **Chen, J.**; Ritter, T.* *Nat. Chem.* **2018**, *10*, 1229–1233.
    - Ye, F.; **Chen, J.**; Ritter, T.* *J. Am. Chem. Soc.* **2017**, *139*, 7184–7187.

- Beyzavi, M. H.; Mandal; D.; Strebl, M. G.; Neumann, C. N.; D'Amato, E. M.; **Chen, J.**; Hooker, J. M.; Ritter, T.* *ACS Cent. Sci.* **2017**, *3*, 944–948.

Mülheim an der Ruhr, September 17, 2020.

_____

(Junting Chen)

ACKNOWLEDGEMENTS

My journey to "*Ithaka-Ph.D."* would not have been possible without the generous financial support from the Max-Planck-Society for research facilities and stipends. Apart from that, I would like to express my very deep gratitude to Professor Tobias Ritter, my supervisor, for his scientific critiques, professional guidance and enthusiastic encouragement. I want to thank him for teaching me how to think about science and to be a real scientist and giving me the freedom to think, design and perform my own projects. I would also like to offer my special thanks to Professor Franziska Schoenebeck and Professor Carsten Bolm for so kindly being co-examiners of this dissertation and offering me professional suggestions.

My great appreciations are always there to all of the senior students and postdocs, who have offered me a lot of help, suggestions and guidance over the past four years. I want to thank Dr. Jiakun Li for guiding me through the fluorination project and teaching me practical lab techniques all the time. I am thankful to Dr. Jonas Börgel and Dr. Heejun Lee for inspiring scientific discussions and always being there to help. I am grateful to have Dr. Matthew Tredwell working next to me and helping me in the radio lab for the first two years, Matt has always been there to share with me his profound knowledge in chemistry and future career. I want to express my special thanks to Dr. Matthew Plutschack, Dr. Constanze Neumann, Dr. Erica D'Amato, Dr. Hassan Beyzavi, Dr. Martin Strebl, Dr. Fei Ye, M. Sc. Xiang Sun. They allowed me to work together with them on their own projects, introduced me the remarkable diversity of the chemistry world, and gave me educational suggestions on how to design, operate and analyze a reaction. Without their help, I would have lost myself on the journey and never know how to enjoy my time. I would like to offer special thanks to Dr. Johannes Lehmann, thank him for helping me draft the German abstract for this thesis. Great thanks is always in my heart to our fantastic lab support team. Without Samira's adept synthetic skills, Daniel's full-time work, Roland's help in radio lab, and of course their great assistance for daily lab work and assistance with the machineries, my research would not have proceeded so efficiently. I am very

grateful for all of the help and support from our analytical departments at MPI. I thank Dirk Kampen for always being so efficient in measuring my MS samples; Markus Leutzsch and Markus Kochius for analyzing and interpreting my tricky NMRs; Georg Bereitenbruch for his professional help with HPLC separations. I am particularly grateful for the assistance given by Sylwia, our sweetest admin. Without her amazing organizing ability and warmhearted kindness, I would have been struggling all the time with the administrative paper work (especially for those German ones). I also want to express my thanks to the administration offices at RWTH Aachen and MPI. Thanks to Tobias again for hiring so many international students, girls especially, so that I could hang out and make good friends with so many amazing girls (Roberta, Marta, Lalita, Samira, Nicola, Yeong-en, Zhen, Wanqi…) after lab work. I thank all of the Ritter group members, past and present, who I have got touch with directly or indirectly, for inspiring, encouraging, advising, and helping me throughout my stay.

I want to thank the UC Irvine and MIT open course wares for sharing so many insightful and educational lecture videos on Youtube. Thanks to the international network, I can grab so many fundamental chemistry knowledges without actually travelling abroad and sitting in a lecture hall. I also express my deepest thanks to our librarians, Alice Lehmann and Renate Lohmer, thank them for helping me lending and ordering articles and books, so that I can access whatever materials I need.

Of course, my families and friends are always there to be my black hole to absorb all of my complaints and frustrations and to back me up and encourage me moving forward, no matter how many hours of jet lag we have. Without them, I would have had so many tough days when the sun was hiding behind the clouds—as long as you can imagine, German winter. Thank them for always being around via Internet to share my good news and bad dreams.

TABLE OF CONTENT

I. REGIO- AND STEREOSELECTIVE THIANTHRENATION OF OLEFINS TO ACCESS VERSATILE ALKENYL ELECTROPHILES

I.1. Introduction

I.1.1. Alkenes

Alkenes, classified as unsaturated hydrocarbons that contain a carbon–carbon double bond (C═C), are among one of the most common compound categories in organic chemistry.[1] They have diverse applications in industry such as the production of plastics, lacquers, detergents and fuels. Therefore, some alkenes, such as, ethene (with a worldwide production over 150 million tons in 2016)[2], propene (with a worldwide production around 90 million tons in 2014)[3] and 1,3-butadiene (in 2020, approx. 13.7 million tons)[4], are often produced in large quantities, and they are all reported to have a continuous growing demand worldwide.

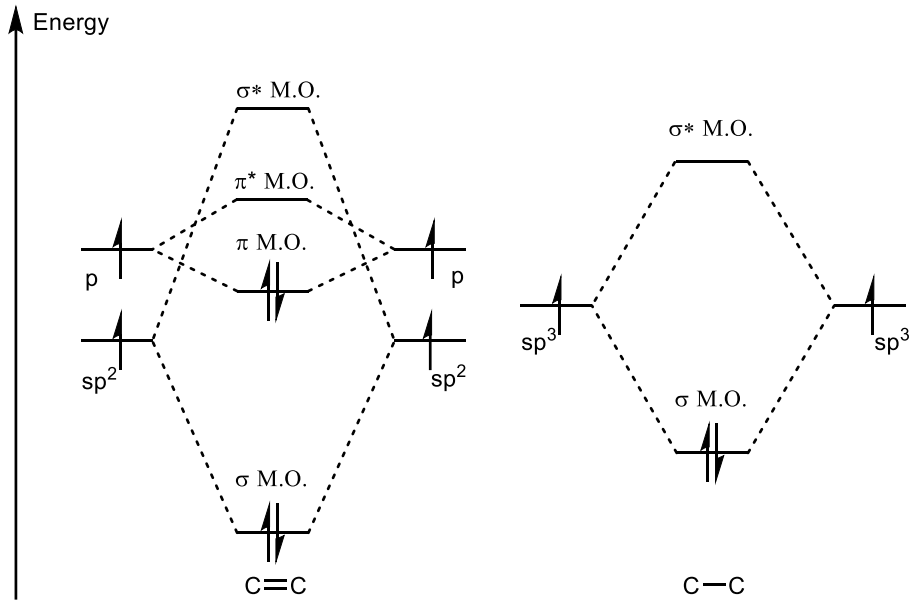

Figure I.1. Molecular orbitals for carbon–carbon double bond and single bond with relative energy comparison.

Structurally, alkenes contain at least one π bond, which manifests high diversification ability in organic synthesis. In general, alkenes are more reactive than alkanes because of the π bond character. We can elucidate this by using molecular orbital theory[5] based on the relative orbital distribution of C═C and C–C (Figure I.1). For carbon atoms on C═C, the higher energy of the highest occupied

molecular orbital (HOMO, Left: π M.O. vs. Right: σ M.O.) makes it a better nucleophile, meanwhile lower energy of the lowest unoccupied molecular orbital (LUMO, Left: π* M.O. vs. Right: σ* M.O.) enhances its electrophilicity. In this sense, alkenes are both better electrophiles and nucleophiles as compared to alkanes.

Generally speaking, alkenes are one of the most versatile functional groups and can be transformed into other useful synthetic groups (Table I.1), mostly via addition reactions: hydrogenation (alkanes), hydration (alcohols), (hydro)halogenation (alkyl halides), oxidation (ketones/aldehydes/carboxylic acids).

Reaction	**Product**	**Reaction**	**Product**
Hydrogenation[6]	alkanes	Sharpless dihydroxylation[7]	diols
Halogen addition reaction[8]	1,2-dihalides	Ozonolysis[9]	aldehydes or ketones
Hydrohalogenation (Markovnikov)[10]	alkyl halides	Diels–Alder reaction[11]	cyclohexenes
Hydrohalogenation (Anti-Markovnikov)[12]	haloalkanes	Epoxidation[13]	epoxides
Hydroamination[14]	amines	Cyclopropanation[15]	cyclopropanes
Hydroformylation[16]	aldehydes	Olefin metathesis[17]	alkenes
Polymerization[18]	polymers	Wacker oxidation[19]	Ketones or aldehydes

Table I.1. Selected transformations based on alkenes.

For olefins containing a terminal C=C, termed as *α*-olefins, olefin metathesis is another favorable approach to functionalization. Such transformations allow for the exchange of fragments between two different alkenes by double bond scission and reformation (Figure I.2). One less developed field for olefins is the direct oxidative functionalization to generate alkenyl functionalities without losing the alkene functional group. Although direct oxidative functionalization of sp^2

hybridized carbon hydrogen bonds on arenes has been widely studied, for alkenes, the most recognizable Wacker oxidation provides ketones or aldehydes, and the double bond C=C functionality is lost in the end.

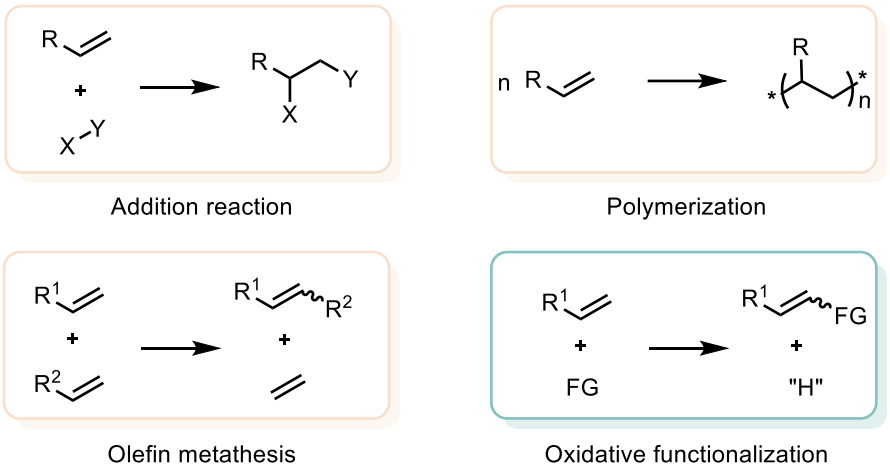

Figure I.2. Most frequently used alkene functionalization categories.

I.1.2. C–H functionalization

C–H bonds are ubiquitous in organic compounds, from natural sources/products to synthetic chemicals. Therefore, the native C–H bonds would ideally be reactive points to build up molecular complexity, since other prefunctionalized starting materials such as substrates containing C–X or C–M bonds usually require tedious multi-step preparative procedures. In addition, ineluctable waste production will be reduced significantly from direct C–H functionalization reactions, which is more progressive in terms of sustainable material development and the goal of environment protection. To achieve selective C–H functionalization, the top challenge involves overcoming the inertness of the C–H bond, with a BDE around 100 kcal/mol (varies depending of the nature of C($sp/sp^2/sp^3$)–H bond). The high-energy barrier not only necessitates a difficult activation, but also renders chemoselectivity problems when various functional groups are present in the same molecule. Another challenge is raised from the abundance of C–H bonds within a molecule, which gives rise to different regioisomers and stereoisomers.

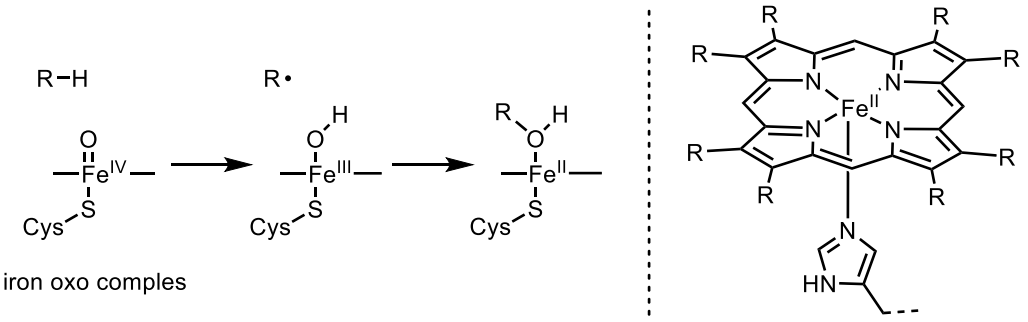

Figure I.3. Part of the mechanistic illustration for P450 catalyzed oxidation of C–H bond (Left) and core structure for heme groups (Right).[20]

Like lab chemical processes, in the human body, cytochromes P450 (CYPs), with a heme (porphyrin-iron) center (Figure I.3), catalyze mono-oxygenation of C–H bonds to maintain the balance of hormones dating back to the very first existence of mammals on earth hundreds of millions of years ago.[21] However, in the field of chemistry, the advances in homogeneous catalysis for C–H functionalization by transition metal complexes started from 1894, where Fenton obtained a compound with a formula of $C_4H_4O_6$ when tartaric acid ($C_4H_6O_6$) interacted with certain oxidants like hydrogen peroxide in the presence of a trace amount of a ferrous salt. [22] The Fenton process (Figure I.4) produces dihydroxymaleic acid from tartaric acid via activation of two C–H bonds to form a C═C bond. Thereafter, no significant effort was devoted to the development of C–H functionalization for 80 years.

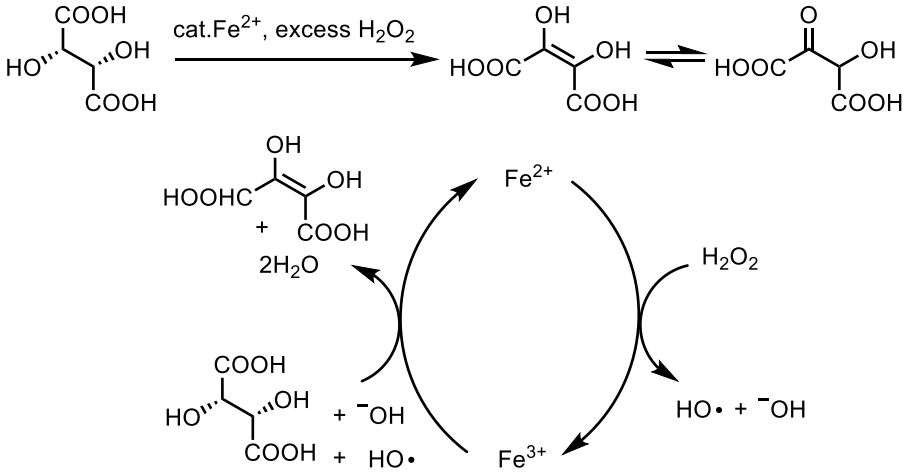

Figure I.4. Illustration of Fenton process.

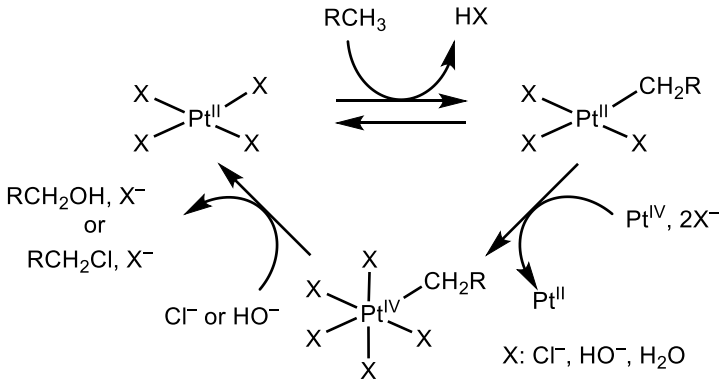

Figure I.5. Shilov's catalyst system and its catalytic cycle.

The next development was not until the 1970s, when Shilov's platinum chemistry enabled C–H functionalization using a high valent metal species: when alkanes were treated with catalytic amount of $Pt^{II}Cl_2$ and stoichiometric $H_2Pt^{IV}Cl_6$, alkyl platinum species were formed, and further addition of water to the reaction mixture lead to alcohol formation.[23] Detailed insight gains into the mechanism in the 1980s allowed revival studies on metal catalysis and C–H functionalization (Figure I.5).[24] Since then, the field of C–H functionalization witnessed its real birth in modern organic chemistry and synthesis.[25]

In the past two decades, rapid development in the direct transformation of C–H bonds was accomplished. The novel and straightforward synthetic avenues allow for quick construction of complexity or diversity from non-prefunctionalized molecules, especially offering an opportunity to streamline the synthesis of new drug candidates by circumventing *de novo* synthetic method development.[26,27] From the perspective of atom-economy, time-saving and synthetic efficiency, C–H functionalization approaches exhibit significant advantages (Figure I.6). Many of them use a transition metal species and constitute mild and selective processes.

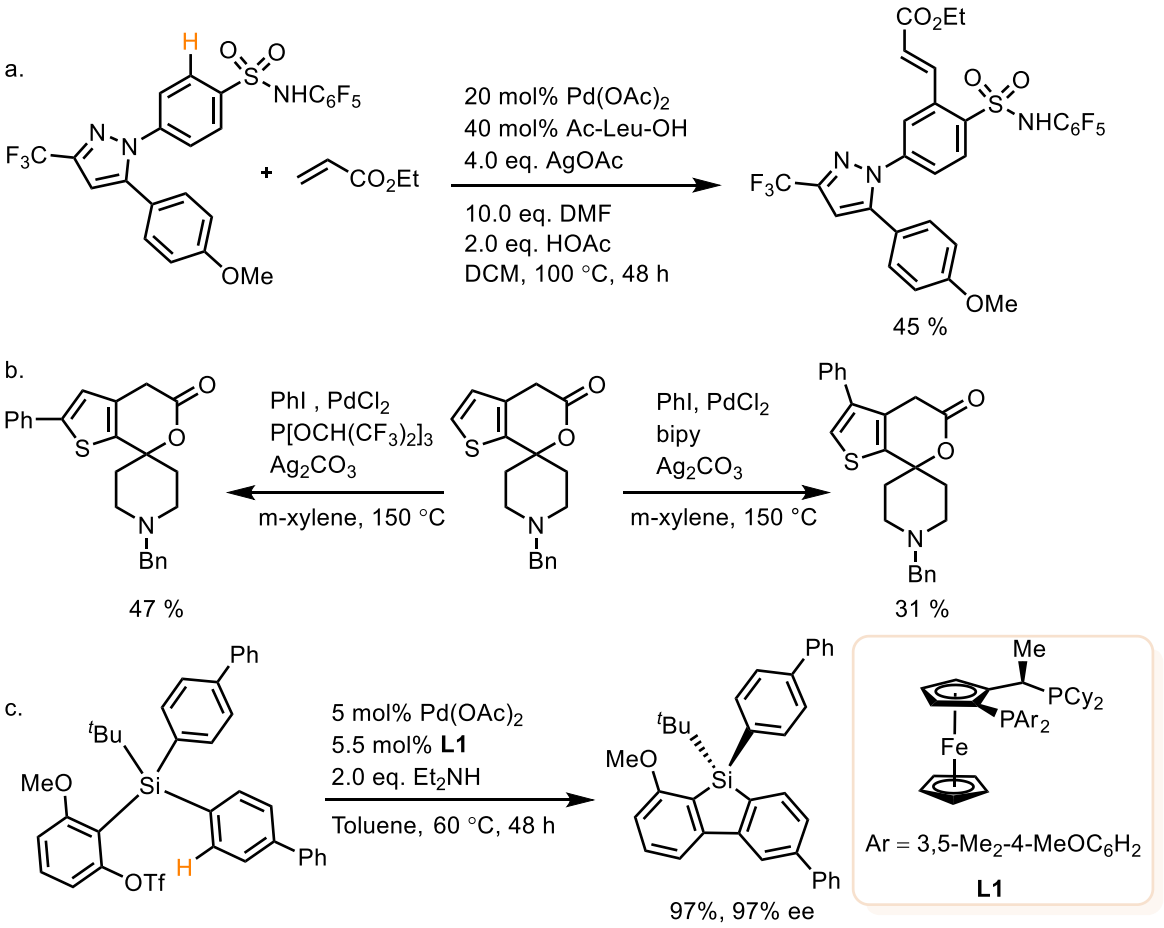

Figure I.6. Examples for direct C–H functionalization reactions in small complex molecules. (a,[28] b,[29] c[30])

In general, all of the methodologies for C–H functionalization fall into two main categories according to functionalization modes (Figure I.7): (a) direct C–H functionalization, reactions often count on the intrinsic electronic or steric properties of the substrates like what CYPs do in the body. Good electrical and sterical matches between substrates and the incoming reagents are crucial to achieve high reactivity and selectivity. (b) Auxiliary directing group facilitated C–H functionalization, reactions where extra groups are introduced to direct a reaction to specific sites. In this case, installation of external chelating groups prior to C–H functionalization and removal afterwards are often unavoidable.

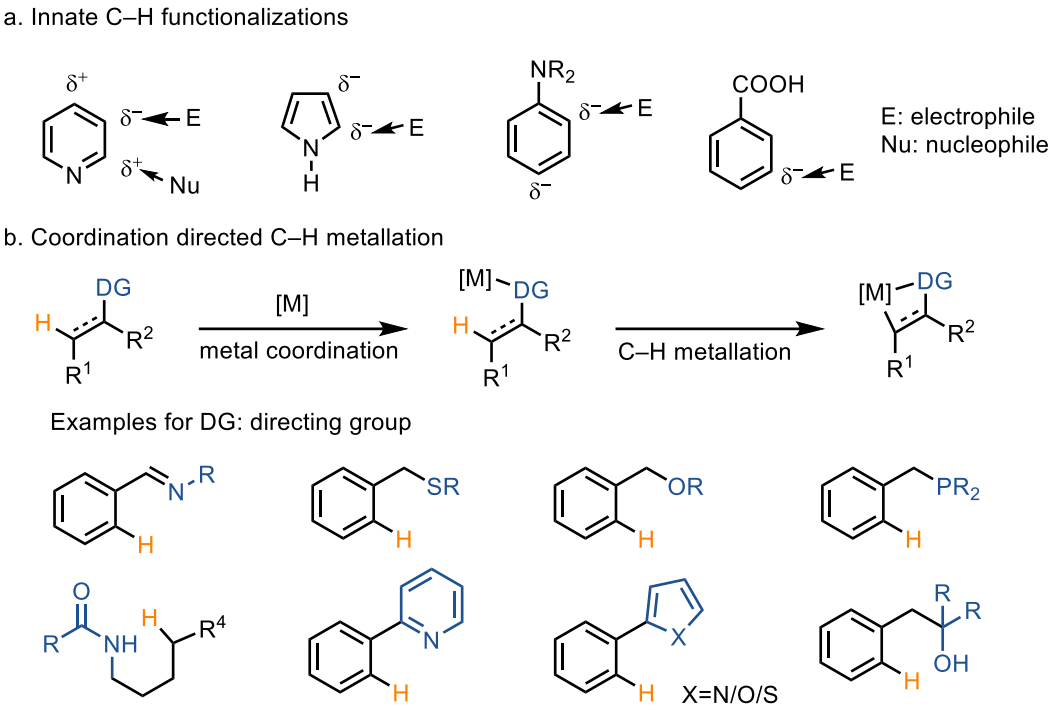

Figure I.7. Strategies for C–H functionalization.

Based on their relative reactivity, C–H functionalization can be selective over sp^3 (alkanes), sp^2 (arenes and alkenes) and sp (alkynes) hybridized C–H bonds. Alkynyl protons are mildly acidic, with pK_a values of around 25, and can be deprotonated with a base such as $NaNH_2$. The resulting acetylides react readily with electrophiles. Thus, no further discussion on alkynyl C–H functionalization is included in this thesis.

I.1.2.1 C–H functionalization of alkanes

In addition to a high activation barrier encountered by functionalization of strong alkyl C–H bonds (BDE ≈ 100 kcal/mol) and selectivity problems raised from different C–H bonds, another challenge is over functionalization: Mono-functionalized products are prone to be functionalized further due to their increased reactivity when compared to the alkane starting materials. For example, alcohols, generated from hydroxylation of alkanes, tend to be further oxidized to aldehydes or ketones.

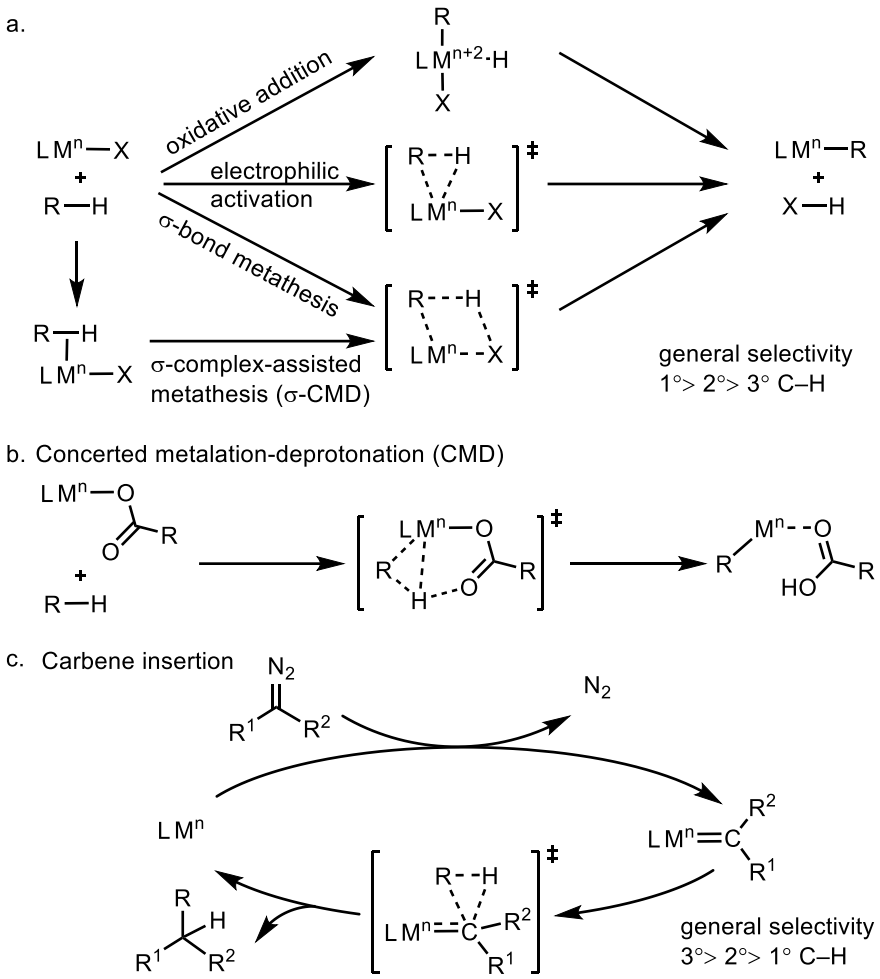

Figure I.8. Reaction pathways for metal-assisted C–H functionalization of alkanes.[31]

For the functionalization of alkanes using a homogenous catalyst, different activation pathways have been proposed in the literature, for example: oxidative addition,[32,33] electrophilic activation,[34,35,36] σ-bond metathesis,[37,38] σ-complex-assisted metathesis,[39,40] concerted metalation-deprotonation,[41,42] and carbene insertion[43,44,45] reactions (Figure I.8). The most widely recognized carbonylation[46] and regioselective borylation[47,48,49] stand out as the text book examples.[50] As their names state, alkyl C–H bonds are transformed to carbonyl and boryl groups, respectively, in a mono-functionalized and selective manner (Figure I.9a and b).

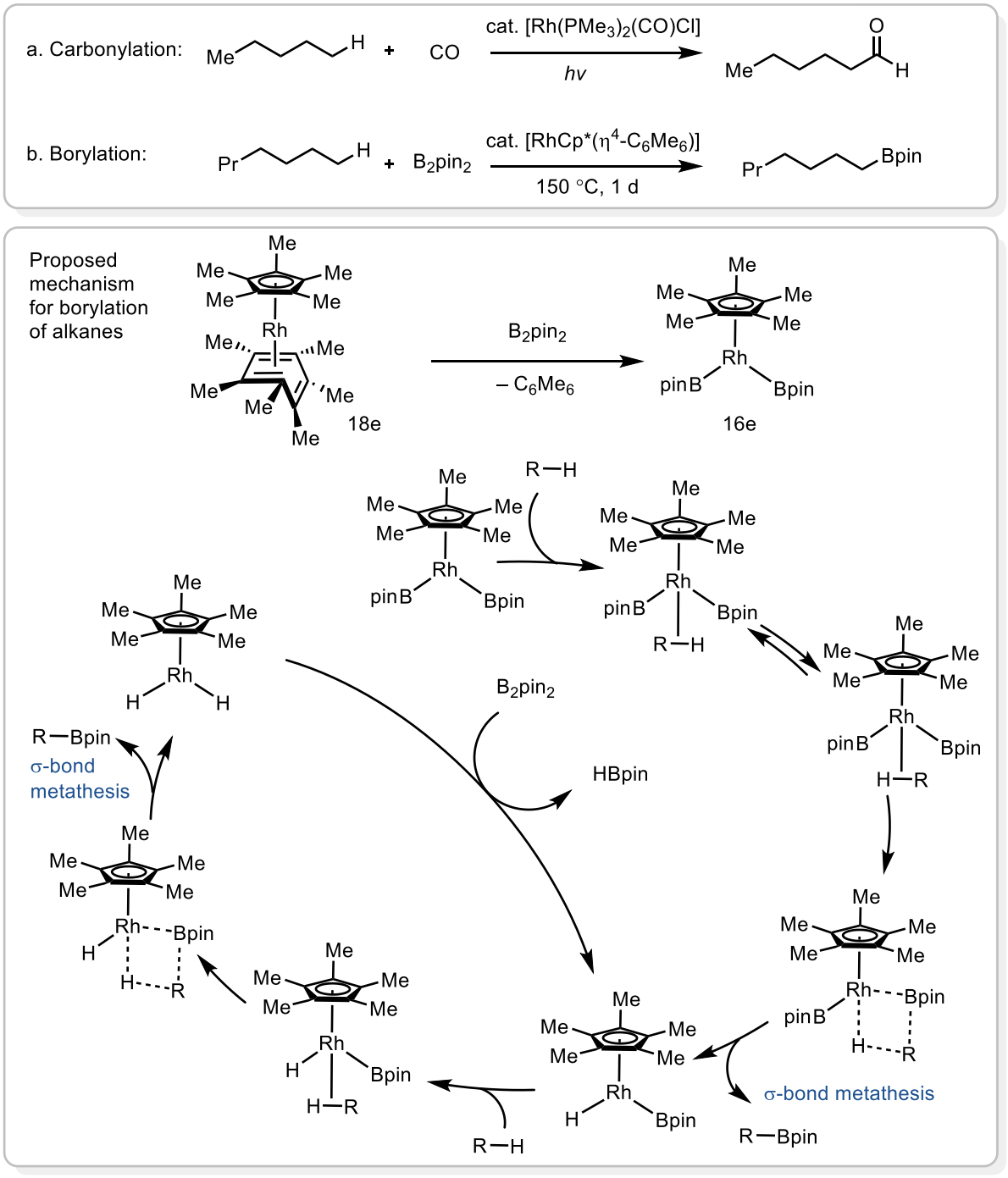

Figure I.9. Carbonylation and borylation of alkanes, and the proposed reaction mechanism for the rhodium catalyzed borylation reaction.

For the rhodium-catalyzed mono-borylation developed by the Hartwig group, preliminary mechanistic data suggest a boryl rhodium complex being responsible for exclusive site-selection of terminal C–H bonds due to kinetic factors, in other terms, from a steric preferred formation of a linear metal-alkyl complex (Figure I.9 Bottom).[51] A conceivable mechanism regarding Cp*Rh(η^4-C_6Me_6) as a pre-catalyst

starts with dissociation of the η^4-C_6Me_6 ligand with simultaneous formation of Cp*Rh(Bpin)$_2$, which reacts with alkane starting materials. The active catalyst Cp*RhH(Bpin) can be generated by σ bond metathesis with concomitant formation of alkyl–Bpin. One interesting observation from this reaction is that the number of moles for alkyl–Bpin produced is greater than the number of moles for B_2pin_2, which indicates the byproduct HBpin can act as Bpin source. Indeed, under similar reaction conditions, alkyl–Bpin can be obtained when HBpin is used instead of B_2pin_2, though with lower yield.

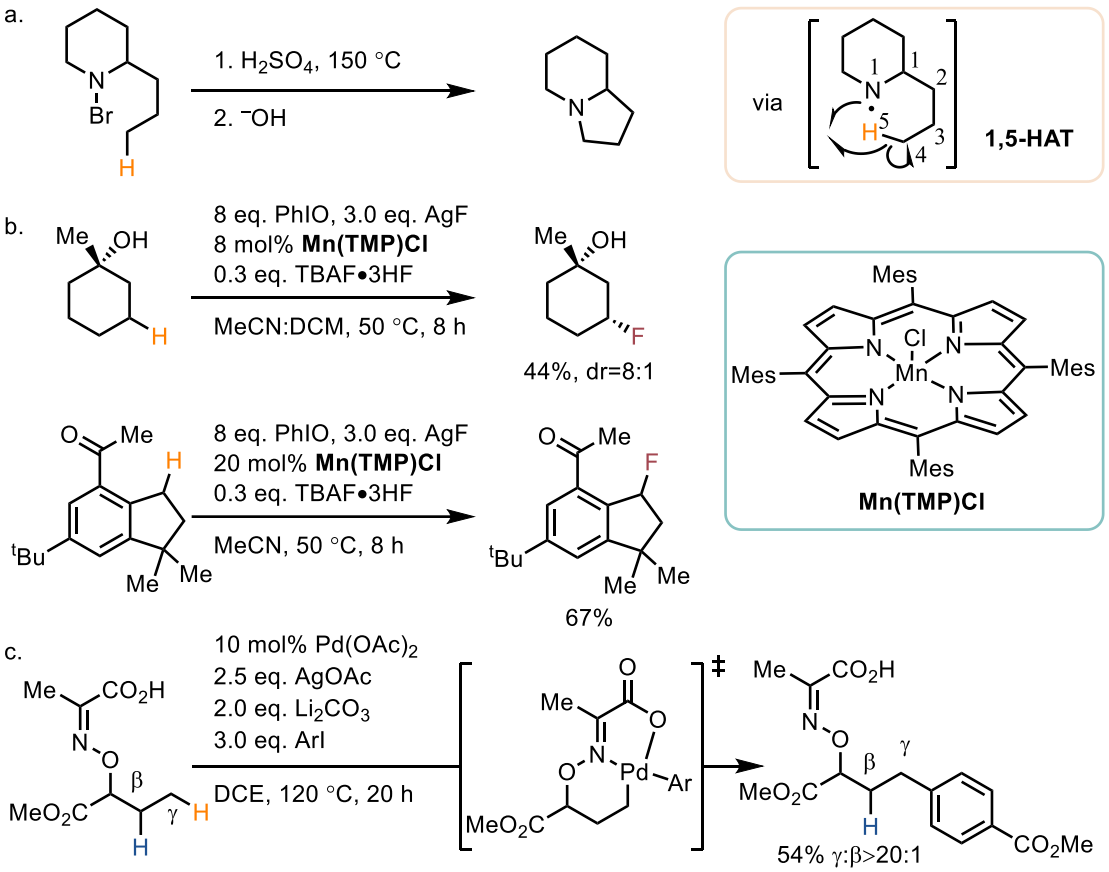

Figure I.10. Examples for selective functionalization of alkanes.

The Hoffmann-Löffler-Freytag reaction allows site-selective amination of alkanes via an intramolecular 1,5-hydrogen atom transfer (1,5-HAT) to a nitrogen centered radical (Figure I.10a).[52,53] With a similar strategy, a positional selective alkylation of unactivated C(sp^3)–H by 1,5-HAT mechanism for pendent amide was recently reported by the Rovis group (Figure I.11). [54] Such a C(sp^3)–C(sp^3) coupling was achieved through photoredox catalysis in combination with nickel catalysis: For the iridium photocatalyst cycle, the photoredox active Ir(III) complex

was activated to the excited state by photons under blue LED irradiation. The excited Ir(III) complex is quenched by an amine anion in a reductive way to generate an amine radical and a reduced Ir(II) species. For the nickel redoxcatalyst cycle, the Ni(I) catalyst reacts with an alkylBr to form a Ni(III)–alkyl species, which is reduced to a Ni(II) complex with concomitant regeneration of Ir(III) complex. The amine radical goes through a 1,5-HAT reaction pathway to afford an alkyl radical which combines to the Ni(II) species to form a Ni(III)–alkyl complex. Reductive elimination from the putative Ni(III)–alkyl species gives the C(sp^3)–C(sp^3) coupling product and regenerates the Ni(I) catalyst.

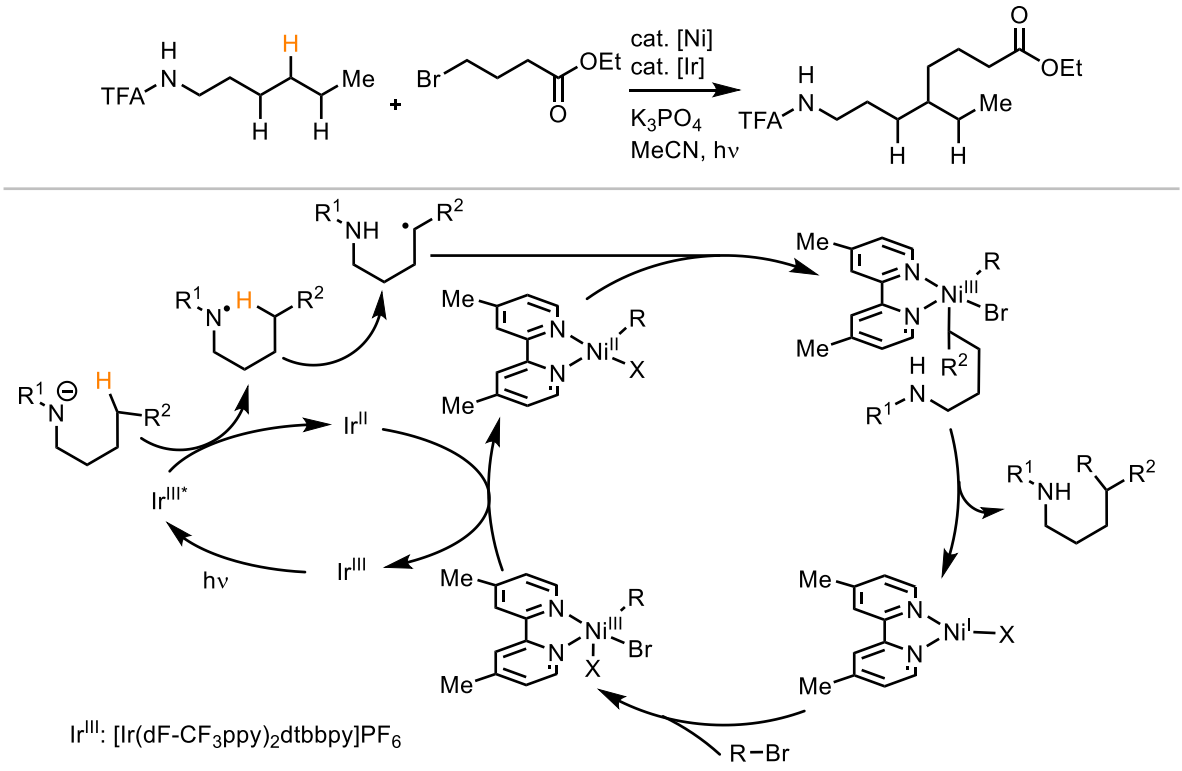

Figure I.11. Selective C(sp^3)–C(sp^3) coupling via 1,5-HAT mechanism.

Bio-inspired manganese porphyrin complexes developed by the Groves group enable efficient one-step conversion of C–H bond to C–F bond, one of the most challenging bond formations (Figure I.10b).[55, 56] Like CYPs, their Mn porphyrin catalysis involves a reactive Mn(V)–oxo intermediate. The authors isolated and characterized a novel *trans*-difluoro Mn(IV) complex, which was further shown to enable efficient fluorine atom transfer to short lived alkyl carbon radicals (Figure I.12b).

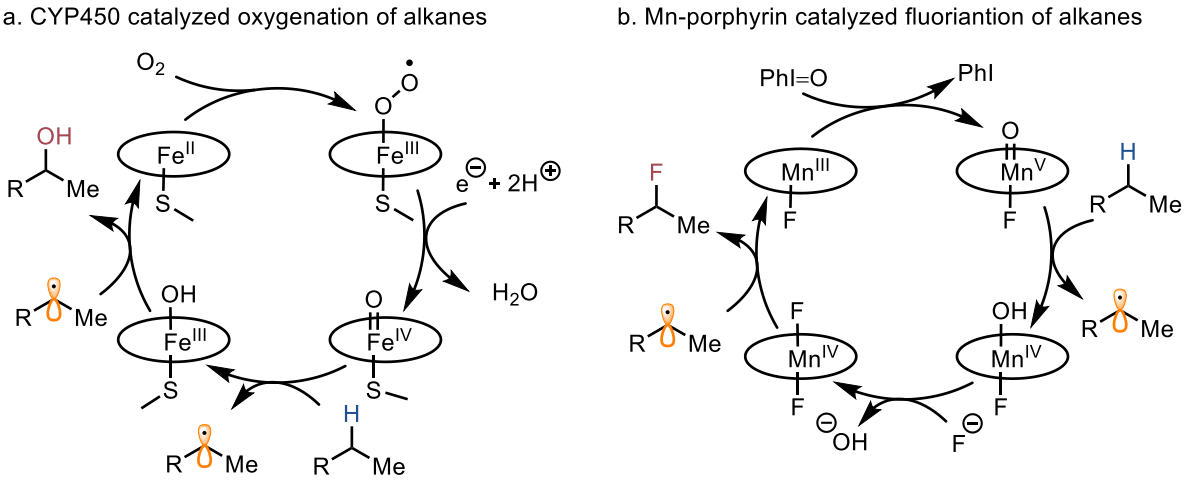

Figure I.12. Proposed mechanisms for metal porphyrin related catalysts catalyzed C–H functionalization of alkanes.

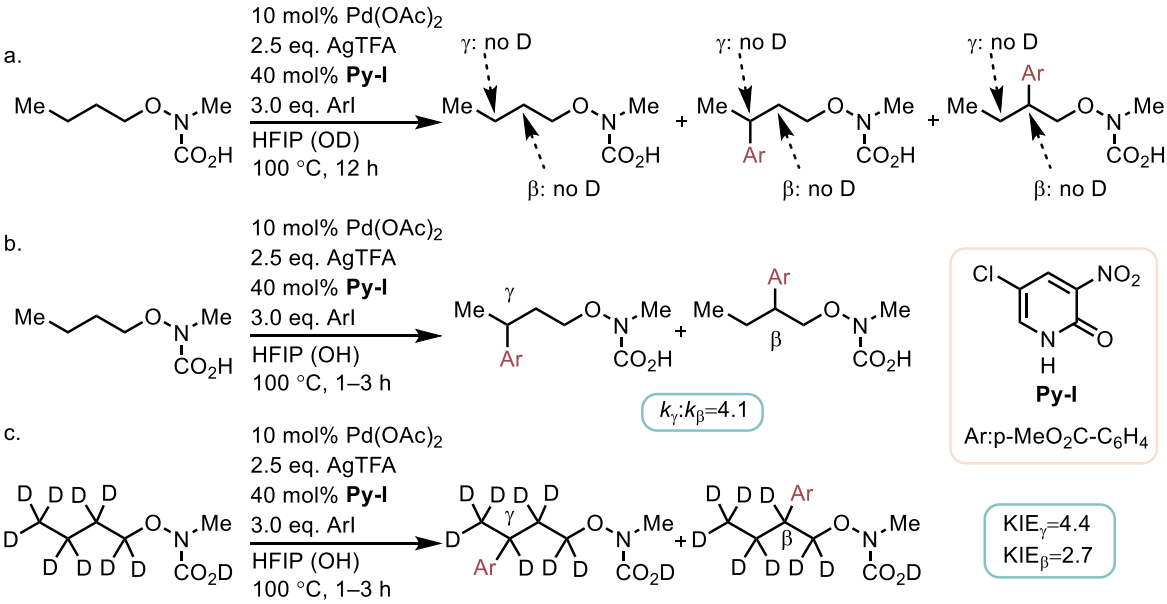

Figure I.13. Mechanistic studies on palladium catalyzed γ-selective C–H activation reaction.

Recent work by the Yu group revealed a strategy for activation of γ-C(sp^3)–H over β-C(sp^3)–H by exploiting directing groups (Figure I.10c).[57] The both kinetically and thermodynamically more favored five-membered counterpart[58,59] is overridden, and the reaction is proposed to proceed through a less favorable six-membered palladacycle intermediate. Deuterium incorporation experiments revealed that the arylation step is sufficiently fast and far over the C–H activation rate (Figure I.13a). Kinetic experiments (Figure I.13b) of intramolecular competition showed that arylation at the γ-C(sp^3) is faster (k_γ/k_β = 4.1). Kinetic isotope effect (KIE)

experiments indicate rate determining C–H cleavage for both γ-C(sp^3)–H over β-C(sp^3)–H bonds (Figure I.13 c: $KIE_\gamma = 4.4$, $KIE_\beta = 2.7$). Overall, the preliminary experimental data allow the authors to suggest the selectivity originating from the C–H cleavage step for this unconventional γ-selective C–H activation reaction.

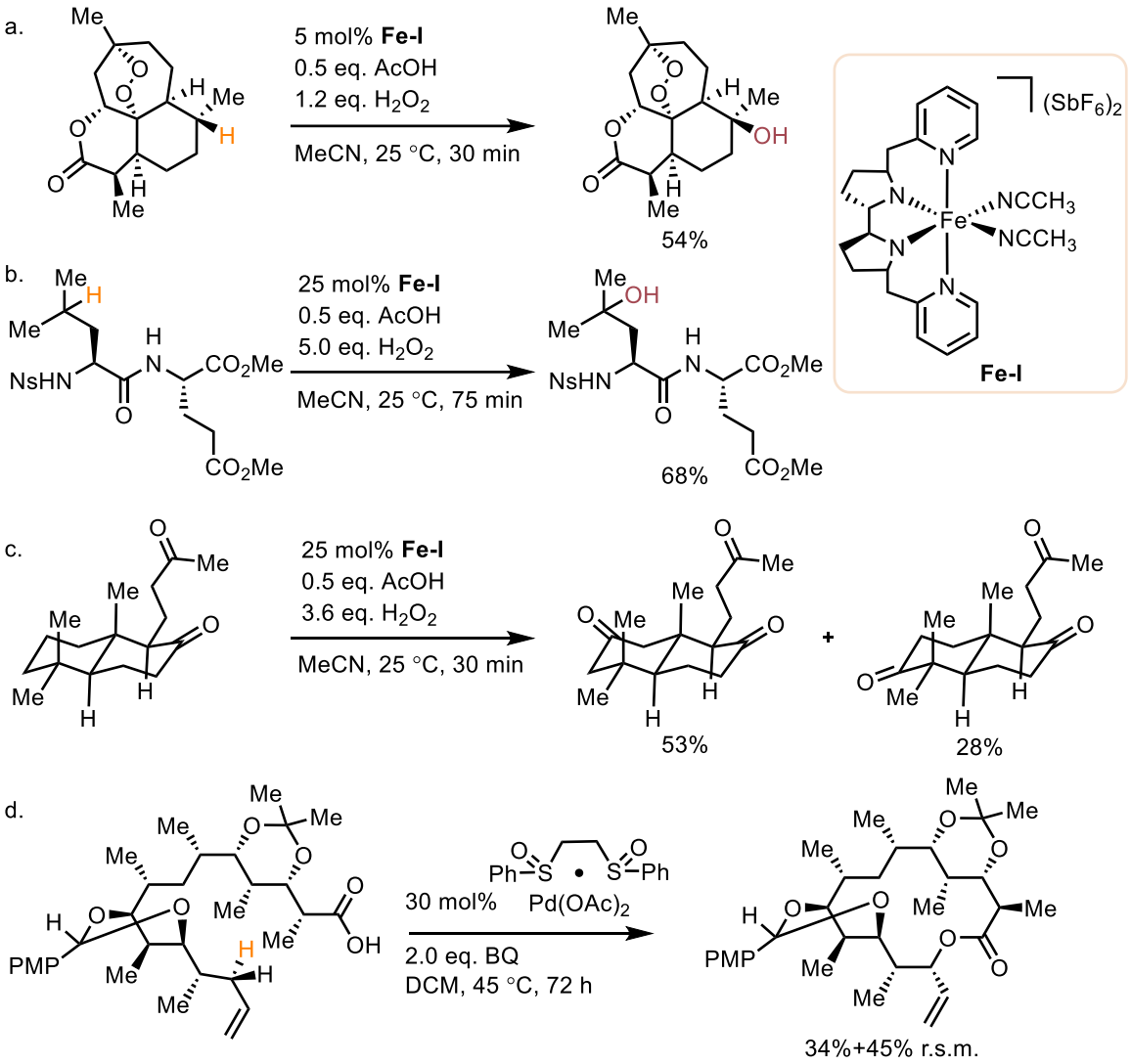

Figure I.14. Streamline syntheses of complex molecules by selective C–H functionalization.

Additional synthesis streamlining methods have been developed by the White group for selective aliphatic C–H oxidation reactions in complex molecule synthesis,[60,61,62] even for small peptides (Figure I.14).[63,64] The White group focused on developing catalysts for site-selective aliphatic C–O bonds formation directly from C–H bonds. In their catalytic systems, the current empirical data regarding the same catalyst system for different substrates (Figure I.14a, b and c)

suggested no need for specific matches between catalysts and substrates to achieve site-selectivity.

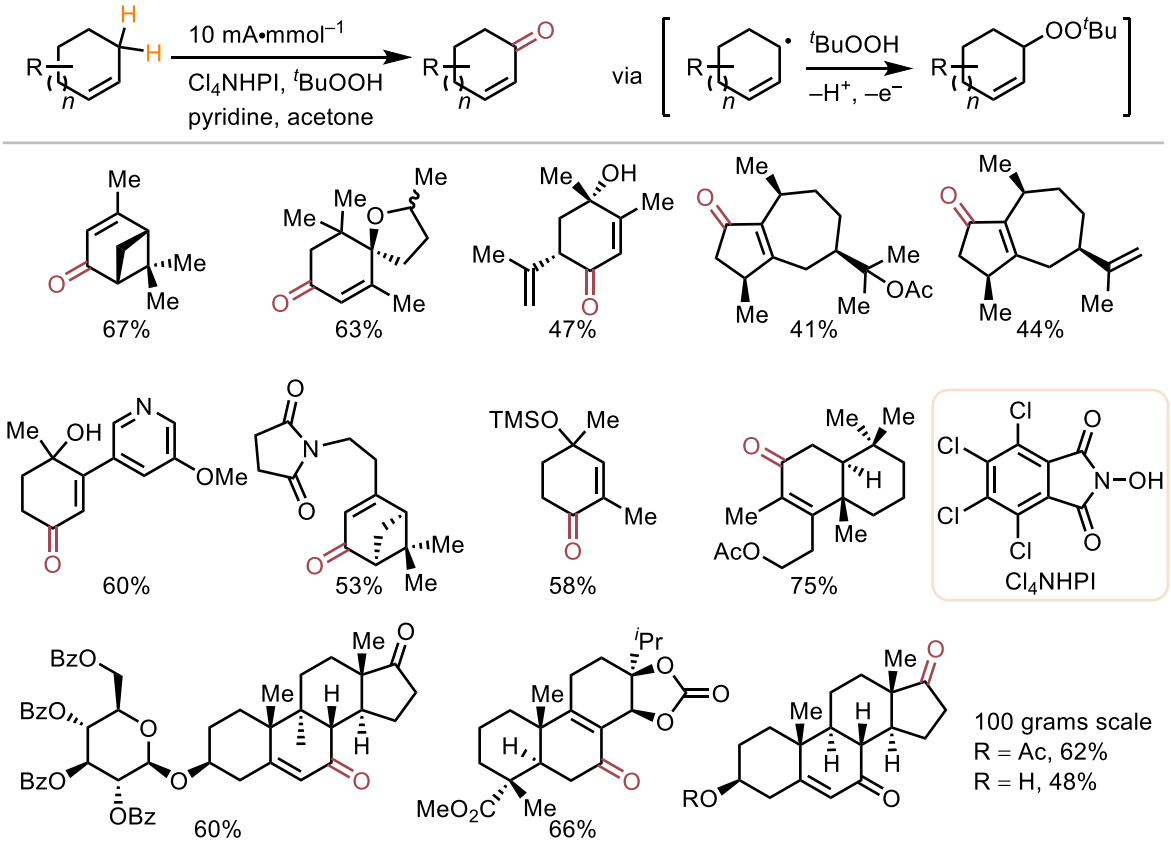

Figure I.15. Electrochemical catalyzed allylic C–H oxidation reaction.

Scalable and sustainable C–H oxidations have also been achieved using electrochemical catalysis..[65,66] The allylic C–H oxidation method (Figure I.15) developed in the Baran group[67] has shown an alternative greener strategy compared to current chemical processes, which often leads to the production of toxic waste[68] when adapted to large-scale industrial settings. Initial mechanistic investigations for this electrochemical allylic oxidation suggest a catalytic *N*-oxyl radical generated from Cl_4NHPI to be responsible for allylic C–H hydrogen atom abstraction and allyl radical formation. Radical combination with the electrochemically derived *tert*-butyl peroxide radical affords an allylic peroxide, which gives the enone product upon elimination of *tert*-butyl alcohol.

I.1.2.2 C–H functionalization of arenes

C–H bonds on arenes are often easier to be functionalized compared to their alkyl counterparts, even though C(sp^2)–H bonds are more inert to homolytic

cleavage than C(sp^3)–H bonds according to BDE. Because aryl C–H bonds can capitalize on the unsaturated aromatic part, more specifically the π bonds, as a "catalytic sector", which can be restored after C(sp^2)–H hydrogen loss. From the point of systematic discussion on the reaction patterns for aromatics towards different incoming reaction partners and the format of hydrogen loss, most of the reactions can be classified into three categories of activation modes involving proton (electrophilic),[69,70,71] hydride (nucleophilic),[72,73,74] or hydrogen atom (radical)[75,76,77] transfer from the aromatic substances. Other transition metal mediated or assisted C–H activation of arenes including oxidative insertion into the C–H σ bond with increasing in oxidation state by two on the metal center,[78,79] or σ bond metathesis between arene C–H σ bond and alkyl metal σ bond,[80] for example an alkyl–Li bond (Figure I.16).[81,82,83]

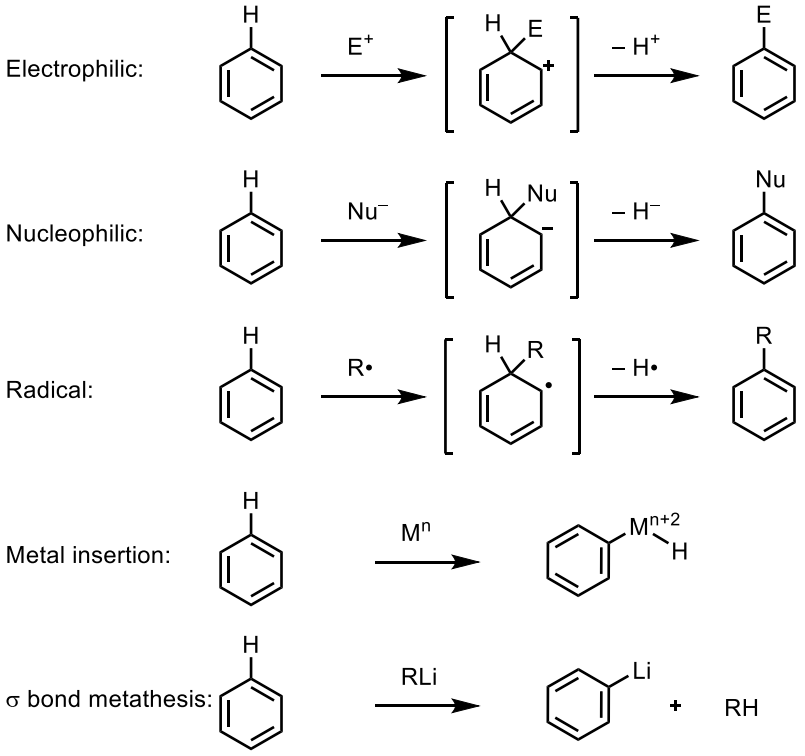

Figure I.16. Aromatic C–H functionalization mechanisms.

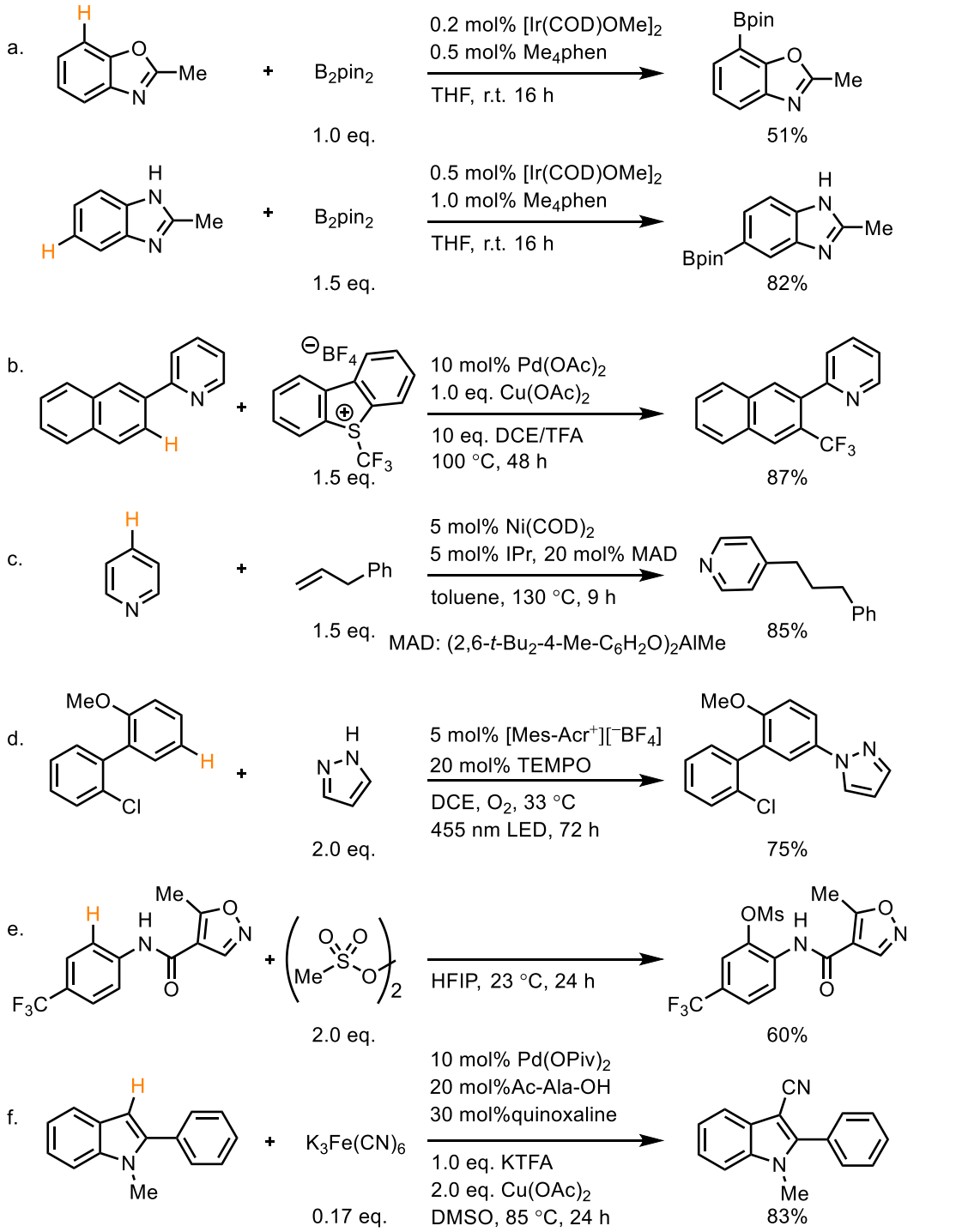

Figure I.17. Examples for C–H functionalization of arenes using recently developed methodologies.

Traditional direct C–H functionalization reactions often suffer from low regioselectivity when more than one aryl C–H bond is present in the substrates.[69,71] For instance, the Friedel-Crafts reaction[69] and the Scholl reaction[84], involve carbon cation intermediates, which often exist as more than one isomer depending on the resonance equilibrium constants. In general, those reactions

suffer from low selectivity, low functional group tolerance, and limited substrate scope, all of which limit their applicability in late-stage C–H functionalization.

For recent advances, which are not restricted to traditionally highlyreactive partners like electron-rich arenes and acrylates, diverse functional groups can be successfully installed. Methods developed vary from directing group assisted site-specific[85,86] to direct site-selective C–H functionalization reactions[87,88,89] to construct C–B,[90,91,92] C–C,[93,94,95] C–N,[96,97,98,] and C–O[99,100] bonds (Figure I.17). Challenging C–F bond formation on complex molecules is also available, although not yet ideal regarding selectivity.[101] For example, the iridium-catalyzed C–H borylation of heteroarenes, developed by the Hartwig group, afforded selective hetero arylboronates when differentiable stereoelectronic characters were present on the substrates (Figure I.17a).[90,91,92] Aryl C–H amination under photoredox conditions, discovered by the Nicewicz group, represented an ideal reaction paradigm, where molecular oxygen was used as the terminal oxidant, and all of the other reagents were used in catalytic amount except for the coupling amine (Figure I.17d).[96] The direct oxygenation of arenes with methylsulfonylperoxide, reported by the Ritter group, demonstrated preference at the positions that are mostly vulnerable in metabolic conditions (Figure I.17e).[88]

The Murai reaction, first reported in 1993,[102] was recognized for its high efficiency and broad substrate scope compared to other C–H activation reactions known before. Generally, a variety of Ru(0) and Ru(II) catalysts work for the Murai reaction, but detailed mechanisms for those reactions have not yet been elucidated. There are two main mechanisms proposed for different catalysts (Figure I.18) based on experimental evidences in combination with density functional theory (DFT) studies. (a) Ru(0) based catalysts such as $[Ru(H_2)(CO)(Ph_3)_3]$ was suggested to go through a Ru(0)–Ru(II)–Ru(0) catalytic cycle under high temperatures.[103,104] (b) Catalyst $[Ru(o\text{-}C_6H_4PPh_2)(H)(CO)(Ph_3)_3]$ which catalyzed the Murai reaction at room temperature, was proposed to involve a Ru(II)–Ru(IV)–Ru(II) catalytic cycle.[105,106]

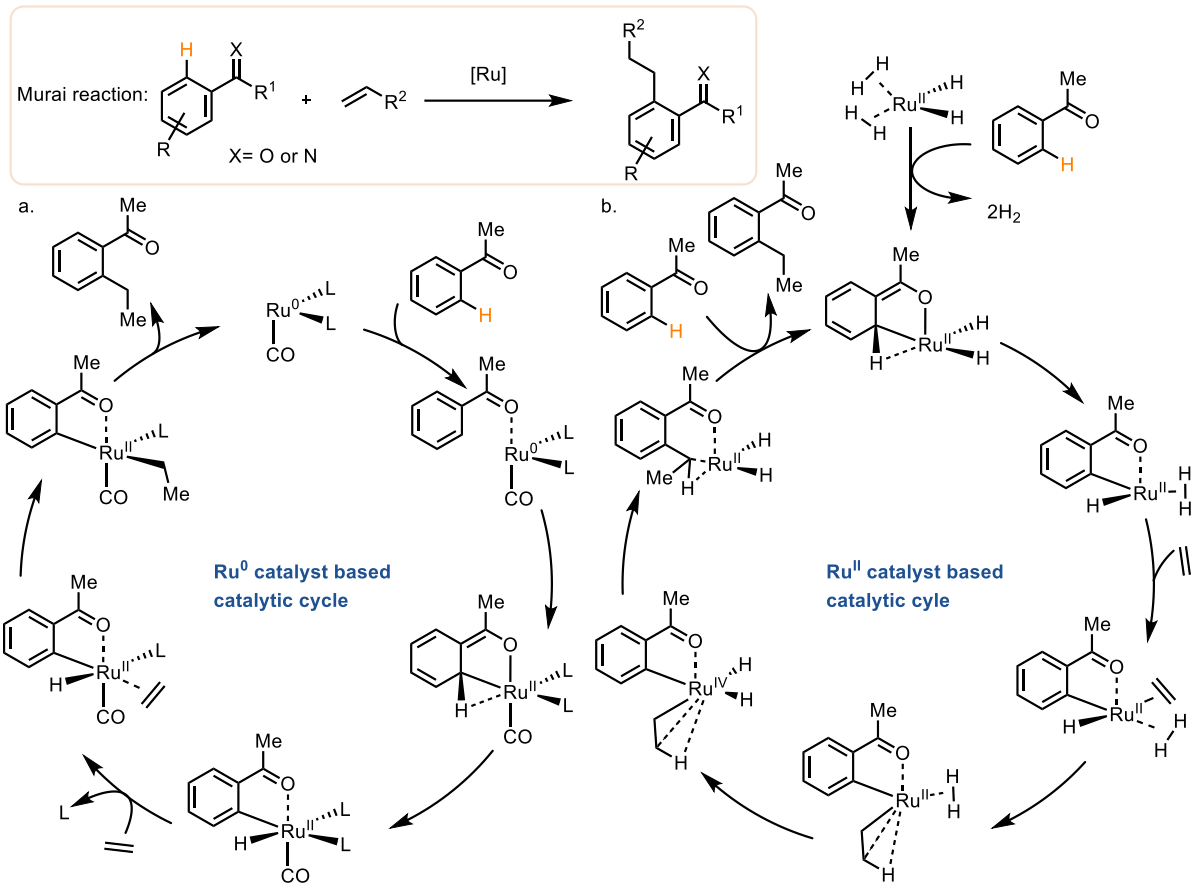

Figure I.18. Ruthenium-catalyzed Murai reaction and plausible mechanisms.

Other than substrate extension, site-selective functionalization research also focused on even less reactive positions, like *meta* C–H bonds on an arene, that are hard to access conventionally, often requiring auxiliary directing groups. Regardless of the advances made for the usual *ortho*-directed functionalization and the generic *para*-favored electrophilic substitution reactions, the intriguing *meta*-selective C–H functionalization is more challenging and hence less developed. This is because the *meta*-position is less activated for electrostatic reasons, while at the same time more difficult to access via directing groups. Such elegant *meta*-functionalization becomes feasible with the iridium catalyzed C–H borylation, developed independently by the Smith[107] and Hartwig groups.[108] The appealing reactivity of borylation is proposed to be an outcome of steric effects on the aromatic ring, which lead to functionalization of the proton that is less adjacent to any other substituents. After that, sequential activation-functionalization facilitated by novel catalysts or in combination with novel directing group allows for

complementary *meta*-selective C–H functionalization, especially those based on copper[109,110], palladium[111] and ruthenium[112,113] catalysts (Figure I.19).

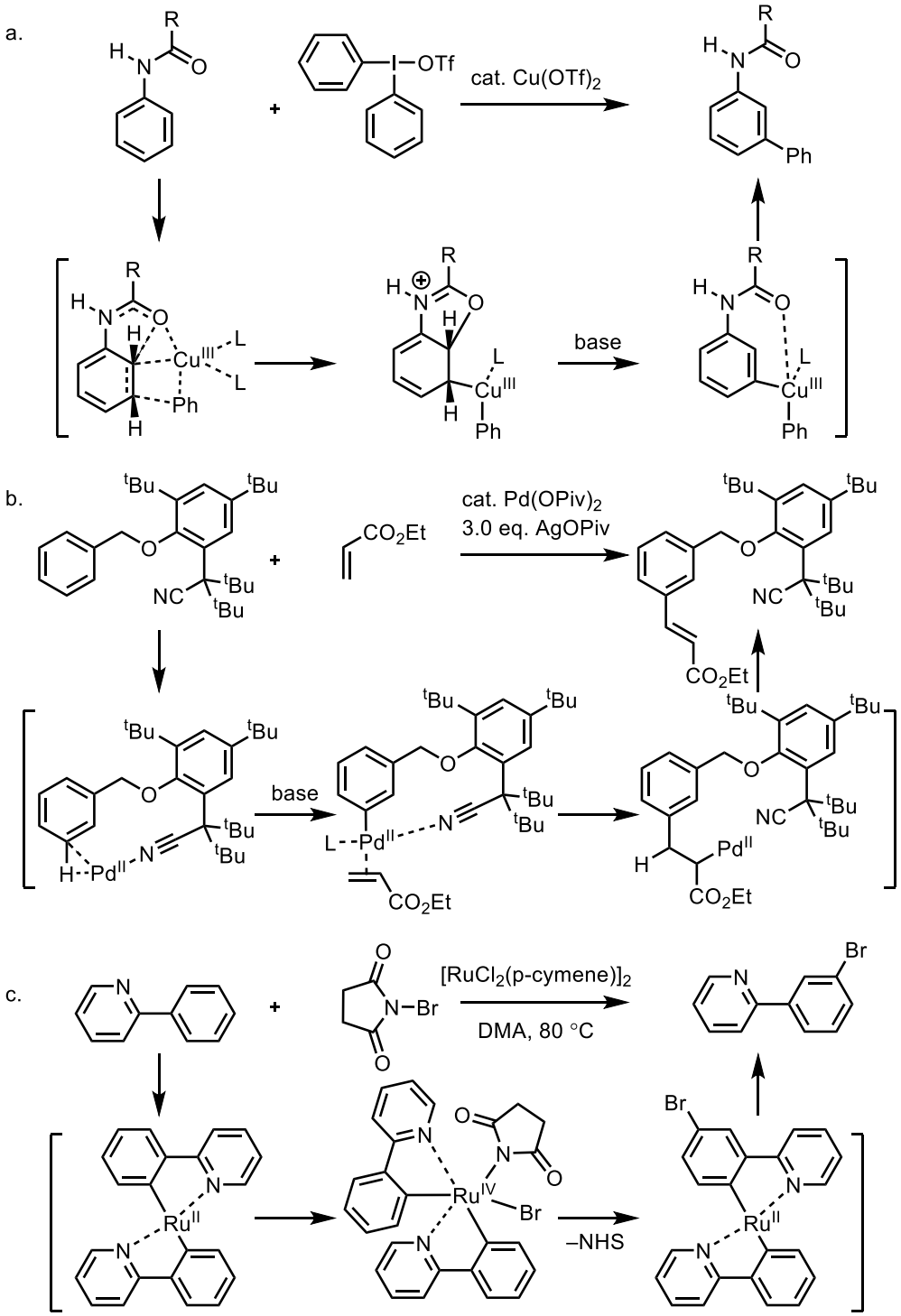

Figure I.19. Copper-, palladium- and ruthenium-catalyzed *meta* C–H functionalization of arenes.

I.1.2.3 C–H functionalization of alkenes

Unlike C–H bonds attached to aromatic systems (Figure I.16), those on alkenes are more difficult to functionalize while preserving the alkene functionality. Normally, direct functionalization of alkenes delivers hydrofunctionalized [114] or vicinal difunctionalized alkanes (*vide ante*, Table I.1),[115,116,117] which possibly can be explained by the higher vulnerability of carbon–carbon π bond compared to the carbon–hydrogen σ bond (*vide ante*, Figure I.1). The difference in reactivity is clear especially when treated with electrophiles, though olefins display C(sp^2)–H bonds like arenes, their reactivity is distinct from arenes: arenes undergo electrophilic C(sp^2)–H substitution (Figure I.16), while olefins typically undergo addition reactions like dihalogenation to generate dihaloalkanes.[118]

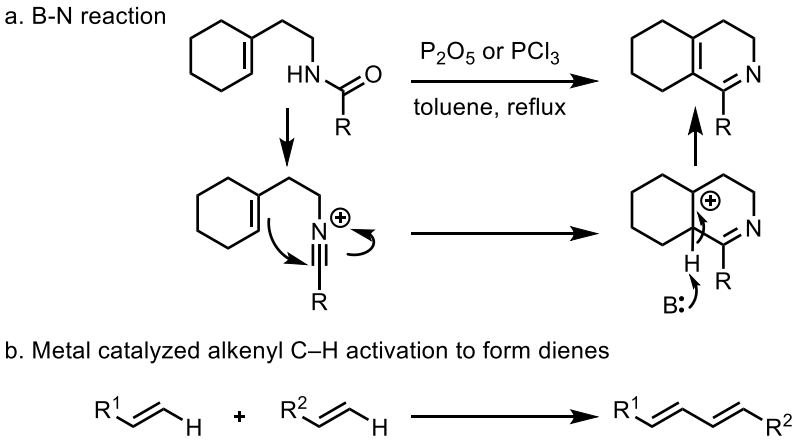

Figure I.20. Bischler-Napieralski (B-N) reaction and metal catalyzed diene formation of alkenes.

Under metal-free conditions, alkene π bonds can be regenerated after hydrogen loss when treated with reactive electrophiles such as in the Bischler-Napieralski (B-N) reaction[119] and it extended versions[120,121,122] to form imines from nitrilium ions (Figure I.20). In the presence of metal catalyst, cross-coupling reactions to afford dienes from simple alkenes are the most generic transformations reported to date for metal catalyzed direct C(sp^2)–H functionalization of alkenes. [123] Transition metals, like palladium, which can undergo β-hydride elimination to form alkenes, are very promising catalysts for C–H functionalization of alkenes. There are still some issues with these catalysts, however, as reported examples with palladium catalysts often lead to

polymerization in the presence of another molecule of alkene through a chain walking process.[124,125]

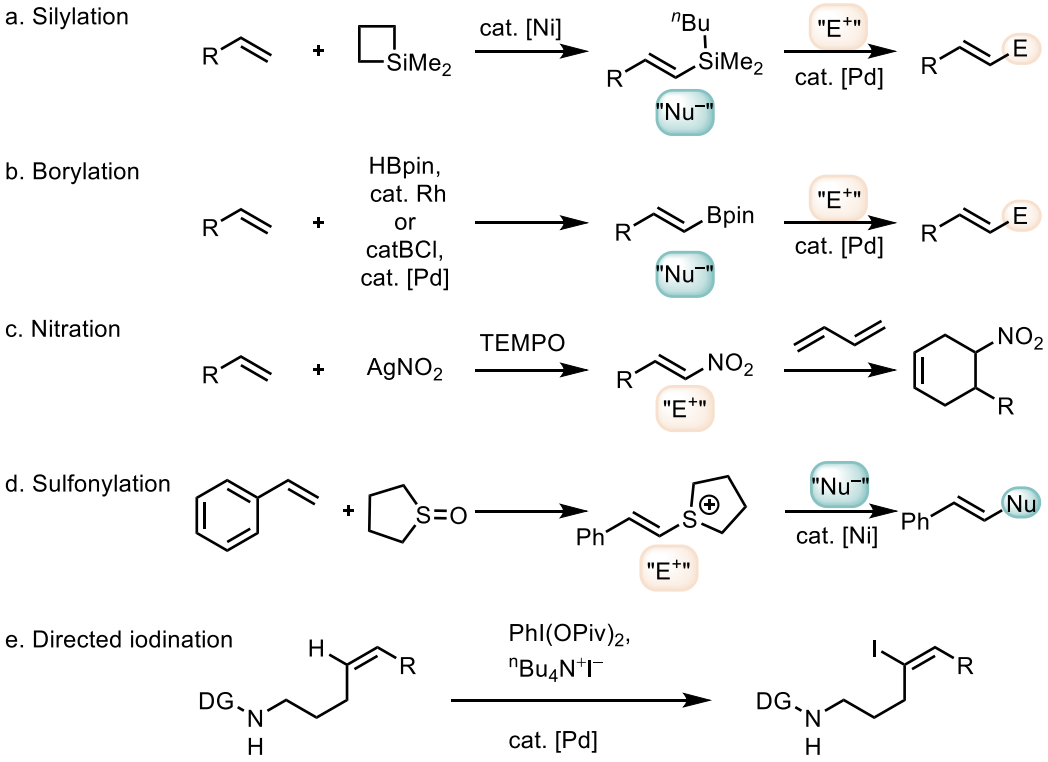

Figure I.21. More examples for direct C–H functionalization of alkenes.

Even though direct C(sp^2)–H functionalization of alkenes is challenging, several alkenyl nucleophiles are available in literature, such as alkenyl silanes[126,127] and boronates (Figure I.21a and b).[128,129] Michael acceptors such as nitroolefins[130,131] and alkenyl nitriles[132] can also be synthesized from alkenes via C(sp^2)–H functionalization (Figure I.21c). Recently, alkenyl electrophiles also became available from alkenes with limited substrate scopes: the Procter group disclosed the synthesis of alkenyl sulfoniums via an interrupted Pummerer approach (Figure I.21d), and the corresponding alkenyl sulfonium salts can act as alkenyl electrophiles for nickel catalyzed Negishi cross-coupling reactions. However, the protocol is limited to styrene-like substrates.[133] In 2019, the Carreira group reported a directed alkenyl C–H functionalization to make alkenyl iodides bearing a picoline-directing group (Figure I.21e).[134] The reaction undergoes an auxiliary group directed concerted metalation deprotonation to form 6-membered alkenyl-palladacycles. In combination with a turnover-limiting C–H activation, the authors are able to obtain all of the alkenyl iodides as single stereoisomers but

directing group installation and removal are necessary. Overall, methods for synthesis of alkenyl electrophiles directly from alkenes, with broad substrate scope and high functional group tolerance, are still in high demand.

I.1.3. Alkenyl electrophiles

Since the rapid development of cross-coupling reactions catalyzed by transition metal complexes from 1970s, organo iodies/bromides play a vital role as cross-coupling partners. They are good coupling partners due to their high reactivity towards transition metal complexes. It can also be explained by their lower bond dissociation energy (BDE), which indicates easier bond cleavage compared to other carbon heteroatom single bonds (Table I.2).[135, 136] The importance of cross-coupling processes using these prefunctionalized substrates have been recognized with the award of the 2010 Nobel Prize in chemistry to Richard F. Heck, Ei-ichi Negishi and Akira Suzuki for their great contributions to the development of palladium catalyzed cross-coupling reactions. From this reason, the development and application of new organo-electrophiles are further encouraged.

single bond	BDE (kcal/mol)	single bond	BDE (kcal/mol)
C–H	99	C–P	70
C–C	83	C–F	116
C–O	86	C–Cl	81
C–N	73	C–Br	68
C–S	65	C–I	51

Table I.2. Bond dissociation energies of carbon heteroatom bonds.

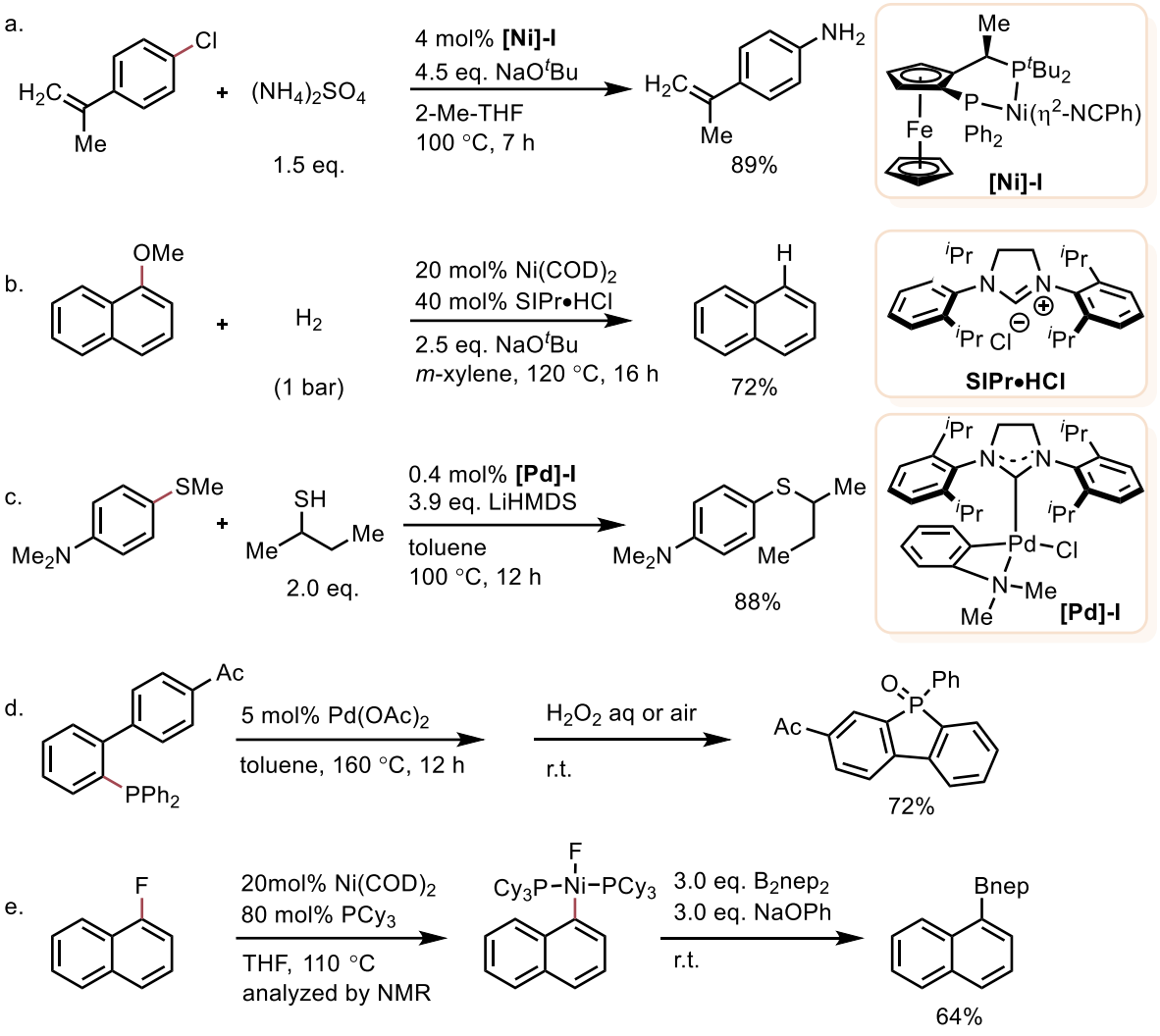

Figure I.22. Activation of carbon heteroatom bonds in modern synthesis.

Recent research in diversification of organo-electrophiles has enabled activation of other less reactive bonds such as C–Cl,[137,138,139] C–F,[140,141,142] C–O,[135,143,144] C–P[100,145,146], and C–S[100,147] bonds (Figure I.22).[148] One major branch of those carbon heteroatom electrophiles are heteroatoms bonded to a sp^2-hybridized carbon, more specifically aryl or alkenyl electrophiles. Aryl electrophiles are more widely available and broadly applied in total synthesis and industrial platforms compared to their alkenyl counterparts. The main reason for this may be the comprehensive distribution of aryl groups in organic molecules. Another possible explanation can be limited accessibility of alkenyl electrophiles.

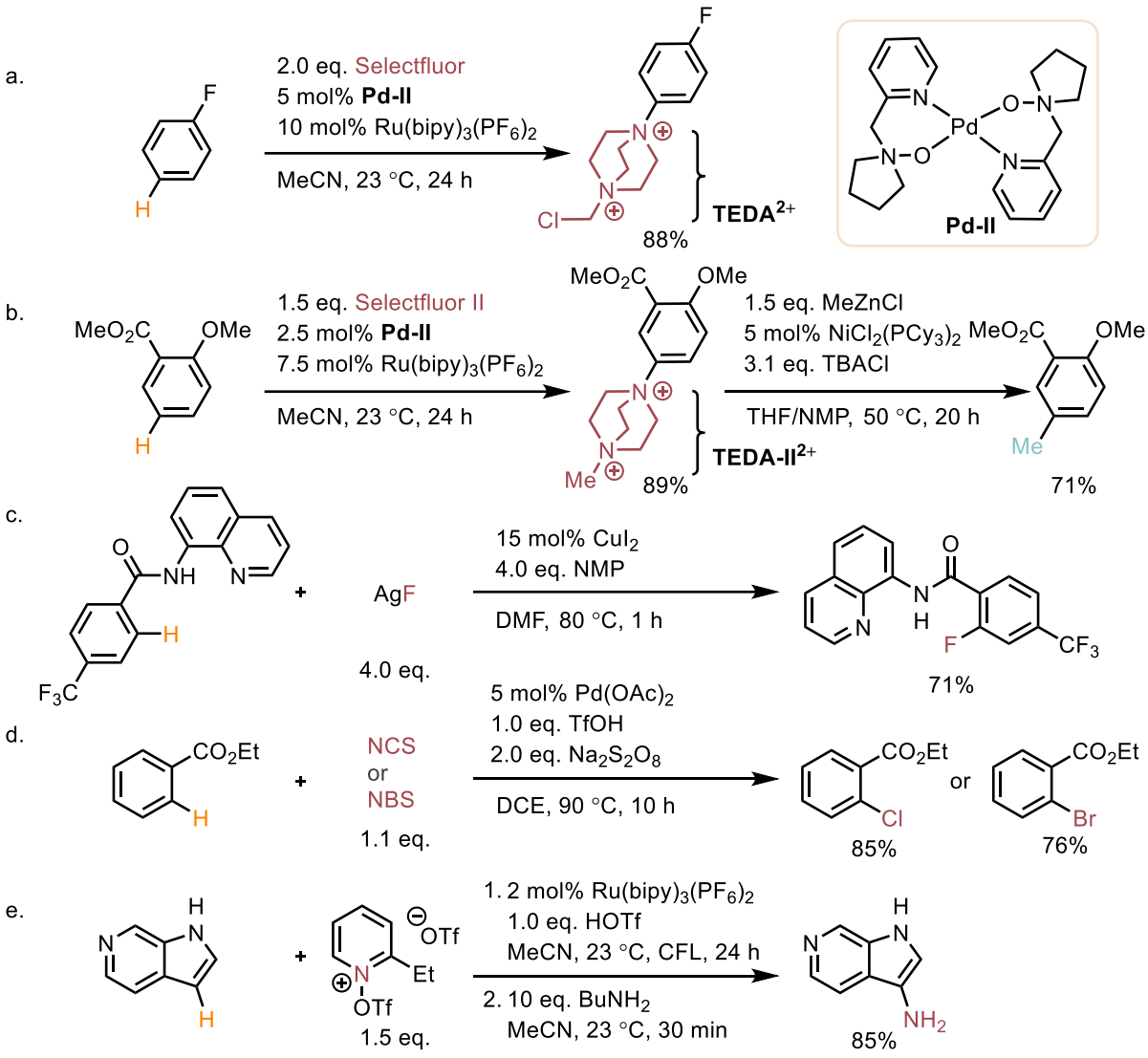

Figure I.23. Examples for modern C–H functionalization of arenes, positional-selective reactions especially.

Most aryl electrophiles, like aryl halides, can be generated from direct C–H halogenation of arenes, in a selective or unselective fashion, such as bromination of arenes, which often delivers regioisomers.[87] P*ara*-Selective Ar-TEDA synthesis (Figure I.23) enables *para*-selective amination of arenes when the Ar-TEDA is treated with a reductant.[89] Although Ar-TEDAs are not widely utilized in other transformations so far, the site-selectivity for C–H functionalization is impressive. Moreover, its second generation, Ar-TEDA-II, synthesized from Selectfluor II in replacement of Selectfluor, is a good aryl electrophile and can be methylated efficiently under nickel catalysis.[149] The most recently published site-selective thianthrenation reaction enables regioselective construction of aryl sulfonium salts,

which can functionalize as good aryl electrophile precursors, which we will discuss in detail in Section I.4. [150] Other directing group facilitated C–H functionalization often requires installation of certain directing groups prior to and removal after C–H functionalization, which would be very powerful when the directing groups are readily available in substrates.[151,152,153] Divergent C–H amination, specifically for complex molecules,[97] delivers (hetero)arylamines which can be used as aryl electrophiles as well when converted to ammonium[154] or diazonium salts.[155]

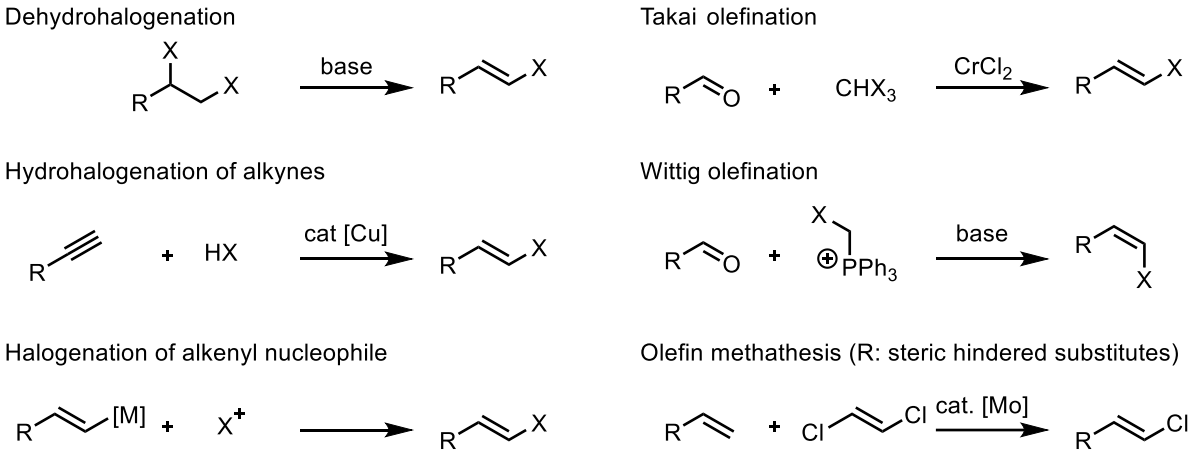

Figure I.24. Synthetic methods for alkenyl halides synthesis.

Nevertheless, alkenyl electrophiles, most commonly alkenyl halides are hard to access in a similar direct C–H functionalization manner (Figure I.24). The production of vinyl chlorides on a scale of millions of tons per year for the synthesis of polyvinyl chloride is achieved by dehydrochlorination of 1,2-dichloroethane.[156] However, for alkenyl halides, where the corresponding vicinal dihalogenated precursors are not readily available, multistep sequences are frequently required, such as dibromination of alkenes followed by the elimination of HBr under harsh conditions.[157] In particular, those sequences often lead to allylic C–H elimination side products and regioisomers. Another method is the prior synthesis of alkenyl nucleophiles, such as alkenyl boronates,[158] alkenyl silanes,[159] or other metal species, followed by treatment with electrophilic halogen sources. Most alkenyl halides like alkenyl bromides can be synthesized from aldehydes or ketones using Takai,[160] Wittig[161] or other[162] olefination reactions, but aldehyde and ketones are often more expensive compared to the corresponding carbon hydrogen counterparts, because they need to be synthesized by hydroformylation

of the corresponding alkenes[163] or by oxidation of the corresponding alcohols.[164] Methods starting from alkynes can also afford alkenyl halides in one step, though they are less widely used considering the smaller availability of alkynes when compared to alkenes.[165,166] In addition, all of those methods listed above often deliver *E*/*Z* mixtures of alkenyl halides.

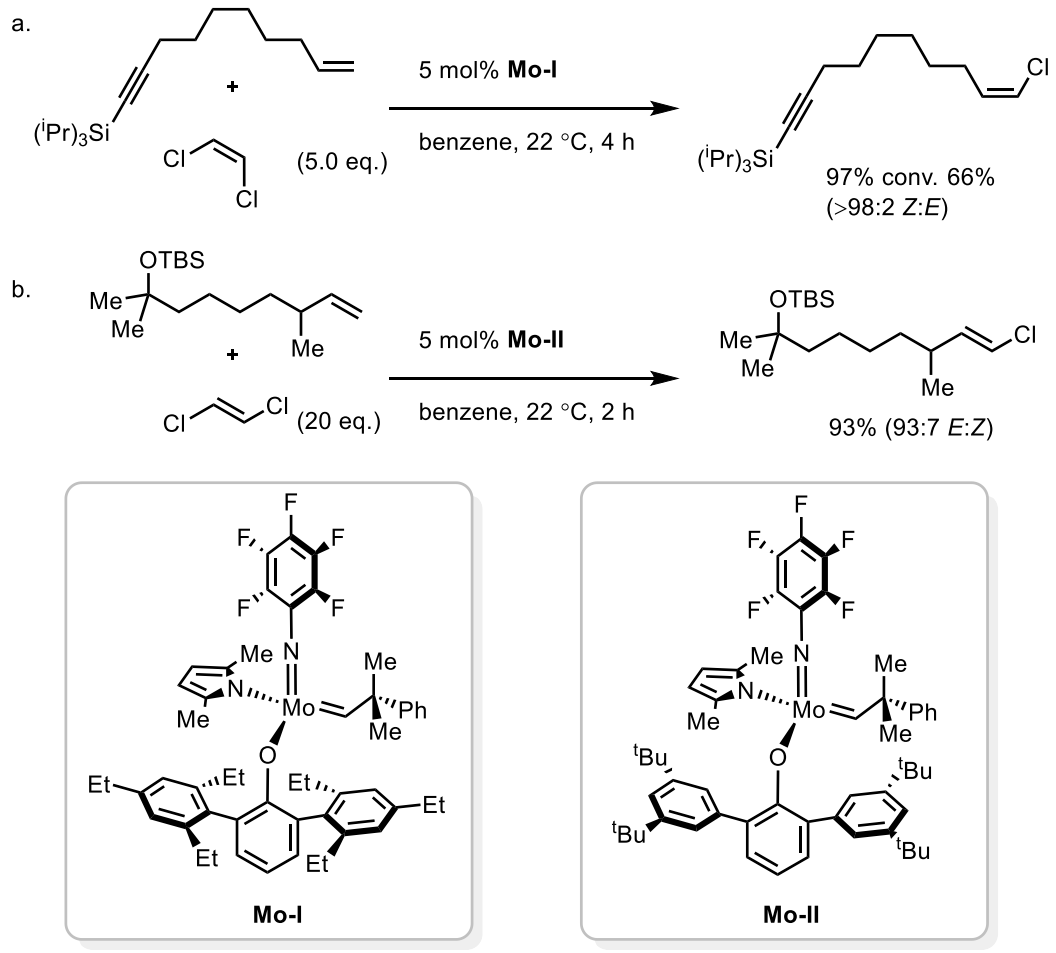

Figure I.25. Molybdenum catalyzed *E*/*Z* selective olefin metathesis examples and catalysts structures.

Modern olefin metathesis catalysts have made great advances in the past two decades, mostly catalyzed by ruthenium carbene complexes developed in the Grubbs group [167,168] and molybdenum and tungsten imido alkylidene catalysts developed in the Schrock and Hoveyda groups.[169,170,171] For applications in the syntheses of alkenyl halides, those catalytic systems enable access to the thermodynamically favorable *Z* alkenes in general: alkenyl chlorides from *Z*-1,2-dichloroethene and *Z* alkenyl fluorides from alkenyl *Z*-bromo-fluoroethene.[172] With sophisticated ligand design and systematic ligand screening, the Hoveyda group

succeeded in synthesizing the thermodynamically less favored *E* alkenyl chlorides from *E*-1,2-dichloroethene, and *E* alkenyl fluorides from *E*-1,2-difluoroethene when bulky substituents are present in the starting materials (Figure I.25).[173]

Besides alkenyl halides,[174,175] sources like alkenyl acetates,[176] alkenyl phosphates,[177,178] alkenyl ethers,[179,180,181] alkenyl thioethers,[182,183] and alkenyl sulfates[184] can also be used as alkenyl electrophiles for Kumada and Suzuki cross-coupling reactions, despite their higher activation energy (Figure I.26 and Table I.2). One outstanding example is Itami's iron catalyzed arylation of alkenyl sulfides with Grignard reagents (Figure I.26e). In contrast to usual palladium and nickel catalyzed reactions where both alkenyl and aryl C–S bonds exist, this iron-catalyzed cross coupling proceeds efficiently at the alkenyl C–S bond. The mechanism for such an intriguing selectivity is unknown so far though.

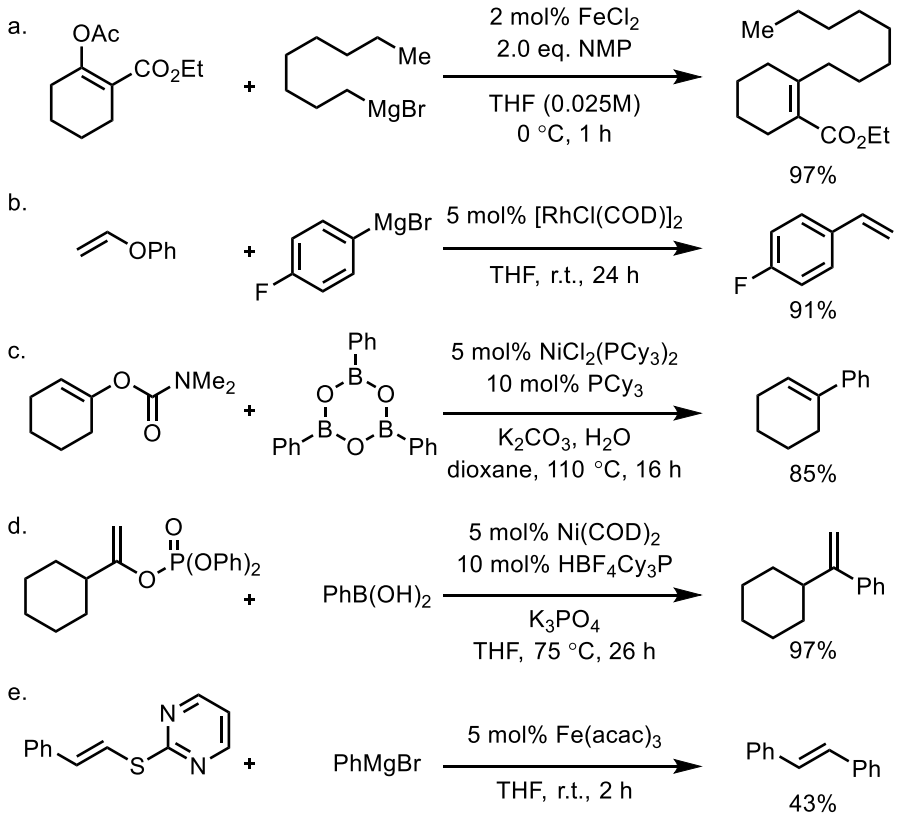

Figure I.26. Other alkenyl electrophiles and their transformations.

Even though diverse classes of alkenyl electrophiles can be used for cross-coupling reactions, the syntheses of those precursors are not trivial. For instance: generation of alkenyl esters from ketones will deliver regioisomers and require several steps with the intermediacy of moisture sensitive enolates,[185] while alkenyl

thioethers syntheses are not so obvious (Figure I.27).[186,187] Either more general methods for the synthesis of known alkenyl electrophiles have to be developed, or new generation of alkenyl electrophiles need to be disclosed.

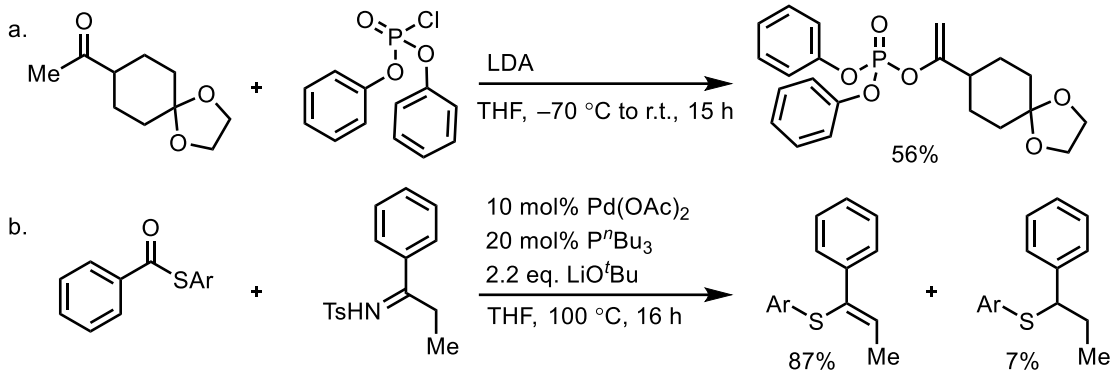

Figure I.27. Examples for the synthesis of alkenyl esters and thioethers.

I.1.4. Site-selective C–H thianthrenation of arenes

In 2019, the Ritter group reported a site-selective thianthrenation of arenes by *in situ* activation of thianthrene-*S*-oxide (**TT**=**O**) or tetrafluorothianthrene-*S*-oxide (**TFT**=**O**) with trifluoroacetic anhydride.[150] The substrate scope of the reaction ranges from electron-rich veratrole to electron-deficient 1,2-dichlorobenzene (Figure I.28). Functional groups such as amines, amides, alcohols, esters, carboxylic acids and heterocycles are all tolerated. The reaction is easy to operate under ambient atmosphere and achieves full conversion within several hours. The thianthrenation reaction is highly regioselective, which even allows for differentiation of different aromatic rings, such as in 2-fluorobiphenyl and famoxadone (Figure I.28 highlighted). The mechanism for such high selectivity is still under investigation, but electronic effects are proposed to override steric biases.

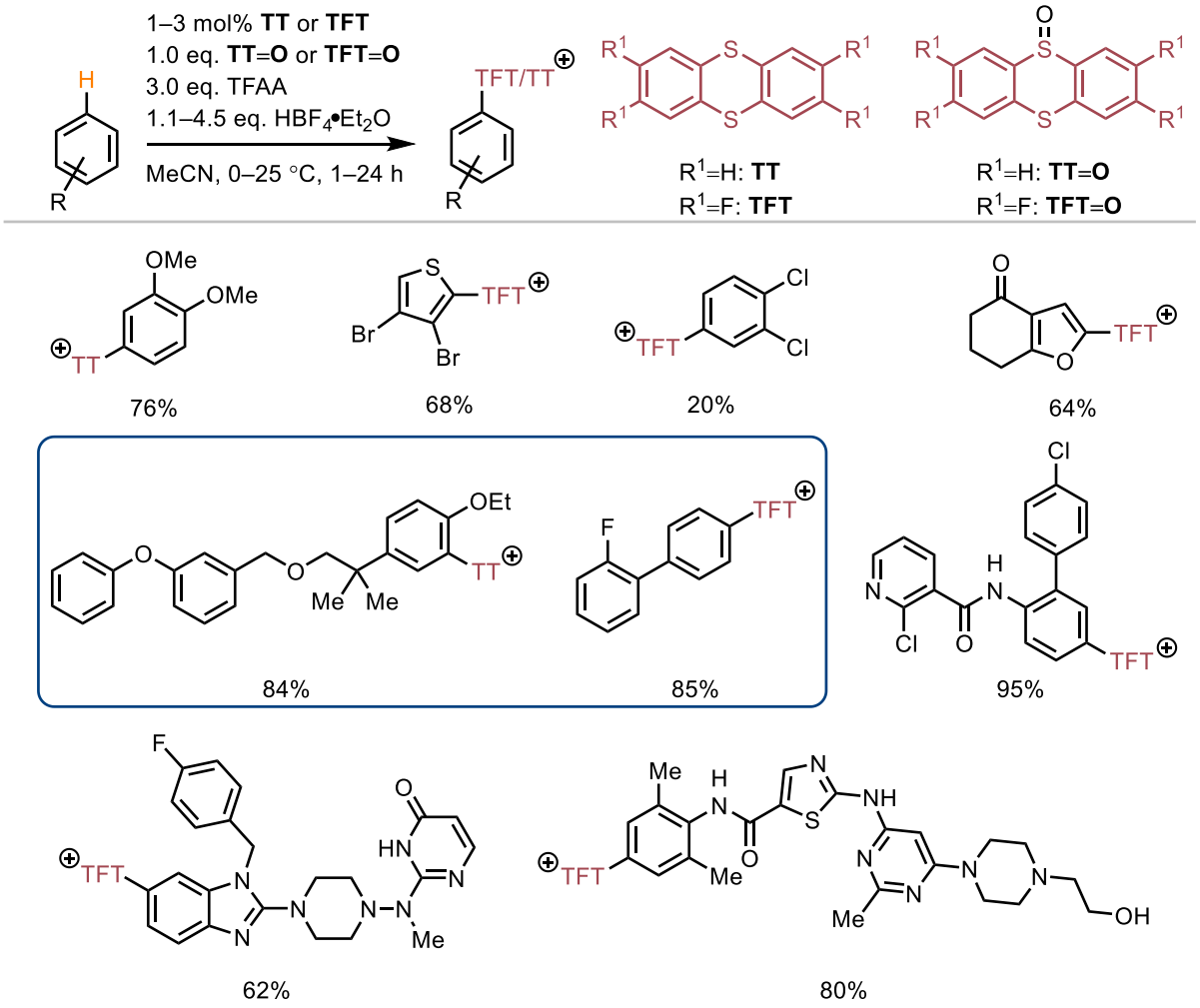

Figure I.28. Example substrates for thianthrenation of arenes.

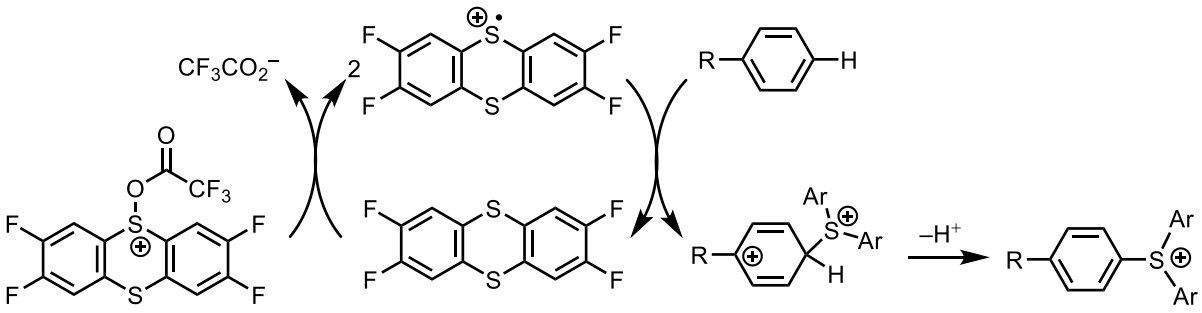

Figure I.29. Possible pathway for site-selective C–H thianthrenation of arenes.

According to preliminary mechanistic studies, thianthrene based radical cations are proposed to be generated through comproportionation between trifluoroacetic anhydride activated **TT**=**O** and thianthrene (**TT**) or **TFT**=**O** and tetrafluorothianthrene (**TFT**) under the reaction conditions. Subsequently, the *in situ* obtained reactive radical cations add to the arene substrates in an electrophilic pathway to form dienyl dications, which are deprotonated to reconstitute the aromatic ring and result in aryl thianthrenium salts (Figure I.29).

The aryl thianthrenium salts are good aryl electrophiles and can be utilized in versatile transition metal catalyzed cross coupling or photoredox catalyzed reactions, such as palladium catalyzed Suzuki coupling and Heck reactions and copper/photoredox catalyzed phosphorylation and (pseudo)halogenation reactions.[150] Further explorations show that aryl thianthrenium salts display unique properties under photoredox conditions, which allows for even challenging C–F,[188] C–N,[189] C–O,[190] C–S[190] and C–CF_3 [191] bonds formation when combine photoredox catalysts and copper(I) salts (Figure I.30).

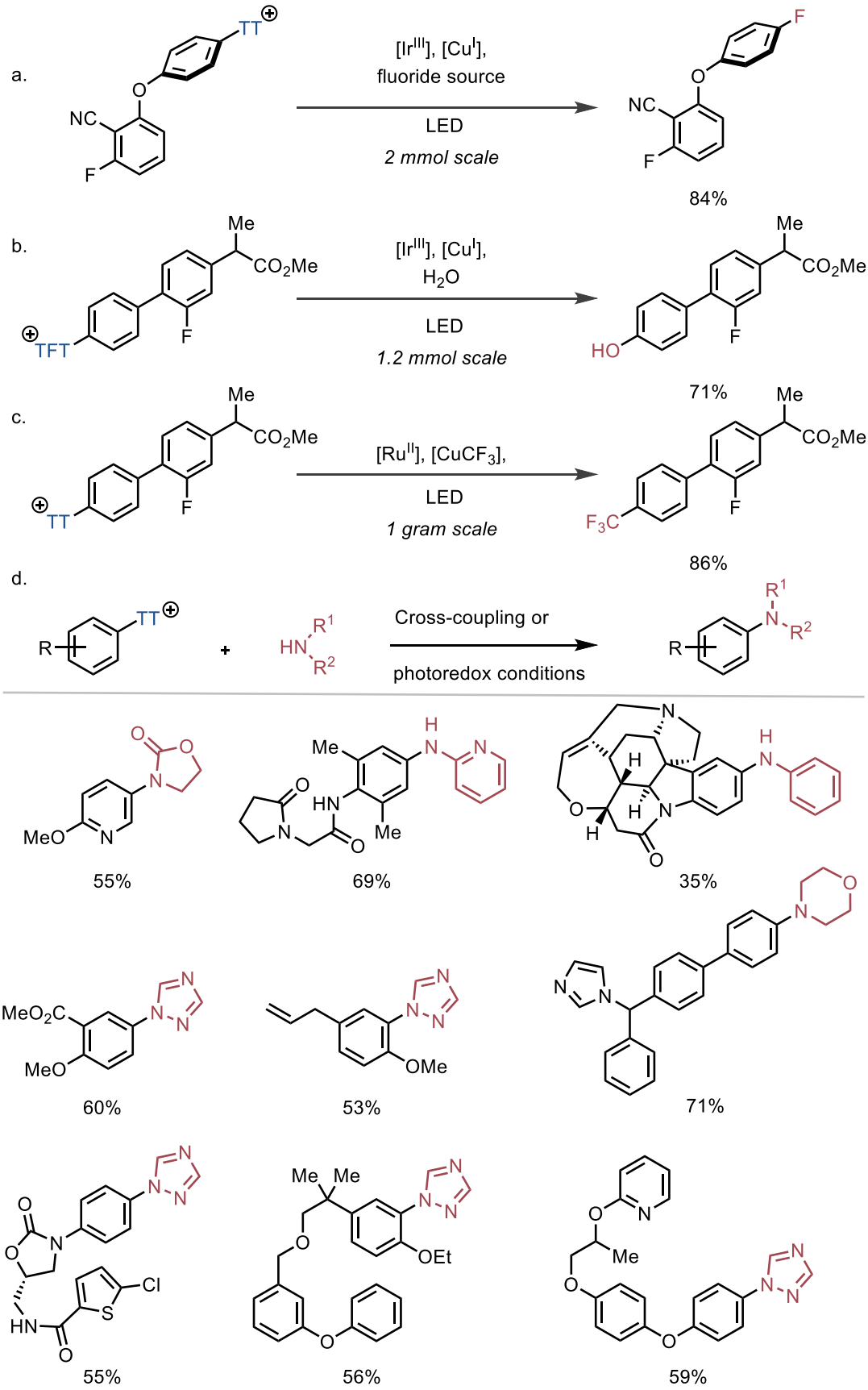

Figure I.30. Scale up examples for C–F, C–O, C–CF_3, and C–N bonds formation from aryl thianthrenium salts.

I.2. Challenges for direct C–H functionalization of alkenes

In general, alkenyl C–H bonds are less reactive compared to the labile alkenyl C=C bond, which challenges direct activation of alkenyl C–H bonds by transition metals. One general strategy applied is taking advantage of the π bond shuttle: breakage and reconstruction of the π bond. As mentioned in the previous Part I.1.2.3, for alkenes, it is difficult to recover the double bond geometry after functionalization to form functionalized alkanes, whilst arenes can be easily restored, possibly benefiting from aromaticity. Besides that, as with every C–H bond functionalization reaction, selective activation of one single C–H is an issue for alkenyl C–H functionalization. Apart from the other existing alkyl and aryl C–H bonds, as shown in Figure I.31, more than one product can be obtained even when only one alkenyl C–H is present in the substrates. Regio- and stereoisomers normally express similar properties when using purification techniques such as flash column chromatography, thus extra purification efforts are required to gain one desired isomer product in high purity. Therefore, regio- and stereoselective C–H functionalization of alkenes remains challenging and promising.

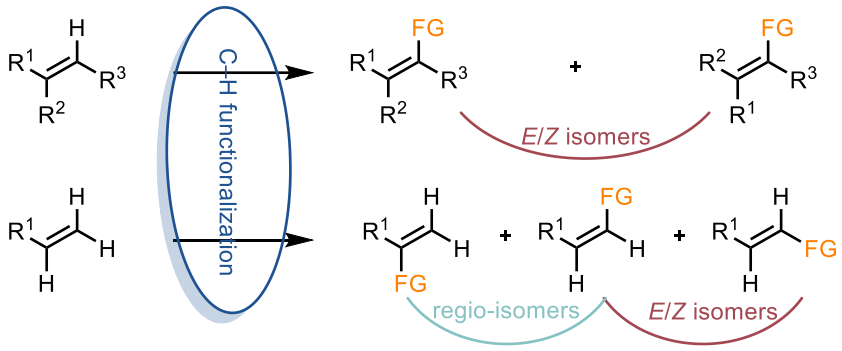

Figure I.31. Possible products from C–H functionalization of alkenes.

I.3. Project design

Alkenes and arenes share similar chemical reactivity in some cases because their highest occupied molecular orbitals (HOMO) are filled π orbitals. For example, both can act as dative ligands when coordinated to metal species via their HOMO → metal LUMO interaction (Figure I.32a). However, when being treated with electrophiles such as dibromide, alkenes undergo dibromination while arenes prefer electrophilic C–H bromination (Figure I.32b).

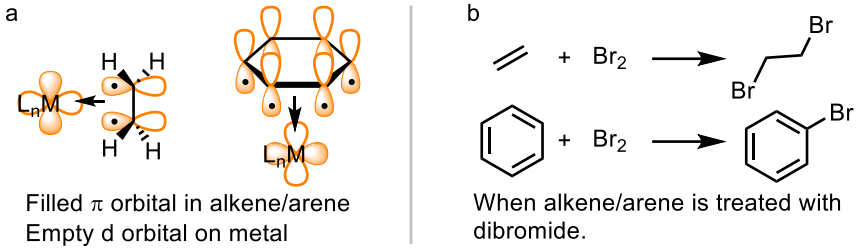

Figure I.32. Examples for similar and distinct reactivity comparison between alkenes and arenes.

Even so, considering the unique reactivity and selectivity we have observed in the C–H thianthrenation of arenes and the broad utility of the resulting aryl thianthrneium salts (*vide ante* Part I.1.4), it is worthwhile to further examine the reactivity and expand the application of the proposed thianthrenium radical cation.

I.4. Results and discussion

Parts of this chapter are taken, with permission, from our published work in Angewandte Chemie International Edition.[192] The alkene thianthrenation reaction has been developed by the author. Experimental data has been collected by the author with help from Dr. Jiakun Li. CV and UV/Vis data were collected by Dr. Matthew B. Plutschack. The author has conducted the mechanistic experiments with input from Dr. Matthew B. Plutschack.

I.4.1. C–H thianthrenation of alkenes

I.4.1.1 General reaction conditions

The overall procedure is straightforward to execute, and no precaution against moisture or oxygen is needed. Under ambient atmosphere, thianthrene-*S*-oxide, alkenes and solvent are added into a reaction vial. Chill the reaction mixture in an ice-water cooling bath before dropwise addition of trifluoroacetic anhydride and triflic acid to yield a lilac mixture. The reaction progress can normally be visualized with fading in color; if not, the reaction was generally stopped after two hours. After concentration, treatment with base and anion exchange, the desired alkenyl thianthrenium tetrafluoroborate salts can be isolated as analytical pure samples using flash column chromatography over silica gel.

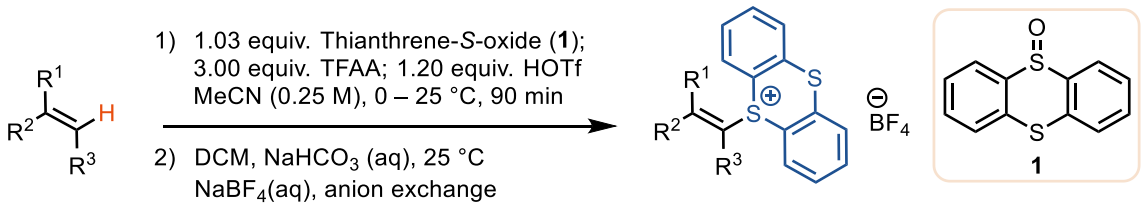

Figure I.33. Regio- and stereoselective thianthrenation of unactivated alkenes.

I.4.1.2 Reaction development

During the course of evaluation for reaction parameters, different *S*-oxides were examined (Table I.3), including tetrahydrothiophene-1-oxide (**1-6**), which showed reactivity for the synthesis of styrenyl sulfonium salts from styrenes. When 1-octene was used as the model substrate, thiophene based *S*-oxides (**1-2** or **1-6**) only afforded trace amount of the desired products under the screened conditions. Minor modification on the thianthrene-*S*-oxide core by changing one sulfur atom to oxygen (phenoxathiine, **1-3**) or nitrogen (phenothiazin, **1-4**) was also detrimental to

this reaction. Only thianthrene based *S*-oxides **TT**=**O** (**1**) and **TFT**=**O** (**1-5**) afforded the corresponding 1-octenyl thianthrenium salts in 92% and 70% yields, respectively, with similar *E*/*Z* ratio. **TT**=**O** was chosen for further substrate scope investigation not only because of its better reactivity, but also due to its easier synthetic accessibility as compared to **TFT**=**O**. So far, thianthrene-*S*-oxide was the optimal reagent for direct and selective C–H functionalization of unactivated alkenes (at least for simple aliphatic alkanes).

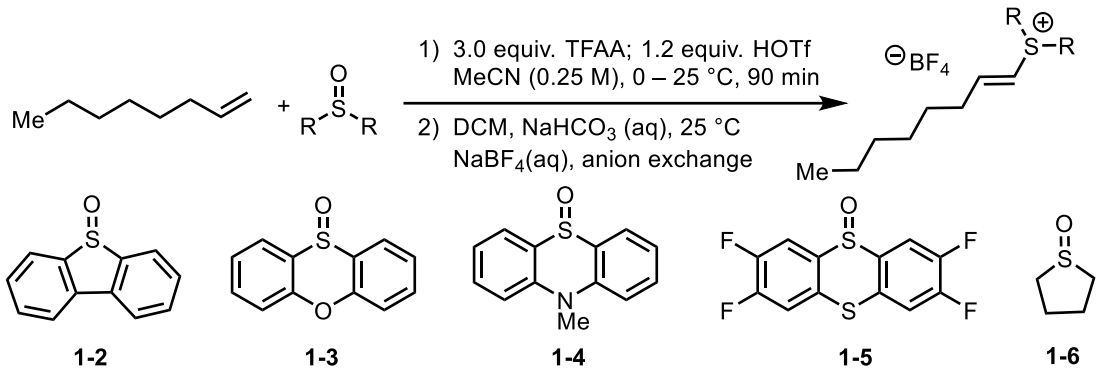

Entry	*S*-oxides	yield
1	**1**	92%[a]
2	**1-2**	<10%[b]
3	**1-3**	<10%[b]
4	**1-4**	0[b]
5	**1-5**	70%[a]
6	**1-6**	trace[b]

Table I.3. *S*-oxide screening table (a: isolated yields; b: based on LC-MS analysis).

Under the optimal reaction conditions, simple terminal mono-substituted, internal symmetrical di-substituted and electronically biased di-substituted olefins were thianthrenated well (Figure I.34). Slight modification on the loading of activating reagents or replacement of triflic acid with weaker acids such as HBF_4•Et_2O was sometimes beneficial for stereoselectivity. For example, the *E*/*Z* ratio increased from 10/1 to 17/1 for alkene **9** upon doubling the triflic acid loading, while maintaining the yield of 71%. For alkene **11**, a single isomer was obtained when HBF_4•Et_2O was used instead of triflic acid, which gave 20/1 *E*/*Z* isomer mixture.

I.4.1.3 Substrate scope

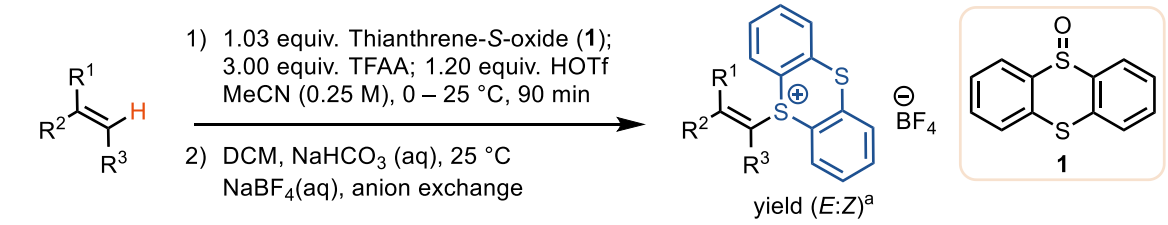

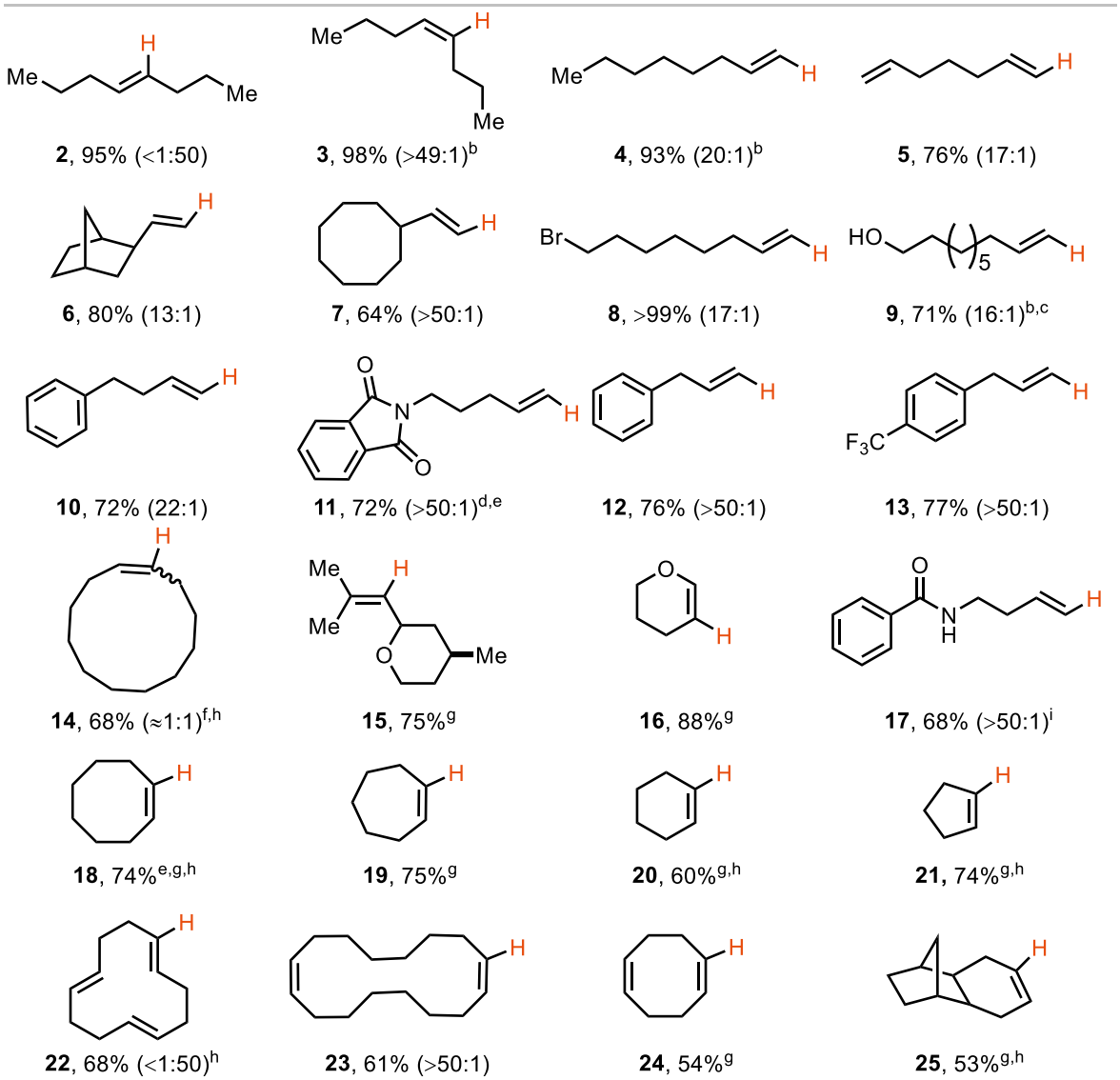

Figure I.34. Substrate table for simple alkenes. (a) 0.500 mmol scale, 1.03 equiv. thianthrene-*S*-oxide (1), 3.00 equiv. trifluoroacetic anhydride (TFAA), 1.20 equiv. trifluoromethanesulfonic acid (HOTf). Isolated yields. *E*/*Z* ratios were determined by ^{1}H-NMR. (b) 2.40 equiv. of HOTf was used to obtain higher *E*/*Z* ratio. (c) The alcohol was partially acylated during the reaction. (d) 1.20 equiv. HBF_4•Et_2O instead of HOTf was used to obtain higher *E*/*Z* ratio. (e) Reaction was performed on 3.00 mmol scale. (f) Cyclododecene starting material used as a mixture of

isomers (*E*/*Z* ≈ 1/2). (g) *E*/*Z* ratio is not applicable. (h) 1.20 equiv. HBF_4•Et_2O instead of HOTf was used to obtain higher yields.

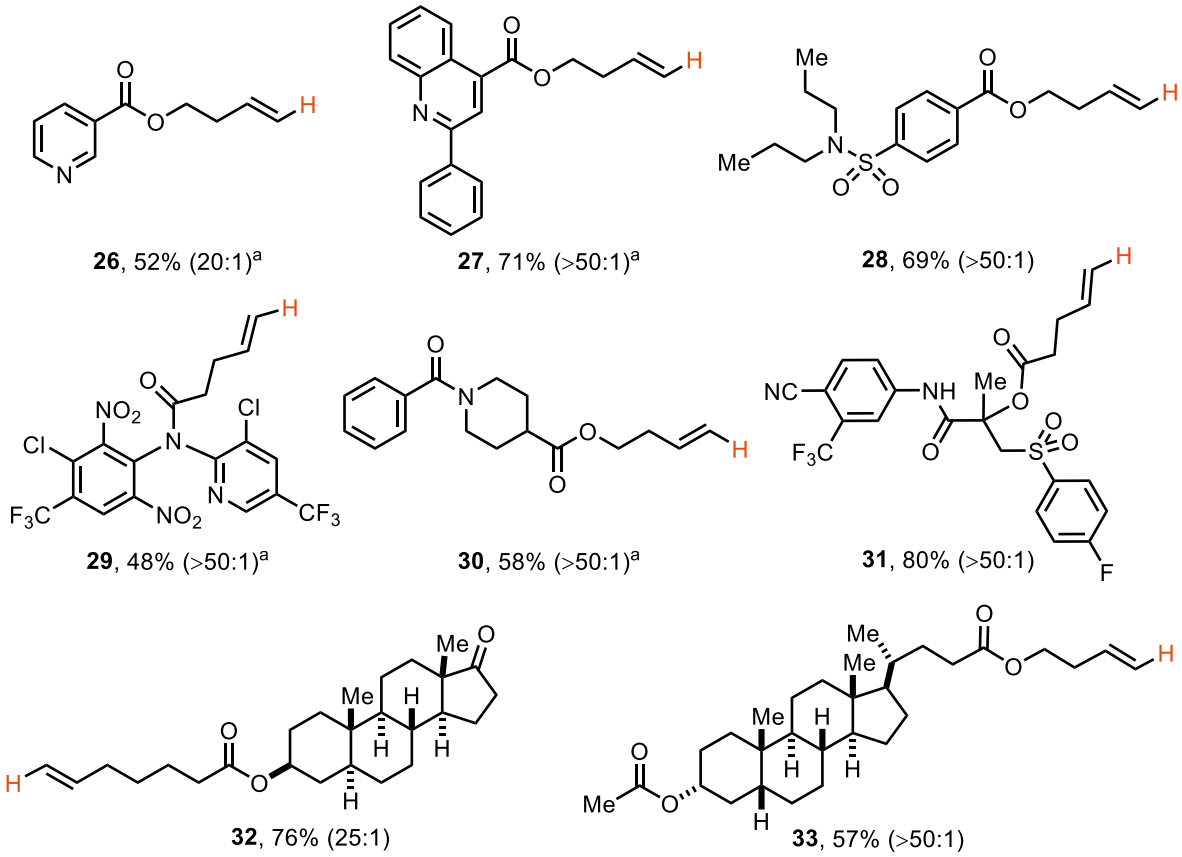

Figure I.35. Substrate table continued with more functionalized/complex molecules. (a) 2.40 equiv. of HOTf was used to obtain higher yields.

For cyclic alkenes such as **14**, **18**, **20**, **21**, **22** and **25**, HBF_4•Et_2O was used to obtain better yields. Regardless of the ring size, good yields were obtained for cyclic alkenes from the 5-membered cyclopentene (**21**) to the 12-membered cyclododecene (**14**). The geometry of the double bonds remains unchanged during the functionalization process, as can be seen from *trans*-(**2**) and *cis*-4-octene (**3**). For the case of cyclododecene **14**, where the starting material consists a mixture of isomers (*E*/*Z* ≈ 1/2), a 1/1 product isomer mixture was obtained, suggesting the reaction rate might be zero order regarding cyclododecene substrates concentration under the discussed reaction conditions. However, the regioselectivity diminishes for other 1,2-di-substituted olefins: thianthrenation of (*E*)-but-2-en-1-yl methyl terephthalate (0.500mmol, stirred at 0 °C for 45 min) gave 44% isolated yield (all 4 stereoisomers were observed based on LC-MS analysis,

the ratio was not determined). For substrates containing more than one alkene functionality (**5**, **22**, **23** and **24**), only mono functionalization was observed, which might be explained by the introduction of a cationic substituent which hinders a subsequent reaction to form the reactive dication sulfur species (thianthrenium dication, *vide infra*) due to electrostatic repulsions.

To further establish the utility of the current C–H functionalization methodology, several more structurally complex and functionalized molecules were tested (Figure I.35). For example, Nicotinic acid (**27**), Cinchophene (**28**), Probenecid (**28**), Fluazinam (**29**), Piperidine (**30**), Bicalutamide (**31**), Epiandorosterone (**32**), and Lithocholic acid (**33**)-derived terminal alkenes were all thianthrenated in mediocre to good yields (between 48% and 80%) with high regio- and stereoselectivity. In the presence of functional groups such as pyridine and quinoline, twice the amount of triflic acid was introduced to obtain higher yields.

Overall, for all *α*-olefins, the *E*-alkenyl thianthrenium salts were isolated as major products, often without detectable *Z* isomer, when analyzed by NMR spectroscopy. Functionalization of internal alkenes proceeded with retention of the double bond geometry for both *E* (**2** and **22**) and *Z* (**3** and **23**) olefins. Steric hindrance in the allylic position does not interfere with productive functionalization (**6** and **7**). Acidic protons such as NH in amides (**17** and **31**) and OH in alcohols (**9**) are well tolerated, though in the alcohol case (**9**), the OH group was partially acylated under the acidic reaction conditions. Vulnerable bis-benzylic and allylic C(sp^3)–H bonds (**12** and **13**) are compatible without double bond isomerization or allylic functionalization. In short, functional groups such as primary alcohols (**9**), imides (**11**), ethers (**15**), amides (**17**), pyridines (**26**), quinolines (**27**), sulfonamides (**28**), nitros (**29**), piperidines (**30**), sulfones (**31**), nitriles (**31**), ketones (**32**), and esters (**32** and **33**) are compatible. Selective monofunctionalization is observed for dienes (**5**, **23**, **24**) and a triene (**22**). The electron neutral and poor arenes remain intact, while electron rich ones undergo aromatic thianthrenation,[189] which leads to a reactivity guideline for further applications as arene (δ^-) > *α*-olefin > arene (δ^0) ≫ arene (δ^+).

I.4.1.4 Limitations

Apart from those successful substrates, additional alkenes were evaluated during the substrate scope examination process. Most of the failed examples (Figure I.36) fall into three different categories according to their outcomes:

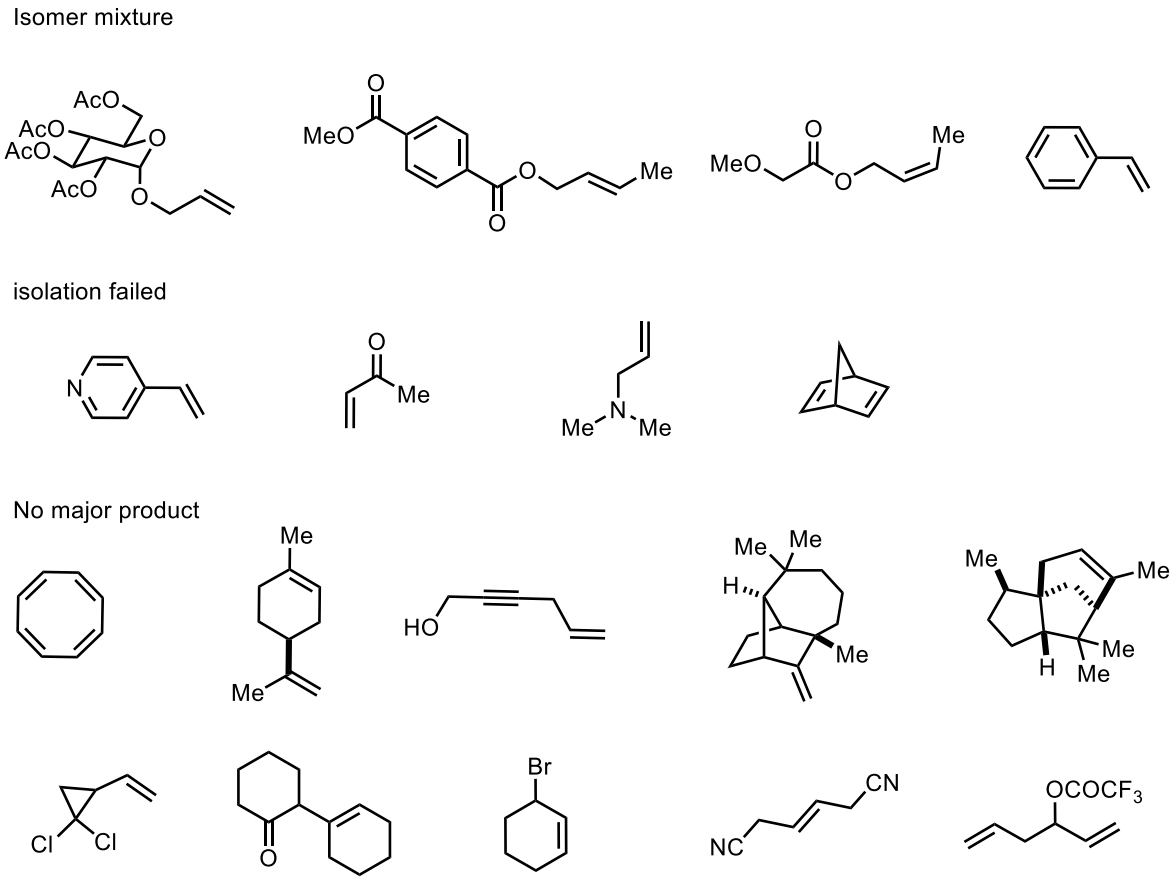

Figure I.36. Failed substrates that did not work or work well.

1) Product isomers were obtained. Either there was acid sensitive functional groups such as acylated saccharide derivative yielded α/β isomers due to anomeric effect and ring closure/opening isomerization (the starting material was a single α isomer), unsymmetrical internal double bond resulted in *E*/*Z* isomer products, or styrene like compounds gave thianthrenation on both the aryl and the alkenyl parts.

2) The desired product mass can be detected by LC-MS from the reaction mixture, but not identifiable on NMR after purification. Decomposition possibly occurred during column chromatography, which means the desired alkenyl thianthrneium salts are not stable enough to be isolated by flash column

chromatography over silica gel. Those compounds either contain basic functional groups such as amines, α,β-unsaturated moieties like acrylates or sterically hindered substituents like in the norbornadiene case. Preliminary trials with other purification methods such as HPLC on C18 packed columns were unsuccessful.

3) LC-MS or TLC analysis cannot identify any major product from the crude reaction mixture. Neither 2,2-disubstituted alkenes nor compounds containing very acidic allylic protons worked in general. All of the thianthrene-*S*-oxide was consumed, suggesting functionalization occurred but possibly resulted in unexpected side reactions such as allylic functionalization.

I.4.2. Studies on alkenyl thianthrenium salts as alkenyl electrophiles

As stated in Part I.1.4, the aryl thianthrenium salts are good aryl electrophiles for transition-metal-catalyzed cross-couplings and photoredox catalysis. If alkenyl thianthrenium salts can also function as alkenyl electrophiles, which are not easily accessible directly from the non-prefunctionalized olefin (*vide ante* Part I.1.3).

I.4.2.1 Transition-metal catalysis

Indeed, like their aromatic counterparts, the alkenyl thianthrenium salts serve as excellent electrophiles in the follow up transformations (Figure I.37). Palladium-catalyzed cross coupling reactions generally proceed with retention of the double bond geometry (**34**, **35**, **36**), and all sp^3, sp^2 and sp hybridized carbon coupling partners were alkenylated well. The alkenyl thianthrenium salts can also serve as suitable alkenyl electrophiles for ruthenium-based catalysis, which enables the synthesis of alkenyl halides (**37**, **38**) and pseudohalides (**39**), stereoselectively. For example, chlorination in the presence of $[Cp^*Ru(MeCN)_3]PF_6$ as catalyst was performed successfully on a gram-scale, and alkenyl trifluoromethyl thioether, which is difficult to access otherwise, is readily obtained.[193] Although Ru(II) catalysts are often proposed to have slow oxidative addition to alkenyl halides,[194] $[Cp^*Ru(MeCN)_3]PF_6$ showed robust catalytic reactivity in the reactions using alkenyl thianthrenium salts as electrophiles.

Sonogashira couplings (Figure I.38) with tri-substituted alkenyl thianthrenium salts (**2-TT** and **3-TT**) with phenylacetylene under palladium catalysis resulted in *E*/*Z* isomer mixtures. The E/Z ratios were as stereoselective as coupling reactions

with alkenyl bromides, suggesting the limitation of the coupling method and not the alkenyl electrophile.[195]

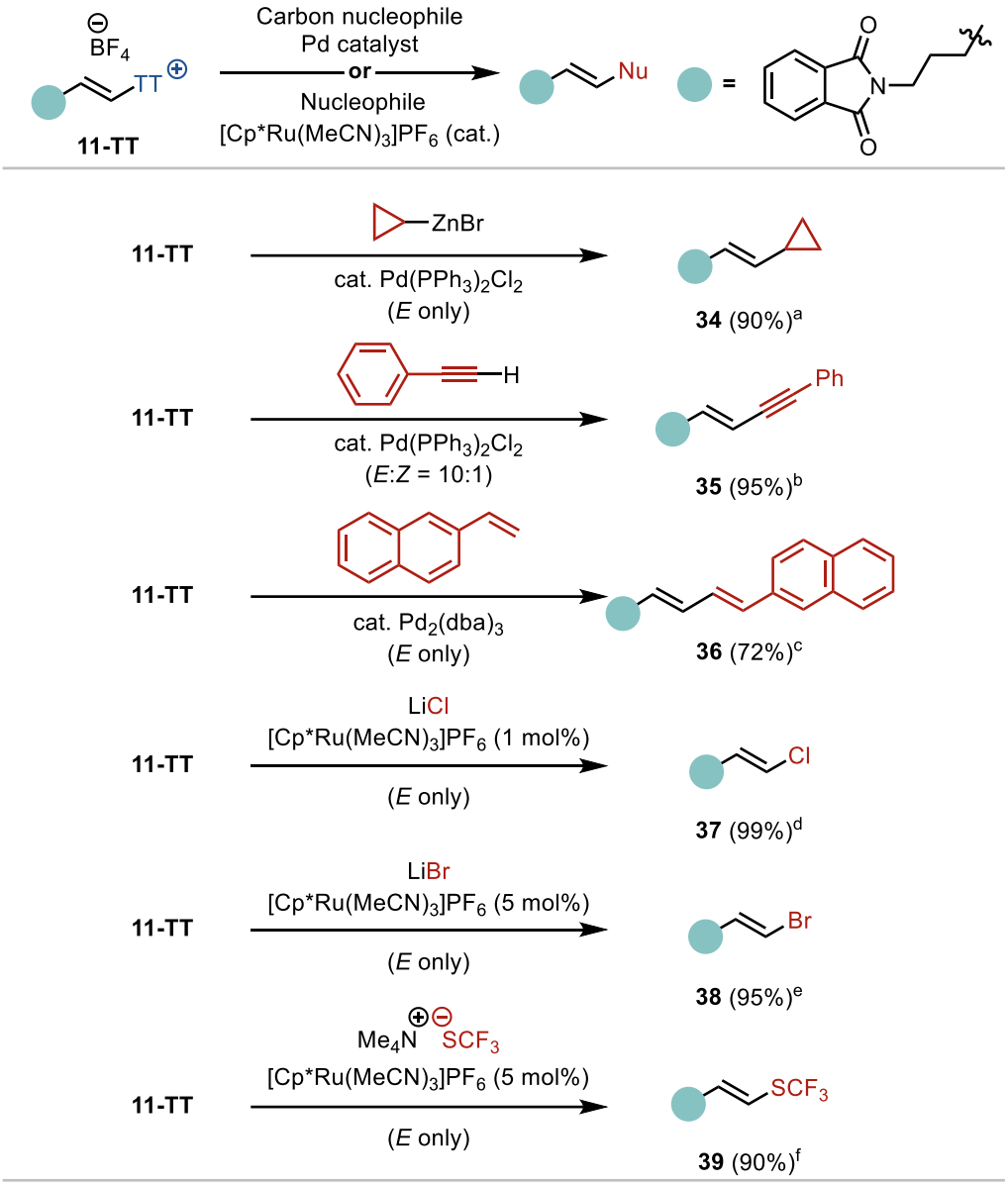

Figure I.37. Synthetic applications of alkenyl thianthrenium salts. (a) CyclopropylZnBr (3.0 equiv.), $Pd(PPh_3)_2Cl_2$ (20 mol%) in THF (0.1 M). (b) Phenylacetylene (2.0 equiv.), N-methylmorpholine (2.0 equiv.), CuI (25 mol%), $Pd(PPh_3)_2Cl_2$ (10 mol%) in THF (0.1 M). (c) 2-Vinylnaphthalene (2.0 equiv.), K_2CO_3 (2.5 equiv.), $Pd_2(dba)_3$ (10 mol%) in DMF (0.1 M). (d) LiCl (1.5 equiv.), $[Cp^*Ru(MeCN)_3]PF_6$ (1 mol%) in THF (0.1 M). (e) LiBr (1.5 equiv.), $[Cp^*Ru(MeCN)_3]PF_6$ (5 mol%) in THF (0.1 M). (f) $[Me_4N^+][^-SCF_3]$ (1.2 equiv.), $[Cp^*Ru(MeCN)_3]PF_6$ (5 mol%) in THF (0.1 M).

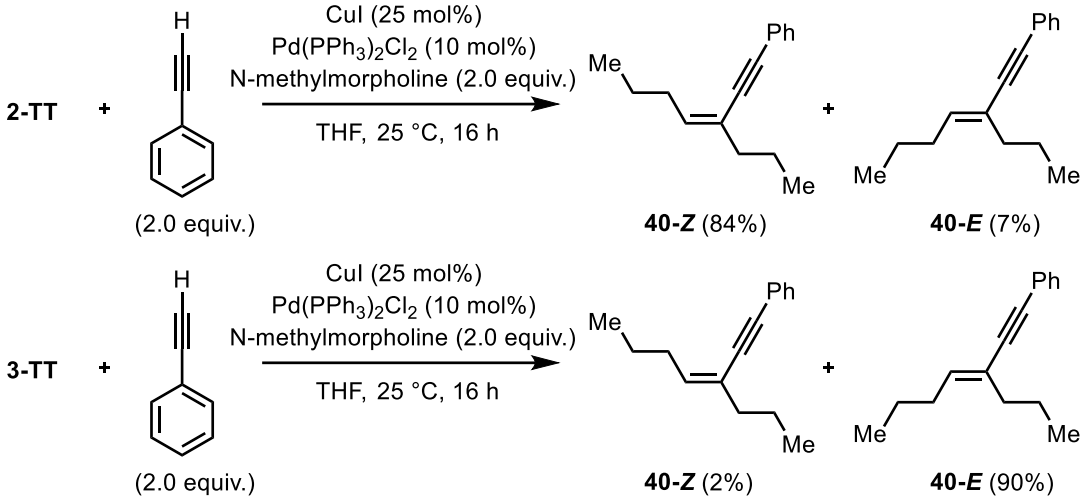

Figure I.38. Sonogashira coupling between tri-substituted alkenyl thianthrenium salts (**2-TT** and **3-TT**) and phenylacetylene.

I.4.2.2 Direct nucleophilic displacement

When alkenyl thianthrenium salt **11-TT** reacted with nucleophiles like cyanide and carboxylate, interesting results were obtained (Figure I.39). For cyanide, cine substitution took place, in which case, the alkenyl thianthrenium salt can possibly viewed as a Michael acceptor—1,4-conjugated addition yields a thianthrenium based ylide which undergoes deprotonation to give the final product **11-CN**. The examination of similar Michael acceptor reactivity on the corresponding alkenyl bromide failed, possibly due to lack of a positively charged electron acceptor like the thianthrenium cation. Unlike the aforementioned ruthenium-catalyzed (pseudo)halogenation reactions, carboxylation of **11-TT** afforded the carboxylated product **11-OCOPh** as a mixture of *E*/*Z* isomers regardless of the presence or the absence of the ruthenium catalyst. In addition, the double bond was shifted one carbon towards the original allylic position. Mykhailo Kondratiuk, a master student in our group, also found aziridine formation when **11-TT** reacted with benzylamine. He is now systematically studying the reactivity of alkenyl thianthrenium salts with different nucleophiles.

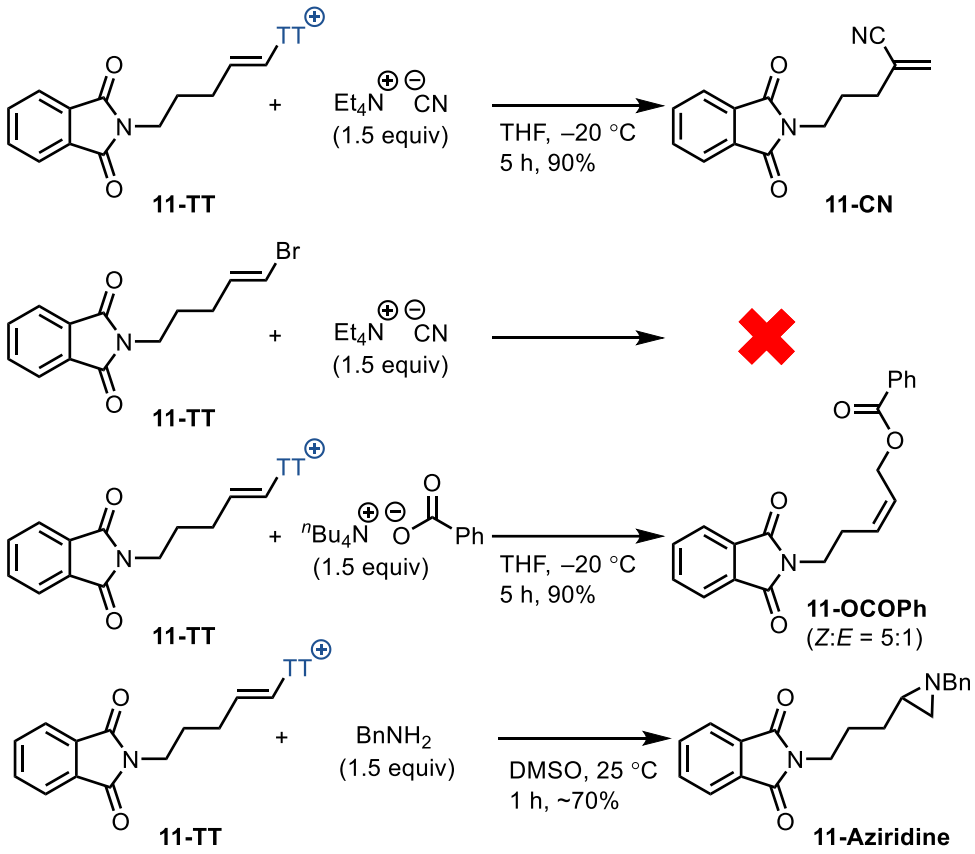

Figure I.39. Direct nucleophilic displacement of alkenyl thianthrenium salts, and their reactivity comparisons with alkenyl bromides.

With the current data in hand, Mykhailo Kondratiuk categorized the reactivity of alkenyl thianthrenium salts with various nucleophiles into three types according to the nucleophilicity of the incoming nucleophiles (Figure I.40). Type I represents strong nucleophiles such as cyanide, where nucleophilic attack happens on the alkenyl carbon adjacent to TT by forming a neutral sulfur ylide intermediate, followed by protonation, and TT elimination to give β-carbon substituted products. Type II requires doubly nucleophilic atoms such as primary amines to afford cyclic compounds with a propylene bridge. Type III shows a completely new reactivity that affords allylic substitution with double bond shift. Detailed explanation and mechanistic investigation are still underway by Mykhailo Kondratiuk.

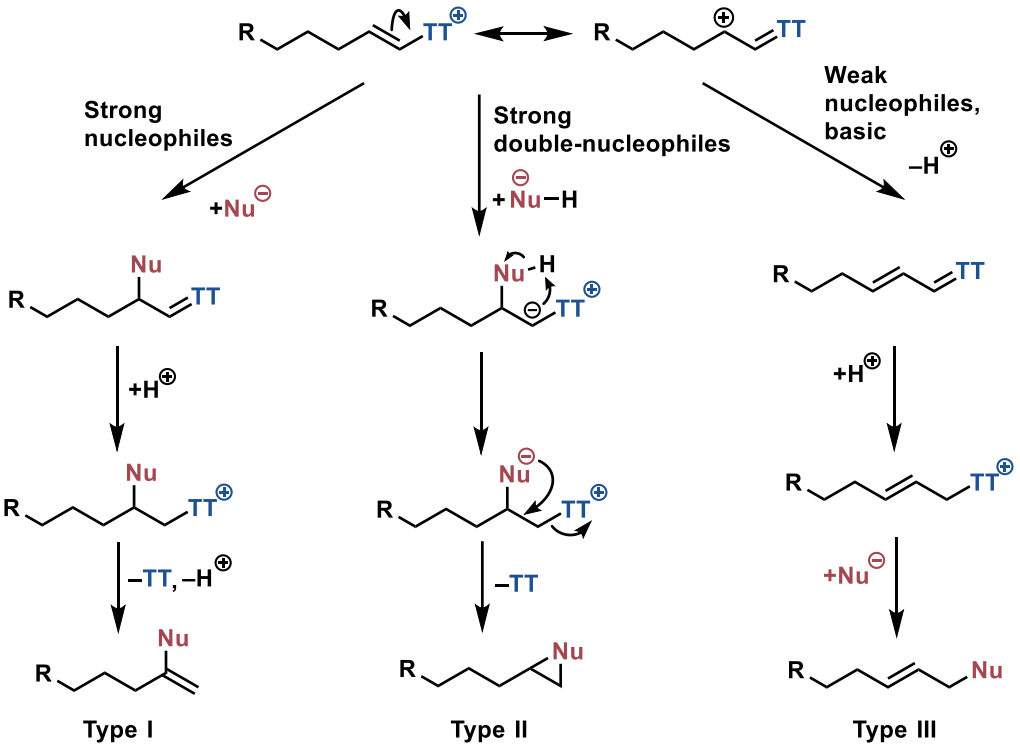

Figure I.40. Plausible reaction pathways for alkenyl thianthrenium salts with different nucleophiles (drafted by Mykhailo Kondratiuk and modified by Junting Chen).

I.4.2.3 Photoredox catalysis

Beyond conventional transition-metal-catalyzed transformations and catalyst-free direct nucleophilic displacement, alkenyl thianthrenium salts are also reactive under photoredox catalysis (Table I.4). However, unlike the transition-metal-catalyzed reactions, retention of the double bond geometry vanished after irradiation. Under the iridium-catalyzed photoredox reaction conditions that we have used for fluorination of aryl thianthrenium salts,[188] the best result obtained for model substrate (**11-TT**) was trifluoromethylation, which yielded *E* isomer in 49% yield. Trials for fluorination and trifluoromethyl thioetherification resulted in *E*/*Z* isomer mixtures, with 5/1 ratio in 79% yield and 8/1 ratio in 53% yield, respectively. Systematic evaluation of different solvents, photoredox catalysts and reagent sources is still on going to improve the yields and stereoselectivity. This *E*/*Z* isomerization phenomenon can be explained by the intermediacy of alkenyl radicals, which can isomerize via a linear π type radical transition state after excitation.[196] Further exploration on the reactivity of alkenyl thianthrenium salts under photoredox catalysis requires the identification of a photocatalyst, which can

reduce the alkenyl thianthrenium salt, yet not lead to alkene isomerization; or other more reactive radical trap reagents such as alkyne, alkenes and other radical sources should be used to outreach the rate for alkenyl radical isomerization.

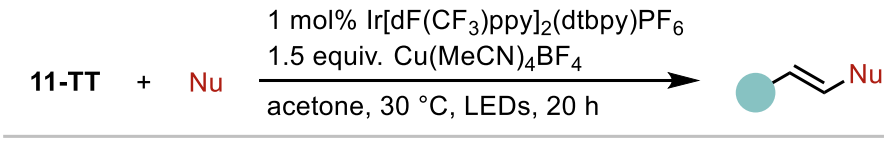

Nu	Reagents	yield (*E*/*Z*)
$F^{\ominus}$	1.2 equiv. CsF	79% (5/1)
$^{\ominus}CF_3$	1.5 equiv. CuSCN, 1.5 equiv. $TMSCF_3$ and 1.5 equiv. CsF in DMF	49% (*E* only)
$^{\ominus}SCF_3$	1.2 equiv. Me_4NSCF_3	53% (8/1)

Table I.4. Functionalization of alkenyl thianthrenium salts with different nucleophiles under photoredox conditions.

All of the results discussed in this section not only show alkenyl thianthrenium salts better alkenyl electrophiles than alkenyl bromides in transition-metal-catalyzed cross-coupling and direct nucleophilic displacement, but also suggest the potential utility of alkenyl thianthrenium salts as alkenyl radical precursors in photoredox catalysis. While under visible-light irradiation, alkenyl radicals are difficult to access from the common alkenyl electrophiles mentioned in Part I.1.3.

I.4.3. Identification of dicationic alkyl thianthrenium species and their role for stereo- and regioselectivity

Preliminary mechanistic research on reaction kinetics showed that, upon addition of triflic acid, an intermediate formed immediately in quantitative yield based on NMR analysis (Figure I.41). The intermediate remained unreacted in the acidic reaction conditions for at least 2 hours. Further characterization showed that *trans*-4-octene (**2**) gave **2-INT** exclusively. After treatment with aqueous $NaHCO_3$, the bicyclic intermediate (**2-INT**) afforded the corresponding alkenyl thianthrenium salt (**2-TT**) as a single isomer (Figure I.42).

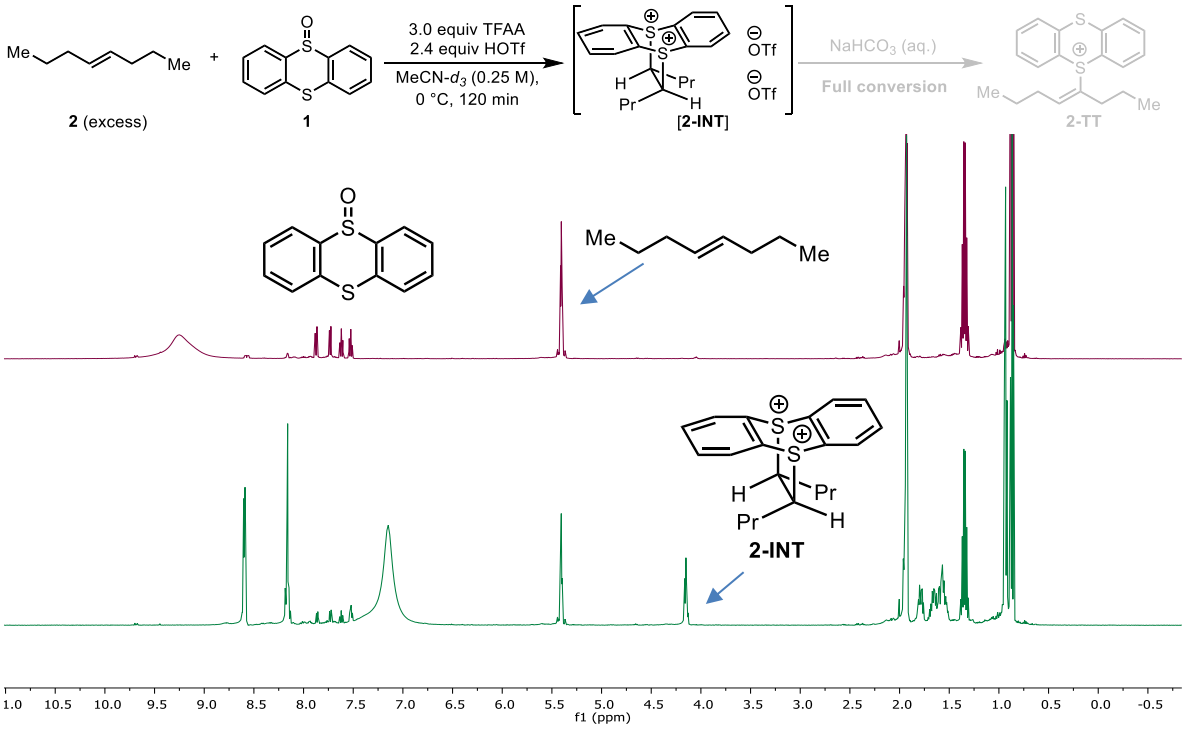

Figure I.41. Evidence for the dicationic thianthrenium salt **2-INT** formation by NMR.

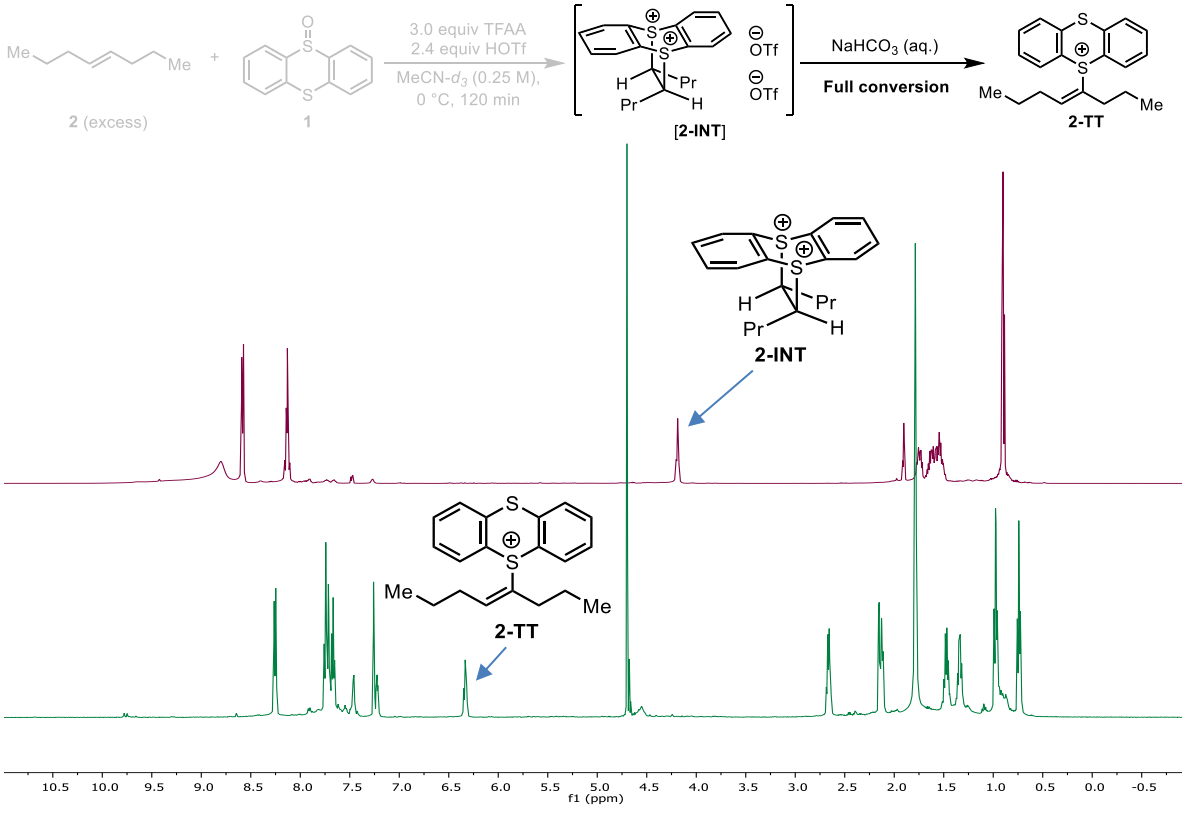

Figure I.42. Evidence for the formation of alkenyl thianthrenium salt **2-TT** from **2-INT**.

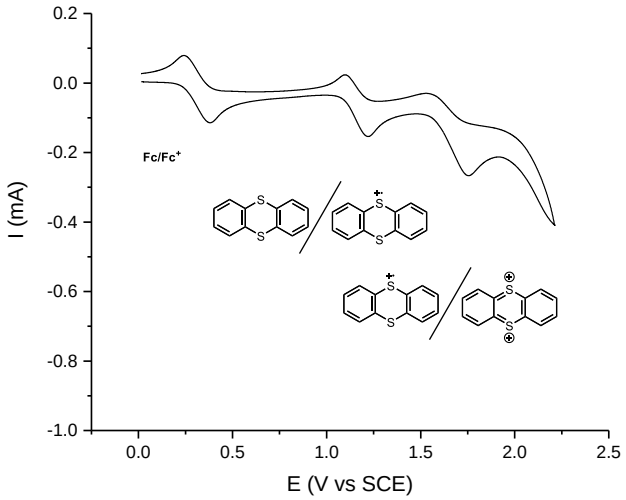

Figure I.43. Cyclic voltammogram for the oxidation of thianthrene (5 mM) in acetonitrile containing sodium triflate (0.1 M), trifluoroacetic anhydride (60 mM), and a ferrocene internal standard (5 mM); sweep rate = 87 $mV \cdot s^{-1}$. Ferrocene internal standard (Fc/Fc^+ = 0.37 V); thianthrene to thianthrene radical cation peak potential = 1.21 V; thianthrene radical cation to thianthrene dication = 1.74 V. (Measured by Dr. Matthew Plutschack)

We proposed such a stereoselective process to be controlled by a stereospecific mechanism, which in this case is consistent with an unusual [4+2] cycloaddition between the olefin substrates and a dicationic thianthrenium dication spieces. To substantiate the validity of the unusual thianthrenium dication as a reaction partner, we tried to observe it by cyclic voltammetry. In the CV analysis (Figure I.43), two oxidation peaks were observed, suggesting two sequential one electron oxidation processes, but the second single electron transfer was electrochemically quasireversible, which might be a result of reduction by solvent or something in the solvent. Considering the relative oxidation potentials, we assigned the first peak (1.21 V) to one electron oxidation of thianthrene to thianthrene radical cation and the second one (1.74 V) as one electron oxidation of thianthrene radical cation to thianthrene dication. Nevertheless, quantitative characterization of their formal potentials requires more sophisticated measurements and is beyond the scope of the current research.

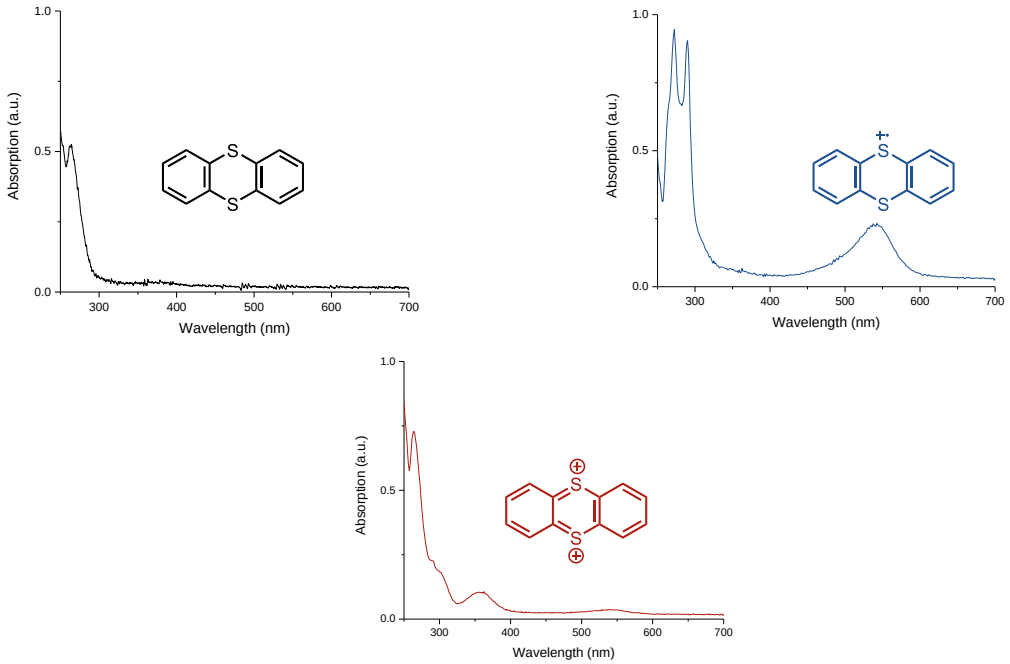

Figure I.44. Constant potential UV/Vis absorption spectra of thianthrene (0.8 mM) in acetonitrile containing trifluoroacetic anhydride, and tetrafluoroboric acid diethyl etherate with an applied potential of 0.0 V (top left), 1.4 V (top right), and 1.8 V (bottom). (Measured by Dr. Matthew Plutschack)

With the relative oxidation potentials in hand, we tried to differentiate the possible species by recording their UV/Vis spectra in an electrical cell at constant potentials. As expected, three different absorption peaks were detected when the corresponding oxidation potentials were applied (Figure I.44). The absorption peak shifted from 530 nm to around 355 nm when the oxidation potential changed from 1.4 V to 1.8 V, which suggests two different species in solution. In combination with the CV data, we proposed the existence of the thianthrene radical dication species, which can react as a 4π diene. We cannot rule out an addition of the thianthrene radical cation to the olefin, followed by single electron oxidation and subsequent cyclization to the bicyclic adducts, but oxidation and cyclization should occur faster than C–C single bond rotation to ensure the observed selectivity. Attempts to thermally induce a cycloreversion of the cycloadduct **2-INT** was not successful, possibly due to its two formal positive charges that also prevented experiments such as flash-vacuum-pyrolysis.

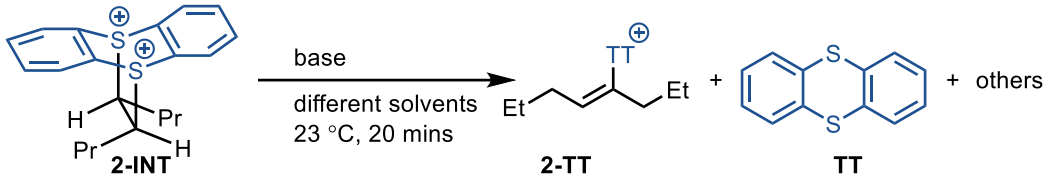

Base	Solvent	Results
$NaHCO_3$	MeOD	Full conv., major **2-TT**, trace **TT**
$NaHCO_3$	DMSO-d_6	Full conv., >80% decomposition to **TT**
Na_2CO_3	MeOD	Full conv., messy, some **2-TT** and **TT**
Na_2CO_3	DMSO-d_6	Full conv., >60% decomposition to **TT**
Na_2CO_3	CD_2Cl_2/MeOD (1/1)	Full conv., major **2-TT**, trace **TT**

Table I.5. Examination of **2-INT** in various solvents and with different bases.

When the base treatment was omitted, dicationic cyclothianthrenium salts can be isolated from the studied cases. Those dicationic cyclothianthrenium salts are relatively stable on bench, for example, no detectable decomposition was observed for **2-INT** when stored in a brown borosilicate vial at room temperature for three months. However, the energetically less favored **3-INT**, synthesized from *cis*-4-octene (**3**), is less stable and decomposes slowly in MeCN-d_3 within an overnight ^{13}C-NMR time scale.

Preliminary examination revealed that deprotonation of dicationic cyclothianthrenium species **2-INT** is sensitive to reaction conditions (Table I.5): relatively basic conditions such as $NaHCO_3$ in combination with DMSO-d_6 resulted in over 80% of decomposition while the same base in MeOD promoted the desired deprotonation reaction. To simplify the deprotonation and purification steps, CH_2Cl_2/H_2O biphasic system was employed. Treatment of either bicycle (**2-INT** or **3-INT**) with mild base, such as aqueous (bi)carbonate, resulted in clean and high-yielding conversion to the corresponding alkenyl thianthrenium salt **2-TT** or **3-TT**, respectively, with complete selectivity of olefin geometry (Figure I.45).

Stereoelectronic considerations dictate that the elimination cannot proceed by an E2 mechanism due to the geometry of the bicycles **2-INT** and **3-INT**, which

prevent an antiperiplanar arrangement of leaving group and proton. An E1 mechanism cannot be excluded but is unlikely due to the near complete degree of fidelity of double bond geometry. Overall, an $E1cB_{irr}$ mechanism where rate-determining deprotonation is followed by a rapid elimination [197, 198] would be consistent with all experimental observations.

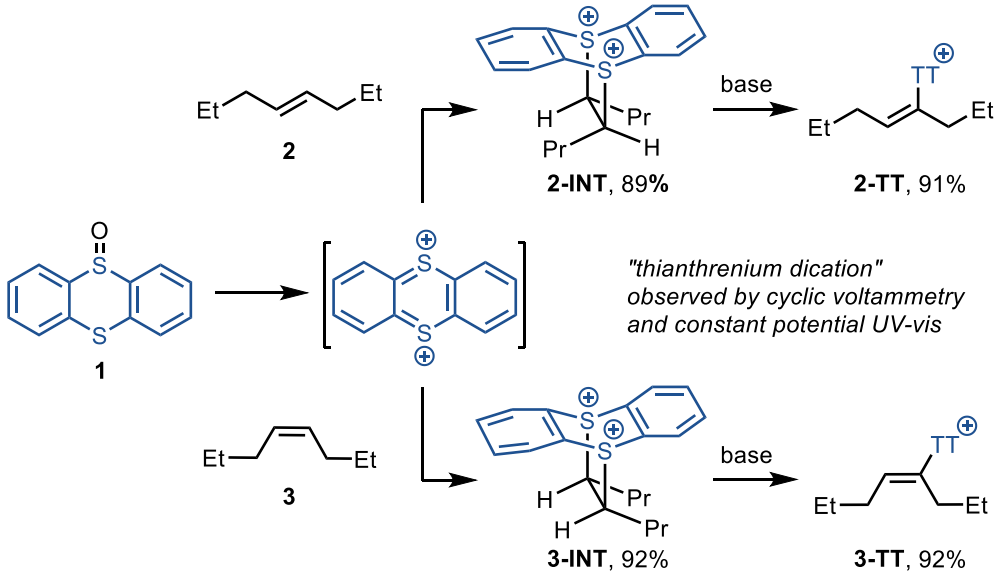

Figure I.45. Mechanism for regioselective thianthrenation of alkenyl C(sp^2)–H bonds.

I.4.4. Preliminary investigation on dicationic alkyl thianthrenium species

After isolation and characterization of the dicationic alkyl thianthrenium compounds **2-INT** and **3-INT**, we examined the [4+2] cycloaddition concept on other internal alkenes, and further explored the utility of dicationic alkyl thianthrenium species as intermediates for *cis*-difunctionalization of alkenes.

By treating alkene substrates with a stoichiometric amount of thianthrenen-*S*-oxide and excess of trifluoroacetic anhydride and triflic acid in MeCN at 0 °C, the desired dicationic alkyl thianthrenium products can be obtained via trituration with diethyl ether after evaporating the volatiles from the reaction mixture (Figure I.46). Super-stoichiometric amount of triflic acid is uitilized to minimize the exchange of triflate couterion by trifluoroacetate in the final products.

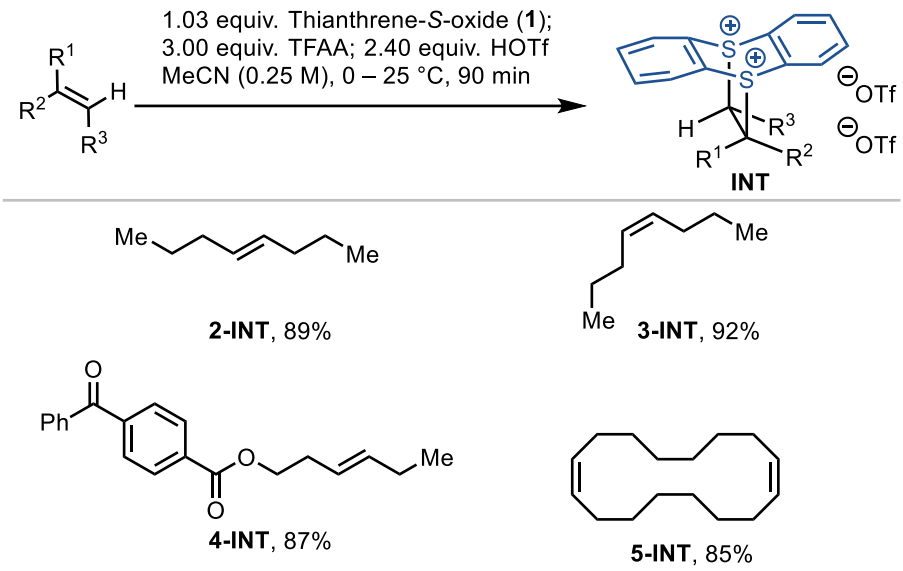

Figure I.46. Substrate table for dicationic thianthrenium formation.

Beyond **2-INT** and **3-INT**, the unsymmetrical internal alkene (*E*)-hex-3-en-1-yl 4-benzoylbenzoate, which gave regio- and stereoisomer mixtures in C–H thianthrenation of alkenes, afforded the dicationic alkyl thianthrneium **4-INT** as a single stereoisomer in 87% yield. Internal alkene (1*Z*,9*Z*)-cyclohexadeca-1,9-diene also gave the desired mono dicationic alkyl thianthrenium **5-INT** in 85% yield. Terminal alkenes are also good substrates under the standard reaction conditions according to Mykhailo Kondratiuk's reports.

Dr. Pascal Stephan Engl found that thianthrene can be oxidized *in situ* by oxidants like Selectfluor, and the resulting reactive species can provide C–H thianthrenated products for arenes. We wondered if the alkyl dicationic product could be harnessed under similar conditions. On the other hand, the bicyclic dicationic species are similar to halonium ions with less ring strain, at least structurally and stereoelectronically. Considering the high reactivity of halonium ions with nucleophiles (even react with a weak nucleophile like water), the electrophilic reactivity of the dicationic alkyl thianthrenium salts seems promising as well, ideally in a diastereoselective fashion. If both assumptions are viable, we have a chance to achieve catalytic *cis*-difunctionalization of alkenes (Figure I.47).

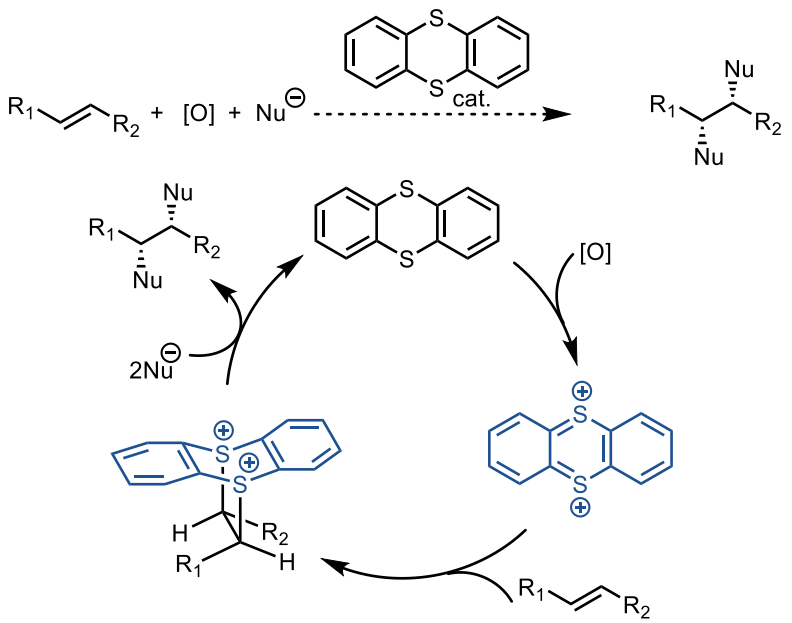

Figure I.47. Proposed catalytic *cis*-difunctionalization of alkenes via thianthrene catalysis.

Initial attempts were made for the proposed catalytic transformations by reacting (*E*)-hex-3-en-1-yl 4-benzoylbenzoate with Selectfluor and 1,3-diphenylurea in the presence of catalytic amount of thianthrene. Unfortunately, only trace amount of alkenyl thianthrenium salts were detected, but it at least suggested the possible intermediacy of alkyl dicationic species from thianthrene and Selectfluor (*vide ante* Part I.4.3).

The electrophilic reactivity of the dicationic alkyl thianthrenium salts were examined by reacting with various nucleophiles. When the reactions were performed in MeCN (Figure I.48), only trace di-substituted products were obtained in two cases, undesirable elimination reactions were observed, and the undesired allylic substituted alkenes, alkynes or conjugated dienes were detected as major products. So far, direct nucleophilic displacement of the dicationic thianthrene has not yet been successful.

Considering both the observation of alkenyl thianthrenium salts under catalytic conditions and the aforementioned ongoing direct nucleophile attack on alkenyl thianthrenium salts (*vide ante* Part I.4.2), a promising direction would be the stereoselective C–H functionalization of alkenes via thianthrene catalysis.

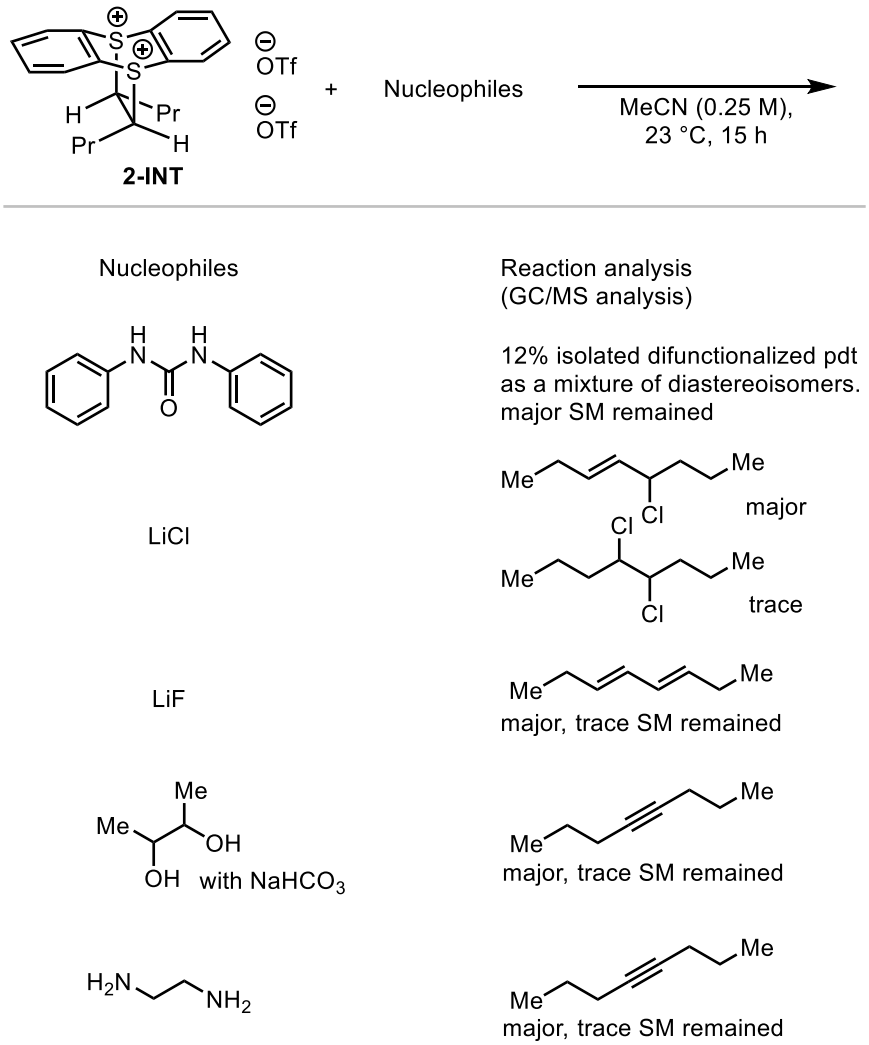

Figure I.48. Reactivity of dicationic thianthrenium salt with nucleophiles.

I.5. Conclusion and outlook

Here, I described a straightforward C–H thianthrenation of alkenes. Unlike the addition to generate functionalized alkanes, which is mostly known for alkene reactions with electrophiles, C–H thianthrenation provides alkenyl thianthrenium products while maintaining the double bond functionality. The reagent we introduced is a thianthrene-*S*-oxide, which can be activated *in situ* with anhydrides and acids to afford a reactive thianthrenium dication species, as characterized by CV and UV/Vis analysis. In the presence of alkenes, the thianthrenium dication acts as a diene and reacts with the alkene dienophile via a stereospecific [4+2] cycloaddition mechanism. When treated with base, the resulting cyclo-dicationic thianthrenium species undergo a proposed rate-determining deprotonation followed by a rapid elimination ($E1cB_{irr}$ mechanism) to afford alkenyl thianthrenium salts. The C–H thianthrenation reaction of terminal olefins is robust, as can be seen by its wide functional group tolerance and excellent regio- and stereoselectivity. The corresponding alkenyl thianthrenium salts are good alkenyl electrophiles in palladium and ruthenium catalyzed cross-coupling reactions to forge alkenyl C–C, C–Cl, C–CF_3 and C–SCF_3 bonds. Overall, the discussed method provides an alternative option for the synthesis of alkenyl electrophiles through direct and stereoselective C–H functionalization of alkenes. Further exploration into the phtoredox reactivity of the alkenyl thianthrenium salts hints at access of alkenyl radicals that are otherwise difficult to obtain.

C–H thianthrenation of alkenes works well for terminal and symmetrical and electronic biased internal olefins, nevertheless, for unsymmetrical internal olefins, thianthrenation gives a mixture of regio- and stereoisomers. For future development of C–H functionalization of alkenes, it would be of interest to target the remaining challenges.

The finding or proposal of the thianthrenium dication reactive species also inspired our group members to evaluate the mechanism for C–H thianthrenation of arenes in a new direction.

II. FLUORINATION OF ARYL THIANTHRENIUM SALTS

II.1. Introduction

The past 20 years witnessed the surge of fluorine chemistry from a subfield in organic chemistry to a multidisciplinary research topic, most outstandingly in applications in pharmaceuticals and agrochemicals.[199,200] As mentioned in many research papers and reports,[201] over 50% of blockbuster drugs contains fluorine, which might be because of the unique electronic (Pauling electron negativity, 4.0), physical (sensitive in nuclear magnetic resonance spectroscopy) and biological properties ($BDE_{C–F} \approx 116$ kcal/mol, resistant to most metabolism systems) introduced by fluorine. For instance, CF_3 can be treated as a bioisostere of an ethyl substituent with higher inhibition potency on matrix metalloprotease-9 (MMP-9; gelatinase B),[202] possibly due to its higher hydrophobicity when accommodated in a tight and deep hydrophobic pocket.[203] Another representative example is Ezetimibe (Figure II.1),[204,205] a cholesterol-absorption inhibitor, to which, the introduction of fluorine dramatically increases the metabolic stability of the lead compound. For the original SCH48461 candidate, the C–H bond at the *para*-position of a phenyl substituent can be easily oxidized to C–OH under metabolic conditions, while the methyl ether of one anisole moiety dealkylated. Since the fluorine atom is similar in size to hydrogen, and C–F bond is one of the strongest organic single C–R bonds, the overall topology of a molecule was not significantly affected, lengthening the drug candidate's half-life with blocked metabolism pathways. Indeed, displacement of those two metabolic vulnerable sites in SCH48461 with fluorides leads to a roughly 400-fold increase in potency for monkey treatments. In 2018, there are 17 new fluorine-containing drugs profiled and introduced to the market with approval from the food and drug administration (FDA).[206] Among those 17 drugs, 30% contain (hetero)aryl fluorides, such as encorafenib, binimetibib, daconitinib and fostamatinib (Figure II.2).

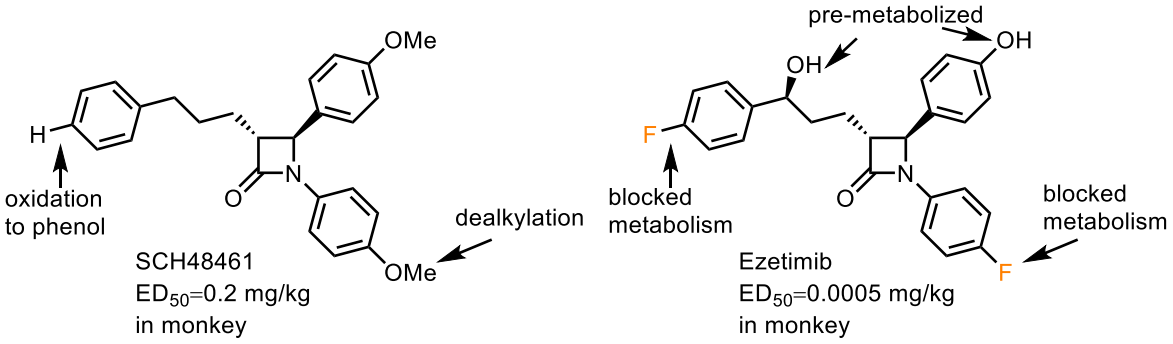

Figure II.1. Replacement of metabolic sensitive sites with biologically more stable C–F bonds increases the potency of the leading compound and leads to the discovery of Ezetimibe.

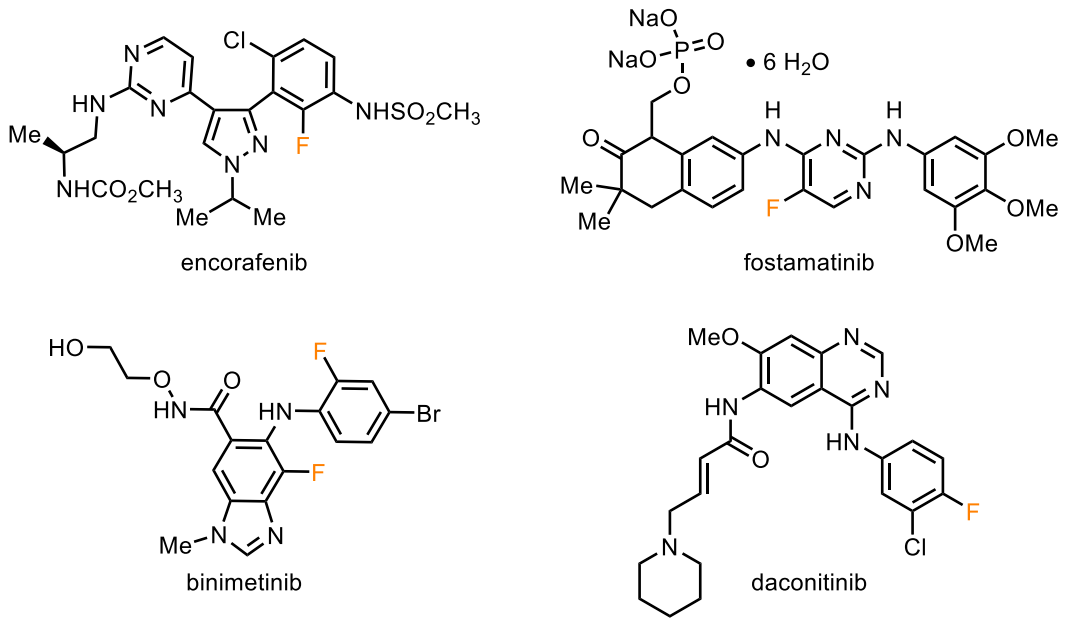

Figure II.2. Examples of aryl fluorides containing drugs approved by FDA in 2018.

One of the fluorine isotopes, ^{18}F, is widely used in positron emission tomography (PET) tracer designs. Since ^{18}F has very short half-life (109.7 min), it needs to be installed at a very late-stage.[207,208] The method targeted in this thesis has not yet been applied to radiochemistry. Therefore, the following discussion will only be in the context of ^{19}F-fluorides.

For most of the aryl fluoride containing drugs, the fluorine atom is often introduced via a building block either in the middle or at the beginning of a synthesis (Figure II.3), which means, *de novo* synthetic design is required if one wants to access targets with different substituents other than fluorine. As mentioned in Part I.1.2, methods enabling direct functionalization of C–H to install

a lynchpin would simplify most diversifications and new drug candidate screening processes. Considering the large population of aryl fluoride and quantity of aryl C–H bonds presented in drug candidates, it is highly demanded to develop a method, which can directly introduce fluorine onto arenes at a late-stage, ideally in a site-selective fashion.

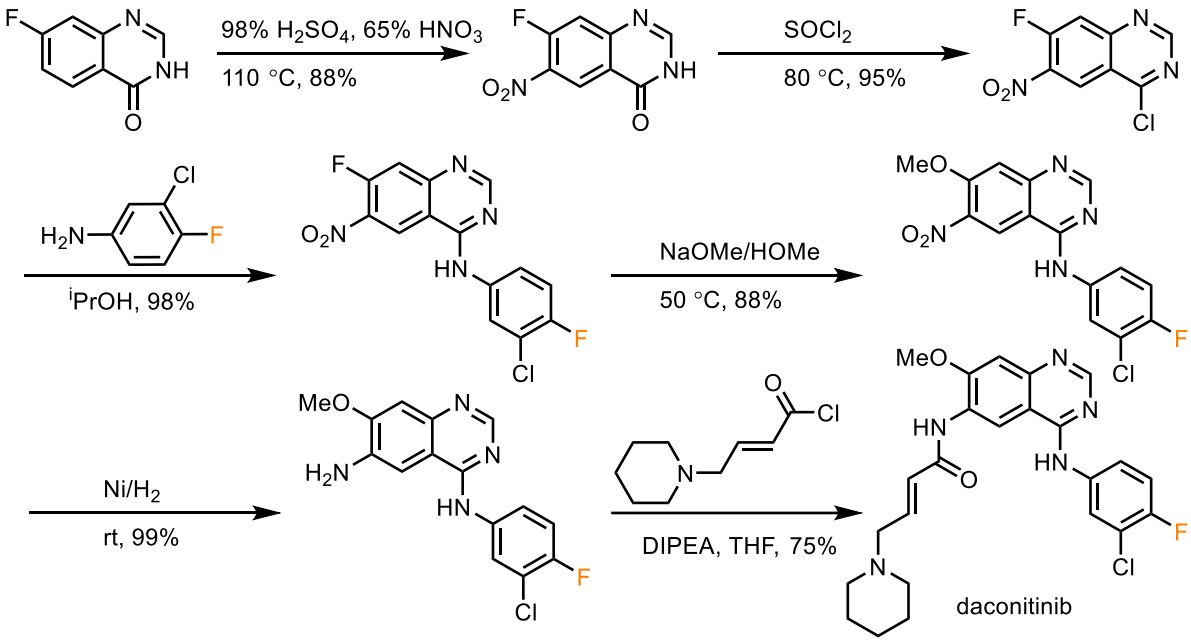

Figure II.3. Synthetic routes to daconitinib.

II.1.1. Late-stage fluorination of arenes

Fluorides on aromatic frameworks are traditionally introduced under harsh conditions that are not compatible with many functional groups, such as employment of elemental fluorine,[209] fluorination of aryldiazonioum salts with HBF_4 (Balz-Schiemann reaction),[210] or nucleophilic aromatic substitution (S_NAr) of electron-deficient aryl nitrates or chlorides (Halex reaction).[211] Since Dupont's report on a principle catalytic fluorination of arenes by CuF_2 using HF as terminal fluoride source and O_2 as oxidant,[212] many methodologies for fluorination of arenes have been published in the past years. Most of them focused on transition metal mediated incorporation of fluorine to a prefunctionalized position such as positions containing borates, stannanes, iodonium salts, and (pseudo)halides using electrophilic fluorinating reagents like Selectfluor, NFSI or alkali fluoride sources. Generally speaking, alkali fluoride sources are more appealing not only for the sake of green production with less waste in industrial synthesis, but also for

their amenability to valuable ^{18}F-labeled compounds. Because ^{18}F-fluoride is readily available while electrophilic ^{18}F-fluorine sources are often synthesized from ^{18}F-fluoride with relative low specific activity (S.A.=radio activity/mass).[213]

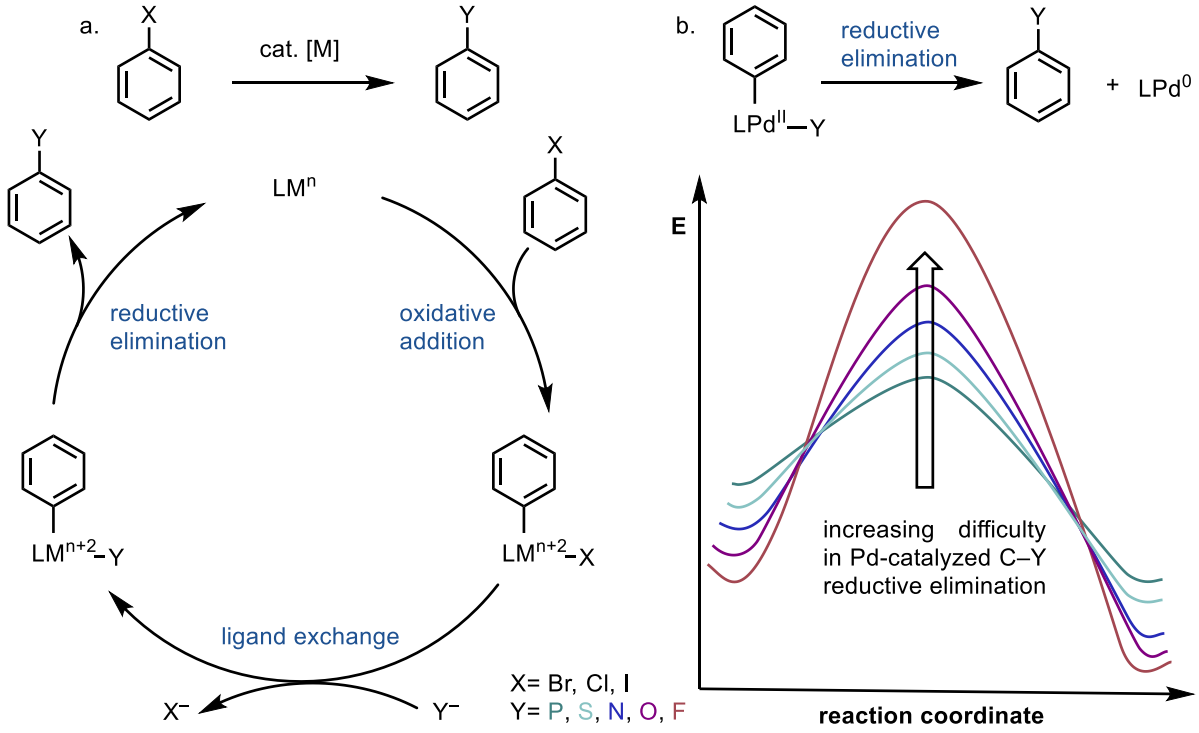

Figure II.4. Metal catalyzed cross coupling reactions, especially palladium catalyzed aryl–hetero bonds formation and their relative energy barriers for reductive elimination from the corresponding aryl–M(L)–X intermediates.

Transition metal promoted aryl–hetero atom bonds formation has been extensively studied since the late 1900s (Figure II.4). Catalytic cross-coupling reactions forging aryl–N, aryl–S, aryl–O bonds provided evidence for the mechanistic feasibility of catalytic aryl–F transformations.[214] In 1997, the very early experiments done by the Grushin group on aryl palladium fluoride ($Pd^{II}F$) complexes failed to give aryl fluorides via reductive elimination. [215] The triphenylphosphine ligated aryl $Pd^{II}F$ complexes $[(Ph_3P)_3Pd(Ar)F]$ prepared from $[(Ph_3P)_3Pd(Ar)I]$ and AgF, were found to be stable in air. Initial studies on reductive elimination only found P–F and P–C products. The first conceptual breakthrough for catalytic fluorination was achieved by the Sanford group in 2006 by using electrophilic fluorine sources in combination with palladium(II) catalysts (Figure II.5a).[216] The silver catalyzed fluorination of arylstannanes was later developed in

the Ritter group, and the substrate scope showed great functional group tolerance (Figure II.5b). [217] Until then, catalytic fluorination was only achievable with electrophilic fluorinating reagents proceeding with strong electrophilic fluorine sources.

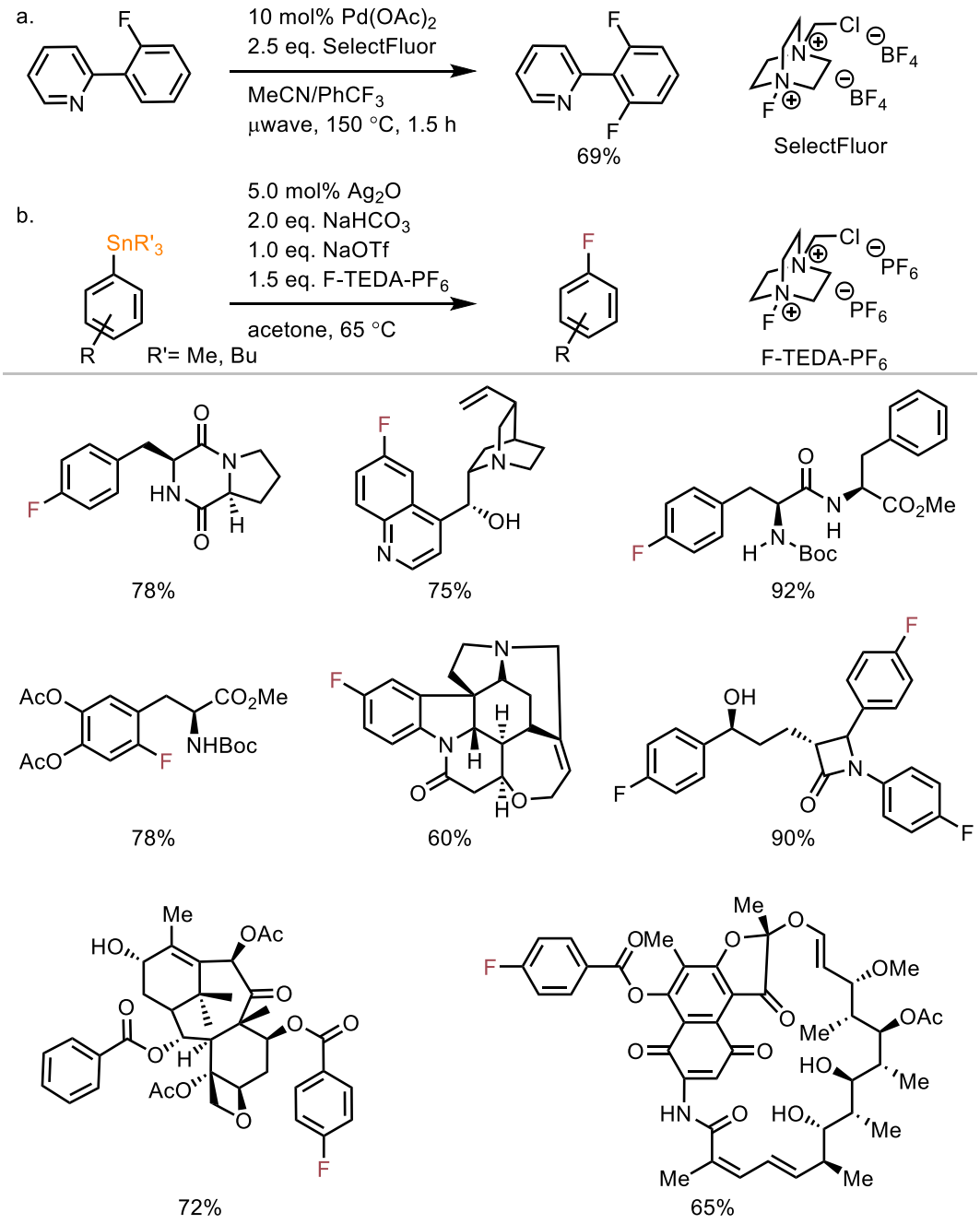

Figure II.5. Palladium and silver catalyzed fluorination reactions using electrophilic fluorinating reagents.

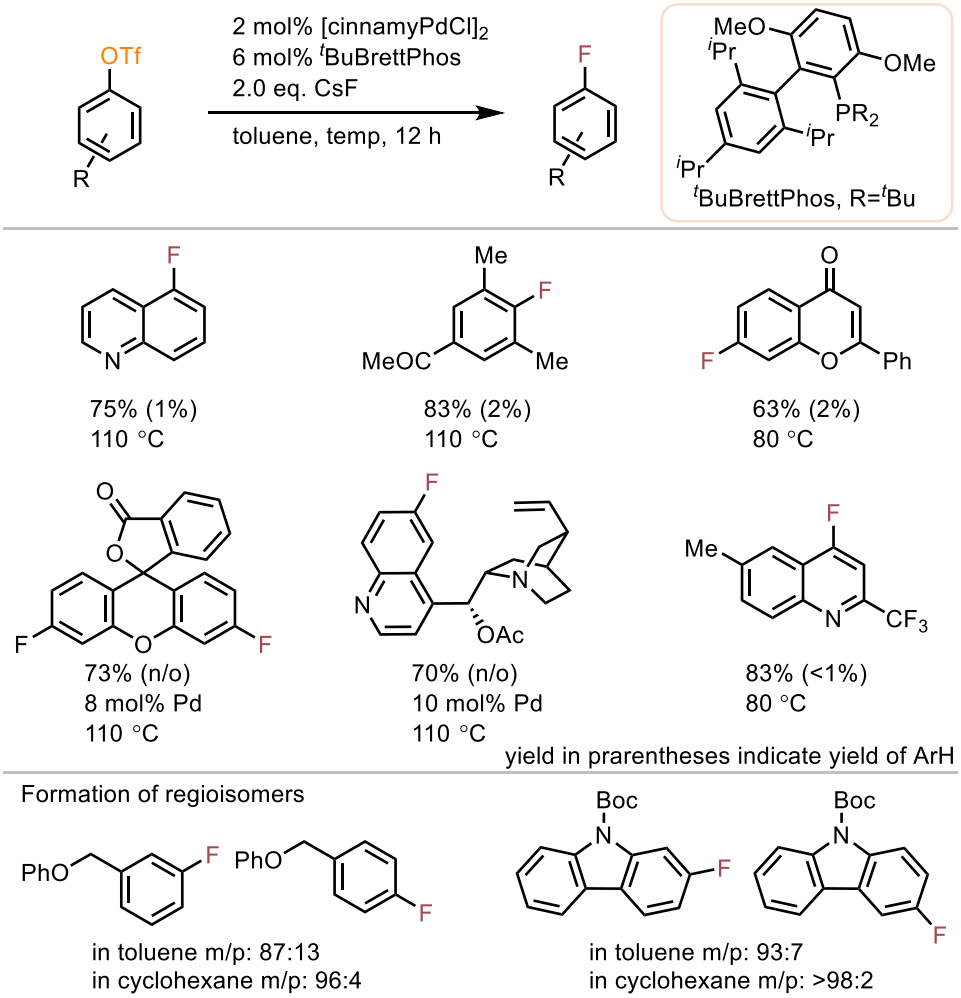

Figure II.6. *t*BuBrettPhos facilitated formation of arylfluoride from aryltriflates via reductive elimination from [BrettPhosPd^{II}(Ar)F] species.

It was not until 2009 that catalytic fluorination with nucleophilic fluorides became possible via palladium catalysis in the presence of fine-tuned BrettPhos ligands developed in the Buchwald group.[218] The reason for such a long time gap for fluoride to be incorporated in metal catalyzed transformations is that there are several fundamental challenges:

1) Formation of aryl–F bond by reductive elimination in transition metal catalysis is difficult, especially for metals at normal oxidation states (with respect to high oxidation states).[219,220] Careful mechanistic investigations done by the Hartwig group for palladium catalyzed aryl–hetero bonds formation revealed that the rate for reductive elimination is associated with the nucleophilicity of coupling nucleophiles in the following order: C–P>C–S>C–N>C–O (Figure II.4 b).[221] One plausible reason for this trend is the increasing ionic character of M–X

bond. On one hand the ionic bond tends to decrease the M–aryl and M–X σ bonds orbital overlap that is responsible for reductive elimination; on the other hand, the thermodynamic stability of aryl–M(L)–X complex is increased, thus the thermodynamic driving force for reductive elimination decreases. Such effect will be more significant when applied to M–F as fluorine is the most electronegative element.

2) Fluoride forms strong hydrogen bonds with protic hydrogens such as protons in water/alcohol/amine, which typically decrease the nucleophilicity of fluoride and weaken the reactivity for S_NAr reactions. While hydrogen bond donors are excluded, fluoride shows more basic characters which leads to undesired side reactions such as deprotonation of nitromethane.[222]

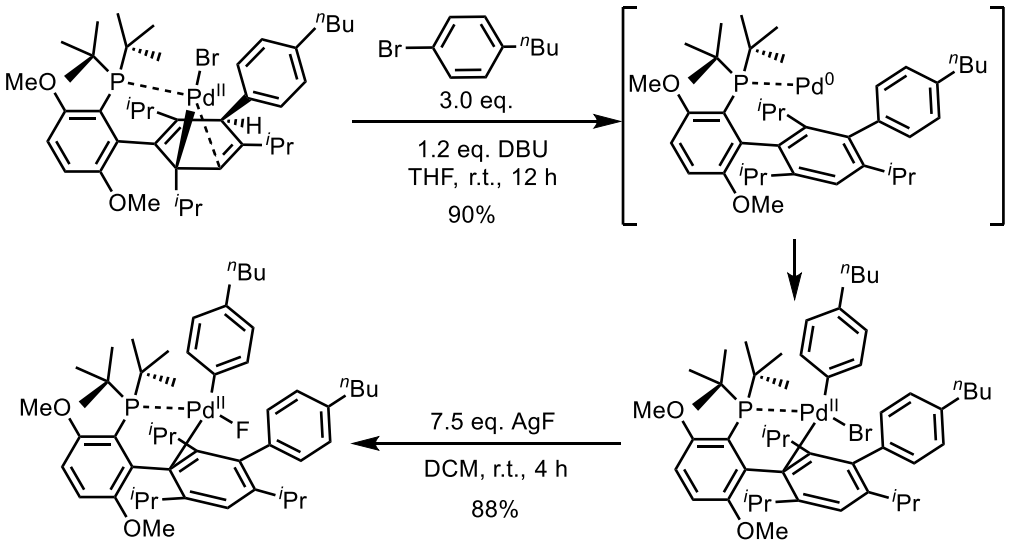

Figure II.7. Preliminary mechanistic data for palladium catalyzed fluorination.

Mechanistic investigation for this discussed palladium catalyzed fluorination system suggested an *in situ* catalyst generation via dearomatization of the palladium catalyst precursor.[223] Upon treatment with base, a palladium(0) species is formed, and reacts with aryl triflates/bromides to give aryl–Pd(L)–X species. After halide exchange, the resulting aryl–Pd(L)–F species afforded the desired aryl fluoride species (Figure II.7). The observation of regioisomers from standard reaction conditions is not fully understood in the moment (Figure II.6), but most likely introduced by intermediacy of palladium aryne intermediates formed under basic conditions. Further ligand examination enables room temperature fluorination of aryl triflates and bromides.[224]

Aryl boron reagents can afford arylfluorides via metal mediation or catalysis in the presence of electrophilic fluorine sources or nucleophilic fluorides in combination with external oxidants. In most cases, one characteristic feature is the incorporation of aryl metal species generated from transmetallation of aryl boron reagents with metal precursors. Metal species like palladium (Figure II.8a),[225] silver (Figure II.8b)[226] and copper (Figure II.8c)[227,228,229] readily generate aryl metal species, which are subsequently oxidized to afford high valent aryl metal fluoride species followed by reductive elimination to deliver the desired arylfluorides. One exception is the Pd(III) catalyzed fluorination of aryl boronic acid and derivatives developed by the Ritter group.[230] Kinetic data suggest a single-electron-transfer (SET) pathway without formation of aryl metal intermediate (Figure II.8d) and a turnover-limiting oxidation of Pd(II) to Pd(III) (rate law showed zero-order dependence on aryl trifluoroborate, first-order on palladium catalyst, saturation kinetics for terpyridine, and a non-integer kinetic order of 1.4 with respect to Selectfluor). On the other hand, **Pd-II** was isolated and characterized when precatalyst **Pd-I** was treated with one equivalent of terpyridine followed by one equivalent of Selectfluor in MeCN. **Pd-II** expresses a similar catalytic reactivity with **Pd-I** for fluorination of arylborates, yet the fluoride radical transfer is not well understood. One limitation of the Pd(III) catalyzed reaction is the inability to access fluorinated heterocycles, which might confine its application, considering the wide variety of heterocycles in drug candidates.

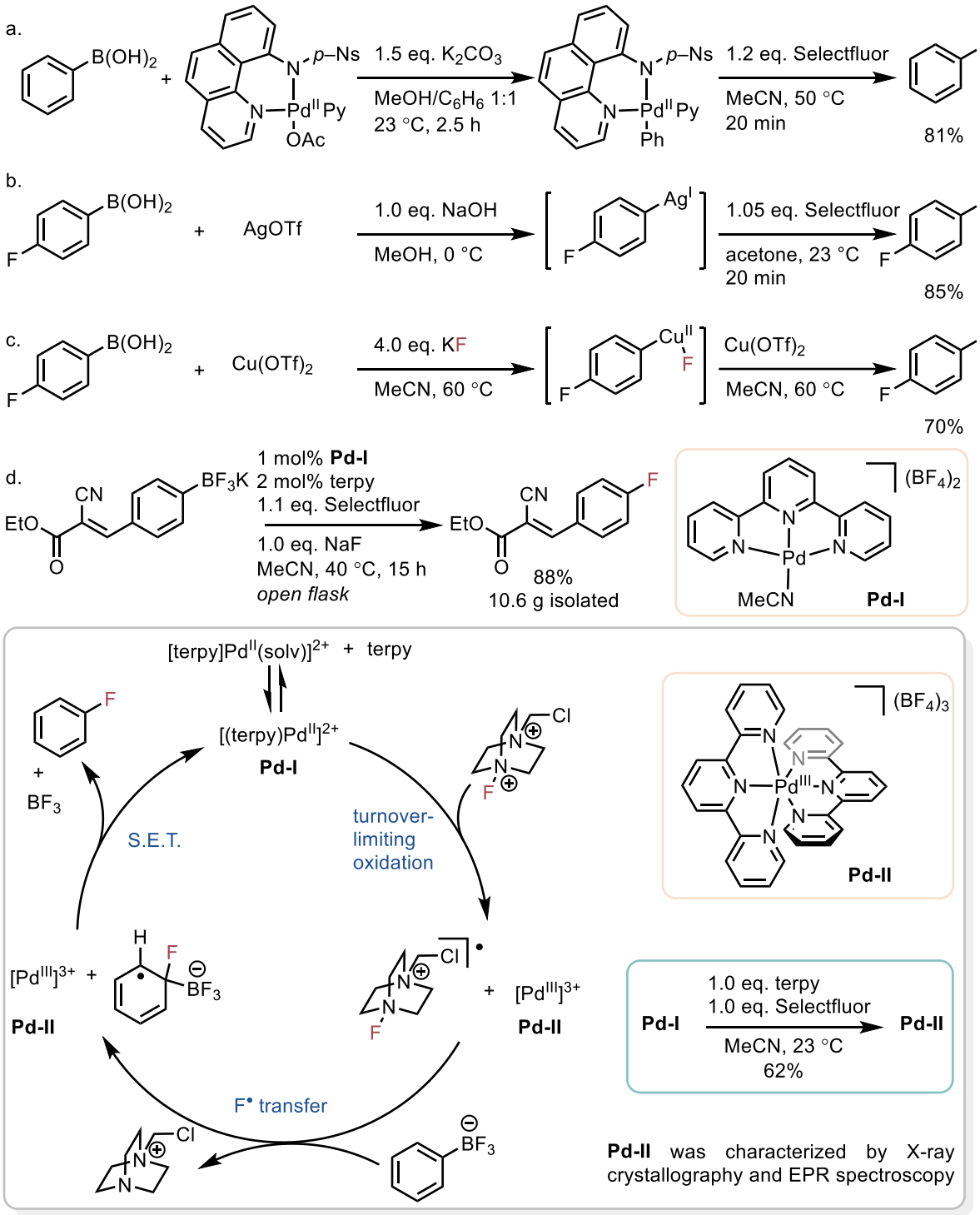

Figure II.8. Examples for fluorination of aryl boron reagents using palladium, silver or copper reagents or catalyst.

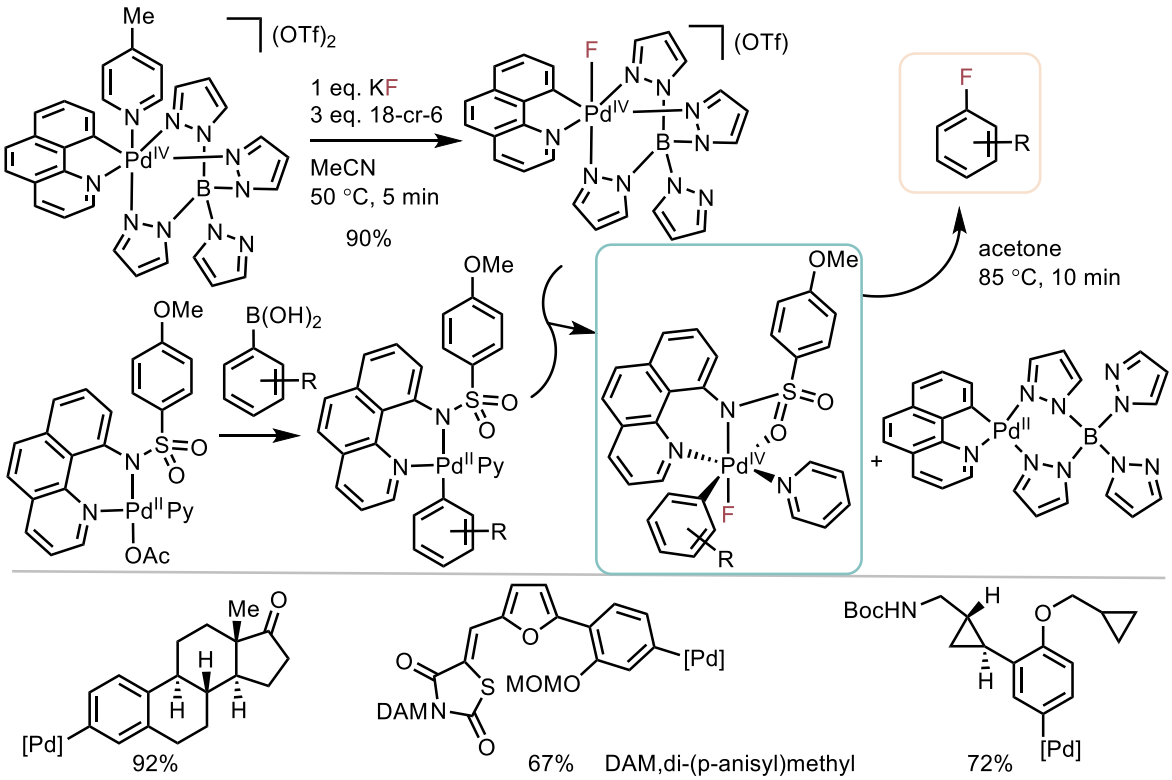

Figure II.9. Fluoride capture by Pd(IV) species and subsequent oxidative fluoride transfer.

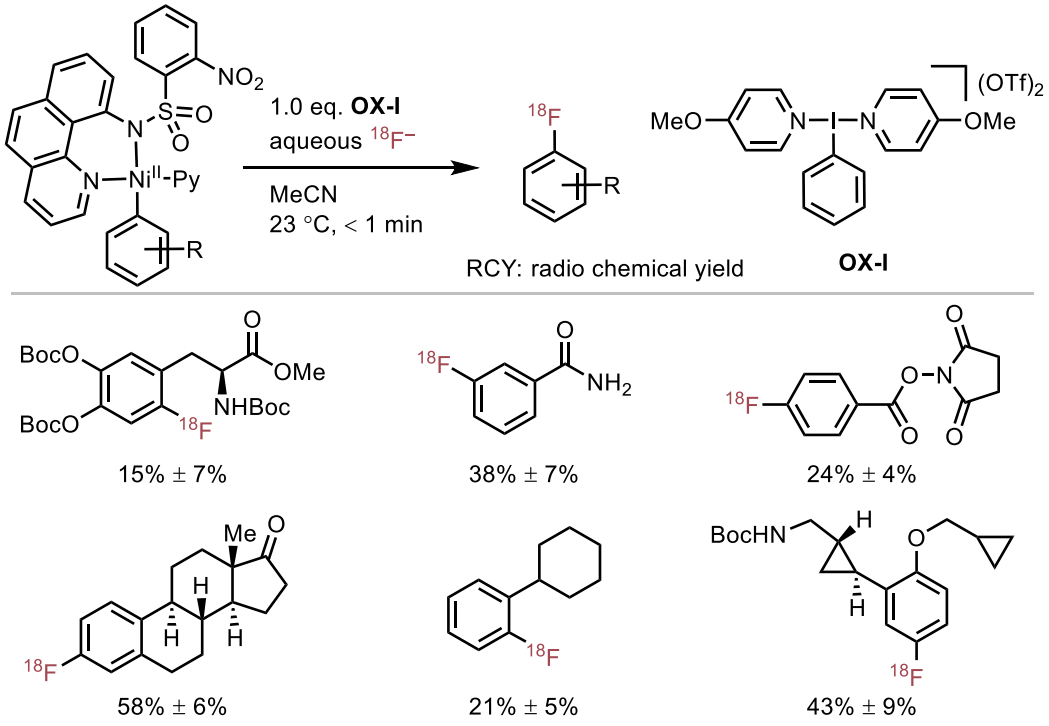

Figure II.10. Nickel(II)-mediated ^{18}F-fluorination within one minute using aqueous ^{18}F-fluoride.

Except for the silver-catalyzed fluorination of arylstannanes (Figure II.5b), methods which offer the most diverse substrate scope and functional group tolerance are those utilizing milder fluorinating reagents in the presence of organometallic intermediates. The Pd(IV) fluorine reagent (Figure II.9) developed by the Ritte group showcases the high applicability of metal mediated transformations for late-stage fluorination by adapting their syntheses to ^{18}F-labeling of aromatic complex molecules.[231] As demonstrated above, a reaction has to be efficient for ^{18}F-synthesis due to the short half-life time of ^{18}F-fluoride, and ^{18}F-fluoride in water is the ideal reagent. Besides, in ^{18}F-chemistry, the ^{18}F-fluoride source is on a nanomole scale, which requires a robust reaction to minimize side products. One striking property of this Pd(IV) fluorine reagent is that it turns a anhydrous fluoride into an electrophilic fluorine source. A similar reagent based on Ni(II) (Figure II.10) was later developed by the same group.[232] The well-defined Ni(II) complex reacts with oxidant and aqueous fluoride at room temperature and affords aryl fluorides within one minute. This new metal mediated fluorination method enables straightforward and practical late-stage ^{18}F-labeling of complex small molecules, which is further established by its successful implementation in producing ^{18}F-5-fluorouracil with a quality and in quantities suitable for PET imaging in humans.[233]

Besides transition metal facilitated C–F bond formation, fluorinating reagents have also been developed over the past ten years, which mainly focus on the deoxyfluorination of phenols. Those reactions might benefit from the inertness of the side products based on oxygen such as 1,3-bis(2,6-diisopropylphenyl)-1,3-dihydro-2*H*-imidazol-2-one (urea like) and SO_3. PhenoFluor[234,235] and its derivative reagents[236,237] stand out with high functional group tolerance and broad substrate scope, and no such a method for deoxyfluorination can compete until today (Figure II.11). The reaction was proposed to proceed through a concerted nucleophilic aromatic substitution (CS_NAr) mechanism to generate the corresponding aryl fluoride and urea.[238] The radioactive version for ^{18}F-deoxyfluorination of phenols based on PhenoFluor structure was successful, albeit the substrate scope is limited to electron-deficient aromatics. PhenoFluor and AlkylFluor are good deoxyfluorinating reagents for aliphatic alcohols as well.[235,237]

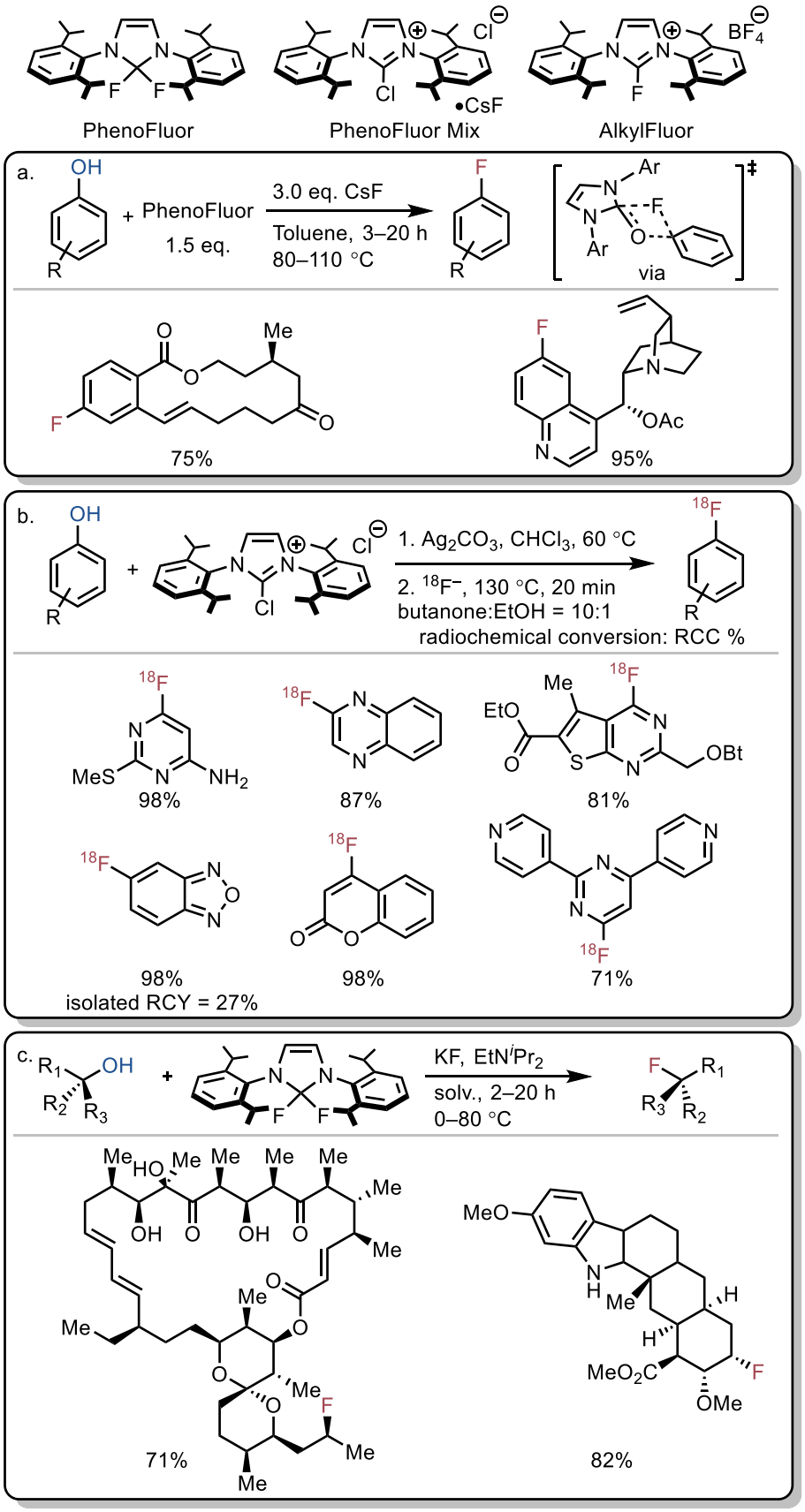

Figure II.11. Structure of PhenoFluor and its derivative reagents and their applications in deoxyfluorination of phenols and alcohols.

The biggest limitation of PhenoFluor-related reagents is the production of a byproduct with high molecular weight, which restricts their broader applications in large-scale synthesis. Deoxyfluorination of phenols using sulfuryl fluoride (SO_2F_2) and tetramethylammonium fluoride (NMe_4F) works well to afford simple aryl fluorides.[239] Despite difficulty in handling gaseous SO_2F_2, this protocol benefits from the reagent with low cost and easy accessibility. The reaction was also proposed to go through a CS_NAr mechanism based on S(VI)–F to give the thermodynamically favorable aryl fluoride and SO_3.

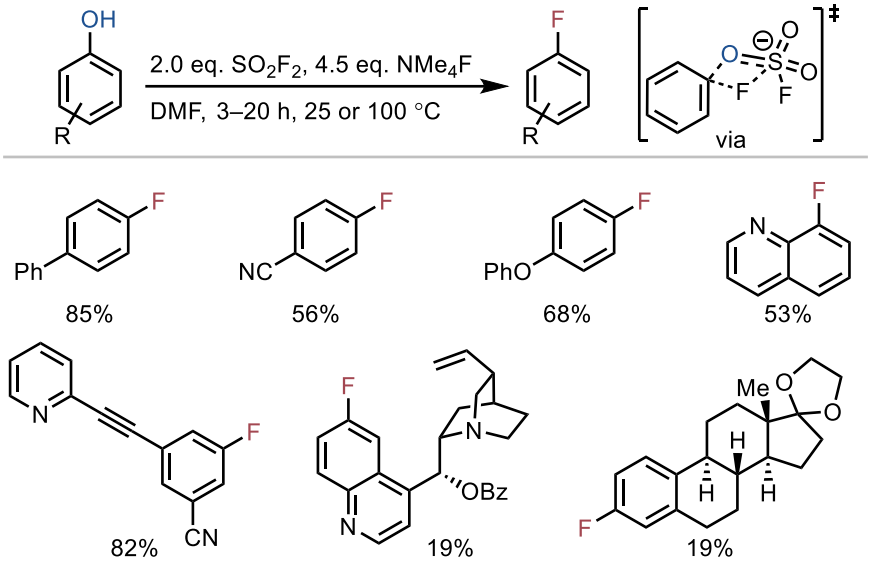

Figure II.12. Deoxyfluorination with PhenoFluor and its derivative reagents.

Above all, fluorine can be introduced to a specific site, albeit most of the functional groups must be pre-installed, and site-selective introduction of boronates or others to aryl C–H bonds is scarce. Methods for fluorination of aryl C–H bonds often suffer from low functional group tolerance or limited substrate scope, because strong electrophilic fluorinating reagents such as fluorine gas or directing groups are required. Selective C–H fluorination of pyridines and diazines has been achieved by the Hartwig group using AgF_2 as both oxidant and fluorinating reagent via Chichibabin mechanism.[240] C–H bonds on the carbon next to nitrogen of heteroarenes are fluorinated exclusively, though with regioisomers when two similar C–H bonds are available.

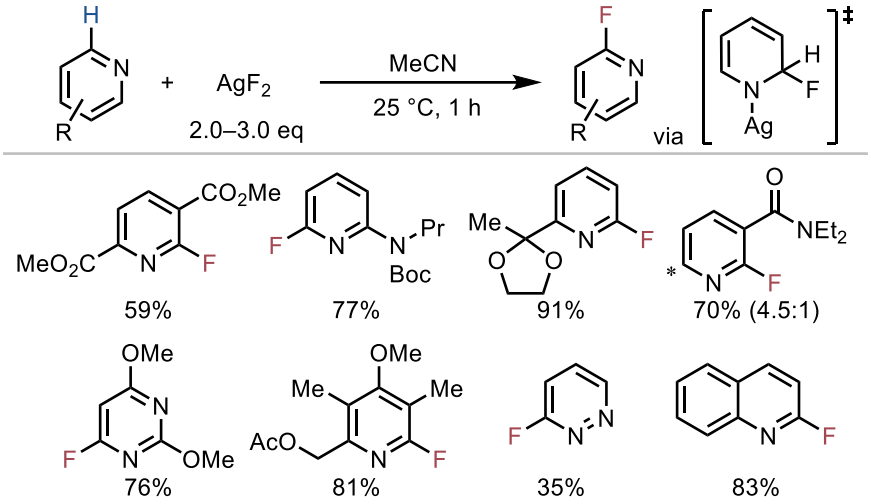

Figure II.13. AgF_2 mediated C–H fluorination of pyridines and diazines.

Recently, the Ritter group published a palladium catalyzed late-stage C–H fluorination, which enables access to fluorinated aromatics that are difficult to access otherwise (Figure II.14).[101] The reaction relies on a fine-tuned ligand system (a tridentate terpyridne and a bidentate 2-chloro-1,10-phenanthroline) and electrophilic fluorine reagent, such as Selectfluor or NFSI, to reach a hypothetical octahedral Pd(IV)–F species, which is proposed to be a highly reactive fluorine radical source. The palladium-catalyzed fluorination reaction worked well with highly functionalized arene substrates, which are not obtainable with Selectfluor or NFSI. However, regioisomers are produced together with the arene starting material and cause purification/isolation obstacles.

For most of the fluorination reactions, conventional heating or strong oxidants are often required for the fluorination to proceed efficiently. Fluorination methods, harnessing green energies, visible light or electricity for example, are eco-friendly alternatives.

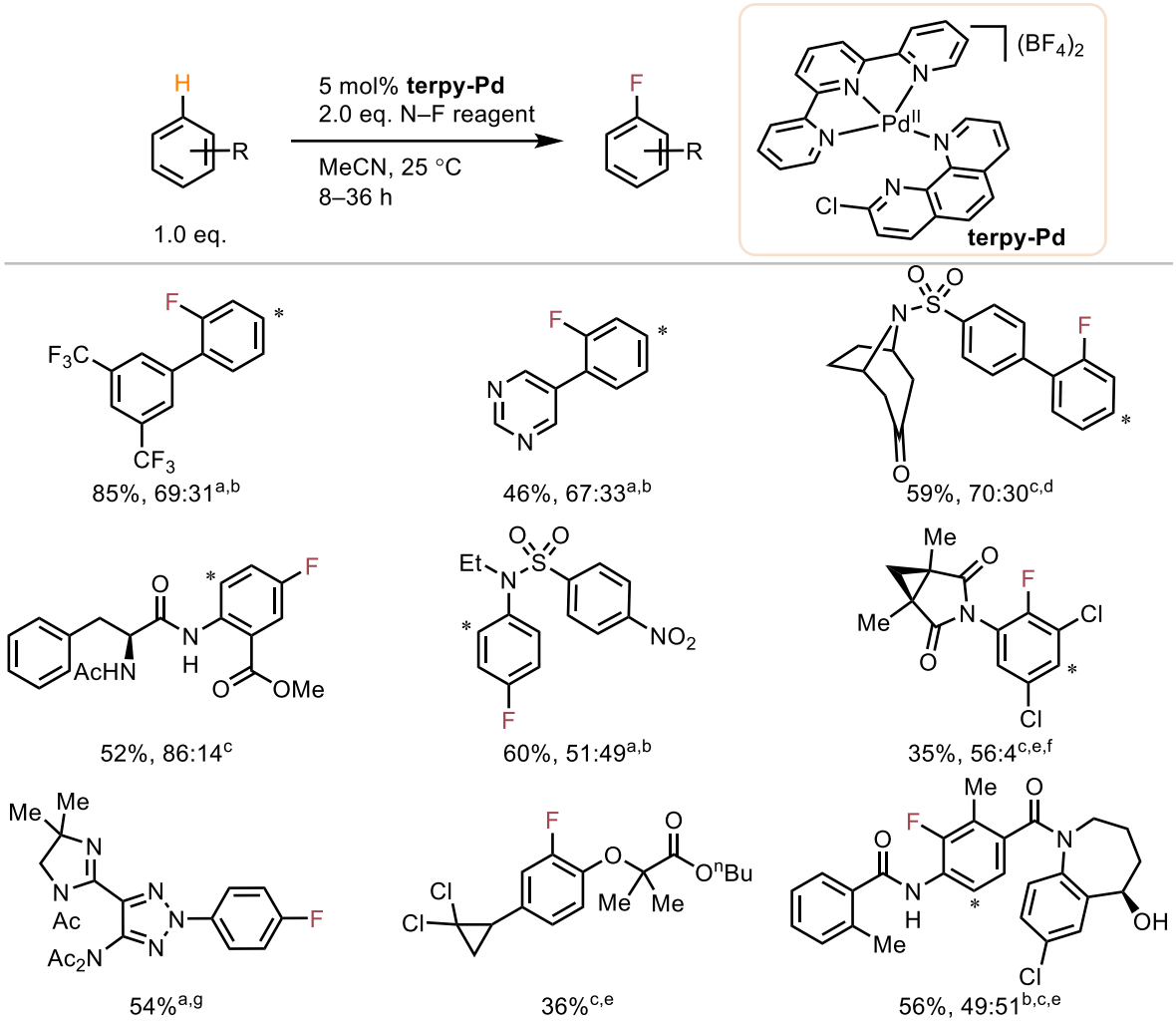

∗: the other regioisomer. a: reaction performed with Selectfluor. b: reaction performed at 50 °C.
c: rection performed with NFSI. d: reaction performed with DCE and MeCN (1:1, v/v, 0.1M).
e: 7.5 mol% catalyst was used. f: reaction performed at 80 °C. g: 10 mol% catalyst was used.

Figure II.14. Palladium-catalyzed electrophilic C–H fluorination of arenes in the absence of auxiliary tags.

II.1.2. Aryl radical precursors in photocatalysis

A renaissance in photocatalysis broke out with the development of organometallic chemistry marching to maturity.[241,242,243] In combination with fine-tuned ligands, metal complexes become reactive under various photoredox conditions, which navigate their application to more diverse bond formation and cleavage processes other than bleaching dark blue pigment. [244] Organo-photoredox catalysts have also been extensively applied to organic synthesis in the past decades,[245] and have similar reactivity to metal-photoredox catalysts. The follow up discussion will take a metal-photoredox catalyst as an example to explain their photochemical properties.

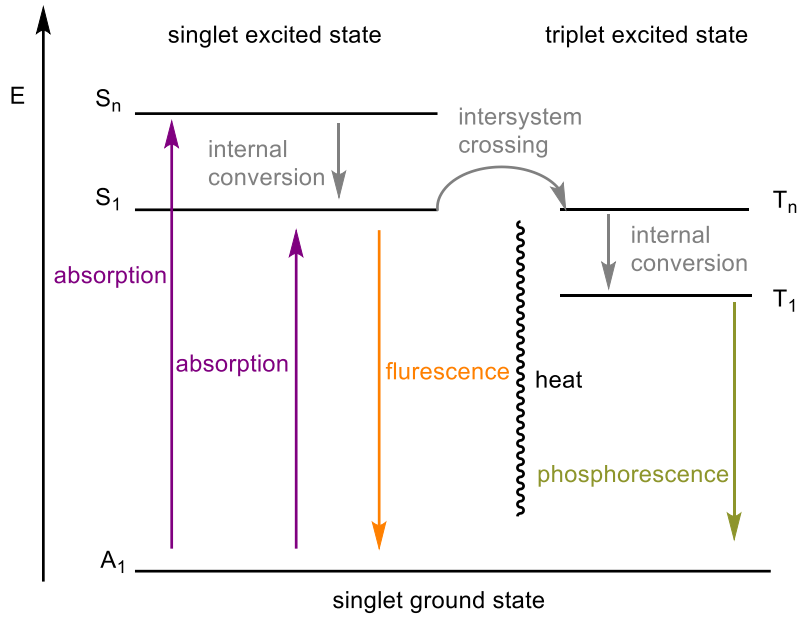

Figure II.15. Jablonski diagram.

As described in quantum mechanics,[246,247] a direct transition from the ground state to a triplet state is symmetry-forbidden according to the parity of the orbital wave functions during radiative processes (Figure II.15). Therefore, a modern photochemical active transition metal sensitizer reaches a singlet excited state via visible light absorption followed by (internal conversion and) intersystem crossing (ISC). A triplet excited state is generated and is mainly responsible for redox chemistry. More specifically, the redox-active excited species are most likely generated via a metal-to-ligand charge transfer where one electron shifts from a metal d orbital (HOMO) to a π* orbital (LUMO) of the ligand. As such, the excited species are both better reductants and oxidants compared to their ground states

considering the frontier molecular orbitals. Indeed, the excited metal complexes can be either oxidized or reduced under certain reaction conditions. When sequenced with another reduction or oxidation process, the ground state complexes can be regenerated, and the redox cycle completed (Figure II.16).

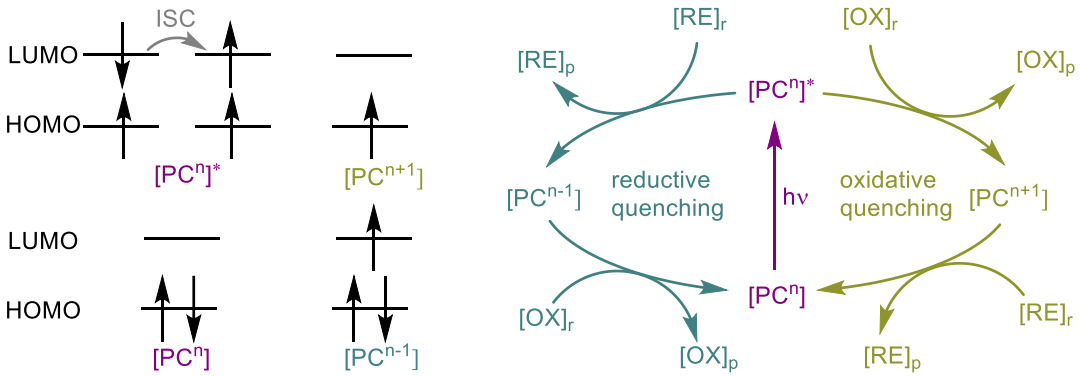

Figure II.16. Possible reaction pathways of the excited metal species under oxidation or reduction conditions.

Both the life-time and redox potential of the excited metal species can be adjusted by ligand modification,[248,249,250] which enables catalysis for a wide range of bond activation and formation that used to require high intensity UV light generated from specialized photoreactors. Therefore, the functional group tolerance of reactions is substantially increased, and substrate scope widened.

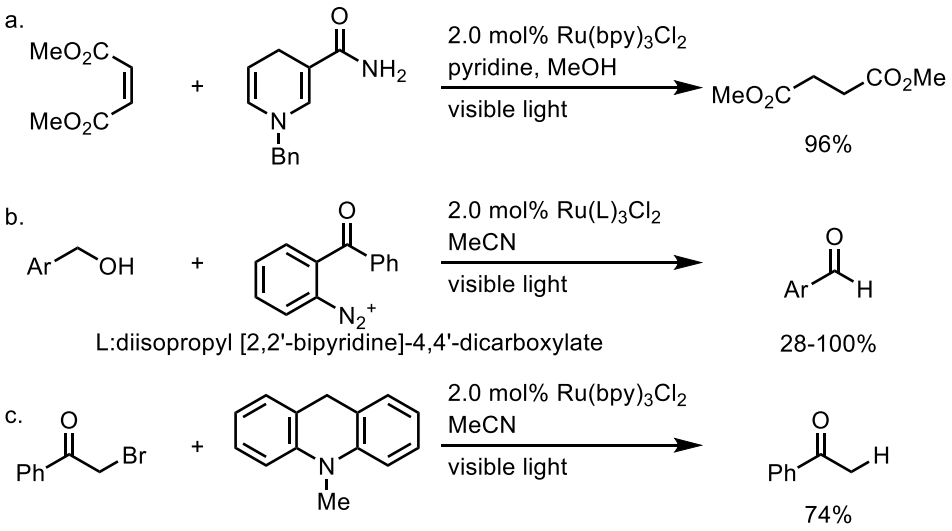

Figure II.17. Early examples of utilizing $Ru(bpy)_3Cl_2$ as a photoredox catalyst in organic synthesis in the 1980s and 1990s.

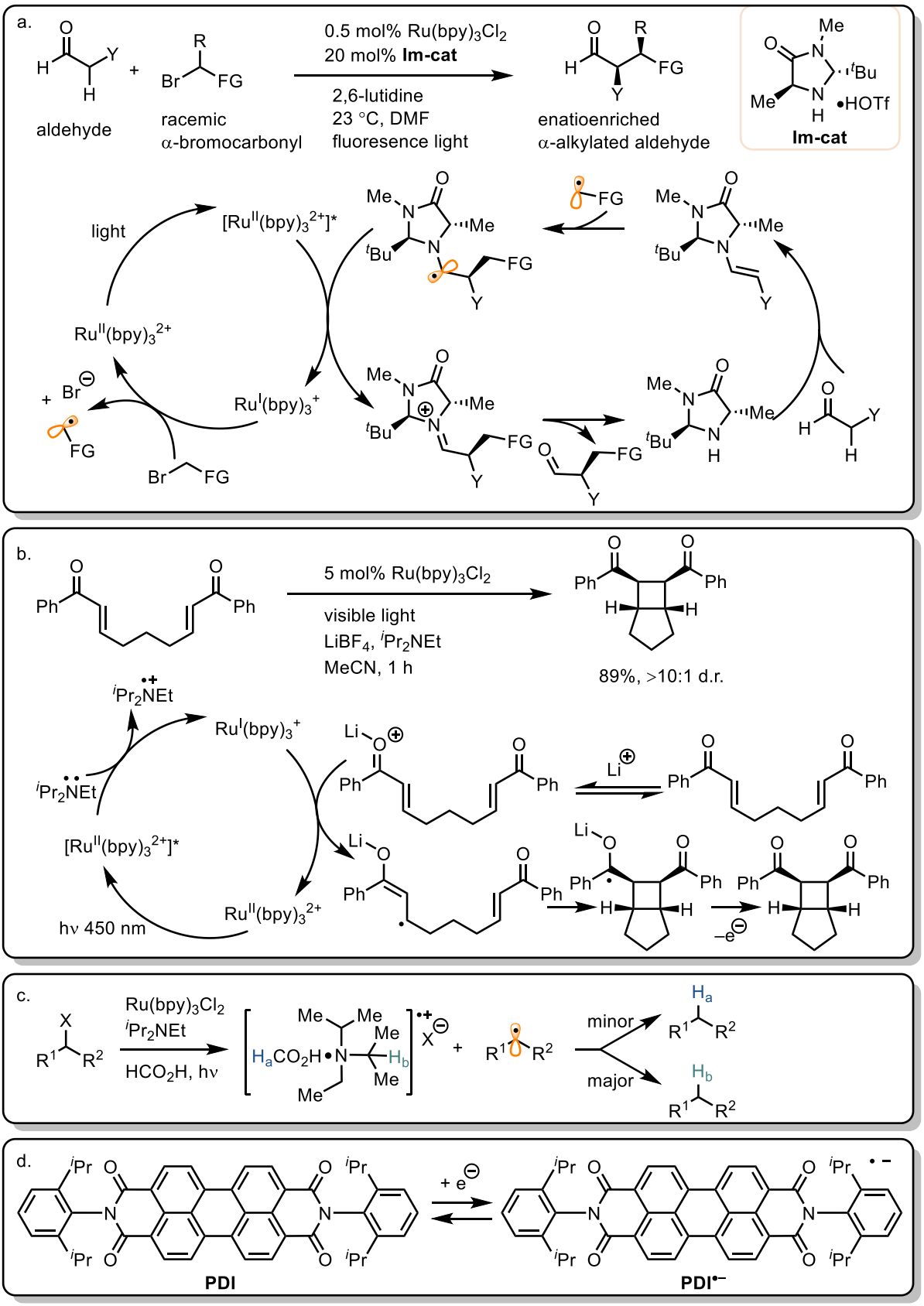

Figure II.18. Reactions, with metallophotoredox catalysts, stimulated the renaissance of photochemistry in organic synthesis.

Previously, these organometallics were used for harvesting light energy for production of chemical fuels. Applications for organic synthesis promoted by visible light were sparked (Figure II.17) in the late 20th,[251,252,253] mainly used for hydrogenation and dehydrogenation reactions. It was not until 2008, as a flash of insight that illuminated this photoredox chemistry area, the Yoon group, the Stephenson group, and the MacMillan group, all independently had the idea of using lightbulbs to solve challenging synthetic problems. In the MacMillan group, by a combination of both $Ru(bpy)_3Cl_2$ photoredox catalyst and an imidazolidinone organocatalyst (**Im-cat**), they harvested a C–C bond adjacent to an aldehyde in asymmetric manner, which was previously elusive (Figure II.18a).[254] The Yoon group harnessed solar energy to address a [2+2] cycloaddition of bis(enone) in the presence of the ruthenium photocatalyst (Figure II.18b).[255] Using the same photocatalyst, the Stephenson group was able to develop a tin-free reductive dehalogenation reaction (Figure II.18c).[256] Later on investigation done by the König group even enabled reduction of aryl halides with visible light irradiation via a consecutive photoinduced electron transfer on perylene diimides N,N-bis(2,6-diisopropylphenyl)perylene3,4,9,10-bis(dicarboximide) (**PDI**, Figure II.18d).[257]

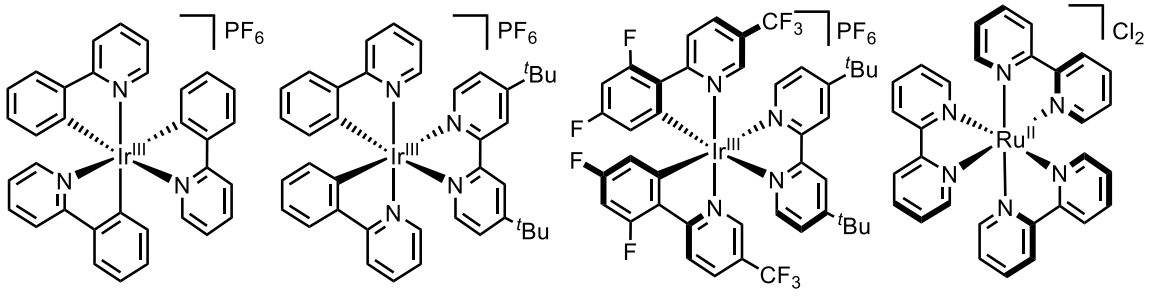

Figure II.19. Some photoredox catalysts with different ligands/metal centers and their corresponding reduction potentials (V vs. SCE).

In addition to diversifying the reaction paradigms beyond hydrogen transfer, another important characteristic of these photoredox catalysts is that their oxidation/reduction potentials are often easy to modulate via ligand modification (Figure II.19). This means a larger variety of redox potentials are available, which enables the use of mild oxidant/reductant in a catalytic system. Metallophotocatalysis, the merge of photoredox catalysis and transition metal

catalysis,[258] allows access to high valent transition metal species in the presence of weak reducing reagents. In addition, fundamental organic steps on conventional metal intermediates can be facilitated either by modulation of the oxidation state on the metal or through energy-transfer-mediated excitation of intermediate metal species. As such, the recently emerged versatile platform permits accomplishment of challenging bond synthesis via new mechanistic pathways that were previously elusive.

In combination with versatile photoredox catalysts, conventional transition metal catalysts evolved catalytic cycles containing co-existent oxidation states, often high oxidation states that are hard to access or proven not compatible with other oxidation states in one pot, for instance Cu(III) and Cu(I) that easily react with each other to form Cu(II) species. The energy barrier for reductive elimination from these high valent metals decreases for most cross-coupling reactions, which enables challenging bond formations like C–O, C–F and C–CF_3 on one hand, and lowers reaction temperatures to near room temperature for conventional C–C and C–N cross coupling on the other hand. The first example reported by the Sanford group regarding C–H arylation of arenes in the presence of auxiliary groups was proposed to be facilitated by a Pd(II)-Pd(III)-Pd(IV)-Pd(II) cycle in combination with a Ru(II)-Ru(II)*-Ru(III)-Ru(II) cycle (Figure II.20a).[259] As data show, the C–C bond formation can be achieved at room temperature, which is not so easy for normal Pd(0)-Pd(II)-Pd(0) cycles at room temperature. A later report by the same group on copper catalyzed trifluoromethylation of arylboronic acid represents one of the most mild and practical reaction conditions for aryl–CF_3 cross coupling to that date (Figure II.20b),[260] as the reaction operates with ICF_3 at 60 °C in the absence of strong acids or bases (trifluoroacetic acid or ^{t}BuOK). Also, the mechanism was proposed to involve an aryl–CF_3 reductive elimination from Cu(III) species in the presence of Cu(I) species. The most outstanding achievement in this field would be the merging of photoredox with nickel catalysis done by the Doyle and MacMillan groups (Figure II.20c),[261] which enables the possibility to access a Ni(0)-Ni(II)-Ni(III)-Ni(I)-Ni(0) cycle. No elusive presence of Ni(0)-Ni(III) species in one catalytic cycle was observed/proposed before. In combination with iridium photocatalyst, a decarboxylative C–C cross coupling was achieved at room temperature.

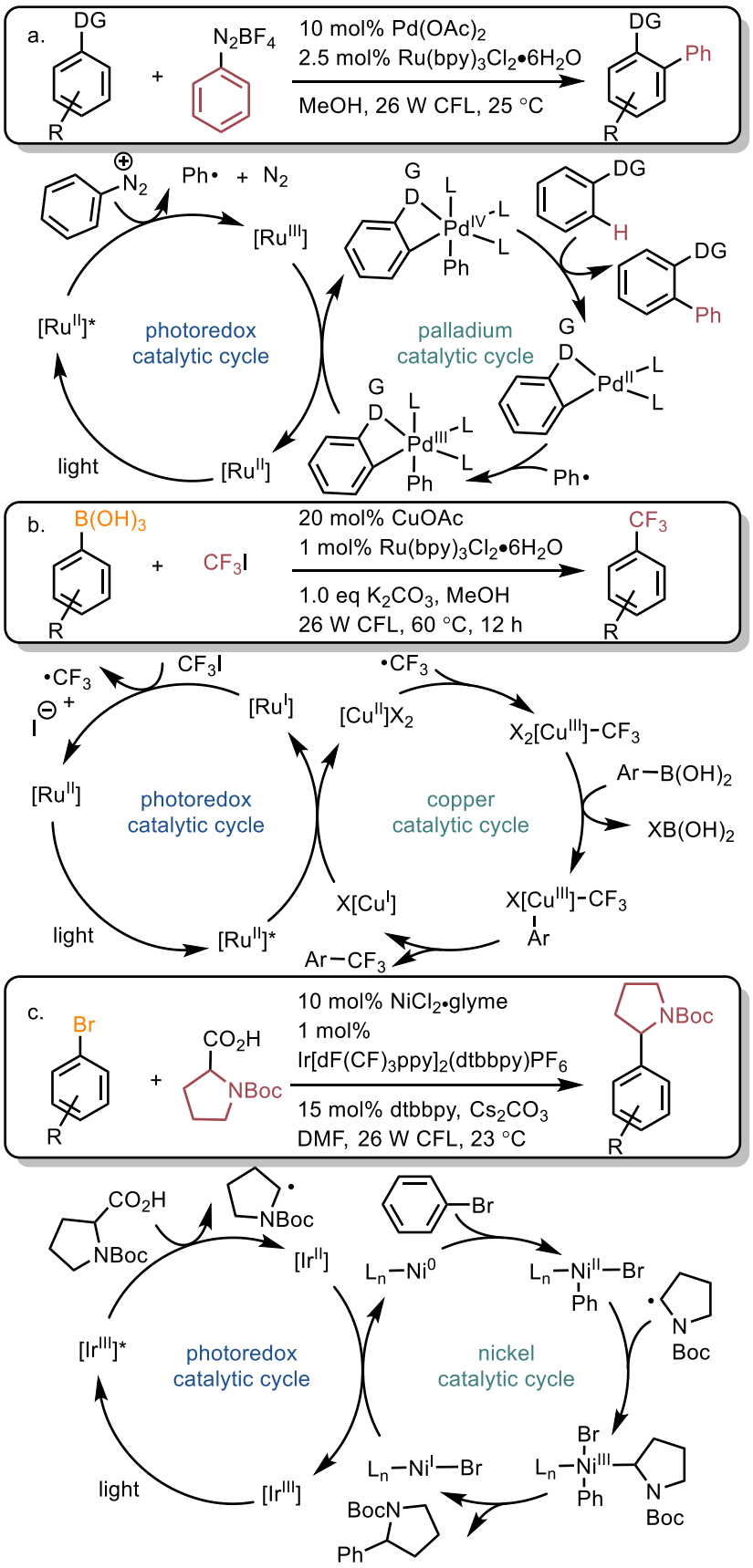

Figure II.20. Metallophotoredox examples at the early stage.

Nevertheless, visible light mediated photoredox functionalization, harnessing aryl radicals, are not so widely applied. Because the most diverse aryl radical precursors, aryl halides, are still very challenging to engage in diverse transformations other than hydrodefunctionalization (Figure II.21a) or reactions compete with hydrogen atom transfer, such as aryl radical trap by (hetero)arenes and alkenes (Figure II.21b).[257] The only aryl radical generation method under visible-light photoredox catalysis was Macmillan's approach, with which aryl radicals can be generated from aryl bromides via bromide radical abstraction by *in situ* formed silyl radicals (Figure II.21c).[262]

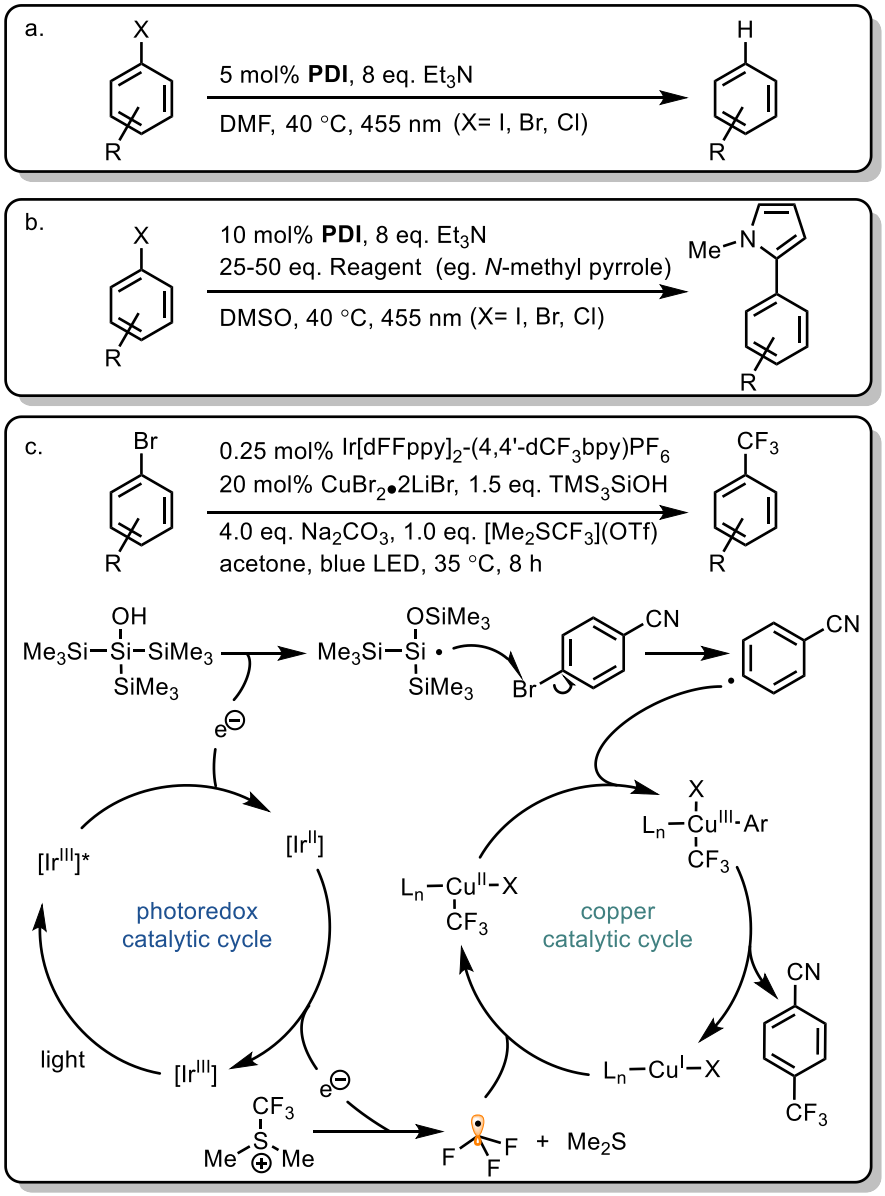

Figure II.21. Visible-light photocatalyzed aryl radical generation from aryl halides.

Generally, the most frequently utilized aryl radical precursors are aryl diazonium salts, diaryl iodonium salts, aryl sulfonyl chlorides, and aryl halides.[263] Under one electron reduction processes, those species can be reduced by one electron to afford radical ions, which undergo mesolytic cleavage to deliver aryl radicals and ions (aryl salts precursors result aryl radicals and neutral species). As shown in the scale chart (Figure II.22), aryl diazoniums and diaryl iodoniums can be easily reduced, which permits their applications in photoredox catalysis under visible light irradiation. However, their relatively low thermo-stability and confined accessibility impose restrictions on their broad applications. Alternatively, aryl sulfonyl chlorides were used for visible-light photocatalyzed desulfonylative C–C cross coupling reactions to generate heterobiaryls with heteroarenes such as pyrrole, thiophene and furan derivatives.[264,265] Stable aryl sulfonyl chlorides also suffer from similar availability limitations. The most convenient, readily available, and stable aryl halides, however, require extreme negative reduction potentials that require ultra-visible (UV) light irradiation or visible-light conditions in combination with super reducing photocatalysts such as **PDI**.[266]

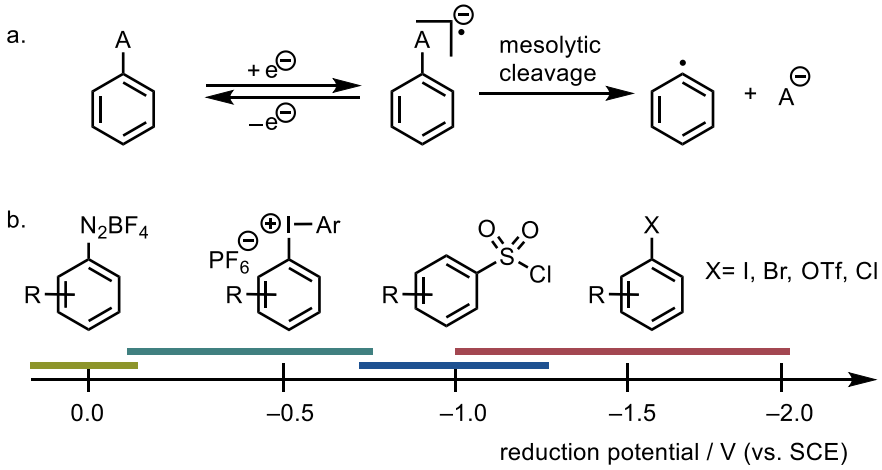

Figure II.22. One electron reduction of aryl radical precursors, and the relative reduction potential of commonly used precursors.

II.2. Challenges for site-selective late-stage fluorination

As mentioned in Part II.1.1, positionally-selective fluorination reactions often require prefunctionalized arenes, which, in most cases, are hard to access selectively via direct C–H functionalization of highly functionalized molecules. One of the most promising and widely applied sequences, iridium-catalyzed C–H borylation of arenes followed by copper-catalyzed Chan-Lam type fluorination, often gives constitutional isomers at the borylation step. Other reported *para*-selective radical substitution reaction can provide aryl TEDA species with only one regioisomer, yet, the most successful follow-up transformation identified so far is reduction to afford amine.

So far, direct C–H fluorination of arenes in a selective fashion is achievable in the presence of auxiliary directing groups, which somehow limit its applicability due to the extra installation and removal steps or restricted accessibility to molecules with directing groups. That being said, a methodology, which affords fluorinated aromatics selectively directly by C–H functionalization of arenes, would be ideal.

II.3. Project design

Considering the high reactivity which aryl thianthrenium salts showed in transition-metal-catalyzed cross coupling and photoredox catalysis (see Part I.1.4), we aimed to identify why aryl thianthrenium salts are so special, whereas the conventional aryl halides are not so broadly applicable. Our interests focused on their photoredox reactivity because challenging bonds such as C–S, C–O, C–N, and C–CF_3 can be formed under photoredox reaction conditions. As for most of other photoredox catalyzed reactions, a radical intermediate was proposed at the start. To further evaluate the radical generation process, we introduced cyclic voltammetry to shed light on redox potentials of aryl thianthrenium salts and the follow up fragmentation rates to give aryl radicals. To show the high reactivity of aryl thianthrenium salt in photoredox catalysis, we attempted the challenging C–F bond formation.

So far, carbon-fluorine reductive elimination has not been reported for any metallophotoredox systems. For C–F reductive elimination to take place, as discussed in Part II.1.1, special ligands are often required especially when fluoride is used as the fluorine source. We are aware of the possibility for C–F bond formation from high-valent transition metals such as Cu(III) at room temperature, most likely in the presence of simple pyridine ligands. Meanwhile, we have successfully achieved C–S, C–O, C–N, and C–CF_3 bond formations from aryl thianthrenium salts when combining photoredox catalysis with copper reagents. Therefore, we started our trials for fluorination of aryl thianthrenium salts using copper reagents under photoredox catalysis.

II.4. Results and discussion

Parts of this chapter are taken, with permission, from our published work in Nature Chemistry.[188] *The fluorination reaction has been developed by the Dr. Ruocheng Sang, the author and Dr. Jiakun Li. The substrate scope was explored by Dr. Jiakun Li, the author and Dr. Ruocheng Sang. X-ray analysis, DFT calculations and EPR data were collected by Dr. Matthew B. Plutschack. Fluorescence quench experiments were executed by Dr. Matthew B. Plutschack and the author. The CV experiments were designed, conducted, and analyzed by Dr. Wonseok Ham and the author. Dr. Jiakun Li and the author have conducted the rest bench chemical mechanistic experiments.*

II.4.1. Fluorination of aryl thianthrenium salts under photoredox catalysis

Under anhydrous and inert argon atmosphere, fluorination of aryl thianthrenium salts takes place in the presence of 1.2 equiv. of CsF, 1.5 equiv. of $Cu(MeCN)_4BF_4$ and 1 mol% of $Ir[dF(CF_3)ppy]_2(dtbpy)PF_6$ in acetone under visible light irradiation at 455 nm.

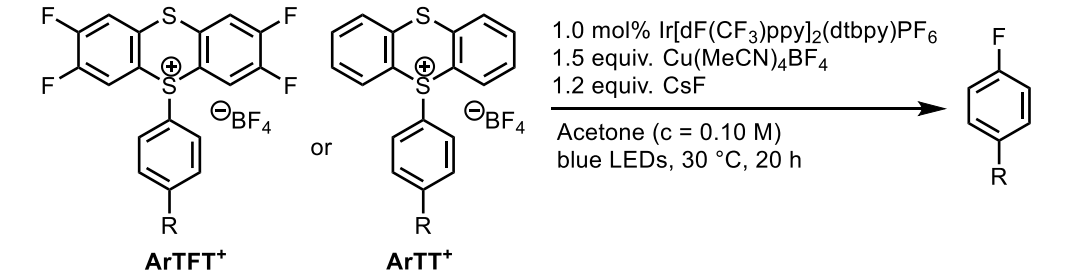

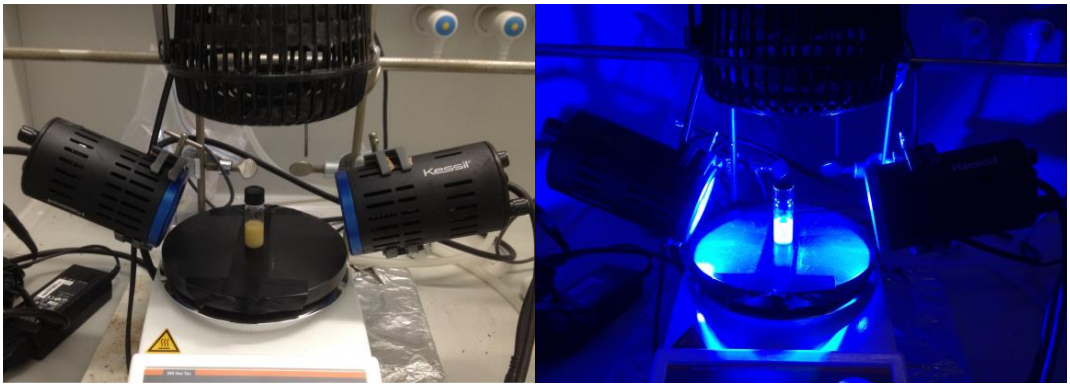

Figure II.23. General reaction conditions for fluorination of aryl thianthrenium salts and its reaction set up.

Control experiments (*vide infra* Part III.3.3) showed that all the reagents are essential to obtain the fluorinated products in high yields. In the absence of

photocatalyst, the C–S bond of aryl thianthreniums fragments with visible light, albeit very slowly (8% conversion over 20 h, Table II.1, entry 2). The fact that fluorination was observed without photocatalyst can be explained by a light induced homolysis of aryl thianthreniums to yield an aryl radical and thianthrene radical cation. Product formation in the absence of CsF (Table II.1, entry 4) can be rationalized by a Balz-Schiemann type reaction where fluoride is abstracted from the tetrafluoroborate counterion. All the reaction components are essential to achieve high selectivity for fluorination over hydrodefunctionalization.

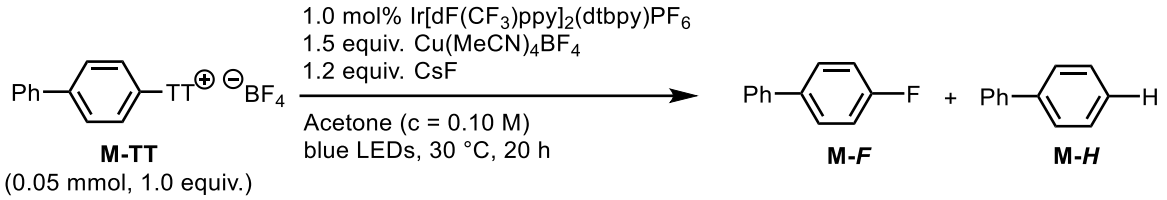

Entry	change of reaction conditions	Yield of **M-*F***[a]	Ratio of **M-*F*/M-*H***[b]
1	none	84%	43:1
2	no $Ir[dF(CF_3)ppy]_2(dtbpy)PF_6$	8%	2.7:1
3	no $Cu(MeCN)_4BF_4$	0%	--
4	no CsF	14%	0.9:1
5	no light	0%	--

Table II.1. Control experiments. (a) Yield was determined by ^{19}F NMR using 4-fluorobenzotrifluoride as an internal standard. (b) Ratios were determined by GC-FID. (in collaboration with Dr. Jiakun Li)

The use of acetone as solvent also had a major effect on the suppression of the hydrodefunctionalization reaction, yet the effect is not clear in the moment. Variation in alkali metal as the source of fluoride showed only slight difference in yields but affected the selectivity for fluorination and hydrodefunctionalization (*vide infra* Part III.3.3.4). Typically, the reaction was performed at 0.1 M concentration (84%), although higher concentrations (0.5 M) did not result in lower yield (85%) in the evaluated cases (*vide infra* Part III.3.3.8). Both aryl thianthrenium ($ArTT^+$) and tetrafluorothianthrenium ($ArTFT^+$) salts can successfully participate in fluorination

(*vide infra* Part III.3.3.2, Figure III.6), with the thianthrenium congeners typically affording higher yield (82% with $ArTT^+$ vs. 59% with $ArTFT^+$).

Evaluation on different copper sources revealed that only Cu(I) salts with less coordinative ligands were effect for the fluorination step. Sources like $CuI/Cu_2O/Cu(BF_4)_2$ only gave hydrodefunctionalized products (*vide infra* Part III.3.3.6). Comparison of different photocatalysts showed that $Ir[dF(CF_3)ppy]_2(dtbpy)PF_6$ was the optimal (*vide infra* Part III.3.3.7), which can be explained by its good redox potential match with aryl thianthreniums.

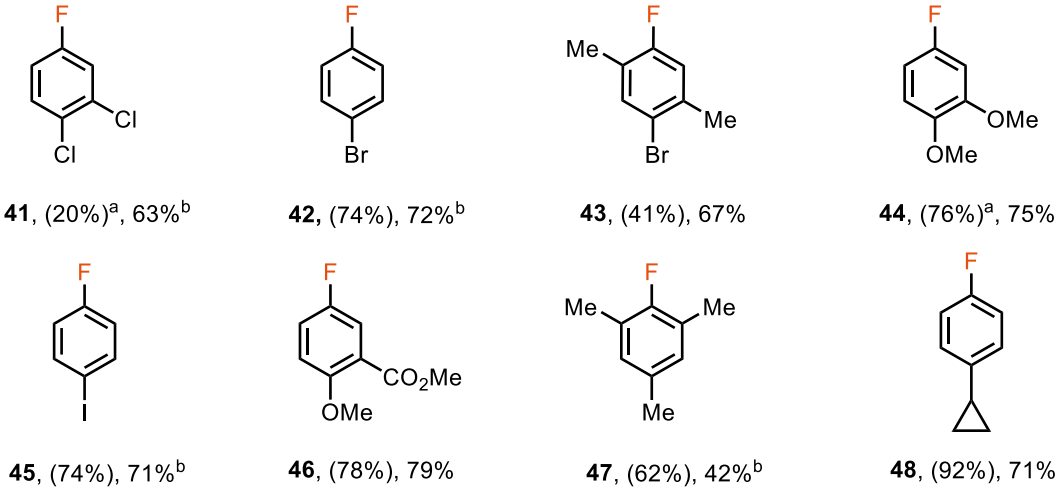

41, (20%)[a], 63%[b] **42,** (74%), 72%[b] **43**, (41%), 67% **44**, (76%)[a], 75%

45, (74%), 71%[b] **46**, (78%), 79% **47**, (62%), 42%[b] **48**, (92%), 71%

Figure II.24. Selected examples for aryl thianthrenium salts with various electronic substituents. Yields in brackets: Yield of the thianthrenation. Second yield: Yield of the fluorination. (a) Yields of volatile fluorides are reported based on ^{19}F NMR integration of reaction mixtures with internal standard. (b) Yield of the thianthrenation from reference 150. (in collaboration with Dr. Jiakun Li and Dr. Ruocheng Sang)

Electronic properties on the arene do not affect much for the fluorination step (Figure II.24). All electron-deficient (**41**, **42**, **45**), -neutral (**43**, **46**, **48**), and -rich arenes (**44** and **47**) gave the fluorinated products in yields between 42% and 79%. Hammett plot analysis with aryl tetrafluorothianthrenium salts also gave a slope of 0.662 ($\rho = 0.662$, Figure II.25), which suggests a rate-determining step for the fluorination reaction being not very sensitive to aryl substituents. In combination with the later electrochemical data, a mechanism involving a rate-determining electron transfer followed by a fast fluorination was proposed. The off-trend phenyl substituent can also be explained by its extended π system, which can enhance

the rate for the single electron transfer step, thus increase its overall fluorination rate.

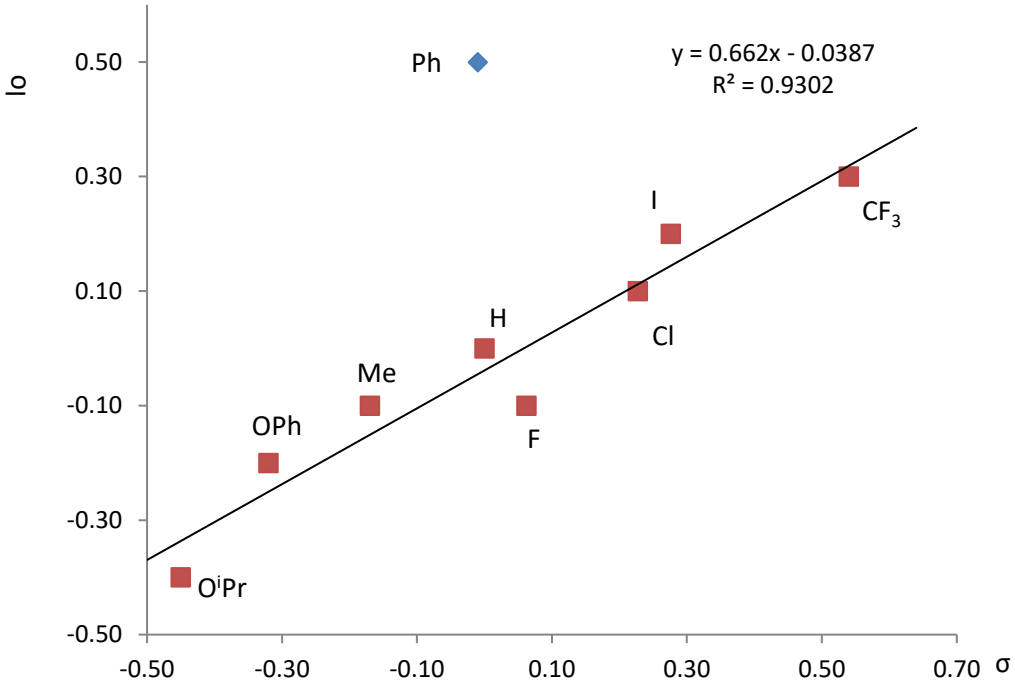

Figure II.25. Hammett-plot for the fluorination of aryl tetrafluorothianthrenium salts.

Substrates bearing *ortho* substituents (**43**, **47**, **49**, **54**) worked well for fluorination, though *ortho* di-substituted mesityl thianthrenium salts gave relatively lower yields. Examination of functional group tolerance was conducted on both small and complex molecules (Figure II.26). The reaction is tolerant towards esters (**46** and **58**), aldehydes (**51**), benzyl ethers (**53**), carbamates (**55**), amides (**52**, **54**, **56**, **58**, **59**), heterocycles (**58**, **59**, **60**, **61**), and acid-sensitive glycosidic linkages (**57**). Protic groups such as alcohols (**50**) and phenols (**49**) and tertiary amines (**60**), which are not compatible with previous nucleophilic or electrophilic transition-metal-catalyzed fluorination reactions, are tolerated in copper-mediated photoredox fluorination. Aryl chlorides (**41**, **54**, **58**, **59**), bromides (**42** and **43**), and iodides (**45** and **60**) that are general aryl electrophiles, did not participate here, possibly due to their high redox potentials which render them inactive aryl radical precursors under visible-light irradiation as discussed in Part II.1.2.

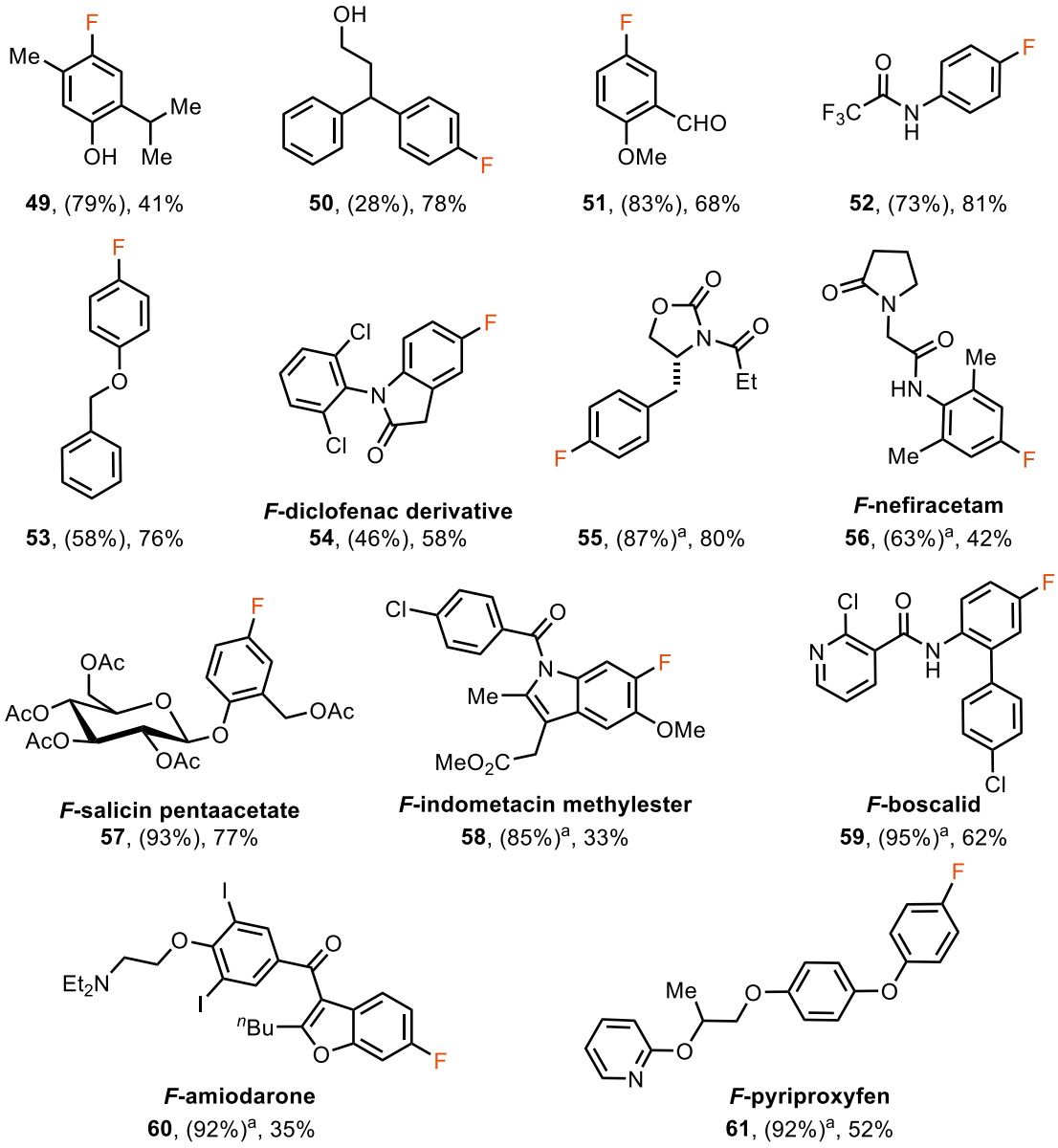

Figure II.26. Continued substrate table containing small complex molecules and various functionalities. Yields in brackets: Yield of the thianthrenation. Second yield: Yield of the fluorination. (a) Yield of the thianthrenation from reference 150. (in collaboration with Dr. Jiakun Li and Dr. Ruocheng Sang)

To further understand the difference in reactivity between aryl thianthrenium salts and aryl halides, competition reactions between anisole-derived thianthrenium salt and various aryl halides were executed under standard photoredox fluorination reaction conditions. As expected from Part II.1.2, no aryl halides were consumed in any examined cases, because aryl halides are not easily reduced by one electron under photoredox conditions. The results are consistent with data in literature: Aryl halides are generally either too difficult to

reduce, or fragmentation to the productive aryl radical is too slow to engage in Cu(III) metallophotoredox catalysis. Electron-rich aryl halides are often prohibitively difficult to reduce, yet the corresponding putative aryl halide anion radicals would fragment rapidly, while the opposite is true for electron-poor aryl halides. Efficient Cu(III) photoredox cross-coupling requires both a suitable reduction potential of the aryl (pseudo)halide which should be positive enough to be accessible by a photoredox catalyst, and a sufficient high fragmentation rate of the aryl halide radical anion to minimize undesired electron transfer processes between the aryl halide anion radical and high-valent metal catalysts. In other words, a high reduction potential is required for productive reduction by common photoredox catalysts in the presence of high valent metals, whereas a high rate constant is required for productive fragmentation. Yet, 4-fluoroanisole was observed in some cases, which suggested, at least, anisole radical is accessible from anisole-derived thianthrenium salts under standard reaction conditions. Thus, we studied the corresponding reduction potential and fragmentation rate for aryl thianthrenium salts by using cyclic voltammetry (*vide infra* Part III.3.6.4). While rate determining electron transfer is only confined to the electrochemical experiments, the fragmentation rate constants are relevant to the catalytic cycle as well since they are not dependent on the rate of reduction.

II.4.2. Systematic investigation on the photoredox properties of aryl thianthrenium salts

Irreversible cyclic voltammograms of aryl thianthrenium salts suggested irreversible electrochemical processes, which, in most case, involve a rate-determining electron transfer step followed by a fast chemical reaction (*vide infra* Part III.3.3.4). Therefore, a linear relationship between peak potential (E_p) and log υ (υ: potential sweep rate) is expected. For acetophenone-derived thianthrenium BF_4, severe nonlinearity in the plot of peak potential (E_p) versus log υ (υ: potential sweep rate) was observed. Such phenomenon was minimized by examining the cyclic voltammogram without phenol additive. The severe nonlinearity observed in the absence of phenol can be explained by the limited proton donor in the electrolyte, which could result in accumulation of aryl radicals around the electrode and therefore affect the observed electron current. For each arylthianthrenium salt, multiple cyclic voltammograms with varied potential sweep rates (ranging from 10

mV/s to 10 V/s) were obtained. To minimized ohmic drop introduced by the accumulated compounds on electrode surfaces, after each measurement, the working electrode was taken out of the glovebox, carefully polished and ultrasonically rinsed in distilled water before the next use. A fresh solution of arylthianthrenium salt, $TBAPF_6$, and phenol was used for each measurement to ensure consistency.

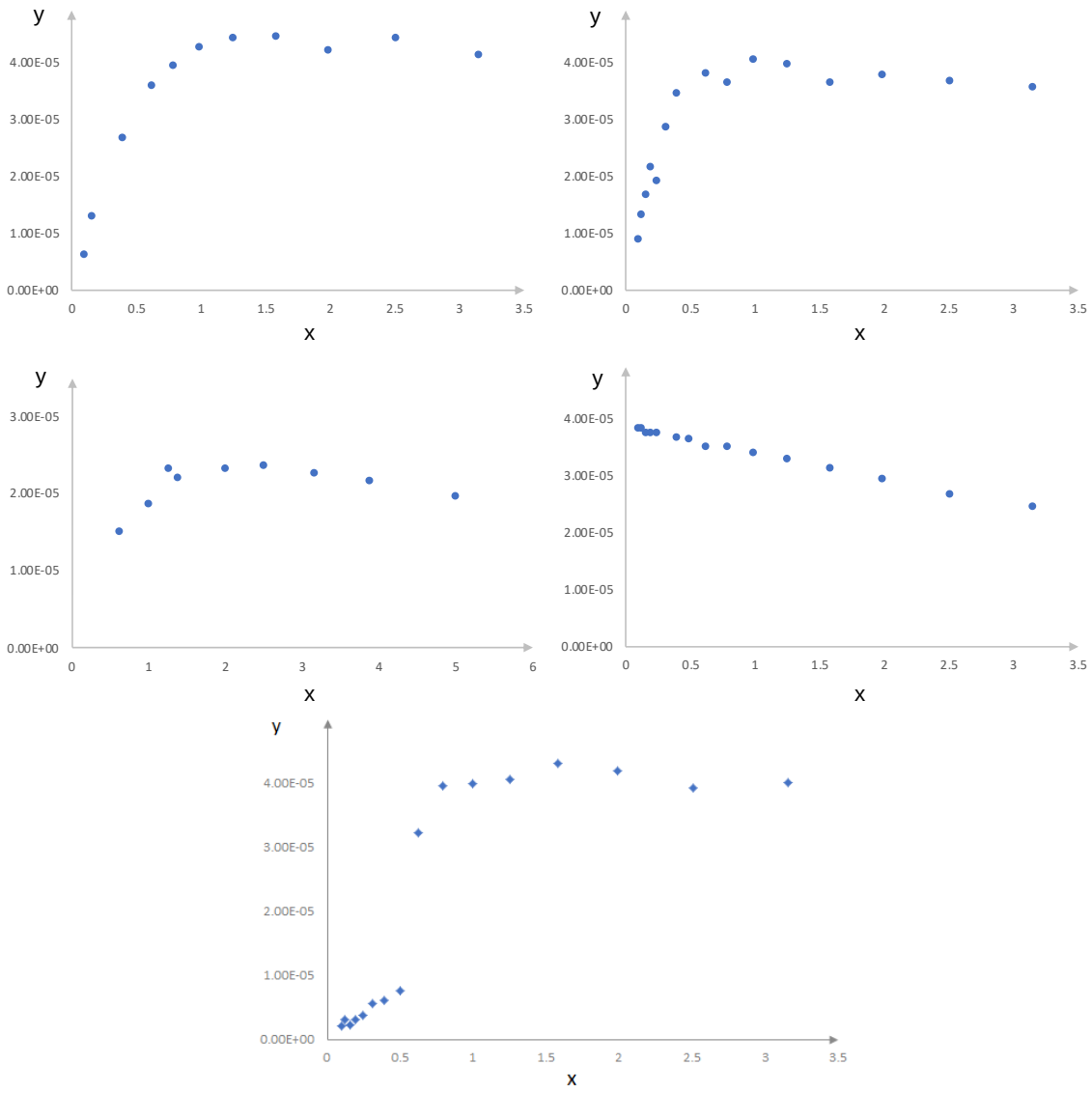

Figure II.27. Plot of $y = I_p/\upsilon^{1/2}$ ($A \cdot s^{1/2} \cdot V^{-1/2}$) versus $x = \upsilon^{1/2}$ ($V^{1/2} \cdot s^{-1/2}$) for arylthianthrenium salt compounds. Top left: anisole-derived thianthrenium BF_4. Top right: benzene-derived thianthrenium BF_4. Middle left: acetophenone-derived thianthrenium BF_4. Middle right: nitrobenzene-derived thianthrenium BF_4. Bottom: isopropoxylbenzene-derived thianthrenium BF_4. (in collaboration with Dr. Wonseok Ham)

Based on the Randles-Sěvćik equation and our analytical conditions (*vide infra* Part III.3.3.4), the diffusion coefficient D was approximated as 1.5×10^{-5} cm^2/s, which is a reasonable estimate for the molecular size of simple arylthianthrenium salts.[267] From known k_S^{el} values of related molecules, we approximate the k_S^{el} value of arylthianthrenium salt compounds to be 0.5 cm/s, which is a conservative guess.[268,269] Theoretically (*vide infra* Part III.3.6.4), the $I_p/\upsilon^{1/2}$ value is expected to be constant regardless of the sweep rate. In practice, except for the nitrobenzene-derived thianthrenium salt, the $I_p/\upsilon^{1/2}$ value is constant only for sufficiently high sweep rates, for which a second cathodic wave is not observable (Figure II.27 and *vide infra* Part III.3.6.4). We assign the first cathodic wave to correspond to the reductive cleavage of arylthianthrenium salt, while the second wave corresponds to an unidentified chemical process that inhibits the arylthianthrenium salt reductive cleavage at low sweep rates. Therefore, only the peak parameters of the first cathodic wave for the range of sweep rates, for which the $I_p/\upsilon^{1/2}$ value is constant, are suited for analysis of the uninhibited arylthianthrenium salt reductive cleavage. The $I_p/\upsilon^{1/2}$ value for the nitrobenzene-derived thianthrenium salt decreases gradually as the sweep rate increases, which we attribute to the inefficiency of diffusion processes at high sweep.[270]

We observed an irreversible cathodic wave corresponding to the reductive fragmentation of 4-methoxyphenyl thianthrenium salt **62** by cyclic voltammetry between –1.2 V and –1.5 V vs. SCE (*vide infra* Part III.3.6.4). While the peak width ($E_{p/2}–E_p$) remains constant at 110 mV, the peak potential (E_p) decreases linearly as a function of sweep rate with a slope of –65 mV, both consistent with the reductive fragmentation proceeding through a stepwise mechanism with rate-determining initial electron transfer. From the data of the first cathodic wave for the appropriate range of sweep rates, plots of peak potentials (E_p) and peak widths ($E_{p/2}–E_p$) versus log υ were constructed for anisole-derived thianthrenium BF_4 (**62**), benzene-derived thianthrenium BF_4 (**70**), acetophenone-derived thianthrenium BF_4 (**71**), nitrobenzene-derived thianthrenium BF_4 (**72**) and isopropoxylbenzene-derived thianthrenium BF_4 (**73**). The apparent transfer coefficient (α_{app}) for each sweep rate was calculated by the equation III–3 (*vide infra* Part III.3.6.4),[271] where T = 298 K. The plot of α_{app} versus log υ was also constructed.

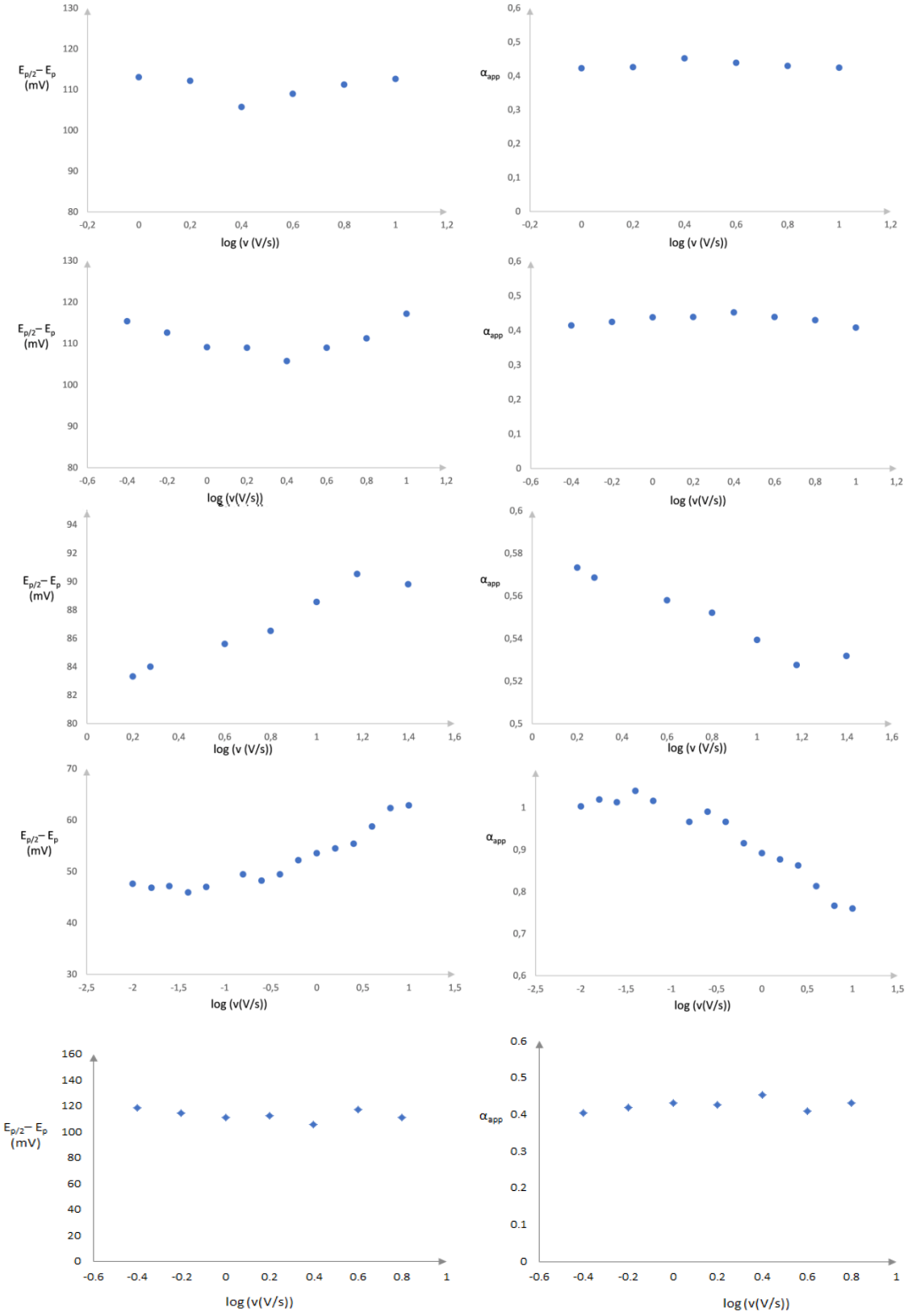

Figure II.28. Plot of ($E_{p/2}$–E_p) (left) and α_{app} (right) versus log υ for arylthianthrenium salt compounds. From top to bottom: anisole-derived thianthrenium BF_4, benzene-derived thianthrenium BF_4, acetophenone-derived

thianthrenium BF_4, nitrobenzene-derived thianthrenium BF_4, isopropoxylbenzene-derived thianthrenium BF_4. (in collaboration with Dr. Wonseok Ham)

For anisole-, bezene-, and *p*-isopropoxylbenzene-derived thianthrenium salts, the α_{app} was approximately constant over the range of sweep rate, indicating that the reductive cleavage occurs through a stepwise mechanism, and the electrochemical cleavage process is under kinetic control by the initial electrode electron transfer. In such a situation, the formal reduction potential (E^0) and fragmentation rate (k_c) were derived based on equations III–2 and III–5 (*vide infra* Part III.3.6.4). For the case of acetophenone- and nitrobenzene-derived thianthrenium salts, while the correlation between the peak potential and log υ appears roughly linear, the peak width increases (and thus α_{app} decreases) as the sweep rate increases. Such CV behavior indicates mixed kinetic control between the initial electron transfer and the subsequent fragmentation reaction. The decrease of α_{app} indicates a transition from mixed kinetic control by electron transfer and the subsequent chemical fragmentation to mainly kinetic control by electron transfer. The variation equations III–6 and III–7 (*vide infra* Part III.3.6.4) could be introduced here. After correlation with the corresponding theoretical curves, E^0 and k_c can be derived accordingly. The standard reduction potential was thus estimated by taking an average of E^0 values (Table II.2) calculated from the combinations of E_p and υ (Eq. III–2 to III-7).

R	**E^0 (V vs. SCE)**	**k_c (s^{-1})**
OMe	–1.51	1.0×10^{12}
H	–1.55	3.9×10^{12}
Ac	–1.25	3.2×10^{8}
NO_2	–0.96	1.6×10^{6}
O*i*Pr	–1.57	5.7×10^{12}

Table II.2. Tabulation of E^0 and k_c values of different *para*-substituted aryl thianthrenium salts. (in collaboration with Dr. Wonseok Ham)

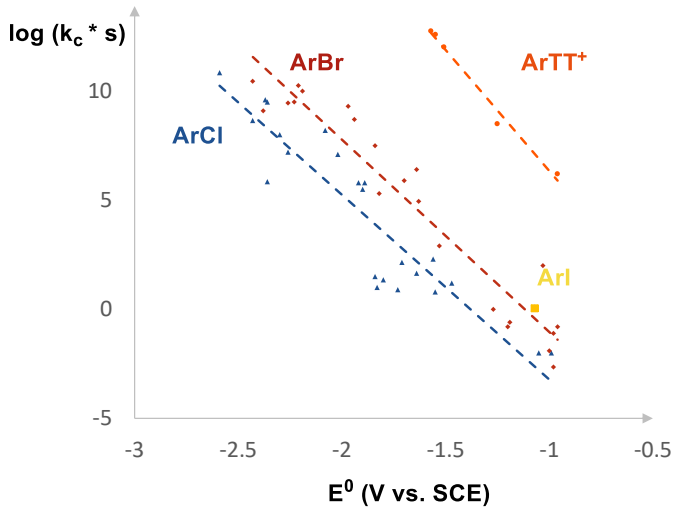

Figure II.29. Correlation between standard reduction potentials and fragmentation rate constants of aryl (pseudo)halides. Blue: aryl chlorides (in DMF).[272] Red: aryl bromides (in DMF).[272] Orange: aryl thianthrenium BF_4 (in MeCN). Yellow: 4-iodo nitrobenzene (in DMF).[273] (Constructed by Dr. Wonseok Ham)

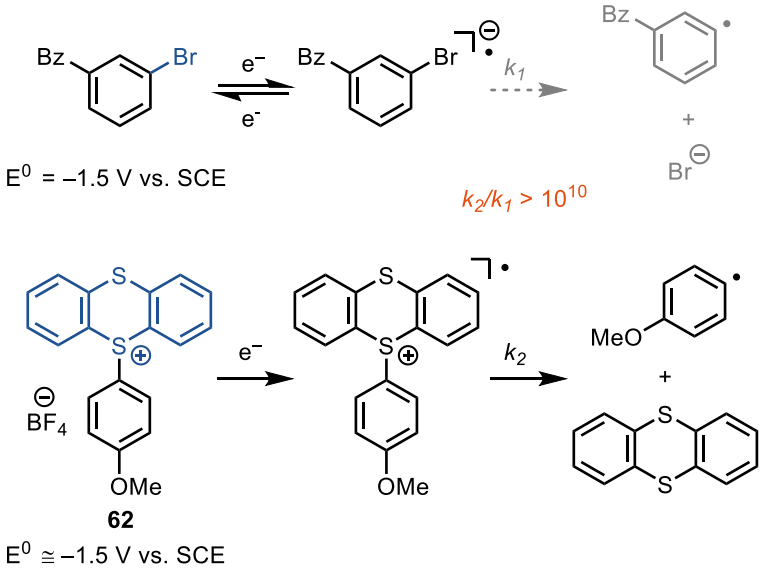

Figure II.30. Comparison between *ortho*-benzyl bromide and anisole-derived thianthrenium salt. (Dr. Wonseok Ham collected the data)

When presenting in a linear free-energy relationship for the standard reduction potentials of aryl halides and the rate constants for fragmentation of the corresponding aryl halide radical anions (Figure II.29). For compounds with similar reduction potentials, anisole-derived thianthrenium salt can exhibit a fragmentation rate that is 10 orders of magnitude faster than conventional aryl bromide (Figure

II.30). We proposed at this moment that due in part to the positive charge, arylthianthreniums are easier to reduce than aryl halides with identical substituents.

Calculation of the actual electron transfer rate constants relevant to our catalytic system additionally requires the knowledge of Marcus reorganization energy values,[274] and is beyond the scope of our work. However, we may combine the data from the electrochemical analysis (Figure II.29) and the Hammett analysis (Figure II.25) to gain insight into the kinetic situation in the catalytic system. In the electrochemical analysis, we found that the reductive cleavage processes of the three electron-rich aryl thianthrenium salts are controlled by the rate-limiting initial reduction at all scan rates employed, while those of the two electron-poor compounds are under mixed control depending on the scan rate. At high scan rates, all compounds except that derived from nitrobenzene (with the σ value that is not covered in our Hammett analysis) are controlled by the initial reduction. Given that the reduction potential difference between the thianthrenium compounds (ranging from –1.57 V to –1.25 V vs. SCE) and the photocatalyst ($E^0(Ir^{III}/Ir^{II})$ = –1.37 V vs. SCE) is small or even negative, the driving force for the initial reduction will also be small. It is conceivable, therefore, that the initial reduction is generally the rate-limiting step in the catalytic system. The positive Hammett ρ found in our analysis is consistent with such a hypothesis.

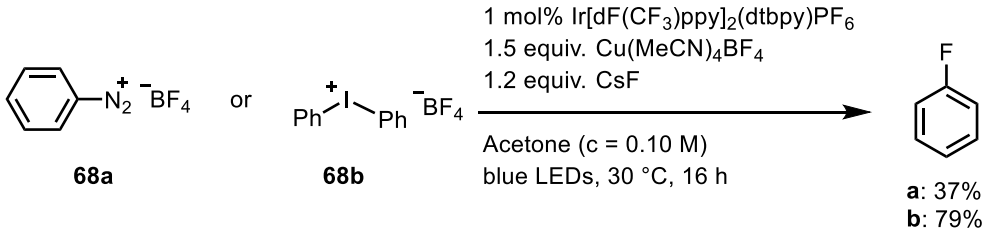

Figure II.31. Photocatalyzed fluorination of diazonium salt and iodonium salt. (in collaboration with Dr. Jiakun Li)

Additional experiments under the optimized reaction conditions were conducted for fluorination of aryldiazonium and diaryl iodonium salts, which have higher reduction potentials than the corresponding halides. The fluorobenzene was obtained in 37% and 79% yield, respectively, upon photolysis in the presence of iridium catalyst and copper(I) salt (Figure II.31). So far, we observed that aryl

radical precursors bearing positive charge on their leaving groups are essential for fluorination under copper-mediated photoredox catalysis, which we credited to faster electron transfer between the photocatalyst and the positively charged aryl salts.

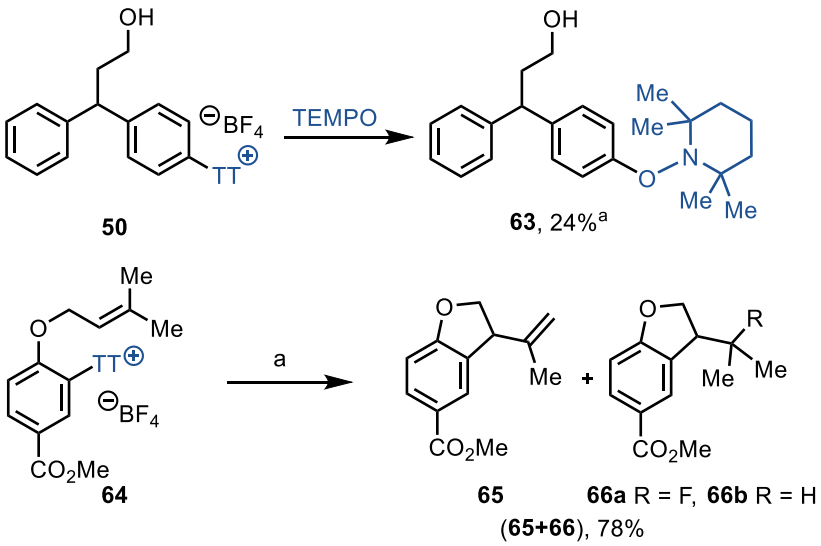

Figure II.32. Top: Radical trapping experiment. Bottom: Cyclization of prenyl ether **64** under standard reaction conditions. (a) standard reaction conditions (in collaboration with Dr. Jiakun Li)

Consistent with the formation of aryl radicals during catalysis, the 2,2,6,6-tetramethylpiperidin-1-oxyl (TEMPO) adduct could be isolated under the reaction conditions upon addition of TEMPO (Figure II.32). Likewise, the same adduct (**63**) was also observed when copper(I) was excluded from the reaction mixture, which rules out the possibility of a copper-mediated C–O coupling between $[ArTT]^+$ **50** and TEMPO. Furthermore, observation of cyclization products (**65** and **66**) in 78% combined yield of the prenyl ether **64** under standard reaction conditions supports a mechanism proceeding through aryl radicals.

A Stern-Volmer experiment (Figure II.33) for the fluorescence of iridium photocatalyst showed a significant quench effect from thianthrene with a rate of 10^9 $M^{-1}\times s^{-1}$, which is two orders of magnitude faster than the quench rate by $[Cu^I]$. Considering the energy match between oxidation potential of thianthrene [E^0 ($TT^{\bullet+}$/TT) = +1.26 V vs. SCE in CH_3CN][275] and reduction potential of photoexcited iridium catalyst [$E^{0'}$ ($^*Ir^{III}/Ir^{II}$) = +1.21 V vs. saturated calomel electrode (SCE) in CH_3CN][276], a reductive quenching cycle for the iridium catalyst was proposed.

Catalytic copper is achievable: fluorination of phenyl tetrafluorothianthrenium salt with 20 mol% $Cu(MeCN)_4BF_4$ afforded fluorobenzene in 65% yield (Figure II.34 a).

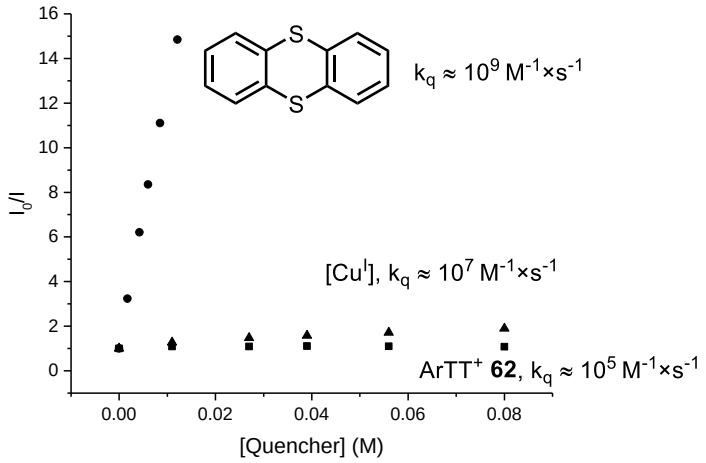

Figure II.33. Stern-Volmer plot of photocatalyst luminescence quenching by **62** (■), Cu(I) (▲), and thianthrene (●). I_0: luminescence intensity without quencher, I: luminescence intensity with quencher; k_q: quenching rate constant. (in collaboration with Dr. Matthew B. Plutschack)

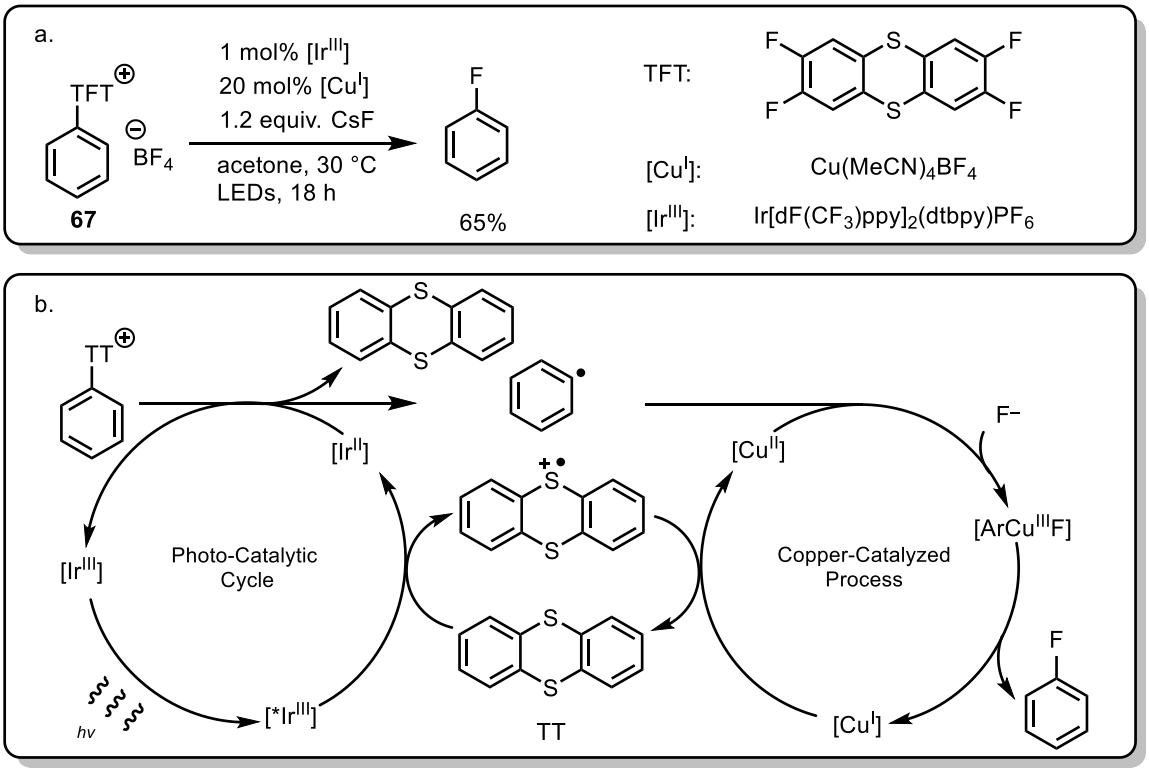

Figure II.34. Fluorination of aryl thianthrenium salts. (a) Specific example of C–H fluorination via arylthianthrenium salt by metallophotoredox catalysis. (b) Proposed mechanism for the fluorination of aryl thianthrenium ($ArTT^+$) salts. (c) Fluorination

of analogous aryl tetrafluorothianthrenium ($ArTFT^+$) salt. (in collaboration with Dr. Jiakun Li)

Based on the results from radical trap reactions, fluorescence quench experiments and catalytic fluorination of phenyl tetrafluorothianthrenium salt, we proposed a plausible mechanism combining a photo-catalytic cycle and a copper-catalyzed process to forge the fluorination of aryl thianthrenium salts under visible-light irradiation (Figure II.34b). As aforementioned, aryl thianthrenium salts can be reduced in the absence of photocatalyst to generate free thianthrene and the hydrodefunctionalized arenes. The free thianthrene yielded from such a decomposition process is presumed to be the initial source for reductive quench of the excited Ir(III) species to generate a thianthrene radical cation and an Ir(II) species. The resulting Ir(II) species undergoes single electron transfer (SET) with the rest aryl thianthrenium salts to regenerate the Ir(III) catalyst. On the other hand, mesolytic cleavage takes place on the resulting aryl thianthrenium radical cations after SET to afford free thianthrene and aryl radicals. The thianthrene radical cation species oxidizes Cu(I), while the resulting Cu(II) species is oxidized to Cu(III) by the aryl radicals. After ligand exchange or fluoride coordination, arylCu(III)F species can be formed and undergo subsequent reductive elimination to produce aryl fluorides and Cu(I) species. Although catalytic Cu is conceivable, a stoichiometric amount of inexpensive Cu(I) salt was utilized to eliminate the undesired amounts of hydrodefunctionalized side-product of complex small molecules.

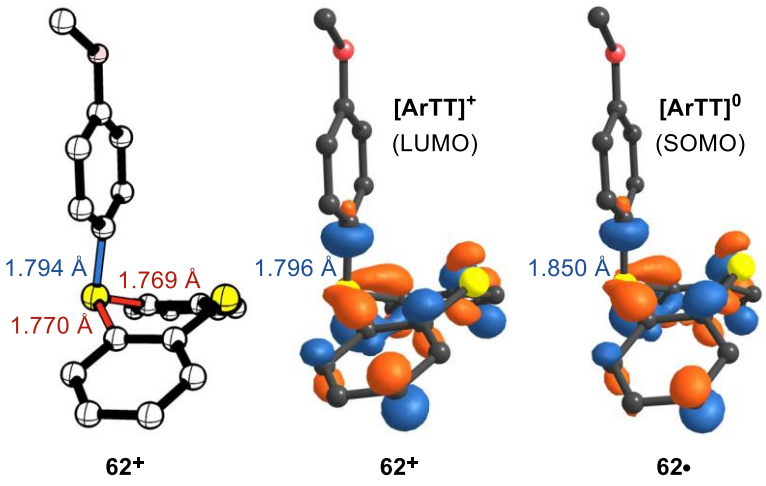

Figure II.35. Structural data for anisole-derived thianthrenium salt **62**. Left: X-ray structure of $[ArTT]^+$ (**62**$^+$) with relevant bond lengths. Middle: lowest unoccupied

molecular orbital of $[ArTT]^+$ (**62**$^+$) calculated by DFT. Right: singly occupied molecular orbital of $[ArTT]^0$ (**62•**) by DFT; *iso*-surface value = 0.06. (Data collected by Dr. Matthew B. Plutschack)

Structurally, arylthianthrenium salts have three C–S bonds, but synthetic utility can only be harnessed if chemoselective cleavage of the exocyclic C–S bond is achieved in preference to the other two endocyclic C–S bonds. X-ray crystallographic analysis of arylthianthrenium salt **62** (Figure II.35 left) shows the aryl substituent in a flagpole position with respect to the dithiine, with a significantly longer C–S bond than the other two C–S bonds within the thianthrene scaffold. Its chemoselective mesolytic cleavage can also be rationalized as a consequence of the antibonding nature of the exocyclic aryl C–S bond in the LUMO of $[ArTT]^+$ (**62**) and its lengthening upon reduction to the $[ArTT]^0$ radical (**62•**), as calculated by DFT (Figure II.35). The larger rate of arylthianthrene radical fragmentation when compared to aryl bromide radical anion fragmentation can thus be explained by the stereoelectronic alignment of the σ* orbital of the exocyclic C–S bond with the π-system of the thianthrene scaffold. Mesolytic cleavage of aryl bromides requires a bending motion to achieve sufficient population of the C–Br σ* orbital, which is orthogonal to the π framework; in both cases, the SOMO has the largest parentage in the π framework but only in the arylthianthreniums is it appropriately aligned to expel the leaving group.[277] The thianthrene-based LUMO of the arylthianthrenium salts can also explain why their reduction potential is less sensitive to substituent effects on the arene, which can be extracted from the length of the respective lines in Figure II.29.

II.5. Conclusion and outlook

In combination with the site-selective thianthrenation of arenes, this general photoredox-Cu(III) fluorination platform enables a two-step positionally-predictable late-stage fluorination of arenes. Copper catalysis is possible for the fluorination. Yet, purification of aryl fluorides from the corresponding hydro-counterparts is challenging. Addition of a stoichiometric amount of inexpensive Cu(I) salt eliminated the undesired amounts of hydrodefunctionalized side-product of complex small molecules that could be observed for reactions with catalytic copper. The proposed catalytic cycle shown in Figure II.34a represents a prototypical fluorination reaction with fluoride, which is catalyzed by an iridium(III) photocatalyst and a copper(I) cross-coupling catalyst, as supported Stern-Volmer analysis, EPR measurements, cyclic voltammetry data, DFT calculations, and radical trapping experiments.

Overall, we have articulated the specific electrochemical, structural, and stereoelectronic requirements for aryl leaving groups to address the challenge of copper(III)-mediated photoredox catalysis as a promising reactivity manifold. In contrast to mononuclear leaving groups such as bromide, complex leaving groups can bear a positive charge that can lower the reduction potential while maintaining the ability to engage in productive redox catalysis if they display appropriate stereoelectronic properties. The conceptual value of our contribution is therefore also to provide a suitable hypothesis for the design of new leaving groups that do not undergo deleterious side reactions and can therefore engage in metallophotoredox catalysis with copper or other metals.

III. EXPERIMENTAL PART

III.1. Materials and methods

All air- and moisture-insensitive reactions were carried out under ambient atmosphere and monitored by thin-layer chromatography (TLC). Concentration under reduced pressure was performed by rotary evaporation at 25–40 °C at an appropriate pressure. Purified compounds were further dried under high vacuum (0.010–0.005 mBar). Yields refer to purified and spectroscopically pure compounds. All air- and moisture-sensitive manipulations were performed using oven-dried glassware (130 °C for a minimum of 12 hours) and standard Schlenk techniques under an atmosphere of argon. A LED Kessil® A160WE was used as the light source. An Edinburgh Instruments spectrofluorometer FS5 was used for Stern-Volmer quenching experiments.

III.1.1. Solvents

Anhydrous acetone was purchased from Fisher Scientific GmbH. Before use, the anhydrous acetone used for fluorination was degassed by repeating freeze-pump-thaw cycling for three times. Anhydrous acetonitrile and tetrahydrofuran were obtained from Phoenix Solvent Drying Systems. All deuterated solvents were purchased from Eur*iso*-Top.

III.1.2. Starting materials

All substrates and reagents were used as received from commercial suppliers or prepared according to published procedures, respectively, unless otherwise stated. Tiny amount of trifluoroacetate counterion residues in the alkenyl thianthrenium salts do not interfere the following up transformations. For convenient operation, CsF was stored in a N_2-filled glovebox after being dried at 200 °C for more than 48 h under high-vacuum.

III.1.3. Spectroscopy and instruments

NMR spectra were recorded on a *Bruker Ascend™ 500* spectrometer operating at 500 MHz, 471 MHz, and 126 MHz, for ^{1}H, ^{19}F, and ^{13}C acquisitions, respectively. Chemical shifts are reported in ppm with the solvent residual peak as the internal standard. For ^{1}H NMR: $CDCl_3$, δ 7.26; CD_2Cl_2, δ 5.32; CD_3CN, δ 1.94;

$(CD_3)_2SO$, δ 2.50. For ^{13}C NMR: $CDCl_3$, δ 77.16; CD_2Cl_2, δ 53.84; CD_3CN, δ 1.32, 118.26; $(CD_3)_2SO$, δ 39.52. ^{19}F NMR spectra were referenced using a unified chemical shift scale based on the ^1H resonance of tetramethylsilane (1% v/v solution in the respective solvent). Data is reported as follows: s = singlet, d = doublet, t = triplet, q = quartet, quin = quintet, sext = sextet, sept = septet, m = multiplet, bs = broad singlet; coupling constants in Hz; integration. The *E*/*Z* ratio was determined by ^1H NMR, quantified by peak integrations of the characteristic *E*/*Z* alkenyl protons.

III.1.4. Chromatography

Thin layer chromatography (TLC) was performed using EMD TLC plates pre-coated with 250 µm thickness silica gel 60 F_{254} plates and visualized by fluorescence quenching under 254 nm UV light, permanganate stain, cerium ammonium molybdate stain, or phosphomolybdic acid stain. Flash chromatography was performed using silica gel (40–63 µm particle size) purchased from Geduran. Preparatory high-performance liquid chromatographic separation was executed on a Shimadzu Prominence Preparative HPLC system with an YMC-Triart C18 HPLC column.

III.1.5. Electrochemical analysis

The potential scale of all displayed voltammograms is referenced to the potential of a silver-wire quasi-reference electrode with a solution of $TBAPF_6$ in acetonitrile (c = 150 mM), which was calibrated after measurements for each compound. All potentials are reported after conversion to voltage versus SCE, and the conversion equation is displayed next to each voltammogram. The raw data regarding differential pulse voltammetry and cyclic voltammetry are processed with Qsoas (http://bip.cnrs-mrs.fr/bip06/qsoas/index.html).

III.2. Experimental data for thianthrenation of alkenes

Parts of this chapter are taken, with permission, from our published work in Angewandte Chemie International Edition.[192] *The alkene thianthrenation reaction has been developed by the author. Experimental data has been collected by the author with help from Dr. Jiakun Li and Dr. Matthew B. Plutschack.*

III.2.1. General procedure for thianthrenation of alkenes

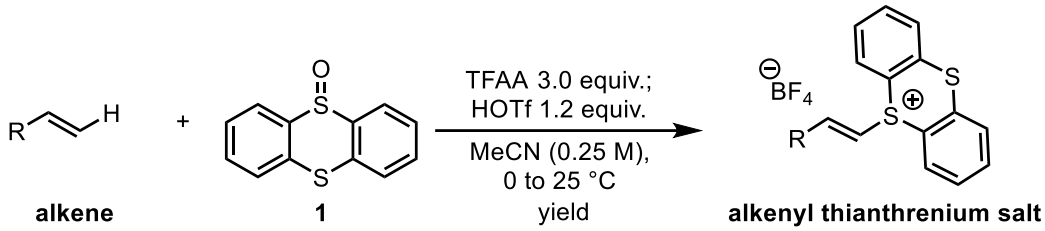

alkene **1** **alkenyl thianthrenium salt**

Under ambient atmosphere, a 20 mL borosilicate vial equipped with a magnetic stir bar was charged with alkene (0.500 mmol, 1.00 equiv.), thianthrene-*S*-oxide (**1**) (120 mg, 0.517 mmol, 1.03 equiv.), and MeCN (2.0 mL, c = 0.25 M). After cooling to 0°C, trifluoroacetic anhydride (0.21 mL, 0.31 g, 1.5 mmol, 3.0 equiv.) was added dropwise within 30 seconds, followed by dropwise addition of HOTf (52 µL, 88 mg, 0.59 mmol, 1.2 equiv.) within 10 seconds. After stirring the lilac mixture at 0 °C for 60 min followed by stirring at 25 °C for 30 min, the resulting light pink mixture was concentrated under reduced pressure and subsequently diluted with CH_2Cl_2 (10 mL). The CH_2Cl_2 solution was poured onto a saturated aqueous $NaHCO_3$ solution (ca. 20 mL). The combined mixture was poured into a separatory funnel, and the layers were separated. The CH_2Cl_2 layer was collected, and the aqueous layer was further extracted with CH_2Cl_2 (2 × ca. 10 mL). The combined CH_2Cl_2 solution was washed with aqueous $NaBF_4$ solution (2 × ca. 20 mL, 5 % w/w). The CH_2Cl_2 layer was dried over Na_2SO_4, filtered, and the solvent was removed under reduced pressure. The residue was purified by chromatography on silica gel eluting with CH_2Cl_2/*i*-PrOH to afford the alkenyl thianthrenium salt.

Synthetic examples for thianthrenation of alkenes

III.2.1.1 *trans*-4-Octene-derived thianthrenium salt **2-TT**

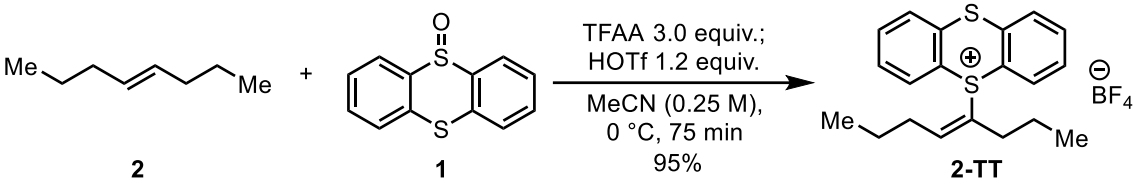

2 **1** **2-TT**

Under ambient atmosphere, a 20 mL borosilicate vial equipped with a magnetic stir bar was charged with *trans*-4-octene (78.5 µL, 56.1 mg, 0.500 mmol, 1.00 equiv.), thianthrene-*S*-oxide (**1**) (120 mg, 0.517 mmol, 1.03 equiv.), and MeCN (2.0 mL, c = 0.25 M). After cooling to 0°C, trifluoroacetic anhydride (0.21 mL, 0.31 g, 1.5 mmol, 3.0 equiv.) was added dropwise within 30 seconds, followed by dropwise addition of HOTf (52 µL, 88 mg, 0.59 mmol, 1.2 equiv.) within 10 seconds. After stirring the lilac mixture at 0 °C for 75 min, the resulting light pink mixture was concentrated under reduced pressure and subsequently diluted with CH_2Cl_2 (10 mL). The CH_2Cl_2 solution was poured onto a saturated aqueous $NaHCO_3$ solution (ca. 20 mL). The combined mixture was poured into a separatory funnel, and the layers were separated. The CH_2Cl_2 layer was collected, and the aqueous layer was further extracted with CH_2Cl_2 (2 × ca. 10 mL). The combined CH_2Cl_2 solution was washed with aqueous $NaBF_4$ solution (2 × ca. 20 mL, 5 % w/w). The CH_2Cl_2 layer was dried over Na_2SO_4, filtered, and the solvent was removed under reduced pressure. The residue was purified by chromatography on silica gel eluting with CH_2Cl_2/*i*-PrOH (100:1, v/v). The product-containing fractions were collected and concentrated under reduced pressure. The residue was further dried in vacuo to afford **2-TT** (*E*/*Z* < 50/1, 197.5 mg, 477 µmol, 95 %) as a colorless solid.

R_f = 0.46 (CH_2Cl_2/MeOH, 15:1, v/v).

NMR Spectroscopy:

^{1}H NMR (500 MHz, CD_2Cl_2, 298 K, δ): 8.01 (dd, *J* = 8.0, 1.3 Hz, 2H), 7.84 – 7.76 (m, 4H), 7.69 (ddd, *J* = 8.1, 7.1, 1.7 Hz, 2H), 6.42 (tt, *J* = 7.6, 1.4 Hz, 1H), 2.72 – 2.65 (m, 2H), 2.19 (m, 2H), 1.55 (h, *J* = 7.3 Hz, 2H), 1.35 (h, *J* = 7.3 Hz, 2H), 1.02 (t, *J* = 7.3 Hz, 3H), 0.76 (t, *J* = 7.3 Hz, 3H).

^{13}C NMR {^{1}H} (126 MHz, CD_2Cl_2, 298 K, δ): 149.4, 136.7, 135.1, 133.7,

131.4, 130.7, 130.5, 117.6, 35.2, 32.9, 22.7, 22.3, 13.9, 13.6.

^{19}F NMR (471 MHz, CD_2Cl_2, 298 K, δ): –152.29 (bs), –152.34 (bs).

HRMS-ESI (m/z) calc'd. for $C_{20}H_{23}S_2^+$ $[M]^+$, 327.12357; found, 327.12306; deviation: +1.56 ppm.

III.2.1.2 *cis*-4-Octene-derived thianthrenium salt **3-TT**

With 1.20 equiv. HOTf:

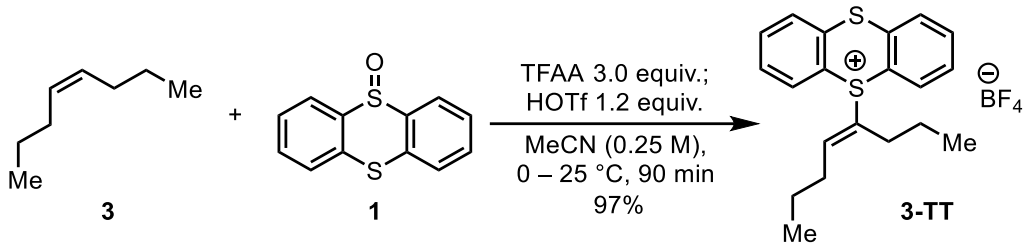

Under ambient atmosphere, a 20 mL borosilicate vial equipped with a magnetic stir bar was charged with *cis*-4-octene (77.8 µL, 56.1 mg, 0.500 mmol, 1.00 equiv.), thianthrene-*S*-oxide (**1**) (120 mg, 0.517 mmol, 1.03 equiv.), and MeCN (2.0 mL, c = 0.25 M). After cooling to 0°C, trifluoroacetic anhydride (0.21 mL, 0.31 g, 1.5 mmol, 3.0 equiv.) was added dropwise within 30 seconds, followed by dropwise addition of HOTf (52 µL, 88 mg, 0.59 mmol, 1.2 equiv.) within 10 seconds. After stirring the lilac mixture at 0 °C for 60 min followed by stirring at 25 °C for 30 min, the resulting purple mixture was concentrated under reduced pressure and subsequently diluted with CH_2Cl_2 (10 mL). The CH_2Cl_2 solution was poured onto a saturated aqueous $NaHCO_3$ solution (ca. 20 mL). The combined mixture was poured into a separatory funnel, and the layers were separated. The CH_2Cl_2 layer was collected, and the aqueous layer was further extracted with CH_2Cl_2 (2 × ca. 10 mL). The combined CH_2Cl_2 solution was washed with aqueous $NaBF_4$ solution (2 × ca. 20 mL, 5 % w/w). The CH_2Cl_2 layer was dried over Na_2SO_4, filtered, and the solvent was removed under reduced pressure. The residue was purified by chromatography on silica gel eluting with CH_2Cl_2/*i*-PrOH (100:1, v/v). The product-containing fractions were collected and concentrated under reduced pressure. The residue was further dried in vacuo to afford **3-TT** (*E*/*Z* ≅ 17/1, 200.6 mg, 484 µmol, 97 %) as a colorless solid. **3-TT** was further purified by chromatography on silica gel eluting with CH_2Cl_2/*i*-PrOH (100:1,

v/v), and fractions containing **3-TT(*E*)** were collected and concentrated under reduced pressure. The residue was further dried in vacuo.

With 2.40 equiv. HOTf:

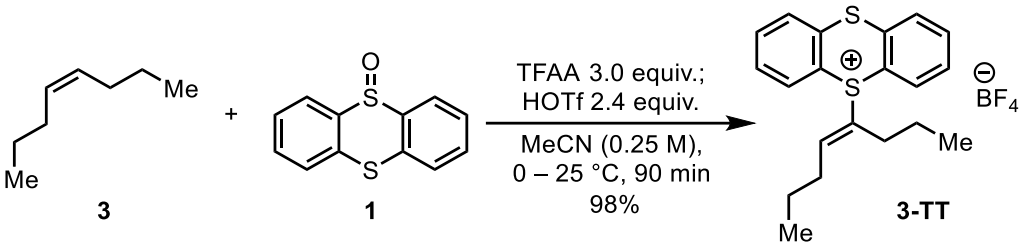

Under ambient atmosphere, a 20 mL borosilicate vial equipped with a magnetic stir bar was charged with *cis*-4-octene (77.8 µL, 56.1 mg, 0.500 mmol, 1.00 equiv.), thianthrene-*S*-oxide (**1**) (120 mg, 0.517 mmol, 1.03 equiv.), and MeCN (2.0 mL, c = 0.25 M). After cooling to 0°C, trifluoroacetic anhydride (0.21 mL, 0.31 g, 1.5 mmol, 3.0 equiv.) was added dropwise within 30 seconds, followed by dropwise addition of HOTf (104 µL, 1766 mg, 1.18 mmol, 2.40 equiv.) within 10 seconds. After stirring the lilac mixture at 0 °C for 60 min followed by stirring at 25 °C for 30 min, the resulting purple mixture was concentrated under reduced pressure and subsequently diluted with CH_2Cl_2 (10 mL). The CH_2Cl_2 solution was poured onto a saturated aqueous $NaHCO_3$ solution (ca. 20 mL). The combined mixture was poured into a separatory funnel, and the layers were separated. The CH_2Cl_2 layer was collected, and the aqueous layer was further extracted with CH_2Cl_2 (2 × ca. 10 mL). The combined CH_2Cl_2 solution was washed with aqueous $NaBF_4$ solution (2 × ca. 20 mL, 5 % w/w). The CH_2Cl_2 layer was dried over Na_2SO_4, filtered, and the solvent was removed under reduced pressure. The residue was purified by chromatography on silica gel eluting with CH_2Cl_2/*i*-PrOH (100:1, v/v). The product-containing fractions were collected and concentrated under reduced pressure. The residue was further dried in vacuo to afford **3-TT** (*E*/*Z* > 49/1, 204.5 mg, 0.488 µmol, 98 %) as a colorless solid.

$\mathbf{R_f}$ = 0.46 (CH_2Cl_2/MeOH, 15:1, v/v).

NMR Spectroscopy:

^{1}H NMR (500 MHz, $CDCl_3$, 298 K, δ): 8.46 (d, *J* = 7.7 Hz, 2H), 7.86 – 7.66 (m, 6H), 5.51 (t, *J* = 7.6 Hz, 1H), 2.13 (m, 4H), 1.30 (m, 4H), 0.81 (t, *J* =7.4 Hz, 6H).

^{13}C NMR {^{1}H} (126 MHz, CD_2Cl_2, 298 K, δ): 142.7, 137.4, 135.5, 135.3, 130.8, 130.6, 123.6, 117.0, 31.9, 30.2, 22.1, 21.9, 13.8, 13.7.

^{19}F NMR (471 MHz, CD_2Cl_2, 298 K, δ): –151.69 (bs), –151.74 (bs).

HRMS-ESI (m/z) calc'd. for $C_{20}H_{23}S_2^+$ $[M]^+$, 327.12357; found, 327.12346; deviation: +0.34 ppm.

III.2.1.3 1-Octene-derived thianthrenium salt **4-TT**

With 1.20 equiv. HOTf:

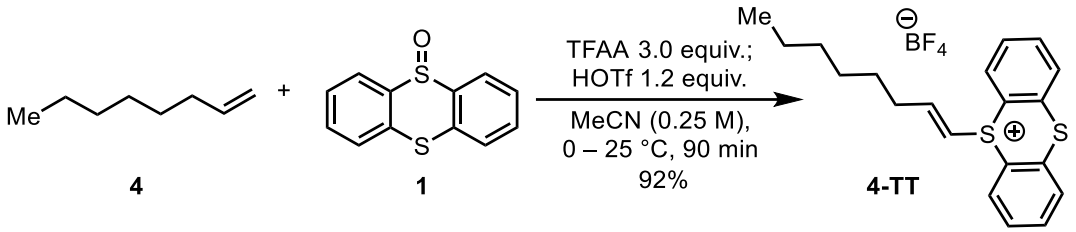

Under ambient atmosphere, a 20 mL borosilicate vial equipped with a magnetic stir bar was charged with 1-octene (78.5 µL, 56.1 mg, 0.500 mmol, 1.00 equiv.), thianthrene-*S*-oxide (**1**) (120 mg, 0.517 mmol, 1.03 equiv.), and MeCN (2.0 mL, c = 0.25 M). After cooling to 0°C, trifluoroacetic anhydride (0.21 -mL, 0.31 g, 1.5 mmol, 3.0 equiv.) was added dropwise within 30 seconds, followed by dropwise addition of HOTf (52 µL, 88 mg, 0.59 mmol, 1.2 equiv.) within 10 seconds. After stirring the lilac mixture at 0 °C for 60 min followed by stirring at 25 °C for 30 min, the resulting purple mixture was concentrated under reduced pressure and subsequently diluted with CH_2Cl_2 (10 mL). The CH_2Cl_2 solution was poured onto a saturated aqueous $NaHCO_3$ solution (ca. 20 mL). The combined mixture was poured into a separatory funnel, and the layers were separated. The CH_2Cl_2 layer was collected, and the aqueous layer was further extracted with CH_2Cl_2 (2 × ca. 10 mL). The combined CH_2Cl_2 solution was washed with aqueous $NaBF_4$ solution (2 × ca. 20 mL, 5 % w/w). The CH_2Cl_2 layer was dried over Na_2SO_4, filtered, and the solvent was removed under reduced pressure. The residue was purified by chromatography on silica gel eluting with CH_2Cl_2/*i*-PrOH (100:1, v/v). The product-containing fractions were collected and concentrated under reduced pressure. The residue was further dried in vacuo to afford **4-TT** (*E*/*Z* ≅ 13/1, 191.2 mg, 462 µmol, 92 %) as a colorless sticky oil. **4-TT** was further purified by chromatography on silica gel eluting with CH_2Cl_2/*i*-PrOH (100:1, v/v),

and fractions containing **4-TT(*E*)** were collected and concentrated under reduced pressure. The residue was further dried in vacuo.

With 2.40 equiv. HOTf:

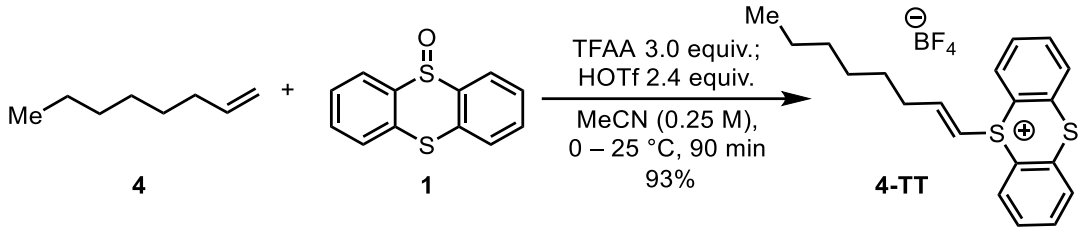

Under ambient atmosphere, a 20 mL borosilicate vial equipped with a magnetic stir bar was charged with 1-octene (78.5 µL, 56.1 mg, 0.500 mmol, 1.00 equiv.), thianthrene-*S*-oxide (**1**) (120 mg, 0.517 mmol, 1.03 equiv.), and MeCN (2.0 mL, c = 0.25 M). After cooling to 0°C, trifluoroacetic anhydride (0.21 -mL, 0.31 g, 1.5 mmol, 3.0 equiv.) was added dropwise within 30 seconds, followed by dropwise addition of HOTf (104 µL, 1766 mg, 1.18 mmol, 2.40 equiv.) within 10 seconds. After stirring the lilac mixture at 0 °C for 60 min followed by stirring at 25 °C for 30 min, the resulting purple mixture was concentrated under reduced pressure and subsequently diluted with CH_2Cl_2 (10 mL). The CH_2Cl_2 solution was cooled to 0 °C for 5 min and poured onto a saturated aqueous $NaHCO_3$ solution (ca. 20 mL) which was prechilled to 0 °C for 5 min. The combined mixture was stirred at 0 °C for 5 min and poured into a separatory funnel, and the layers were separated. The CH_2Cl_2 layer was collected, and the aqueous layer was further extracted with CH_2Cl_2 (2 × ca. 10 mL). The combined CH_2Cl_2 solution was washed with aqueous $NaBF_4$ solution (2 × ca. 20 mL, 5 % w/w). The CH_2Cl_2 layer was dried over Na_2SO_4, filtered, and the solvent was removed under reduced pressure. The residue was purified by chromatography on silica gel eluting with CH_2Cl_2/*i*-PrOH (100:1, v/v). The product-containing fractions were collected and concentrated under reduced pressure. The residue was further dried in vacuo to afford **4-TT** (*E*/*Z* ≅ 20/1, 192.3 mg, 464 µmol, 93 %) as a colorless sticky oil.

R_f = 0.46 (CH_2Cl_2/MeOH, 15:1, v/v).

NMR Spectroscopy:

^{1}H NMR (500 MHz, CD_2Cl_2, 298 K, δ): 8.24 (d, *J* = 7.9 Hz, 2H), 7.89 (d, *J* = 8.0 Hz, 2H), 7.78 (t, *J* = 7.8 Hz, 2H), 7.71 (t, *J* = 7.7 Hz, 2H), 7.10 (dt, *J*

= 14.9, 7.5 Hz, 1H), 6.55 (dt, *J* = 14.8, 1.5 Hz, 1H), 2.27 (m, 2H), 1.43 – 1.35 (m, 2H), 1.31 – 1.12 (m, 6H), 0.87 – 0.76 (m, 3H).

^{13}C NMR {^{1}H} (126 MHz, CD_2Cl_2, 298 K, δ): 157.4, 136.3, 135.1, 133.7, 130.8, 130.7, 120.8, 109.8, 33.8, 31.8, 29.1, 27.7, 22.9, 14.2.

^{19}F NMR (471 MHz, CD_2Cl_2, 298 K, δ): –151.05 (bs), –151.11 (bs).

HRMS-ESI (m/z) calc'd. for $C_{20}H_{23}S_2^+$ $[M]^+$, 327.12357; found, 327.12302; deviation: +1.68 ppm.

III.2.1.4 10-Undecen-1-ol-derived thianthrenium salts **9-TT(OTFA)** and **9-TT(OH)**

With 1.20 equiv. HOTf:

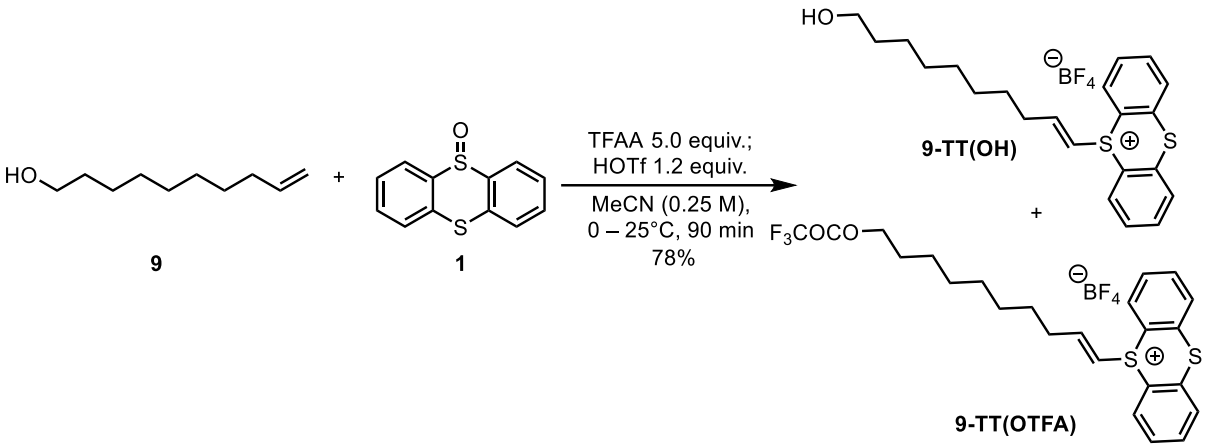

Under ambient atmosphere, a 20 mL borosilicate vial equipped with a magnetic stir bar was charged with 10-undecen-1-ol (78.1 mg, 0.500 mmol, 1.00 equiv.), thianthrene-*S*-oxide (**1**) (120 mg, 0.517 mmol, 1.03 equiv.), and MeCN (2.0 mL, c = 0.25 M). After cooling to 0°C, trifluoroacetic anhydride (0.35 mL, 0.31 g, 1.5 mmol, 5.0 equiv.) was added dropwise within 30 seconds, followed by dropwise addition of HOTf (52 µL, 88 mg, 0.59 mmol, 1.2 equiv.) within 10 seconds. After stirring the lilac mixture at 0 °C for 60 min followed by stirring at 25 °C for 30 min, the resulting purple mixture was concentrated under reduced pressure and subsequently diluted with CH_2Cl_2 (10 mL). The CH_2Cl_2 solution was poured onto a saturated aqueous $NaHCO_3$ solution (ca. 20 mL). The combined mixture was poured into a separatory funnel, and the layers were separated. The CH_2Cl_2 layer was collected, and the aqueous layer was further extracted with CH_2Cl_2 (2 × ca. 10 mL). The combined CH_2Cl_2 solution was washed

with aqueous $NaBF_4$ solution (2 × ca. 20 mL, 5 % w/w). The CH_2Cl_2 layer was dried over Na_2SO_4, filtered, and the solvent was removed under reduced pressure. The residue was purified by chromatography on silica gel eluting with CH_2Cl_2/*i*-PrOH (100:1, v/v). The product-containing fractions were collected and concentrated under reduced pressure. The residue was further dried in vacuo to afford **9-TT(OTFA)** (*E*/*Z* ≅ 14/1, 130.0 mg, 229 µmol, 46 %) as a colorless sticky oil and **9-TT(OH)** (*E*/*Z* ≅ 10/1, 75.4 mg, 160 µmol, 32 %) as a colorless sticky oil. **9-TT(OTFA)** was further purified by chromatography on silica gel eluting with CH_2Cl_2/*i*-PrOH (100:1, v/v), and fractions containing **9-TT(OTFA)(*E*)** were collected and concentrated under reduced pressure. The residue was further dried in vacuo.

With 2.40 equiv. HOTf:

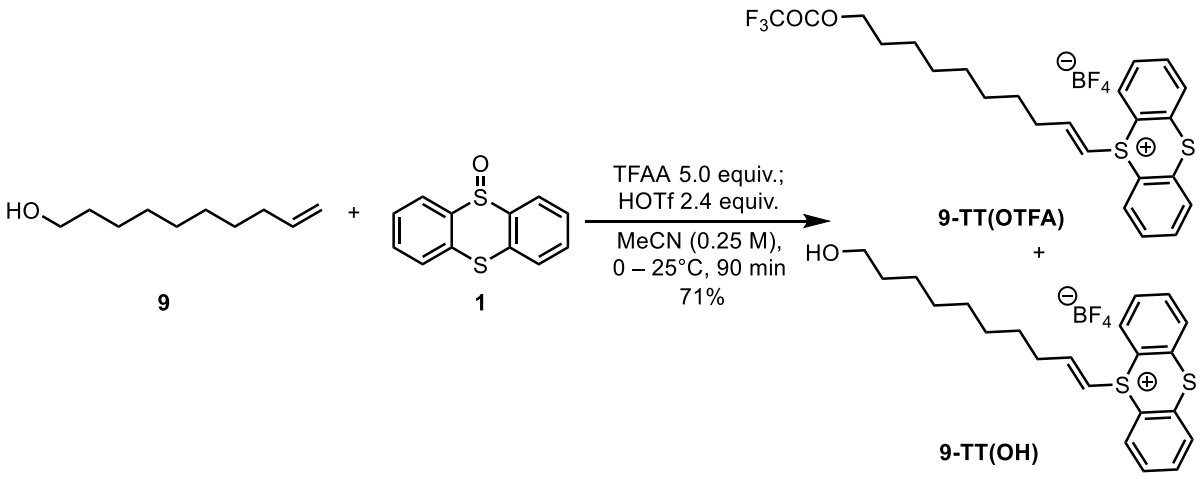

Under ambient atmosphere, a 20 mL borosilicate vial equipped with a magnetic stir bar was charged with 10-undecen-1-ol (78.1 mg, 0.500 mmol, 1.00 equiv.), thianthrene-*S*-oxide (**1**) (120 mg, 0.517 mmol, 1.03 equiv.), and MeCN (2.0 mL, c = 0.25 M). After cooling to 0°C, trifluoroacetic anhydride (0.35 mL, 0.31 g, 1.5 mmol, 5.0 equiv.) was added dropwise within 30 seconds, followed by dropwise addition of HOTf (104 µL, 176 mg, 1.18 mmol, 2.40 equiv.) within 10 seconds. After stirring the lilac mixture at 0 °C for 60 min followed by stirring at 25 °C for 30 min, the resulting light purple mixture was concentrated under reduced pressure and subsequently diluted with CH_2Cl_2 (10 mL). The CH_2Cl_2 solution was cooled to 0 °C for 5 min and poured onto a saturated aqueous $NaHCO_3$ solution (ca. 20 mL) which was prechilled to 0 °C for 5 min. The

combined mixture was stirred at 0 °C for 5 min and poured into a separatory funnel, and the layers were separated. The CH_2Cl_2 layer was collected, and the aqueous layer was further extracted with CH_2Cl_2 (2 × ca. 10 mL). The combined CH_2Cl_2 solution was washed with aqueous $NaBF_4$ solution (2 × ca. 20 mL, 5 % w/w).The CH_2Cl_2 layer was dried over Na_2SO_4, filtered, and the solvent was removed under reduced pressure. The residue was purified by chromatography on silica gel eluting with CH_2Cl_2/*i*-PrOH (100:1 to 50:1, v/v). The product-containing fractions were collected and concentrated under reduced pressure. The residue was further dried in vacuo to afford **9-TT(OTFA)** (*E*/*Z* ≅ 31/1, 150.9 mg, 272 µmol, 54 %) as a light yellow sticky oil and **9-TT(OH)** (*E*/*Z* ≅ 16/1, 39.2 mg, 86 µmol, 17 %) as a light yellow sticky oil.

R_f = 0.46 (CH_2Cl_2/MeOH, 15:1, v/v) for **9-TT(OTFA)**.

R_f = 0.32 (CH_2Cl_2/MeOH, 15:1, v/v). for **9-TT(OH)**

NMR Spectroscopy for 9-TT(OTFA):

^{1}H NMR (500 MHz, CD_2Cl_2, 298 K, δ) 8.17 (d, *J* = 7.9 Hz, 2H), 7.80 (d, *J* = 7.9 Hz, 2H), 7.69 (tt, *J* = 7.8, 1.5 Hz, 2H), 7.65 – 7.60 (m, 2H), 7.08 – 6.99 (m, 1H), 6.47 (dt, *J* = 14.8, 1.6 Hz, 1H), 4.24 (t, *J* = 6.7 Hz, 2H), 2.23 – 2.13 (m, 2H), 1.69 – 1.56 (m, 2H), 1.33 (p, *J* = 7.1 Hz, 2H), 1.28 – 1.22 (m, 2H), 1.21 – 1.10 (m, 6H).

^{13}C NMR {^{1}H} (126 MHz, CD_2Cl_2, 298 K, δ): 158.6 (2C), 137.7, 136.0, 135.1, 132.3, 132.1, 122.2, 116.5 (q, J = 284.5 Hz), 111.3, 70.4, 35.2, 30.8, 30.7, 30.7, 29.9, 29.1, 27.1.

^{19}F NMR (471 MHz, CD_2Cl_2, 298 K, δ): –73.62 (s), –148.95 (bs), –149.01 (bs).

HRMS-ESI (m/z) 9-TT(OTFA) calc'd. for $C_{24}H_{26}F_3O_2S_2^+$ $[M]^+$, 467.13208; found, 467.13153; deviation: +1.19 ppm.

NMR Spectroscopy for 9-TT(OH):

^{1}H NMR (500 MHz, CD_2Cl_2, 298 K, δ) 10.19 (dd, *J* = 8.0, 1.4 Hz, 2H), 9.86 (dd, *J* = 7.9, 1.3 Hz, 2H), 9.75 (td, *J* = 7.7, 1.4 Hz, 2H), 9.65 (td, *J* =

7.7, 1.3 Hz, 2H), 9.06 (dt, *J* = 14.7, 6.9 Hz, 1H), 8.52 (dt, *J* = 14.8, 1.5 Hz, 1H), 6.28 (t, *J* = 6.7 Hz, 2H), 4.27 – 4.09 (m, 2H), 3.66 (dq, *J* = 8.4, 6.7 Hz, 2H), 3.36 (t, *J* = 7.5 Hz, 2H), 3.32 – 3.15 (m, 8H).

^{13}C NMR {^{1}H} (126 MHz, CD_2Cl_2, 298 K, δ): 157.3, 136.3, 135.1, 133.6, 130.8, 130.7, 120.7, 109.8, 63.1, 33.7, 33.2, 29.6, 29.5, 29.2, 27.7, 26.1.

^{19}F NMR (471 MHz, CD_2Cl_2, 298 K, δ): –150.67 (bs), –150.72 (bs).

HRMS-ESI (m/z) 9-TT(OH) calc'd. for $C_{22}H_{27}OS_2^+$ $[M]^+$, 371.14978; found, 371.14910; deviation: +1.85 ppm.

III.2.1.5 Pent-4-en-1-yl-phthalimide-derived thianthrenium salt **11-TT**

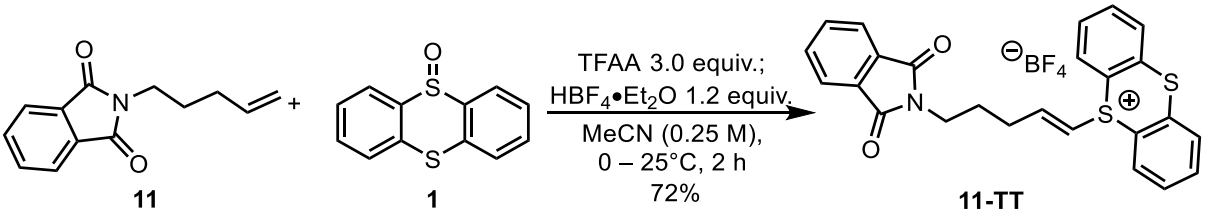

Under ambient atmosphere, a 20 mL borosilicate vial equipped with a magnetic stir bar was charged with pent-4-en-1-yl-phthalimide[1] (645 mg, 3.00 mmol, 1.00 equiv.), thianthrene-*S*-oxide (**1**) (696 mg, 3.00 mmol, 1.00 equiv.), and MeCN (12 mL, c = 0.25 M). After cooling to 0°C, trifluoroacetic anhydride (1.26 mL, 1.86 g, 9.00 mmol, 3.00 equiv.) was added dropwise within 30 seconds, followed by dropwise addition of HBF_4•OEt_2 (522 µL, 3.60 mmol, 1.2 equiv.) within 10 seconds. After stirring the lilac mixture at 0 °C for 60 min followed by stirring at 25 °C for 60 min, the resulting purple mixture was concentrated under reduced pressure and subsequently diluted with CH_2Cl_2 (10 mL). The CH_2Cl_2 solution was poured onto a saturated aqueous $NaHCO_3$ solution (ca. 20 mL). The combined mixture was poured into a separatory funnel, and the layers were separated. The CH_2Cl_2 layer was collected, and the aqueous layer was further extracted with CH_2Cl_2 (2 × ca. 10 mL). The combined CH_2Cl_2 solution was washed with aqueous $NaBF_4$ solution (2 × ca. 20 mL, 5 % w/w). The CH_2Cl_2 layer was dried over Na_2SO_4, filtered, and the solvent was removed under reduced pressure. The residue was purified by chromatography on silica gel eluting with CH_2Cl_2/*i*-PrOH (100:1, v/v). The product-containing fractions were collected and concentrated

under reduced pressure. The residue was further dried in vacuo to afford **11-TT** (*E*/*Z* > 50/1, 1.12 g, 2.17 mmol, 72 %) as a colorless solid.

R_f = 0.40 (CH_2Cl_2/MeOH, 15:1, v/v).

NMR Spectroscopy:

^{1}H NMR (500 MHz, CD_2Cl_2, 298 K, δ 8.24 (dd, *J* = 7.9, 1.3 Hz, 2H), 7.89 (dd, *J* = 7.9, 1.3 Hz, 2H), 7.82 – 7.74 (m, 4H), 7.76 – 7.67 (m, 4H), 7.06 (ddd, *J* = 14.0, 7.3, 6.3 Hz, 1H), 6.61 (dd, *J* = 14.8, 1.4 Hz, 1H), 3.60 (t, *J* = 6.8 Hz, 2H), 2.33 (q, *J* = 8.1, 7.5 Hz, 2H), 1.80 (p, *J* = 7.2 Hz, 2H).

^{13}C NMR {^{1}H} (126 MHz, CD_2Cl_2, 298 K, δ): 168.7, 155.2, 136.5, 135.1, 134.6, 133.9, 132.5, 130.9, 130.8, 123.6, 120.6, 110.9, 37.2, 30.9, 26.8.

^{19}F NMR (471 MHz, CD_2Cl_2, 298 K, δ): –151.07(bs), –151.12 (bs).

HRMS-ESI (m/z) calc'd. for $C_{25}H_{20}NO_2S_2^+$ $[M]^+$, 430.09299 found, 430.09273; deviation: +0.63 ppm.

III.2.1.6 Allylbenzol-derived thianthrenium salt **12-TT**

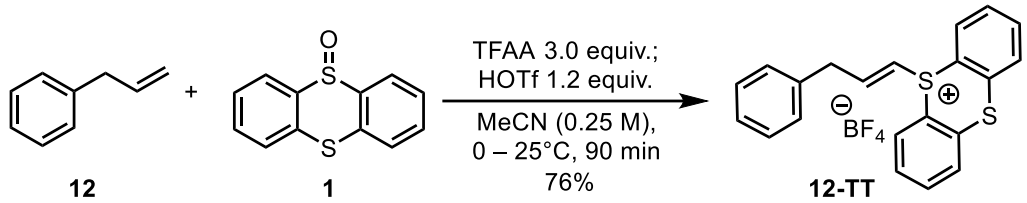

12 **1** **12-TT**

Under ambient atmosphere, a 20 mL borosilicate vial equipped with a magnetic stir bar was charged with allylbenzol (66.4 µL, 59.1 mg, 0.500 mmol, 1.00 equiv.), thianthrene-*S*-oxide (**1**) (120 mg, 0.517 mmol, 1.03 equiv.), and MeCN (2.0 mL, c = 0.25 M). After cooling to 0°C, trifluoroacetic anhydride (0.21 mL, 0.31 g, 1.5 mmol, 3.0 equiv.) was added dropwise within 30 seconds, followed by dropwise addition of HOTf (52 µL, 88 mg, 0.59 mmol, 1.2 equiv.) within 10 seconds. After stirring the lilac mixture at 0 °C for 60 min followed by stirring at 25 °C for 30 min, the resulting purple mixture was concentrated under reduced pressure and subsequently diluted with CH_2Cl_2 (10 mL). The CH_2Cl_2 solution was poured onto a saturated aqueous $NaHCO_3$ solution (ca. 20 mL). The combined mixture was poured into a separatory funnel, and the layers were separated. The CH_2Cl_2 layer was collected, and the aqueous layer was further

extracted with CH_2Cl_2 (2 × ca. 10 mL). The combined CH_2Cl_2 solution was washed with aqueous $NaBF_4$ solution (2 × ca. 20 mL, 5 % w/w). The CH_2Cl_2 layer was dried over Na_2SO_4, filtered, and the solvent was removed under reduced pressure. The residue was purified by chromatography on silica gel eluting with CH_2Cl_2/*i*-PrOH (100:1, v/v). The product-containing fractions were collected and concentrated under reduced pressure. The residue was further dried in vacuo to afford **12-TT** (*E*/*Z* > 50/1, 158.9 mg, 378 µmol, 76 %) as a colorless solid.

$\mathbf{R_f}$ = 0.46 (CH_2Cl_2/MeOH, 15:1, v/v).

NMR Spectroscopy:

^{1}H NMR (500 MHz, CD_2Cl_2, 298 K, δ) 8.22 (dd, *J* = 7.9, 1.4 Hz, 2H), 7.88 (dt, *J* = 8.0, 1.4 Hz, 2H), 7.77 (tt, *J* = 7.8, 1.4 Hz, 2H), 7.69 (td, *J* = 7.7, 1.3 Hz, 2H), 7.31 – 7.26 (m, 2H), 7.26 – 7.21 (m, 1H), 7.18 (dt, *J* = 14.8, 6.7 Hz, 1H), 7.11 – 7.08 (m, 2H), 6.50 (dt, *J* = 14.8, 1.6 Hz, 1H), 3.60 (dd, *J* = 6.7, 1.6 Hz, 2H).

^{13}C NMR {^{1}H} (126 MHz, CD_2Cl_2, 298 K, δ): 154.8, 136.5, 135.8, 135.1, 133.9, 130.9, 130.8, 129.5, 129.3, 127.8, 120.5, 111.2, 39.6.

^{19}F NMR (471 MHz, CD_2Cl_2, 298 K, δ): –150.87 (bs), –150.92 (bs).

HRMS-ESI (m/z) calc'd. for $C_{21}H_{17}S_2^+$ $[M]^+$, 333.07662; found, 333.07610; deviation: +1.56 ppm.

III.2.1.7 1-Allyl-4-(trifluormethyl)-benzol-derived thianthrenium salt **13-TT**

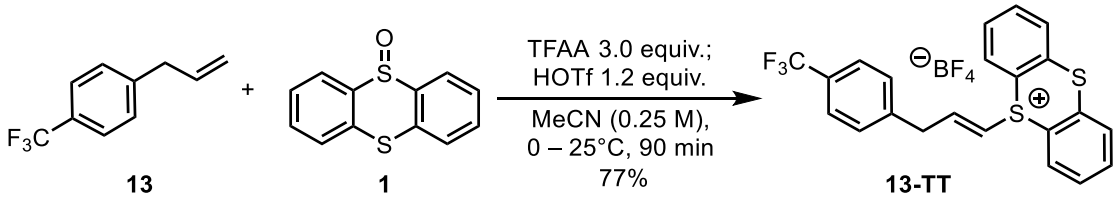

Under ambient atmosphere, a 20 mL borosilicate vial equipped with a magnetic stir bar was charged with 1-allyl-4-(trifluormethyl)-benzol (83.9 µL, 93.1 mg, 0.500 mmol, 1.00 equiv.), thianthrene-*S*-oxide (**1**) (120 mg, 0.517 mmol, 1.03 equiv.), and MeCN (2.0 mL, c = 0.25 M). After cooling to 0°C, trifluoroacetic anhydride (0.21 mL, 0.31 g, 1.5 mmol, 3.0 equiv.) was added dropwise within 30 seconds, followed by dropwise addition of HOTf (52 µL, 88 mg, 0.59 mmol, 1.2 equiv.) within 10 seconds. After stirring the lilac mixture at 0 °C for 60 min

followed by stirring at 25 °C for 30 min, the resulting purple mixture was concentrated under reduced pressure and subsequently diluted with CH_2Cl_2 (10 mL). The CH_2Cl_2 solution was poured onto a saturated aqueous $NaHCO_3$ solution (ca. 20 mL). The combined mixture was poured into a separatory funnel, and the layers were separated. The CH_2Cl_2 layer was collected, and the aqueous layer was further extracted with CH_2Cl_2 (2 × ca. 10 mL). The combined CH_2Cl_2 solution was washed with aqueous $NaBF_4$ solution (2 × ca. 20 mL, 5 % w/w). The CH_2Cl_2 layer was dried over Na_2SO_4, filtered, and the solvent was removed under reduced pressure. The residue was purified by chromatography on silica gel eluting with CH_2Cl_2/*i*-PrOH (100:1, v/v). The product-containing fractions were collected and concentrated under reduced pressure. The residue was further dried in vacuo to afford **13-TT** (*E*/*Z* > 50/1, 187.0 mg, 383 µmol, 77 %) as a colorless solid.

R_f = 0.46 (CH_2Cl_2/MeOH, 15:1, v/v).

NMR Spectroscopy:

^{1}H NMR (500 MHz, CD_2Cl_2, 298 K, δ) 8.21 (dd, *J* = 8.0, 1.4 Hz, 2H), 7.88 (dd, *J* = 8.0, 1.3 Hz, 2H), 7.77 (td, *J* = 7.7, 1.3 Hz, 2H), 7.67 (td, *J* = 7.7, 1.4 Hz, 2H), 7.52 (d, *J* = 8.0 Hz, 2H), 7.28 (d, *J* = 8.0 Hz, 2H), 7.15 (dt, *J* = 14.8, 6.9 Hz, 1H), 6.56 (dt, *J* = 14.8, 1.5 Hz, 1H), 3.67 (dd, *J* = 6.8, 1.5 Hz, 2H).

^{13}C NMR {^{1}H} (126 MHz, CD_2Cl_2, 298 K, δ): 153.1, 140.3, 136.4, 135.2, 133.7, 130.9, 130.6, 129.8, 129.5, 126.2 (q, *J* = 3.8 Hz), 124.6 (q, *J* = 271.8 Hz), 120.1, 112.1, 39.0.

^{19}F NMR (471 MHz, CD_2Cl_2, 298 K, δ): –62.73, –150.27 (bs), –150.37 (bs).

HRMS-ESI (m/z) calc'd. for $C_{12}H_{16}F_3S_2^+$ $[M]^+$, 401.06400; found, 401.06332; deviation: +1.71 ppm.

III.2.1.8 Cyclododecene-derived thianthrenium salt **14-TT**

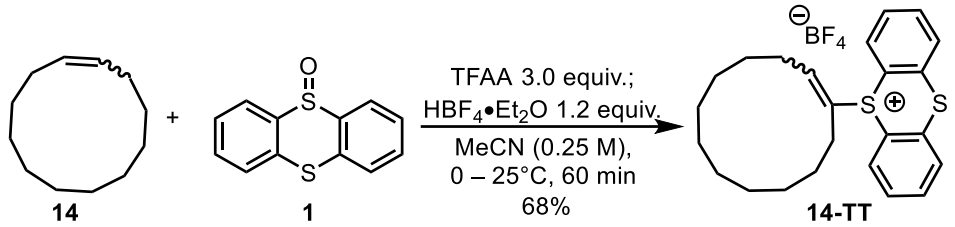

Under ambient atmosphere, a 20 mL borosilicate vial equipped with a magnetic stir bar was charged with cyclododecene (E/Z ≅ 1/2, 96.7 µL, 83.2 mg, 0.500 mmol, 1.00 equiv.), thianthrene-*S*-oxide (**1**) (120 mg, 0.517 mmol, 1.03 equiv.), and MeCN (2.0 mL, c = 0.25 M). After cooling to 0°C, trifluoroacetic anhydride (0.21 mL, 0.31 g, 1.5 mmol, 3.0 equiv.) was added dropwise within 30 seconds, followed by dropwise addition of $HBF_4{\cdot}OEt_2$ (87 µL, 0.60 mmol, 1.2 equiv.) within 10 seconds. After stirring the lilac mixture at 0 °C for 60 min, the resulting pink mixture was concentrated under reduced pressure and subsequently diluted with CH_2Cl_2 (10 mL). The CH_2Cl_2 solution was poured onto a saturated aqueous $NaHCO_3$ solution (ca. 20 mL). The combined mixture was poured into a separatory funnel, and the layers were separated. The CH_2Cl_2 layer was collected, and the aqueous layer was further extracted with CH_2Cl_2 (2 × ca. 10 mL). The combined CH_2Cl_2 solution was washed with aqueous $NaBF_4$ solution (2 × ca. 20 mL, 5 % w/w). The CH_2Cl_2 layer was dried over Na_2SO_4, filtered, and the solvent was removed under reduced pressure. The residue was purified by chromatography on silica gel eluting with CH_2Cl_2/*i*-PrOH (100:1, v/v). The product-containing fractions were collected and concentrated under reduced pressure. The residue was further dried in vacuo to afford **14-TT** (*E*/*Z* ≅ 1/1, 159.0 mg, 339 µmol, 68 %) as a colorless solid.

R_f = 0.46 (CH_2Cl_2/MeOH, 15:1, v/v).

NMR Spectroscopy:

^{1}H NMR (500 MHz, CD_2Cl_2, 298 K, δ) 8.22 (dd, *J* = 7.9, 1.4 Hz, 1H), 8.11 (dd, *J* = 8.1, 1.4 Hz, 1H), 7.92 (dd, *J* = 7.9, 1.4 Hz, 1H), 7.84 (td, *J* = 7.8, 1.4 Hz, 2H), 7.80 (td, *J* = 7.7, 1.4 Hz, 1H), 7.76 (td, *J* = 7.6, 1.4 Hz,1H), 7.74 – 7.67 (m, 1H), 6.49 (t, *J* = 7.7 Hz, 0.4H), 5.39 (t, *J* = 8.2 Hz, 0.5H), 2.67 – 2.59 (m, 1H), 2.39 – 2.32 (m, 1H), 2.22 (t, *J* = 7.2 Hz, 1H), 2.20 – 2.16 (m, 1H), 1.77 – 1.70 (m, 1H), 1.58 – 1.49 (m, 2H), 1.43 – 1.27 (m,

8H), 1.28 – 1.21 (m, 2H), 1.21 – 1.13 (m, 2H), 1.13 – 1.06 (m, 1H).

^{13}C NMR {^{1}H} (126 MHz, CD_2Cl_2, 298 K, δ): 150.4, 142.3, 137.8, 137.6, 135.5, 135.5, 135.3, 134.5, 131.2, 131.0, 130.8, 130.7, 130.6, 124.4, 117.9, 117.1, 34.8, 30.4, 27.4, 26.4, 26.1, 26.0, 25.9, 25.69, 25.67, 25.2, 25.1, 24.9, 24.8, 24.7, 24.23, 24.16, 22.9, 22.4.

^{19}F NMR (471 MHz, CD_2Cl_2, 298 K, δ): –152.16 (bs), –152.21 (bs).

HRMS-ESI (m/z) calc'd. for $C_{24}H_{29}S_2^+$ $[M]^+$, 381.17052; found, 381.17032; deviation: +0.53 ppm.

III.2.1.9 3,4-Dihydro-2*H*-pyrane-derived thianthrenium salt **16-TT**

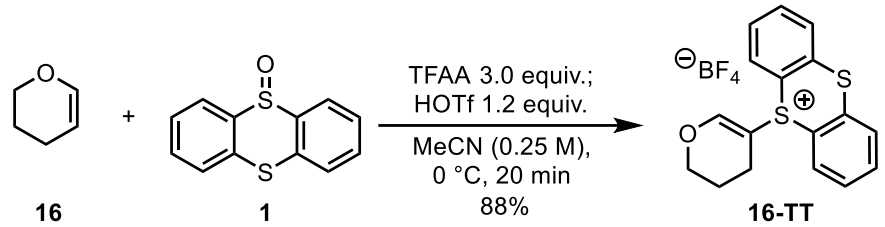

16 **1** **16-TT**

Under ambient atmosphere, a 20 mL borosilicate vial equipped with a magnetic stir bar was charged with 3,4-dihydro-2*H*-pyrane (45.7 µL, 42.1 mg, 0.500 mmol, 1.00 equiv.), thianthrene-*S*-oxide (**1**) (120 mg, 0.517 mmol, 1.03 equiv.), and MeCN (2.0 mL, c = 0.25 M). After cooling to 0°C, trifluoroacetic anhydride (0.21 mL, 0.31 g, 1.5 mmol, 3.0 equiv.) was added dropwise within 30 seconds, followed by dropwise addition of HOTf (52 µL, 88 mg, 0.59 mmol, 1.2 equiv.) within 10 seconds. After stirring the lilac mixture at 0 °C for 20 min, the resulting yellow mixture was concentrated under reduced pressure and subsequently diluted with CH_2Cl_2 (10 mL). The CH_2Cl_2 solution was poured onto a saturated aqueous $NaHCO_3$ solution (ca. 20 mL). The combined mixture was poured into a separatory funnel, and the layers were separated. The CH_2Cl_2 layer was collected, and the aqueous layer was further extracted with CH_2Cl_2 (2 × ca. 10 mL). The combined CH_2Cl_2 solution was washed with aqueous $NaBF_4$ solution (2 × ca. 20 mL, 5 % w/w). The CH_2Cl_2 layer was dried over Na_2SO_4, filtered, and the solvent was removed under reduced pressure. The residue was purified by chromatography on silica gel eluting with CH_2Cl_2/*i*-PrOH (100:1, v/v). The product-containing fractions were collected and concentrated under reduced pressure. The

residue was further dried in vacuo to afford **16-TT** (169.0 mg, 438 µmol, 88 %) as a colorless solid.

$\mathbf{R_f}$ = 0.46 (CH_2Cl_2/MeOH, 15:1, v/v).

NMR Spectroscopy:

^{1}H NMR (500 MHz, CD_2Cl_2, 298 K, δ) 8.07 (dd, *J* = 7.9, 1.2 Hz, 2H), 7.79 – 7.73 (m, 5H), 7.69 (ddd, *J* = 8.6, 6.6, 2.0 Hz, 2H), 4.18 – 4.14 (t, *J* = 5.9 Hz, 2H), 2.21 (t, *J* = 6.3 Hz, 2H), 1.95 (p, *J* = 6.1 Hz, 2H).

^{13}C NMR {^{1}H} (126 MHz, CD_2Cl_2, 298 K, δ): 159.6, 136.2, 134.6, 133.0, 130.6, 130.0, 118.6, 103.0, 68.3, 21.8, 20.2.

^{19}F NMR (471 MHz, CD_2Cl_2, 298 K, δ): –151.57 (bs), –151.59 (bs).

HRMS-ESI (m/z) calc'd. for $C_{22}H_{25}OS_2^+$ $[M]^+$, 369.13413; found, 369.13432; deviation: –0.50 ppm.

III.2.1.10 *N*-(But-3-en-1-yl)benzamide-derived thianthrenium salt **17-TT**

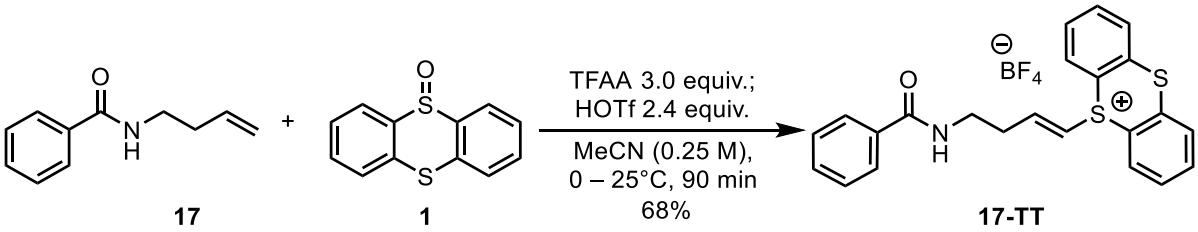

Under ambient atmosphere, a 20 mL borosilicate vial equipped with a magnetic stir bar was charged with *N*-(but-3-en-1-yl)benzamide[2] (109 mg, 0.500 mmol, 1.00 equiv.), thianthrene-*S*-oxide (**1**) (120 mg, 0.517 mmol, 1.03 equiv.), and MeCN (2.0 mL, c = 0.25 M). After cooling to 0°C, HOTf (52 µL, 88 mg, 0.59 mmol, 1.2 equiv.) within 10 seconds, followed by dropwise addition of trifluoroacetic anhydride (0.21 mL, 0.31 g, 1.5 mmol, 3.0 equiv.) within 30 seconds, followed by dropwise addition of HOTf (52 µL, 88 mg, 0.59 mmol, 1.2 equiv.) within 10 seconds. After stirring the lilac mixture at 0 °C for 60 min followed by stirring at 25 °C for 30 min, the resulting purple mixture was concentrated under reduced pressure and subsequently diluted with CH_2Cl_2 (10 mL). The CH_2Cl_2 solution was poured onto a saturated aqueous $NaHCO_3$ solution (ca. 20 mL). The combined mixture was poured into a separatory funnel, and the layers were

separated. The CH_2Cl_2 layer was collected, and the aqueous layer was further extracted with CH_2Cl_2 (2 × ca. 10 mL). The combined CH_2Cl_2 solution was washed with aqueous $NaBF_4$ solution (2 × ca. 20 mL, 5 % w/w). The CH_2Cl_2 layer was dried over Na_2SO_4, filtered, and the solvent was removed under reduced pressure. The residue was purified by chromatography on silica gel eluting with CH_2Cl_2/*i*-PrOH (70:1 to 30:1, v/v). The product-containing fractions were collected and concentrated under reduced pressure. The residue was further dried in vacuo to afford **10-TT** (*E*/*Z* > 50/1, 163.0 mg, 342 µmol, 68 %) as a beige solid.

$\mathbf{R_f}$ = 0.21 (CH_2Cl_2/MeOH, 15:1, v/v).

NMR Spectroscopy:

^{1}H NMR (500 MHz, CD_2Cl_2, 298 K, δ) 8.09 (dd, *J* = 8.0, 1.4 Hz, 2H), 7.76 (dd, *J* = 7.9, 1.4 Hz, 2H), 7.66 (t, *J* = 7.8 Hz, 4H), 7.56 (td, *J* = 7.7, 1.4 Hz, 2H), 7.44 (td, *J* = 7.4, 1.4 Hz, 1H), 7.35 – 7.31 (m, 2H), 7.31 – 7.26 (m, 1H), 7.26 – 7.20 (m, 1H), 6.64 (dd, *J* = 14.8, 1.4 Hz, 1H), 3.55 (q, *J* = 6.1 Hz, 2H), 2.61 (q, *J* = 6.5 Hz, 2H).

^{13}C NMR {^{1}H} (126 MHz, CD_2Cl_2, 298 K, δ): 167.7, 155.9, 136.0, 134.9, 134.5, 133.3, 131.8, 130.7, 130.5, 128.9, 127.5, 120.8, 111.2, 37.9, 34.2.

^{19}F NMR (471 MHz, $CDCl_3$, 298 K, δ): –149.98 (bs), –150.03 (bs).

HRMS-ESI (m/z) calc'd. for $C_{23}H_{20}NOS_2^+$ $[M]^+$, 390.09808; found, 390.09744; deviation: +1.65 ppm.

III.2.1.11 Cyclooctene-derived thianthrenium salt **18-TT**

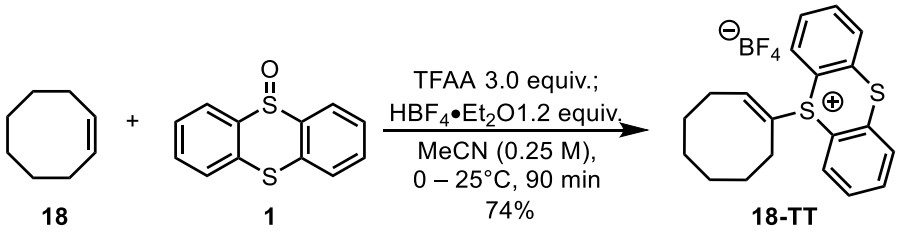

Under ambient atmosphere, a 20 mL borosilicate vial equipped with a magnetic stir bar was charged with cyclooctene (389 µL, 331 mg, 3.00 mmol, 1.00 equiv.), thianthrene-*S*-oxide (**1**) (696 mg, 3.00 mmol, 1.00 equiv.), and MeCN (12 mL, c = 0.25 M). After cooling to 0°C, trifluoroacetic anhydride (1.26 mL, 1.86 g, 9.00 mmol, 3.00 equiv.) was added dropwise within 30 seconds, followed

by dropwise addition of HBF_4•OEt_2 (522 µL, 4.20 mmol, 1.20 equiv.) within 10 seconds. After stirring the lilac mixture at 0 °C for 60 min followed by stirring at 25 °C for 30 min, the resulting purple mixture was concentrated under reduced pressure and subsequently diluted with CH_2Cl_2 (20 mL). The CH_2Cl_2 solution was poured onto a saturated aqueous $NaHCO_3$ solution (ca. 20 mL). The combined mixture was poured into a separatory funnel, and the layers were separated. The CH_2Cl_2 layer was collected, and the aqueous layer was further extracted with CH_2Cl_2 (2 × ca. 10 mL). The combined CH_2Cl_2 solution was washed with aqueous $NaBF_4$ solution (2 × ca. 20 mL, 5 % w/w). The CH_2Cl_2 layer was dried over Na_2SO_4, filtered, and the solvent was removed under reduced pressure. The residue was purified by chromatography on silica gel eluting with CH_2Cl_2/*i*-PrOH (100:1, v/v). The product-containing fractions were collected and concentrated under reduced pressure. The residue was further dried in vacuo to afford **18-TT** (920 mg, 2.23 mmol, 74 %) as a colorless solid.

R_f = 0.46 (CH_2Cl_2/MeOH, 15:1, v/v).

NMR Spectroscopy:

^{1}H NMR (500 MHz, CD_2Cl_2, 298 K, δ) 8.22 (dd, *J* = 7.9, 1.5 Hz, 2H), 7.89 (dd, *J* = 8.1, 1.6 Hz, 2H), 7.84 (td, *J* = 7.6, 1.5 Hz, 2H), 7.75 (td, *J* = 7.7, 1.6 Hz, 2H), 5.76 (dd, *J* = 9.1, 7.8 Hz, 1H), 2.50 (t, *J* = 6.3 Hz, 2H), 2.29 – 2.22 (m, 2H), 1.57 (p, *J* = 6.1 Hz, 2H), 1.43 – 1.33 (m, 4H), 1.03 (p, *J* = 5.9 Hz, 2H).

^{13}C NMR {^{1}H} (126 MHz, CD_2Cl_2, 298 K, δ): 143.3, 137.4, 135.6 (d, *J* = 1.7 Hz), 135.3, 130.72, 130.67, 123.8, 116.8 (d, *J* = 2.4 Hz), 29.5, 28.6, 28.4, 28.3, 26.3, 25.6.

^{19}F NMR (471 MHz, CD_2Cl_2, 298 K, δ): –152.30 (bs), –152.34 (bs).

HRMS-ESI (m/z) calc'd. for $C_{20}H_{21}S_2^+$ $[M]^+$, 325.10792; found, 325.10728; deviation: +1.97 ppm.

III.2.1.12 Cycloheptene-derived thianthrenium salt **19-TT**

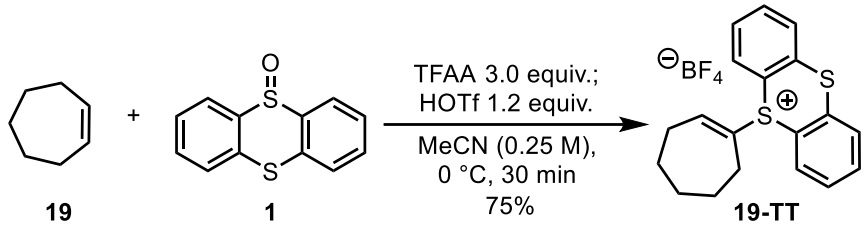

Under ambient atmosphere, a 20 mL borosilicate vial equipped with a magnetic stir bar was charged with cycloheptene (58.6 µL,486.1 mg, 0.500 mmol, 1.00 equiv.), thianthrene-*S*-oxide (**1**) (120 mg, 0.517 mmol, 1.03 equiv.), and MeCN (2.0 mL, c = 0.25 M). After cooling to 0°C, trifluoroacetic anhydride (0.21 mL, 0.31 g, 1.5 mmol, 3.0 equiv.) was added dropwise within 30 seconds, followed by dropwise addition of HOTf (52 µL, 88 mg, 0.59 mmol, 1.2 equiv.) within 10 seconds. After stirring the lilac mixture at 0 °C for 30 min, the resulting pink mixture was concentrated under reduced pressure and subsequently diluted with CH_2Cl_2 (10 mL). The CH_2Cl_2 solution was poured onto a saturated aqueous $NaHCO_3$ solution (ca. 20 mL). The combined mixture was poured into a separatory funnel, and the layers were separated. The CH_2Cl_2 layer was collected, and the aqueous layer was further extracted with CH_2Cl_2 (2 × ca. 10 mL). The combined CH_2Cl_2 solution was washed with aqueous $NaBF_4$ solution (2 × ca. 20 mL, 5 % w/w). The CH_2Cl_2 layer was dried over Na_2SO_4, filtered, and the solvent was removed under reduced pressure. The residue was purified by chromatography on silica gel eluting with CH_2Cl_2/*i*-PrOH (100:1, v/v). The product-containing fractions were collected and concentrated under reduced pressure. The residue was further dried in vacuo to afford **19-TT** (149.3 mg, 375 µmol, 75 %) as a colorless solid.

$\mathbf{R_f}$ = 0.46 (CH_2Cl_2/MeOH, 15:1, v/v).

NMR Spectroscopy:

^{1}H NMR (500 MHz, CD_2Cl_2, 298 K, δ) 8.20 (d, *J* = 8.0 Hz, 2H), 7.89 (d, *J* = 7.9 Hz, 2H), 7.83 (t, *J* = 7.7 Hz, 2H), 7.74 (t, *J* = 7.6 Hz, 2H), 5.92 (t, *J* = 6.6 Hz, 1H), 2.28 (dq, *J* = 11.4, 5.9 Hz, 4H), 1.67 (dp, *J* = 11.6, 5.1, 4.7 Hz, 2H), 1.49 (p, *J* = 5.8 Hz, 2H), 1.34 (p, *J* = 5.8 Hz, 2H).

^{13}C NMR {^{1}H} (126 MHz, CD_2Cl_2, 298 K, δ): 145.1, 137.1 (d, *J* = 2.1 Hz), 135.4 (d, *J* = 3.7 Hz), 135.3, 130.8 (d, *J* = 2.0 Hz), 130.6, 124.6, 117.6 (d,

J = 2.2 Hz), 31.0, 30.6, 29.9, 26.1, 25.4.

^{19}F NMR (471 MHz, CD_2Cl_2, 298 K, δ): –151.78 (bs), –151.83 (bs).

HRMS-ESI (m/z) calc'd. for $C_{19}H_{19}S_2^+$ $[M]^+$, 311.09227; found, 311.09166; deviation: +1.96 ppm.

III.2.1.13 Cyclohexene-derived thianthrenium salt **20-TT**

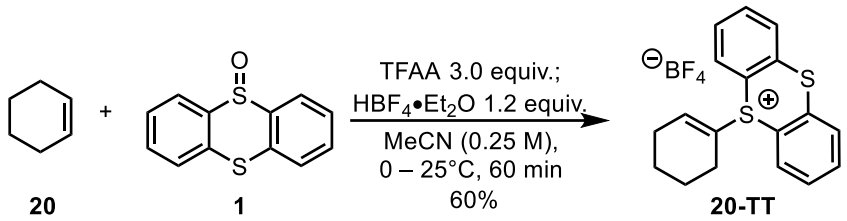

Under ambient atmosphere, a 20 mL borosilicate vial equipped with a magnetic stir bar was charged with cyclohexene (50.6 µL, 41.1 mg, 0.500 mmol, 1.00 equiv.), thianthrene-*S*-oxide (**1**) (120 mg, 0.517 mmol, 1.03 equiv.), and MeCN (2.0 mL, c = 0.25 M). After cooling to 0°C, trifluoroacetic anhydride (0.21 mL, 0.31 g, 1.5 mmol, 3.0 equiv.) was added dropwise within 30 seconds, followed by dropwise addition of HBF_4•OEt_2 (87 µL, 0.59 mmol, 1.2 equiv.) within 10 seconds. After stirring the lilac mixture at 0 °C for 45 min followed by stirring at 25 °C for 15 min, the resulting purple mixture was concentrated under reduced pressure and subsequently diluted with CH_2Cl_2 (10 mL). The CH_2Cl_2 solution was poured onto a saturated aqueous $NaHCO_3$ solution (ca. 20 mL). The combined mixture was poured into a separatory funnel, and the layers were separated. The CH_2Cl_2 layer was collected, and the aqueous layer was further extracted with CH_2Cl_2 (2 × ca. 10 mL). The combined CH_2Cl_2 solution was washed with aqueous $NaBF_4$ solution (2 × ca. 20 mL, 5 % w/w). The CH_2Cl_2 layer was dried over Na_2SO_4, filtered, and the solvent was removed under reduced pressure. The residue was purified by chromatography on silica gel eluting with CH_2Cl_2/*i*-PrOH (100:1, v/v). The product-containing fractions were collected and concentrated under reduced pressure. The residue was further dried in vacuo to afford **20-TT** (115.5 mg, 301 µmol, 60 %) as a colorless solid.

R_f = 0.46 (CH_2Cl_2/MeOH, 15:1, v/v).

NMR Spectroscopy:

^{1}H NMR (500 MHz, CD_2Cl_2, 298 K, δ) 8.19 (d, *J* = 7.9 Hz, 2H), 7.88 (d, *J*

= 7.9 Hz, 2H), 7.82 (t, *J* = 7.7 Hz, 2H), 7.75 – 7.70 (m, 2H), 6.05 (d, *J* = 4.1 Hz, 1H), 2.23 – 2.17 (m, 2H), 1.99 – 1.93 (m, 2H), 1.73 – 1.66 (m, 2H), 1.59 – 1.52 (m, 2H).

^{13}C NMR {^{1}H} (126 MHz, CD_2Cl_2, 298 K, δ): 142.0, 137.1, 135.4, 135.2, 130.7, 130.5, 123.8, 117.1, 27.7, 25.9, 23.0, 20.8.

^{19}F NMR (471 MHz, CD_2Cl_2, 298 K, δ): –149.84 (bs), –149.92 (bs).

HRMS-ESI (m/z) calc'd. for $C_{18}H_{17}S_2^+$ $[M]^+$, 297.07662; found, 297.07647; deviation: +0.51 ppm.

III.2.1.14 Cyclopentene-derived thianthrenium salt **21-TT**

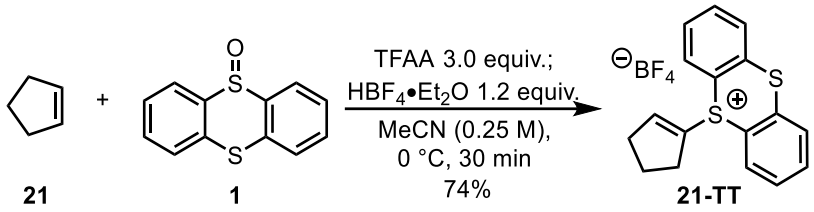

Under ambient atmosphere, a 20 mL borosilicate vial equipped with a magnetic stir bar was charged with cyclopentene (45.8 µL, 34.1 mg, 0.500 mmol, 1.00 equiv.), thianthrene-*S*-oxide (**1**) (120 mg, 0.517 mmol, 1.03 equiv.), and MeCN (2.0 mL, c = 0.25 M). After cooling to 0°C, trifluoroacetic anhydride (0.21 mL, 0.31 g, 1.5 mmol, 3.0 equiv.) was added dropwise within 30 seconds, followed by dropwise addition of HBF_4•OEt_2 (87 µL, 0.60 mmol, 1.2 equiv.) within 10 seconds. After stirring the lilac mixture at 0 °C for 30 min, the resulting light purple mixture was concentrated under reduced pressure and subsequently diluted with CH_2Cl_2 (10 mL). The CH_2Cl_2 solution was poured onto a saturated aqueous $NaHCO_3$ solution (ca. 20 mL). The combined mixture was poured into a separatory funnel, and the layers were separated. The CH_2Cl_2 layer was collected, and the aqueous layer was further extracted with CH_2Cl_2 (2 × ca. 10 mL). The combined CH_2Cl_2 solution was washed with aqueous $NaBF_4$ solution (2 × ca. 20 mL, 5 % w/w). The CH_2Cl_2 layer was dried over Na_2SO_4, filtered, and the solvent was removed under reduced pressure. The residue was purified by chromatography on silica gel eluting with CH_2Cl_2/*i*-PrOH (100:1, v/v). The product-containing fractions were collected and concentrated under reduced pressure. The residue was further dried in vacuo to afford **21-TT** (136.6 mg, 369 µmol, 74 %) as a colorless solid.

R_f = 0.46 (CH_2Cl_2/MeOH, 15:1, v/v).

NMR Spectroscopy:

^{1}H NMR (500 MHz, CD_2Cl_2, 298 K, δ): 8.22 (dd, *J* = 7.9, 1.4 Hz, 2H), 7.87 (dd, *J* = 8.0, 1.4 Hz, 2H), 7.82 (td, *J* = 7.6, 1.4 Hz, 2H), 7.72 (td, *J* = 7.7, 1.4 Hz, 2H), 6.27 (p, *J* = 2.2 Hz, 1H), 2.55 – 2.50 (m, 2H), 2.38 – 2.33 (m, 2H), 2.03 (p, *J* = 7.6 Hz, 2H).

^{13}C NMR {^{1}H} (126 MHz, CD_2Cl_2, 298 K, δ): 148.5, 136.9, 135.3, 134.4, 130.6, 130.5, 124.7, 117.7, 34.0, 32.9, 23.8.

^{19}F NMR (471 MHz, CD_2Cl_2, 298 K, δ): –151.52 (bs), –151.59 (bs).

HRMS-ESI (m/z) calc'd. for $C_{17}H_{15}S_2^+$ $[M]^+$, 283.06097; found, 283.06045; deviation: +1.84 ppm.

III.2.1.15 (*E,E,E*)-1,5,9-Cyclododecatriene-derived thianthrenium salt **22-TT**

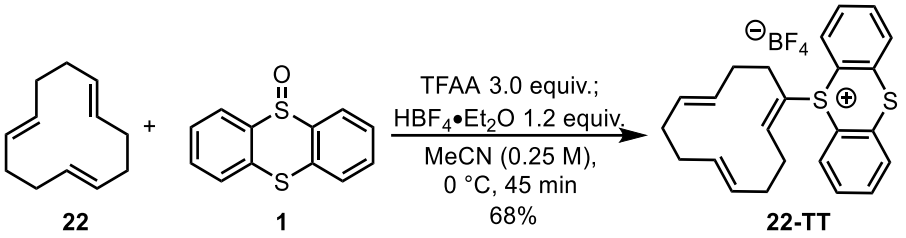

22 **1** **22-TT**

Under ambient atmosphere, a 20 mL borosilicate vial equipped with a magnetic stir bar was charged with (*E,E,E*)-1,5,9-cyclododecatriene (91.2 µL, 81.1 mg, 0.500 mmol, 1.00 equiv.), thianthrene-*S*-oxide (**1**) (120 mg, 0.517 mmol, 1.03 equiv.), and MeCN (2.0 mL, c = 0.25 M). After cooling to 0°C, trifluoroacetic anhydride (0.21 mL, 0.31 g, 1.5 mmol, 3.0 equiv.) was added dropwise within 30 seconds, followed by dropwise addition of $HBF_4{\cdot}OEt_2$ (87 µL, 0.60 mmol, 1.2 equiv.) within 10 seconds. After stirring the lilac mixture at 0 °C for 45 min, the resulting purple mixture was concentrated under reduced pressure and subsequently diluted with CH_2Cl_2 (10 mL). The CH_2Cl_2 solution was poured onto a saturated aqueous $NaHCO_3$ solution (ca. 20 mL). The combined mixture was poured into a separatory funnel, and the layers were separated. The CH_2Cl_2 layer was collected, and the aqueous layer was further extracted with CH_2Cl_2 (2 × ca. 10 mL). The combined CH_2Cl_2 solution was washed with aqueous $NaBF_4$ solution (2 × ca. 20 mL, 5 % w/w). The CH_2Cl_2 layer was dried over Na_2SO_4, filtered, and the solvent was removed under reduced pressure. The residue was purified by

chromatography on silica gel eluting with CH_2Cl_2/*i*-PrOH (100:1, v/v). The product-containing fractions were collected and concentrated under reduced pressure. The residue was further dried in vacuo to afford **22-TT** (157.4 mg, 339 µmol, 68 %) as a colorless solid.

$\mathbf{R_f}$ = 0.46 (CH_2Cl_2/MeOH, 15:1, v/v).

NMR Spectroscopy:

^{1}H NMR (500 MHz, CD_2Cl_2, 298 K, δ): 8.06 – 8.02 (m, 2H), 7.83 – 7.77 (m, 4H), 7.70 (m, *J* = 8.1, 6.4, 2.4 Hz, 2H), 6.03 (t, *J* = 7.4 Hz, 1H), 5.31 – 5.25 (m, 1H), 5.21 – 5.10 (m, 1H), 4.94 – 4.84 (m, 1H), 4.71 – 4.59 (m, 1H), 2.84 (td, *J* = 7.2, 5.4 Hz, 2H), 2.46 – 2.40 (m, 2H), 2.35 (m, *J* = 6.6 Hz, 2H), 2.11 – 2.04 (m, 2H), 2.01 (m, *J* = 7.1, 5.9, 3.3 Hz, 2H), 1.68 (m, *J* = 6.7 Hz, 2H).

^{13}C NMR {^{1}H} (126 MHz, CD_2Cl_2, 298 K, δ): 154.1, 137.0, 135.2, 134.4, 134.2, 134.0, 130.6, 130.4, 130.0, 129.6, 128.6, 117.3, 35.1, 32.6, 32.1, 32.0, 31.9, 30.3.

^{19}F NMR (471 MHz, CD_2Cl_2, 298 K, δ): –152.13 (bs), –152.18 (bs).

HRMS-ESI (m/z) calc'd. for $C_{24}H_{25}S_2^+$ $[M]^+$, 377.13922; found, 377.13857; deviation: +1.72 ppm.

III.2.1.16 1,9-Cyclohexadecadiene-derived thianthrenium salt **23-TT**

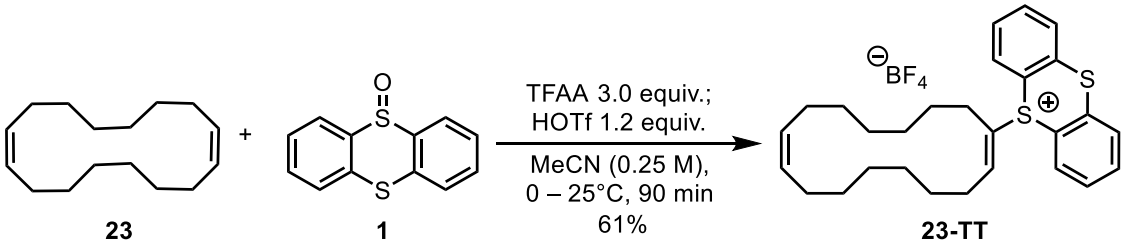

Under ambient atmosphere, a 20 mL borosilicate vial equipped with a magnetic stir bar was charged with 1,9-cyclohexadecadiene (110 mg, 0.500 mmol, 1.00 equiv.), thianthrene-*S*-oxide (**1**) (120 mg, 0.517 mmol, 1.03 equiv.), and MeCN (2.0 mL, c = 0.25 M). After cooling to 0°C, trifluoroacetic anhydride (0.21 mL, 0.31 g, 1.5 mmol, 3.0 equiv.) was added dropwise within 30 seconds, followed by dropwise addition of HOTf (52 µL, 88 mg, 0.59 mmol, 1.2 equiv.)

within 10 seconds. After stirring the lilac mixture at 0 °C for 60 min followed by stirring at 25 °C for 30 min, the resulting purple mixture was concentrated under reduced pressure and subsequently diluted with CH_2Cl_2 (10 mL). The CH_2Cl_2 solution was poured onto a saturated aqueous $NaHCO_3$ solution (ca. 20 mL). The combined mixture was poured into a separatory funnel, and the layers were separated. The CH_2Cl_2 layer was collected, and the aqueous layer was further extracted with CH_2Cl_2 (2 × ca. 10 mL). The combined CH_2Cl_2 solution was washed with aqueous $NaBF_4$ solution (2 × ca. 20 mL, 5 % w/w). The CH_2Cl_2 layer was dried over Na_2SO_4, filtered, and the solvent was removed under reduced pressure. The residue was purified by chromatography on silica gel eluting with CH_2Cl_2/*i*-PrOH (100:1, v/v). The product-containing fractions were collected and concentrated under reduced pressure. The residue was further dried in vacuo to afford **23-TT** (159.0 mg, 304 µmol, 61 %) as a colorless solid.

R_f = 0.46 (CH_2Cl_2/MeOH, 15:1, v/v).

NMR Spectroscopy:

^{1}H NMR (500 MHz, CD_2Cl_2, 298 K, δ): 8.22 (d, *J* = 7.9 Hz, 2H), 7.89 – 7.80 (m, 4H), 7.72 (t, *J* = 7.6 Hz, 2H), 5.51 (t, *J* = 8.3 Hz, 1H), 5.31 – 5.24 (m, 2H), 2.25 – 2.15 (m, 2H), 2.08 (q, *J* = 8.0 Hz, 2H), 1.97 (m, 4H), 1.35 – 1.10 (m, 16H).

^{13}C NMR {^{1}H} (126 MHz, CD_2Cl_2, 298 K, δ): 142.2, 137.3, 135.4, 135.3, 130.7, 130.5, 130.4, 130.1, 123.7, 116.9, 29.3, 29.1, 28.9, 28.5, 28.3, 28.08, 28.03, 28.01, 27.97, 27.7, 27.1, 26.9.

^{19}F NMR (471 MHz, CD_2Cl_2, 298 K, δ): –151.37 (bs), –151.42 (bs).

HRMS-ESI (m/z) calc'd. for $C_{28}H_{35}S_2^+$ $[M]^+$, 435.21747; found, 435.21674; deviation: +1.68 ppm.

III.2.1.17 1,5-Cyclooctadiene-derived thianthrenium salt **24-TT**

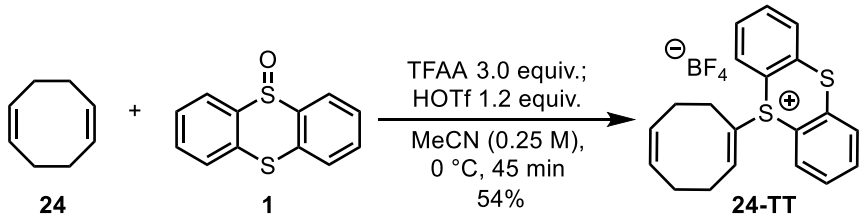

24 **1** **24-TT**

Under ambient atmosphere, a 20 mL borosilicate vial equipped with a magnetic stir bar was charged with 1,5-cyclooctadiene (61.3 µL, 54.1 mg, 0.500 mmol, 1.00 equiv.), thianthrene-*S*-oxide (**1**) (120 mg, 0.517 mmol, 1.03 equiv.), and MeCN (2.0 mL, c = 0.25 M). After cooling to 0°C, trifluoroacetic anhydride (0.21 mL, 0.31 g, 1.5 mmol, 3.0 equiv.) was added dropwise within 30 seconds, followed by dropwise addition of HOTf (52 µL, 88 mg, 0.59 mmol, 1.2 equiv.) within 10 seconds. After stirring the lilac mixture at 0 °C for 45 min, the resulting purple mixture was concentrated under reduced pressure and subsequently diluted with CH_2Cl_2 (10 mL). The CH_2Cl_2 solution was poured onto a saturated aqueous $NaHCO_3$ solution (ca. 20 mL). The combined mixture was poured into a separatory funnel, and the layers were separated. The CH_2Cl_2 layer was collected, and the aqueous layer was further extracted with CH_2Cl_2 (2 × ca. 10 mL). The combined CH_2Cl_2 solution was washed with aqueous $NaBF_4$ solution (2 × ca. 20 mL, 5 % w/w). The CH_2Cl_2 layer was dried over Na_2SO_4, filtered, and the solvent was removed under reduced pressure. The residue was purified by chromatography on silica gel eluting with CH_2Cl_2/*i*-PrOH (100:1, v/v). The product-containing fractions were collected and concentrated under reduced pressure. The residue was further dried in vacuo to afford **24-TT** (110.0 mg, 268 µmol, 54 %) as a colorless solid.

R_f = 0.46 (CH_2Cl_2/MeOH, 15:1, v/v).

NMR Spectroscopy:

^{1}H NMR (500 MHz, $CDCl_3$, 298 K, δ): 8.37 – 8.31 (m, 2H), 7.81 – 7.75 (m, 4H), 7.70 (ddd, *J* = 8.6, 6.8, 2.1 Hz, 2H), 5.84 (t, *J* = 6.5 Hz, 1H), 5.53 – 5.44 (m, 1H), 5.32 – 5.24 (m, 1H), 2.64 (t, *J* = 6.9 Hz, 2H), 2.49 (q, *J* = 6.6 Hz, 2H), 2.33 (q, *J* = 6.9 Hz, 2H), 2.02 (q, *J* = 6.8 Hz, 2H).

^{13}C NMR {^{1}H} (126 MHz, $CDCl_3$, 298 K, δ): 142.2, 136.8, 135.6, 135.1, 130.5, 130.2, 129.0, 127.3, 124.1, 117.5, 29.6, 28.9, 27.1, 26.1.

^{19}F NMR (471 MHz, $CDCl_3$, 298 K, δ): –151.67 (bs), –151.72 (bs).

HRMS-ESI (m/z) calc'd. for $C_{20}H_{19}S_2^+$ $[M]^+$, 323.09227; found, 323.09220; deviation: +0.22 ppm.

III.2.1.18 Tricyclo[6.2.1.02,7]undeca-4-ene-derived thianthrenium salt **25-TT**

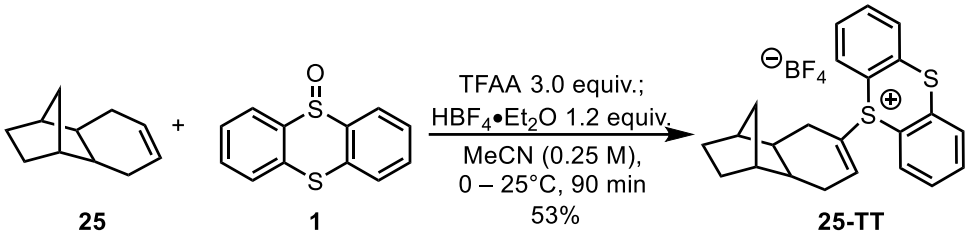

Under ambient atmosphere, a 20 mL borosilicate vial equipped with a magnetic stir bar was charged with tricyclo[6.2.1.02,7]undeca-4-ene (74.1 mg, 0.500 mmol, 1.00 equiv.), thianthrene-*S*-oxide (**1**) (120 mg, 0.517 mmol, 1.03 equiv.), and MeCN (2.0 mL, c = 0.25 M). After cooling to 0°C, trifluoroacetic anhydride (0.21 mL, 0.31 g, 1.5 mmol, 3.0 equiv.) was added dropwise within 30 seconds, followed by dropwise addition of HBF_4•OEt_2 (87 µL, 0.59 mmol, 1.2 equiv.) within 10 seconds. After stirring the lilac mixture at 0 °C for 60 min followed by stirring at 25 °C for 30 min, the resulting purple mixture was concentrated under reduced pressure and subsequently diluted with CH_2Cl_2 (10 mL). The CH_2Cl_2 solution was poured onto a saturated aqueous $NaHCO_3$ solution (ca. 20 mL). The combined mixture was poured into a separatory funnel, and the layers were separated. The CH_2Cl_2 layer was collected, and the aqueous layer was further extracted with CH_2Cl_2 (2 × ca. 10 mL). The combined CH_2Cl_2 solution was washed with aqueous $NaBF_4$ solution (2 × ca. 20 mL, 5 % w/w). The CH_2Cl_2 layer was dried over Na_2SO_4, filtered, and the solvent was removed under reduced pressure. The residue was purified by chromatography on silica gel eluting with CH_2Cl_2/*i*-PrOH (100:1, v/v). The product-containing fractions were collected and concentrated under reduced pressure. The residue was further dried in vacuo to afford **25-TT** (119.1 mg, 265 µmol, 53 %) as a colorless solid.

R_f = 0.46 (CH_2Cl_2/MeOH, 15:1, v/v).

NMR Spectroscopy:

^{1}H NMR (500 MHz, CD_2Cl_2, 298 K, δ): 8.19 (dd, *J* = 8.0, 1.4 Hz, 2H), 7.87 (ddd, *J* = 8.0, 3.8, 1.4 Hz, 2H), 7.81 (tdd, *J* = 7.8, 3.1, 1.4 Hz, 2H), 7.73 (tdd, *J* = 7.5, 3.0, 1.4 Hz, 2H), 6.01 (dd, *J* = 7.6, 2.4 Hz, 1H), 2.49 – 2.42 (m, 1H), 2.25 – 2.17 (m, 1H), 1.95 – 1.90 (m, 1H), 1.89 – 1.83 (m, 1H), 1.66 – 1.54 (m, 4H), 1.51 – 1.40 (m, 3H), 1.18 – 1.06 (m, 2H), 1.05

– 0.98 (m, 1H).

^{13}C NMR {^{1}H} (126 MHz, CD_2Cl_2, 298 K, δ): 142.9, 136.9, 135.4, 135.3, 135.2, 134.9, 130.8, 130.7, 130.5, 121.3, 117.5, 117.3, 44.4, 43.6, 43.3, 42.6, 33.6, 31.1, 29.7, 29.6, 29.5.

^{19}F NMR (471 MHz, CD_2Cl_2, 298 K, δ): –151.72 (bs), –151.78 (bs).

HRMS-ESI (m/z) calc'd. for $C_{23}H_{23}S_2^+$ $[M]^+$, 363.12357; found, 363.12354; deviation: +0.08 ppm.

III.2.1.19 Probenecid-derived thianthrenium salt **28-TT**

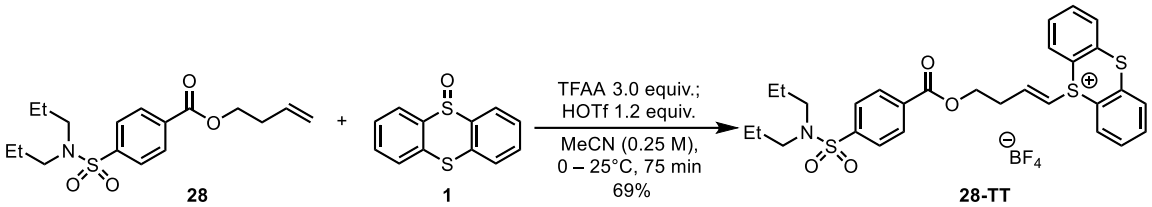

Under ambient atmosphere, a 20 mL borosilicate vial equipped with a magnetic stir bar was charged with Probenecid-derived alkene **28** (170 mg, 0.500 mmol, 1.00 equiv.), thianthrene-*S*-oxide (**1**) (120 mg, 0.517 mmol, 1.03 equiv.), and MeCN (2.0 mL, c = 0.25 M). After cooling to 0°C, trifluoroacetic anhydride (0.21 mL, 0.31 g, 1.5 mmol, 3.0 equiv.) was added dropwise within 30 seconds, followed by dropwise addition of HOTf (52 µL, 88 mg, 0.59 mmol, 1.2 equiv.) within 10 seconds. After stirring the lilac mixture at 0 °C for 45 min followed by stirring at 25 °C for 30 min, the resulting purple mixture was concentrated under reduced pressure and subsequently diluted with CH_2Cl_2 (10 mL). The CH_2Cl_2 solution was poured onto a saturated aqueous $NaHCO_3$ solution (ca. 20 mL). The combined mixture was poured into a separatory funnel, and the layers were separated. The CH_2Cl_2 layer was collected, and the aqueous layer was further extracted with CH_2Cl_2 (2 × ca. 10 mL). The combined CH_2Cl_2 solution was washed with aqueous $NaBF_4$ solution (2 × ca. 20 mL, 5 % w/w). The CH_2Cl_2 layer was dried over Na_2SO_4, filtered, and the solvent was removed under reduced pressure. The residue was purified by chromatography on silica gel eluting with CH_2Cl_2/*i*-PrOH (90:1 to 60:1, v/v). The product-containing fractions were collected and concentrated under reduced pressure. The residue was further dried in vacuo to afford **28-TT** (*E*/*Z* > 50/1, 220.0 mg, 343 µmol, 69 %) as a colorless solid.

R_f = 0.46 (CH_2Cl_2/MeOH, 20:1, v/v).

NMR Spectroscopy:

^{1}H NMR (500 MHz, CD_3Cl, 298 K, δ): 8.36 – 8.31 (m, 2H), 7.99 (d, *J* = 8.2 Hz, 2H), 7.79 (d, *J* = 8.1 Hz, 2H), 7.76 – 7.68 (m, 4H), 7.64 (td, *J* = 7.5, 1.7 Hz, 2H), 7.29 (dt, *J* = 14.6, 7.2 Hz, 1H), 6.70 (d, *J* = 14.7 Hz, 1H), 4.44 (t, *J* = 6.0 Hz, 2H), 3.15 – 3.06 (m, 4H), 2.76 (q, *J* = 6.3 Hz, 2H), 1.55 (h, *J* = 7.4 Hz, 4H), 0.87 (t, *J* = 7.3 Hz, 6H).

^{13}C NMR {^{1}H} (126 MHz, CD_3Cl, 298 K, δ): 164.8, 151.6, 144.5, 135.5, 134.5, 134.0, 132.8, 130.4, 130.2, 130.0, 127.1, 119.9, 112.0, 62.0, 50.0, 32.4, 22.0, 11.2.

^{19}F NMR (471 MHz, CD_3Cl, 298 K, δ): –150.25 (bs), –150.30 (bs).

HRMS-ESI (m/z) calc'd. for $C_{29}H_{32}NO_4S_3^+$ $[M]^+$, 554.14880; found, 554.14880; deviation: 0.00 ppm.

III.2.1.20 Fluazinam-derived thianthrenium salt **29-TT**

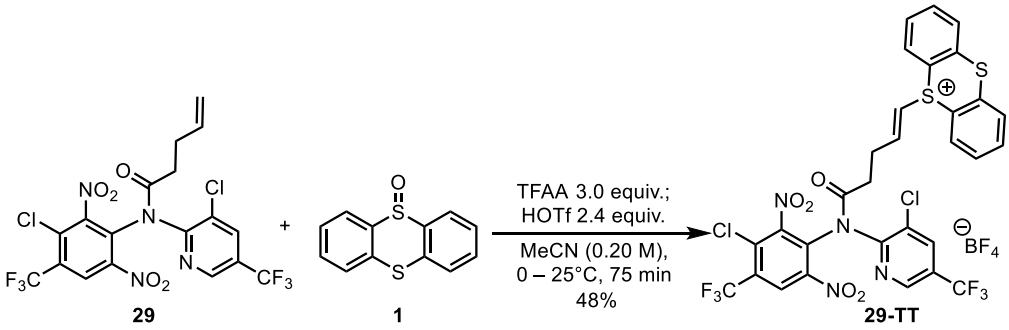

Under ambient atmosphere, a 20 mL borosilicate vial equipped with a magnetic stir bar was charged with Fluazinam-derived alkene **29** (109 mg, 0.200 mmol, 1.00 equiv.), thianthrene-*S*-oxide (**1**) (48 mg, 0.206 mmol, 1.03 equiv.), and MeCN (1.0 mL, c = 0.20 M). After cooling to 0°C, HOTf (20 µL, 35 mg, 0.24 mmol, 1.2 equiv.) within 10 seconds was added dropwise within 30 seconds, followed by dropwise addition of trifluoroacetic anhydride (84 µL, 64 mg, 0.60 mmol, 3.0 equiv.) and HOTf (20 µL, 35 mg, 0.24 mmol, 1.2 equiv.). After stirring the lilac mixture at 0 °C for 45 min followed by stirring at 25 °C for 30 min, the resulting purple mixture was concentrated under reduced pressure and subsequently diluted with CH_2Cl_2 (10 mL). The CH_2Cl_2 solution was poured onto a saturated aqueous $NaHCO_3$ solution (ca. 20 mL). The combined mixture was

poured into a separatory funnel, and the layers were separated. The CH_2Cl_2 layer was collected, and the aqueous layer was further extracted with CH_2Cl_2 (2 × ca. 10 mL). The combined CH_2Cl_2 solution was washed with aqueous $NaBF_4$ solution (2 × ca. 20 mL, 5 % w/w). The CH_2Cl_2 layer was dried over Na_2SO_4, filtered, and the solvent was removed under reduced pressure. The residue was purified by chromatography on silica gel eluting with CH_2Cl_2/*i*-PrOH (100:1, v/v). The product-containing fractions were collected and concentrated under reduced pressure. The residue was further dried in vacuo to afford **29-TT** (*E*/*Z* > 50/1, 81.3 mg, 95.8 µmol, 48 %) as a yellow solid.

R_f = 0.46 (CH_2Cl_2/MeOH, 20:1, v/v).

NMR Spectroscopy:

^{1}H NMR (600 MHz, CD_3Cl, 298 K, δ): 8.74 (s, 1H), 8.40 (s, 1H), 8.23 (d, *J* = 7.9 Hz, 1H), 8.20 (d, *J* = 7.9 Hz, 1H), 7.98 (s, 1H), 7.84 – 7.78 (m, 2H), 7.74 – 7.70 (m, 2H), 7.69 – 7.63 (m, 2H), 7.14 – 7.06 (m, 1H), 6.55 (d, *J* = 14.6 Hz, 1H), 2.91 – 2.79 (m, 2H), 2.78 – 2.70 (m, 1H), 2.60 – 2.51 (m, 1H).

^{13}C NMR {^{1}H} (151 MHz, CD_3Cl, 268 K, δ): 170.3, 154.3, 151.0, 150.6, 147.2, 143.6 (d, *J* = 4.0 Hz), 136.7, 135.7, 135.6, 134.4, 134.3, 134.0, 133.5, 132.5(d, *J* = 34.6 Hz), 130.5, 130.4, 130.25, 130.23, 129.4, 129.3, 129.1, 127.2, 126.7 (q, *J* = 34.1 Hz), 122.1 (d, *J* = 273.2 Hz), 120.6 (d, *J* = 274.9 Hz), 120.2, 119.8, 111.0, 32.6, 27.3.

^{19}F NMR (471 MHz, CD_3Cl, 298 K, δ): –62.29 (s), –63.24 (s), –150.63 (bs), –150.69 (bs).

HRMS-ESI (m/z) calc'd. for $C_{30}H_{17}Cl_2F_6N_4O_5S_2^+$ $[M]^+$, 760.99162; found, 760.99226; deviation: –0.48 ppm.

III.2.1.21 Bicalutamide-derived thianthrenium salt **31-TT**

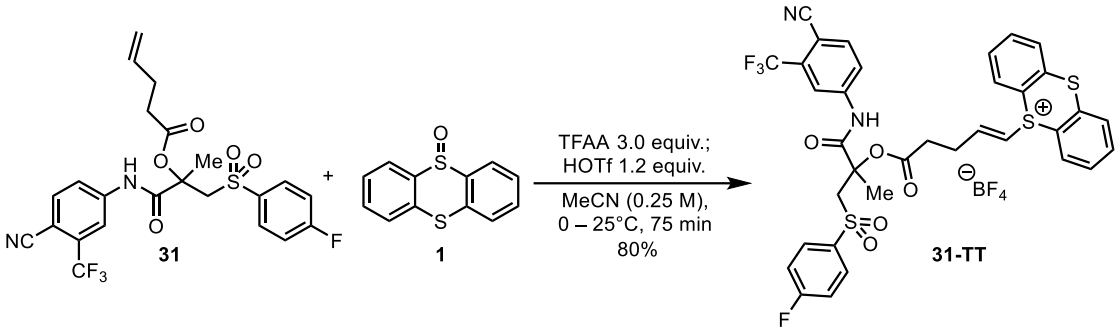

Under ambient atmosphere, a 20 mL borosilicate vial equipped with a magnetic stir bar was charged with Bicalutamide-derived alkene **31** (128 mg, 0.250 mmol, 1.00 equiv.), thianthrene-*S*-oxide (**1**) (60 mg, 0.258 mmol, 1.03 equiv.), and MeCN (2.0 mL, c = 0.13 M). After cooling to 0°C, trifluoroacetic anhydride (0.11 mL, 0.16 g, 0.75 mmol, 3.0 equiv.) was added dropwise within 30 seconds, followed by dropwise addition of HOTf (26 µL, 44 mg, 0.30 mmol, 1.2 equiv.) within 10 seconds. After stirring the lilac mixture at 0 °C for 60 min followed by stirring at 25 °C for 15 min, the resulting pink mixture was concentrated under reduced pressure and subsequently diluted with CH_2Cl_2 (10 mL). The CH_2Cl_2 solution was poured onto a saturated aqueous $NaHCO_3$ solution (ca. 20 mL). The combined mixture was poured into a separatory funnel, and the layers were separated. The CH_2Cl_2 layer was collected, and the aqueous layer was further extracted with CH_2Cl_2 (2 × ca. 10 mL). The combined CH_2Cl_2 solution was washed with aqueous $NaBF_4$ solution (2 × ca. 20 mL, 5 % w/w). The CH_2Cl_2 layer was dried over Na_2SO_4, filtered, and the solvent was removed under reduced pressure. The residue was purified by chromatography on silica gel eluting with CH_2Cl_2/*i*-PrOH (80:1 to 50:1, v/v). The product-containing fractions were collected and concentrated under reduced pressure. The residue was further dried in vacuo to afford **31-TT** (*E*/*Z* > 50/1, 163.2 mg, 200 µmol, 80 %) as a colorless solid.

R_f = 0.46 (CH_2Cl_2/MeOH, 20:1, v/v).

NMR Spectroscopy:

^{1}H NMR (500 MHz, CD_3Cl, 298 K, δ): 9.34 (s, 1H), 8.24 (d, *J* = 2.2 Hz, 1H), 8.16 (d, *J* = 7.9 Hz, 1H), 8.11 (d, *J* = 7.9 Hz, 1H), 7.91 (dd, *J* = 8.6, 2.1 Hz, 1H), 7.88 – 7.79 (m, 4H), 7.77 – 7.68 (m, 2H), 7.67 – 7.56 (m, 3H), 7.28 (dt, *J* = 14.3, 6.8 Hz, 1H), 7.12 (t, *J* = 8.5 Hz, 2H), 6.74 (d, *J* =

14.7 Hz, 1H), 4.17 (d, *J* = 14.5 Hz, 1H), 4.01 (d, *J* = 14.5 Hz, 1H), 3.02 – 2.93 (m, 1H), 2.91 – 2.82 (m, 1H), 2.78 – 2.55 (m, 2H), 1.70 (s, 3H).

^{13}C NMR {^{1}H} (126 MHz, CD_3Cl, 298 K, δ): 171.0, 169.3, 165.8 (d, *J* = 257.4 Hz), 155.8, 141.9, 135.4, 135.4, 135.3, 135.2, 134.32, 134.25, 133.2, 132.9, 132.7, 132.5, 131.3, 131.2, 130.3, 130.2, 130.1, 130.0, 123.1, 122.2 (q, *J* = 274.1 Hz), 120.2 (d, *J* = 8.7 Hz), 118.1, 116.4 (d, *J* = 22.6 Hz), 115.7, 110.2, 103.9, 79.7, 57.4, 53.4, 31.5, 27.7, 23.9.

^{19}F NMR (471 MHz, CD_3Cl, 298 K, δ): –62.00, –102.47 (m), –148.12 (bs), –148.17 (bs).

HRMS-ESI (m/z) calc'd. for $C_{35}H_{27}N_2O_5S_2F_4^+$ $[M]^+$, 727.10128; found, 727.10209; deviation: –1.11 ppm.

III.2.2. Evaluation of different *S*-oxides

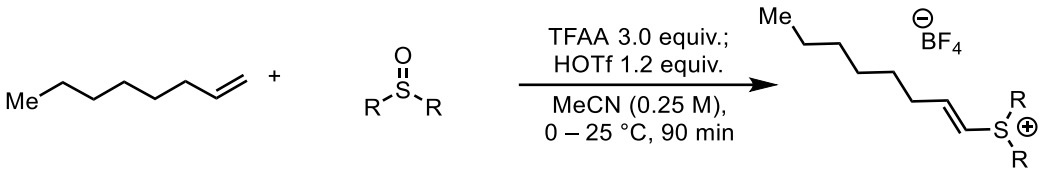

Under ambient atmosphere, a 20 mL borosilicate vial equipped with a magnetic stir bar was charged with 1-octene (78.5 µL, 56.1 mg, 0.500 mmol, 1.00 equiv.), *S*-oxide (0.517 mmol, 1.03 equiv.), and MeCN (2.0 mL, c = 0.25 M). After cooling to 0°C, trifluoroacetic anhydride (0.21 -mL, 0.31 g, 1.5 mmol, 3.0 equiv.) was added dropwise within 30 seconds, followed by dropwise addition of HOTf (52 µL, 88 mg, 0.59 mmol, 1.2 equiv.) within 10 seconds. After stirring the lilac mixture at 0 °C for 60 min followed by stirring at 25 °C for 30 min, the resulting purple mixture was concentrated under reduced pressure and subsequently diluted with CH_2Cl_2 (10 mL). The CH_2Cl_2 solution was poured onto a saturated aqueous $NaHCO_3$ solution (ca. 20 mL). The combined mixture was poured into a separatory funnel, and the layers were separated. The CH_2Cl_2 layer was collected, and the aqueous layer was further extracted with CH_2Cl_2 (2 × ca. 10 mL). The combined CH_2Cl_2 solution was washed with aqueous $NaBF_4$ solution (2 × ca. 20 mL, 5 % w/w). The CH_2Cl_2 layer was dried over Na_2SO_4, filtered, and the solvent was removed under reduced pressure. The residue was checked by TLC and

LCMS or purified by chromatography on silica gel to obtain the yield for alkenyl sulfonium salts.

III.2.3. Mechanistic experiments

III.2.3.1 NMR studies of the reaction kinetics

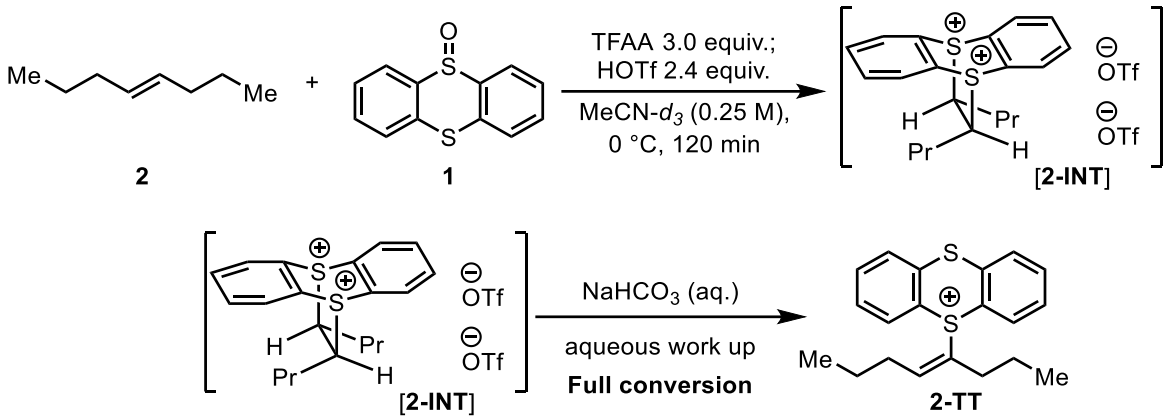

Under ambient atmosphere, a 4 mL borosilicate vial equipped with a magnetic stir bar was charged with *trans*-4-octene (78.5 µL, 56.1 mg, 0.500 mmol, 1.00 equiv.), thianthrene-*S*-oxide (**1**) (60 mg, 0.26 mmol, 0.52 equiv.), and CD_3CN (1.0 mL, c = 0.50 M). After cooling to 0°C, trifluoroacetic anhydride (0.11 mL, 0.16 g, 0.75 mmol, 3.0 equiv.) was added dropwise within 30 seconds, an aliquot (0.20 mL) was taken out and diluted in 0.5 mL CD_3CN, and ^{1}H-NMR was measured for this sample. HOTf (52 µL, 88 mg, 0.59 mmol, 2.4 equiv.) was added dropwise within 10 seconds, during the course of stirring the lilac mixture at 0 °C for 120 min, an aliquot (0.20 mL) was taken out and diluted in 0.5 mL CD_3CN, and ^{1}H-NMR was measured for the samples at the time of 30”, 2’30”, 4’30”, 7’, 10’, 15’, 20’, 30’, 40’, 60’, 90’, and 120’. The resulting light pink mixture was concentrated under reduced pressure and ^{1}H-NMR was checked for the residue. Subsequently the residue was diluted with CD_3Cl (2 mL). A saturated aqueous $NaHCO_3$ solution (ca. 5.0 mL) was slowly added into the CD_3Cl solution, the resulting organic phase was separated and measure by ^{1}H-NMR. Full conversion of thianthrenium dication **2-INT** to the alkenyl thianthrenium salt **2-TT** was observed.

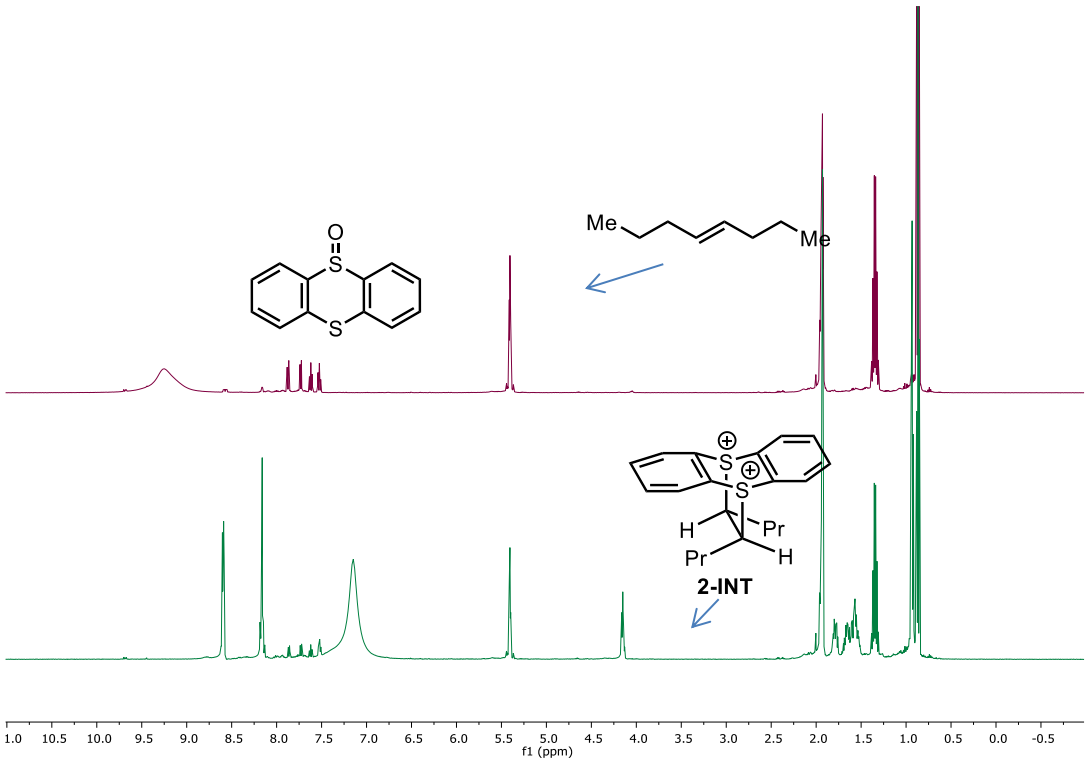

Figure III.1. NMR spectra for the reaction of thianthrene-*S*-oxide, trifluoroacetic anhydride with trans-4-octene before and after addition of triflic acid.

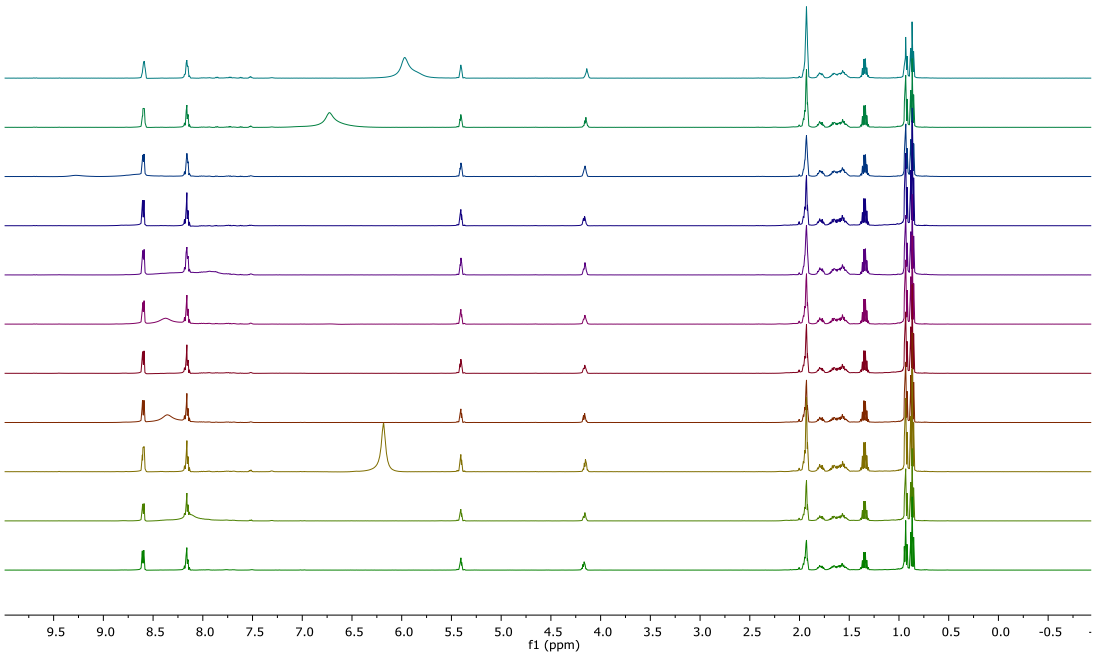

Figure III.2. NMR spectra for the reaction of thianthrene-*S*-oxide, trifluoroacetic anhydride with trans-4-octene after addition of triflic acid between 2'30" and 120' (from top to bottom: 2'30", 4'30", 7', 10', 15', 20', 30', 40', 60', 90', and 120').

Synthesis of dicationic thianthrenium salts

III.2.3.2 *trans*-4-Octene-derived thianthrenium dication **2-INT**

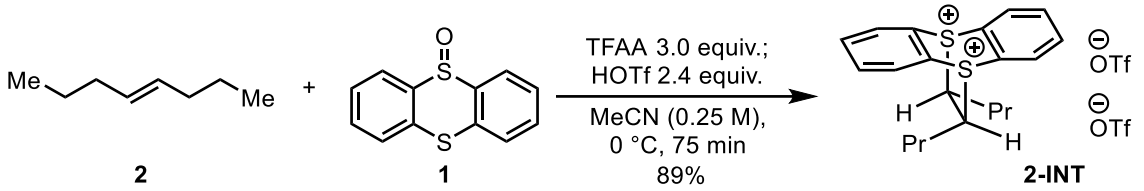

2 **1** **2-INT**

Under ambient atmosphere, a 20 mL borosilicate vial equipped with a magnetic stir bar was charged with *trans*-4-octene (78.5 µL, 56.1 mg, 0.500 mmol, 1.00 equiv.), thianthrene-*S*-oxide (**1**) (120 mg, 0.517 mmol, 1.03 equiv.), and MeCN (2.0 mL, c = 0.25 M). After cooling to 0°C, trifluoroacetic anhydride (0.21 mL, 0.31 g, 1.5 mmol, 3.0 equiv.) was added dropwise within 30 seconds, followed by dropwise addition of HOTf (104 µL, 176 mg, 1.08 mmol, 2.4 equiv.) within 10 seconds. After stirring the lilac mixture at 0 °C for 75 min, the resulting light pink mixture was concentrated under reduced pressure and subsequently diluted with CH_2Cl_2 (2 mL). The CH_2Cl_2 solution was poured onto a stirring solution of Et_2O (ca. 20 mL), and colorless precipitates formed immediately. The colorless solid was collected on a filter frit and rinsed with Et_2O (3 × ca. 5 mL). The solid was collected and further dried in vacuo to afford **2-INT** (280.0 mg, 447 µmol, 89 %) as a colorless solid.

NMR Spectroscopy:

^{1}H NMR (500 MHz, CD_3CN, 298 K, δ): 8.65 – 8.60 (m, 4H), 8.20 – 8.12 (m, 4H), 4.32 – 4.25 (m, 2H), 1.81 – 1.72 (m, 2H), 1.71 – 1.49 (m, 6H), 0.93 (t, *J* = 7.1 Hz, 6H).

^{13}C NMR {^{1}H} (126 MHz, CD_3CN, 298 K, δ): 137.6 – 137.4 (m, 4C), 125.9, 125.0 – 120.5 (m), 122.8, 60.9, 35.0, 20.9, 13.6.

^{19}F NMR (471 MHz, CD_3CN, 298 K, δ): –79.27 (s).

HRMS-ESI (m/z) calc'd. for $C_{20}H_{24}S_2^{2+}$ $[M]^{2+}$, 164.06542; found, 164.06541; deviation: +0.08 ppm.

III.2.3.3 *cis*-4-Octene-derived thianthrenium dication **3-INT**

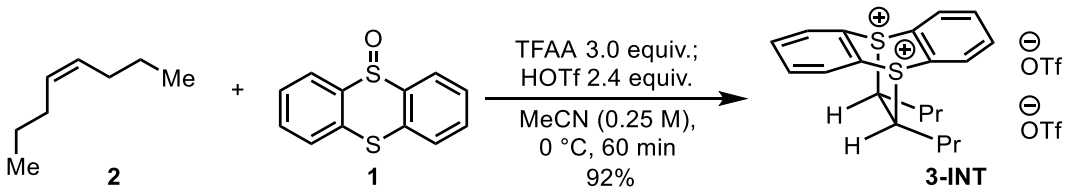

2 **1** **3-INT**

Under ambient atmosphere, a 20 mL borosilicate vial equipped with a magnetic stir bar was charged with *cis*-4-octene (78.5 µL, 56.1 mg, 0.500 mmol, 1.00 equiv.), thianthrene-*S*-oxide (**1**) (120 mg, 0.517 mmol, 1.03 equiv.), and MeCN (2.0 mL, c = 0.25 M). After cooling to 0°C, trifluoroacetic anhydride (0.21 mL, 0.31 g, 1.5 mmol, 3.0 equiv.) was added dropwise within 30 seconds, followed by dropwise addition of HOTf (104 µL, 176 mg, 1.08 mmol, 2.4 equiv.) within 10 seconds. After stirring the lilac mixture at 0 °C for 60 min, the resulting yellow mixture was concentrated under reduced pressure and subsequently diluted with CH_2Cl_2 (2 mL). The CH_2Cl_2 solution was poured onto a stirring solution of Et_2O (ca. 20 mL), and colorless precipitates formed immediately. The colorless solid was collected on a filter frit and rinsed with Et_2O (3 × ca. 5 mL) The solid was collected and further dried in vacuo to afford **3-INT** (287.2 mg, 459 µmol, 92 %) as a beige solid.

NMR Spectroscopy:

^{1}H NMR (500 MHz, CD_3CN, 298 K, δ): 8.66 (dd, *J* = 5.8, 3.4 Hz, 2H), 8.60 (dd, *J* = 5.9, 3.4 Hz, 2H), 8.19 (dd, *J* = 5.8, 3.3 Hz, 2H), 8.12 (dd, *J* = 5.9, 3.4 Hz, 2H), 4.81 – 4.68 (m, 2H), 1.98 – 1.90 (m, 2H, overlapped with CD_3CN), 1.89 – 1.77 (m, 2H), 1.71 – 1.60 (m, 2H), 1.43 – 1.23 (m, 2H), 0.97 (t, *J* = 7.2 Hz, 6H).

^{13}C NMR {^{1}H} (151 MHz, CD_3CN, 298 K, δ): 137.4, 137.3, 136.6, 136.5, 125.8, 123.3, 121.5 (q, *J* = 320.6 Hz), 59.2, 30.1, 21.1, 13.3.

^{19}F NMR (471 MHz, CD_3CN, 298 K, δ): –79.26 (s).

HRMS-ESI (m/z) calc'd. for $C_{20}H_{24}S_2^{2+}$ $[M]^{2+}$, 164.06542; found, 164.06525; deviation: +1.05 ppm.

III.2.3.4 Studies on dicationic thianthrenium salts

Synthesis of 2-TT from 2-INT

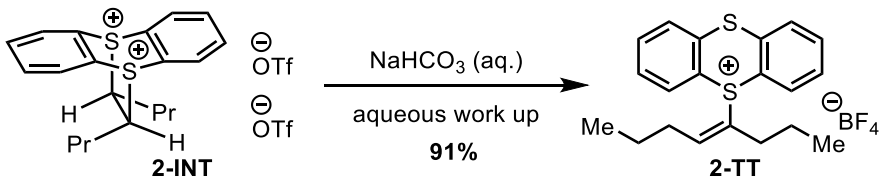

Under ambient atmosphere, a 20 mL borosilicate vial was charged with *cis*-4-octene-derived thianthrenium dication **2-INT** (100 mg, 160 µmol, 1.00 equiv.). The

beige solid was dissolved with CH_2Cl_2 (10 mL) and poured onto a saturated aqueous $NaHCO_3$ solution (ca. 10 mL). The combined mixture was poured into a separatory funnel, and the layers were separated. The CH_2Cl_2 layer was collected, and the aqueous layer was further extracted with CH_2Cl_2 (2 × ca. 10 mL). The combined CH_2Cl_2 solution was washed with aqueous $NaBF_4$ solution (2 × ca. 10 mL, 5 % w/w). The CH_2Cl_2 layer was dried over Na_2SO_4, filtered, and the solvent was removed under reduced pressure. The residue was triturated with Et_2O (3 × 5.0 mL), and Et_2O was removed by pipette. The solid was collected and further dried in vacuo to afford **2-TT** (*E*/*Z* < 50/1, 60.1 mg, 145 µmol, 91 %) as a colorless solid.

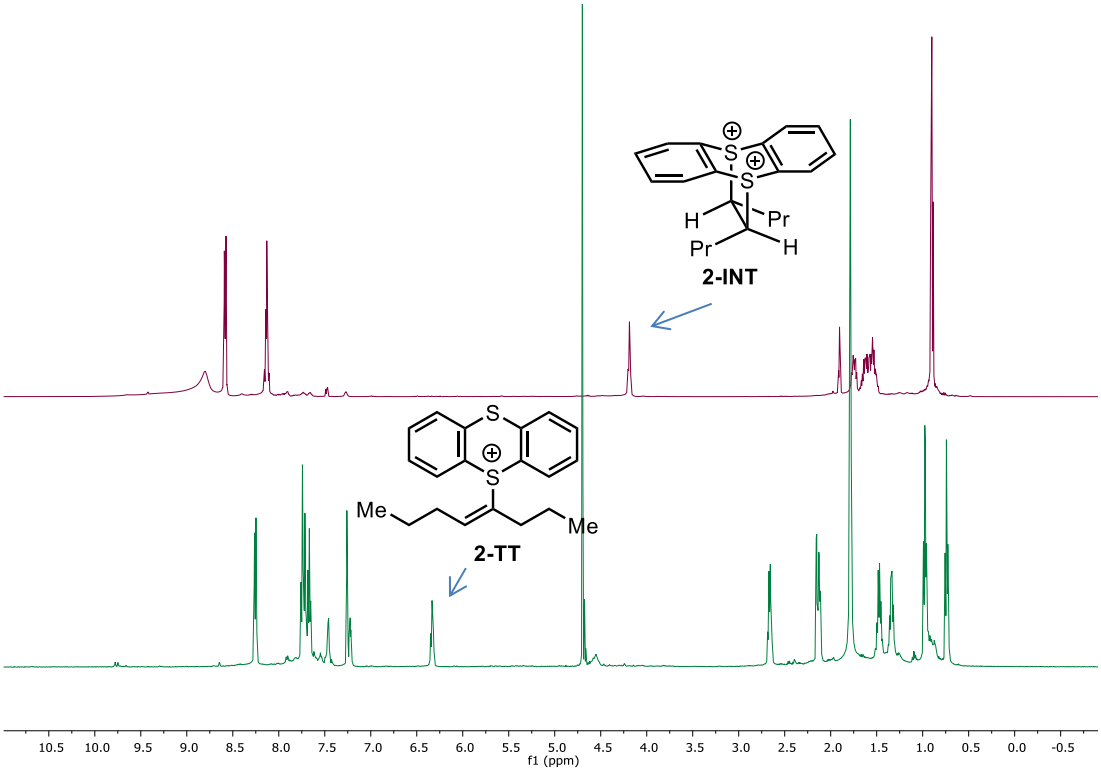

Figure III.3. NMR spectra for the reaction for *trans*-4-octene-derived thianthrenium salt before and after deprotonation (top: concentrated residue; bottom: after deprotonation).

Synthesis of 3-TT from 3-INT

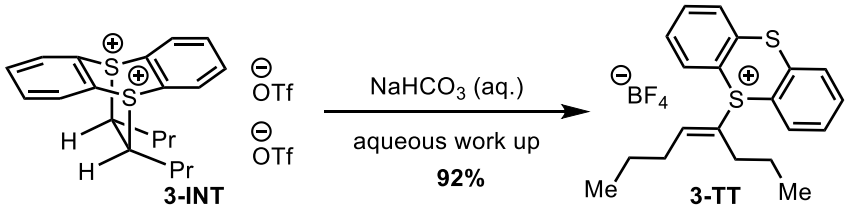

Under ambient atmosphere, a 20 mL borosilicate vial was charged with *cis*-4-octene-derived thianthrenium dication **3-INT** (100 mg, 160 µmol, 1.00 equiv.). The beige solid was dissolved with CH_2Cl_2 (10 mL) and poured onto a saturated aqueous $NaHCO_3$ solution (ca. 10 mL). The combined mixture was poured into a separatory funnel, and the layers were separated. The CH_2Cl_2 layer was collected, and the aqueous layer was further extracted with CH_2Cl_2 (2 × ca. 10 mL). The combined CH_2Cl_2 solution was washed with aqueous $NaBF_4$ solution (2 × ca. 10 mL, 5 % w/w). The CH_2Cl_2 layer was dried over Na_2SO_4, filtered, and the solvent was removed under reduced pressure. The residue was triturated with Et_2O (3 × 5.0 mL), and Et_2O was removed by pipette. The solid was collected and further dried in vacuo to afford **3-TT** (*E*/*Z* > 50/1, 62.2 mg, 148 µmol, 92 %) as a colorless solid. (When the reaction was executed in D_2O with $NaHCO_3$, only **3-TT** was observed, no H/D scrambling was detected.)

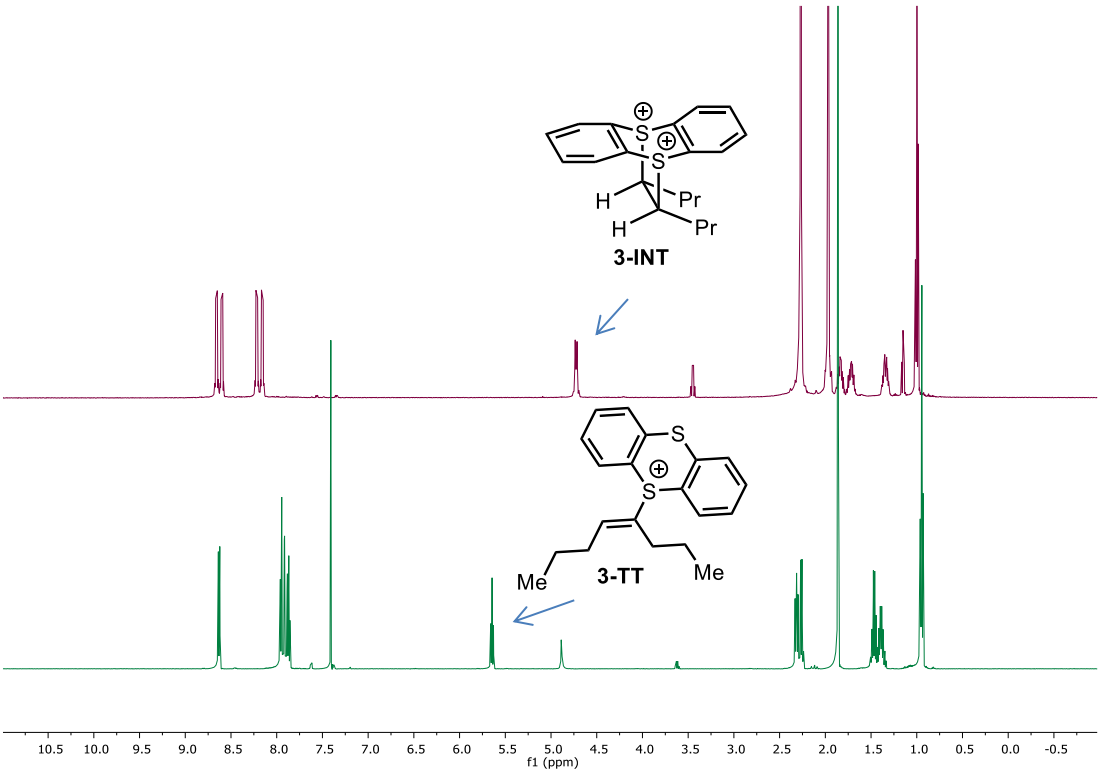

Figure III.4. NMR spectra for the reaction *cis*-4-octene-derived thianthrenium salt before and after deprotonation (top: concentrated residue; bottom: after deprotonation).

III.2.4. Functionalization of alkyl thianthrenium salts

III.2.4.1 Cyclopropyl-pent-4-en-1-yl-phthalimide (**34**)

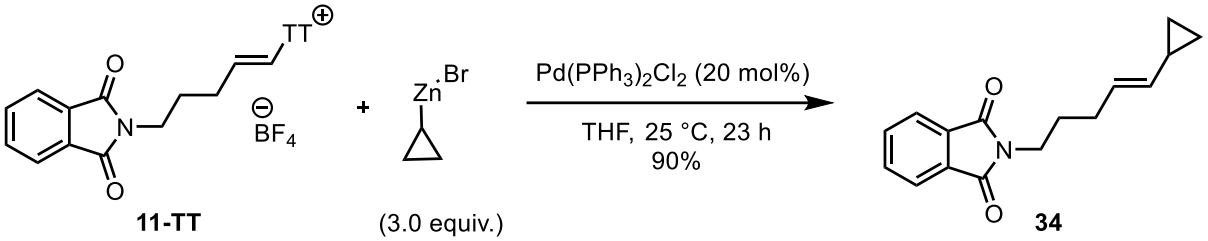

To a 4-mL borosilicate vial equipped with a stir bar was added $Pd(PPh_3)_2Cl_2$ (28 mg, 0.040 mmol, 20 mol%), and alkenyl thianthrenium salt **11-TT** (104 mg, 0.200 mmol, 1.00 equiv.). The vial was transferred into a N_2-filled glovebox. After addition of cyclopropylzinc bromide solution (1.2 mL, 0.50 M in THF, 0.60 mmol, 3.0 equiv.) and THF (0.80 mL, c = 0.10 M), the vial was capped, transferred out of the glovebox and placed on a stirring plate. After being stirred at 25 °C for 23 h, the reaction mixture was diluted with CH_2Cl_2 (2 mL), and the resulting mixture was filtered through a short pad of Celite® using CH_2Cl_2 (5 mL) as eluent. The filtrate was collected and concentrated by rotary evaporation. The residue was purified by chromatography on silica gel eluting with hexanes/ethyl acetate (40:1 to 10:1, v/v) to afford **34** (46.0 mg, 0.180 mmol, 90%) as a colorless solid.

R_f = 0.30 (hexanes/ethyl acetate, 10:1, v/v).

NMR Spectroscopy:

^{1}H NMR (500 MHz, $CDCl_3$, 298 K, δ): 7.83 (dd, *J* = 5.4, 3.1 Hz, 2H), 7.70 (dd, *J* = 5.5, 3.0 Hz, 2H), 5.47 (dt, *J* = 15.3, 6.7 Hz, 1H), 4.98 (dd, *J* = 15.3, 8.6 Hz, 1H), 3.68 (t, *J* = 7.3 Hz, 2H), 2.10 – 2.00 (m, 2H), 1.74 (p, *J* = 7.4 Hz, 2H), 1.35 – 1.24 (m, 1H), 0.65 – 0.56 (m, 2H), 0.33 – 0.23 (m, 2H).

^{13}C NMR {^{1}H} (126 MHz, $CDCl_3$, 298 K, δ): 168.4, 134.82, 133.8, 132.2, 126.3, 123.1, 37.7, 29.8, 28.2, 13.5, 6.3.

HRMS-ESI (m/z) calc'd. for $C_{16}H_{17}NO_2Na^+$ $[M+Na]^+$, 278.11514; found, 278.11500; deviation: +0.53 ppm.

III.2.4.2 Phenylacetylenyl-pent-4-en-1-yl-phthalimide (**35**)

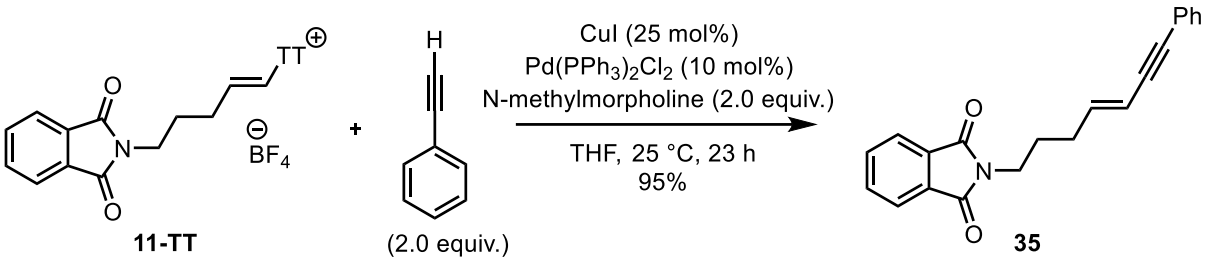

To a 4-mL borosilicate vial equipped with a stir bar was added $Pd(PPh_3)_2Cl_2$ (7.0 mg, 0.010 mmol, 10 mol%), CuI (4.8 mg, 0.025 mmol, 25 mol%), and alkenyl thianthrenium salt **11-TT** (51.7 mg, 0.100 mmol, 1.00 equiv.). The vial was transferred into a N_2-filled glovebox. After addition of THF (1.0 mL, c = 0.10 M), phenylacetylene (22.0 µL, 20.5 mg, 0.200mmol, 2.00 equiv.), and N-methylmorpholine (22.0 µL, 20.3 mg, 0.200 mmol, 2.00 equiv.), the vial was capped, transferred out of the glovebox, and placed on a stirring plate. After being stirred at 25 °C for 23 h, the reaction mixture was diluted with CH_2Cl_2 (2 mL), and the resulting mixture was filtered through a short pad of Celite® using CH_2Cl_2 (5 mL) as eluent. The filtrate was collected and concentrated by rotary evaporation. The residue was purified by chromatography on silica gel eluting with hexanes/ethyl acetate (40:1 to 10:1, v/v) to afford **35** (30.0 mg, 0.095 mmol, 95%, *E*/*Z* ≅ 10/1) as a yellow solid.

R_f = 0.26 (hexanes/ethyl acetate, 10:1, v/v).

NMR Spectroscopy:

^{1}H NMR (500 MHz, $CDCl_3$, 298 K, δ): 7.70 (dd, *J* = 5.5, 3.1 Hz, 2H), 7.56 (dd, *J* = 5.4, 3.0 Hz, 2H), 7.28 – 7.24 (m, 2H), 7.14 (m, 3H), 6.08 (dt, *J* = 15.7, 7.0 Hz, 1H), 5.60 (dt, *J* = 15.8, 1.6 Hz, 1H), 3.58 (t, *J* = 7.1 Hz, 2H), 2.15 – 2.05 (m, 2H), 1.69 (p, *J* = 7.3 Hz, 2H).

^{13}C NMR {^{1}H} (126 MHz, $CDCl_3$, 298 K, δ): 168.3, 142.9, 133.9, 132.1, 131.4, 128.2, 127.9, 123.4, 123.2, 110.6, 88.3, 87.9, 37.4, 30.5, 27.

HRMS-ESI (m/z) calc'd. for $C_{21}H_{17}NO_2Na^+$ $[M+Na]^+$, 338.11514; found, 338.11551; deviation: –1.07 ppm.

III.2.4.3 Vinylnaphthalenyl-pent-4-en-1-yl-phthalimide (**36**)

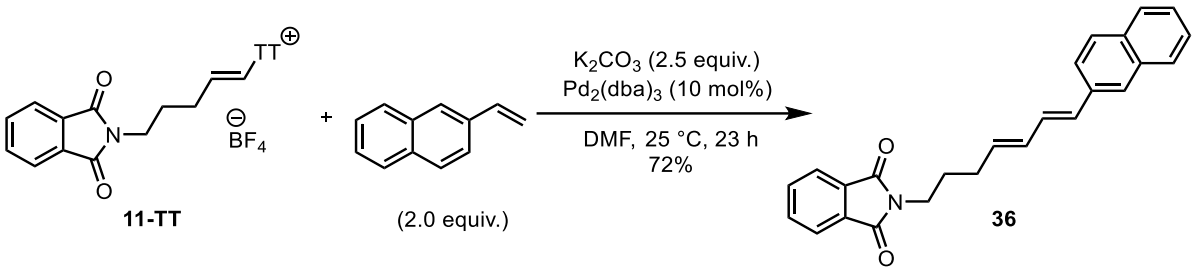

To a 4-mL borosilicate vial equipped with a stir bar was added $Pd_2(dba)_3$ (14 mg, 0.010 mmol, 10 mol%), 2-vinylnaphthalene (30.8 mg, 0.200 mmol, 2.00 equiv.), K_2CO_3 (34.6 mg, 0.250 mmol, 2.50 equiv.), and alkenyl thianthrenium salt **11-TT** (51.7 mg, 0.100 mmol, 1.00 equiv.). The vial was transferred into a N_2-filled glovebox. After addition of THF (1.0 mL, c = 0.10 M), the vial was capped, transferred out of the glovebox, and placed on a stirring plate. After being stirred at 25 °C for 23 h, the reaction mixture was diluted with CH_2Cl_2 (2 mL), and the resulting mixture was filtered through a short pad of Celite® using CH_2Cl_2 (5 mL) as eluent. The filtrate was collected and concentrated by rotary evaporation. The residue was purified by chromatography on silica gel eluting with hexanes/ethyl acetate (40:1 to 10:1, v/v) to afford **36** (26.4 mg, 0.072 mmol, 72%) as a colorless solid.

R_f = 0.25 (hexanes/ethyl acetate, 10:1, v/v).

NMR Spectroscopy:

^{1}H NMR (500 MHz, CD_2Cl_2, 298 K, δ): 7.84 – 7.81 (m, 2H), 7.78 (t, *J* = 8.5 Hz, 3H), 7.72 – 7.69 (m, 3H), 7.59 (dd, *J* = 8.7, 1.7 Hz, 1H), 7.47 – 7.40 (m, 2H), 6.86 (dd, *J* = 15.7, 10.4 Hz, 1H), 6.60 (d, *J* = 15.6 Hz, 1H), 6.31 (dd, *J* = 15.2, 10.4 Hz, 1H), 5.89 (dt, *J* = 14.6, 7.0 Hz, 1H), 3.71 (t, *J* = 7.2 Hz, 2H), 2.24 (q, *J* = 7.3 Hz, 2H), 1.84 (p, *J* = 7.3 Hz, 2H).

^{13}C NMR {^{1}H} (126 MHz, $CDCl_3$, 298 K, δ): 168.6, 135.2, 134.2, 134.1, 133.9, 133.0, 132.3, 131.6, 130.8, 129.6, 128.3, 128.1, 127.8, 126.4, 126.2, 125.9, 123.6, 123.4, 37.8, 30.4, 28.1.

HRMS-ESI (m/z) calc'd. for $C_{25}H_{22}NO_2$ $[M+H]^+$, 368.16450; found, 368.16436; deviation: +0.39 ppm.

III.2.4.4 Chloro-pent-4-en-1-yl-phthalimide (**37**)

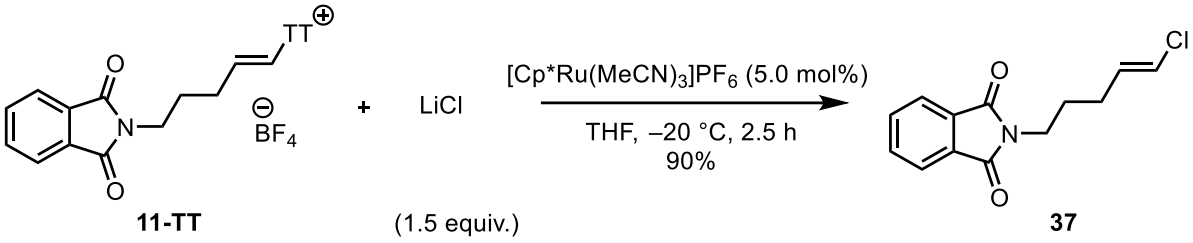

11-TT (1.5 equiv.) **37**

To a 4-mL borosilicate vial equipped with a stir bar was added LiCl (12.7 mg, 0.300 mmol, 1.50 equiv.) and alkenyl thianthrenium salt **11-TT** (104 mg, 0.200 mmol, 1.00 equiv.). The vial was transferred into a N_2-filled glovebox. After addition of $[Cp^*Ru(MeCN)_3]PF_6$ (5.0 mg, 10 µmol, 5.0 mol%) and THF (2.0 mL, c = 0.10 M, THF was pre-cooled to –20 °C), the vial was capped and placed in a cooling well (temperature at round –20 °C) which was pre-cooled in a dry ice-acetonitrile cooling bath. After being stirred at –20 °C for 2.5 h, the vial was transferred out of the glovebox, and the reaction mixture was concentrated by rotary evaporation. The residue was purified by chromatography on silica gel eluting with hexanes/ethyl acetate (40:1 to 10:1, v/v) to afford **37** (45.6 mg, 0.181 mmol, 90%) as a colorless solid.

Gram scale reaction

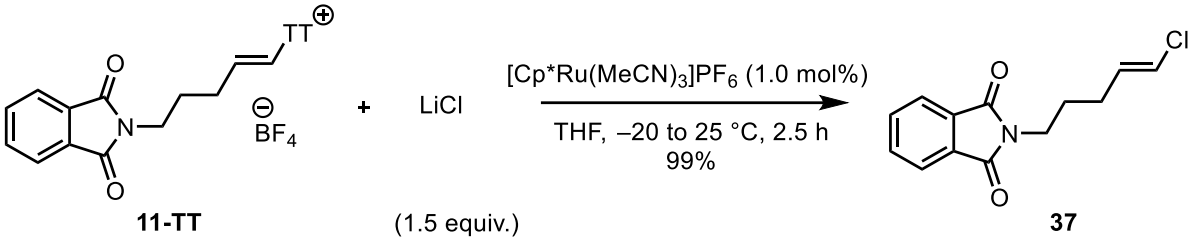

11-TT (1.5 equiv.) **37**

To a 100-mL round-bottomed flask equipped with a stir bar was added LiCl (127 mg, 3.00 mmol, 1.50 equiv.) and alkenyl thianthrenium salt **11-TT** (1.04 g, 2.00 mmol, 1.00 equiv.). The flask was transferred into a N_2-filled glovebox. After addition of $[Cp^*Ru(MeCN)_3]PF_6$ (11 mg, 5.0 µmol, 1.0 mol%) and THF (20 mL, c = 0.10 M, THF was pre-cooled to –20 °C), the flask was capped with a rubber septum and placed in a cooling well (temperature at round –20 °C) which was pre-cooled in a dry ice-acetonitrile cooling bath. After being stirred at –20 °C for 2 h, the flask was transferred out of the glovebox, and the reaction mixture was stirred

at 25 °C for 30 min further and subsequently concentrated by rotary evaporation. The residue was purified by chromatography on silica gel eluting with hexanes/ethyl acetate (60:1 to 10:1, v/v) to afford **37** (495 mg, 1.99 mmol, 99%) as a colorless solid.

R_f = 0.32 (hexanes/ethyl acetate, 10:1, v/v).

NMR Spectroscopy:

^{1}H NMR (500 MHz, $CDCl_3$, 298 K, δ): 7.84 (dd, *J* = 5.4, 3.1 Hz, 2H), 7.71 (dd, *J* = 5.5, 3.0 Hz, 2H), 6.00 (dt, *J* = 13.2, 1.4 Hz, 1H), 5.89 (dt, *J* = 13.5, 7.2 Hz, 1H), 3.69 (t, *J* = 7.1 Hz, 2H), 2.12 (qd, *J* = 7.3, 1.4 Hz, 2H), 1.78 (p, *J* = 7.3 Hz, 2H).

^{13}C NMR {^{1}H} (126 MHz, $CDCl_3$, 298 K, δ): 168.6, 134.2, 132.5, 132.3, 123.8, 118.2, 37.5, 28.5, 27.9.

HRMS-ESI (m/z) calc'd. for $C_{13}H_{13}NO_2Cl$ $[M+H]^+$, 250.06293; found, 250.06264; deviation: +1.17 ppm.

III.2.4.5 Bromo-pent-4-en-1-yl-phthalimide (**38**)

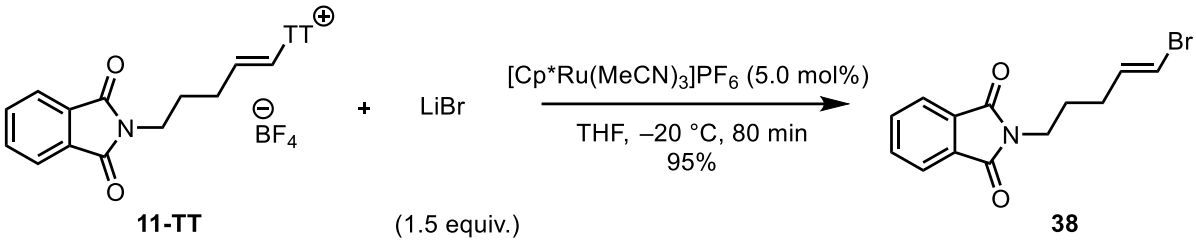

To a 4-mL borosilicate vial equipped with a stir bar was added LiBr (26.1 mg, 0.300 mmol, 1.50 equiv.) and alkenyl thianthrenium salt **11-TT** (104 mg, 0.200 mmol, 1.00 equiv.). The vial was transferred into a N_2-filled glovebox. After addition of $[Cp^*Ru(MeCN)_3]PF_6$ (5.0 mg, 10 µmol, 5.0 mol%) and THF (2.0 mL, c = 0.10 M, THF was pre-cooled to –20 °C), the vial was capped and placed in a cooling well (temperature at round –20 °C) which was pre-cooled in a dry ice-acetonitrile cooling bath. After being stirred at –20 °C for 80 min, the vial was transferred out of the glovebox, and the reaction mixture was concentrated by rotary evaporation. The residue was purified by chromatography on silica gel eluting with hexanes/ethyl acetate (40:1 to 10:1, v/v) to afford **38** (55.7 mg, 0.190 mmol, 95%) as a colorless solid.

R_f = 0.32 (hexanes/ethyl acetate, 10:1, v/v).

NMR Spectroscopy:

^{1}H NMR (500 MHz, $CDCl_3$, 298 K, δ): 7.84 (dd, *J* = 5.4, 3.0 Hz, 2H), 7.71 (dd, *J* = 5.5, 3.0 Hz, 2H), 6.17 (dt, *J* = 13.8, 6.9 Hz, 1H), 6.09 (dd, *J* = 13.5, 1.1 Hz, 1H), 3.70 (t, *J* = 7.0 Hz, 2H), 2.14 – 2.07 (m, 2H), 1.80 (p, *J* = 7.2 Hz, 2H).

^{13}C NMR {^{1}H} (126 MHz, $CDCl_3$, 298 K, δ): 168.1, 136.2, 133.7, 131.8, 123.0, 105.1, 36.9, 30.0, 27.1.

HRMS-ESI (m/z) calc'd. for $C_{13}H_{13}NO_2Br$ $[M+H]^+$, 294.01242; found, 294.01217; deviation: +0.88 ppm.

III.2.4.6 Trifluoromethylsulfuryl-pent-4-en-1-yl-phthalimide (**39**)

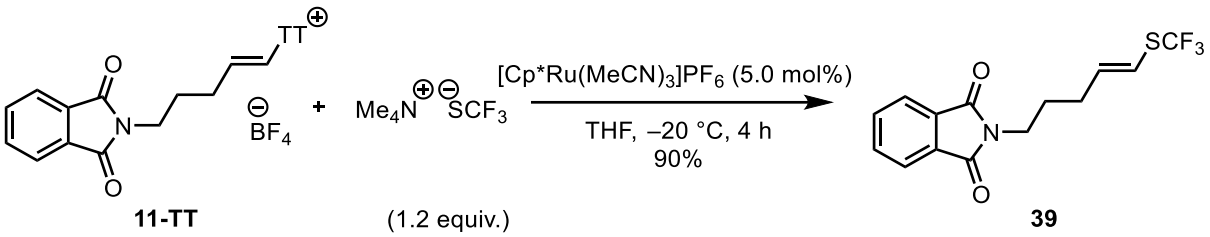

To a 4-mL borosilicate vial equipped with a stir bar was added alkenyl thianthrenium salt **11-TT** (51.7 mg, 0.100 mmol, 1.00 equiv.). The vial was transferred into a N_2-filled glovebox. After addition of tetramethyl ammonium trifluoromethylsulfide[3] (21.0 mg, 0.120 mmol, 1.20 equiv.), $[Cp^*Ru(MeCN)_3]PF_6$ (2.5 mg, 5.0 μmol, 5.0 mol%), and THF (1.0 mL, c = 0.10 M, THF was pre-cooled to –20 °C), the vial was capped and placed in a cooling well (temperature at round –20 °C) which was pre-cooled in a dry ice-acetonitrile cooling bath. After being stirred at –20 °C for 4 h, the vial was transferred out of the glovebox, and the reaction mixture was concentrated by rotary evaporation. The residue was purified by chromatography on silica gel eluting with hexanes/ethyl acetate (40:1 to 10:1, v/v) to afford **39** (28.3 mg, 89.8 μmol, 90%) as a colorless solid.

R_f = 0.32 (hexanes/ethyl acetate, 10:1, v/v).

NMR Spectroscopy:

^{1}H NMR (500 MHz, $CDCl_3$, 298 K, δ): 7.85 (dd, *J* = 5.4, 3.1 Hz, 2H), 7.72 (dd, *J* = 5.4, 3.1 Hz, 2H), 6.23 (dt, *J* = 13.9, 6.8 Hz, 1H), 6.13 (d, *J* = 14.9 Hz, 1H), 3.71 (t, *J* = 7.1 Hz, 2H), 2.25 (q, *J* = 7.2 Hz, 2H), 1.83 (p, *J* = 7.3 Hz, 2H).

^{13}C NMR {^{1}H} (126 MHz, $CDCl_3$, 298 K, δ): 168.3, 144.1, 134.0, 132.0, 129.6 (q, *J* = 307.4 Hz), 123.3, 112.9 (q, *J* = 2.9 Hz), 37.2, 30.4, 27.3.

^{19}F NMR (471 MHz, CD_2Cl_2, 298 K, δ): –43.16 (s).

HRMS-ESI (m/z) calc'd. for $C_{14}H_{12}F_3NO_2SNa$ $[M+Na]^+$, 338.04330; found, 338.04296; deviation: +1.02 ppm.

III.2.4.7 Cyano-pent-4-en-1-yl-phthalimide (**11-CN**)

With Ru catalyst

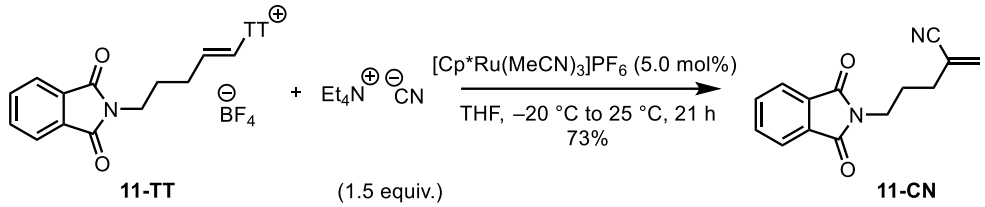

To a 4-mL borosilicate vial equipped with a stir bar was added LiBr (46.9 mg, 0.300 mmol, 1.50 equiv.) and alkenyl thianthrenium salt **11-TT** (104 mg, 0.200 mmol, 1.00 equiv.). The vial was transferred into a N_2-filled glovebox. After addition of $[Cp^*Ru(MeCN)_3]PF_6$ (5.0 mg, 0.010 mmol, 5.0 mol%) and THF (2.0 mL, c = 0.10 M), the vial was capped and placed in a cooling well (temperature at round –20 °C) which was pre-cooled in a dry ice-acetonitrile cooling bath. The reaction mixture was stirred in a cooling well for 21 h, during which the temperature was slowly increased to 25 °C. The vial was then transferred out of the glovebox, and the reaction mixture was concentrated by rotary evaporation. The residue was purified by chromatography on silica gel eluting with hexanes/ethyl acetate (40:1 to 10:1, v/v) to afford **11-CN** (35.2 mg, 0.147 mmol, 73%) as a colorless solid.

Without Ru catalyst

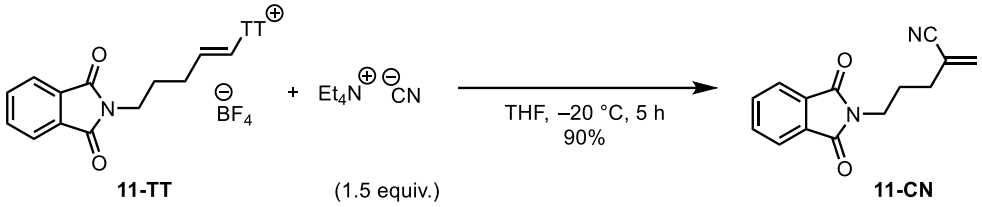

To a 4-mL borosilicate vial equipped with a stir bar was added LiBr (46.9 mg, 0.300 mmol, 1.50 equiv.) and alkenyl thianthrenium salt **11-TT** (104 mg, 0.200 mmol, 1.00 equiv.). The vial was transferred into a N_2-filled glovebox. After addition of THF (2.0 mL, c = 0.10 M), the vial was capped and placed in a cooling well (temperature at round –20 °C) which was pre-cooled in a dry ice-acetonitrile cooling bath. The reaction mixture was stirred in a cooling well for 5 h. The vial was then transferred out of the glovebox, and the reaction mixture was concentrated by rotary evaporation. The residue was purified by chromatography on silica gel eluting with hexanes/ethyl acetate (40:1 to 10:1, v/v) to afford **11-CN** (43.3 mg, 0.180 mmol, 90%) as a colorless solid.

$\mathbf{R_f}$ = 0.35 (hexanes/ethylacetate, 10:1, v/v).

NMR Spectroscopy:

^{1}H NMR (500 MHz, $CDCl_3$, 298 K, δ): 7.85 (ddd, *J* = 4.9, 3.2, 1.3 Hz, 2H), 7.73 (ddd, *J* = 5.0, 3.3, 1.5 Hz, 2H), 5.89 (s, 1H), 5.80 (d, *J* = 1.6 Hz, 1H), 3.73 (td, *J* = 6.8, 1.3 Hz, 2H), 2.36 – 2.28 (m, 2H), 2.02 – 1.92 (m, 2H).

^{13}C NMR {^{1}H} (126 MHz, $CDCl_3$, 298 K, δ): 168.3, 134.1, 132.0, 131.1, 123.3, 121.8, 118.3, 36.7, 31.9, 26.5.

GC-EI (m/z) calc'd. for $C_{14}H_{12}N_2O_2$ [M], 240.089327; found, 240.089090; deviation: +0.99 ppm.

III.2.4.8 Phenylacetylenyl-4-octene (**40**)

For tri-substituted thianthrenium salt 2-TT

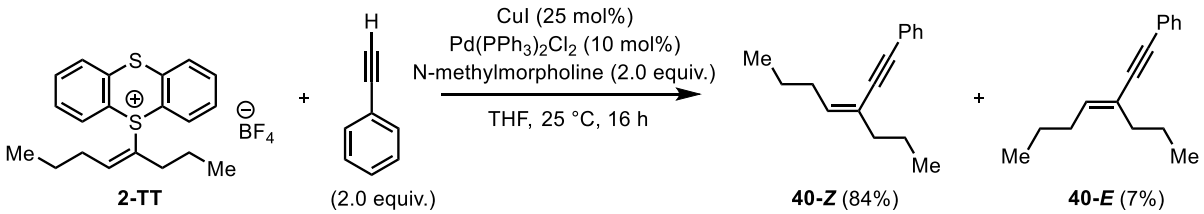

2-TT (2.0 equiv.) **40-*Z*** (84%) **40-*E*** (7%)

To a 4-mL borosilicate vial equipped with a stir bar was added $Pd(PPh_3)_2Cl_2$ (14 mg, 20 µmol, 10 mol%), CuI (9.6 mg, 50 µmol, 25 mol%), and alkenyl thianthrenium salt **2-TT** (82.8 mg, 0.200 mmol, 1.00 equiv.). The vial was transferred into a N_2-filled glovebox. After addition of THF (2.0 mL, c = 0.10 M), phenylacetylene (43.9 µL, 40.9 mg, 0.400mmol, 2.00 equiv.), and N-methylmorpholine (44.0 µL, 40.5 mg, 0.400 mmol, 2.00 equiv.), the vial was capped, transferred out of the glovebox, and placed on a stirring plate. After being stirred at 25 °C for 16 h, the reaction mixture was diluted with CH_2Cl_2 (2 mL), and the resulting mixture was filtered through a short pad of Celite® using CH_2Cl_2 (5 mL) as eluent. The filtrate was collected and concentrated by rotary evaporation. The residue was purified by chromatography on silica gel eluting with pentane to afford **40-*Z*** (35.5 mg, 0.167 mmol, 84%) as a colorless oil and **40-*E*** (3.0 mg, 14 µmol, 7%) as a colorless oil.

For tri-substituted thianthrenium salt 3-TT

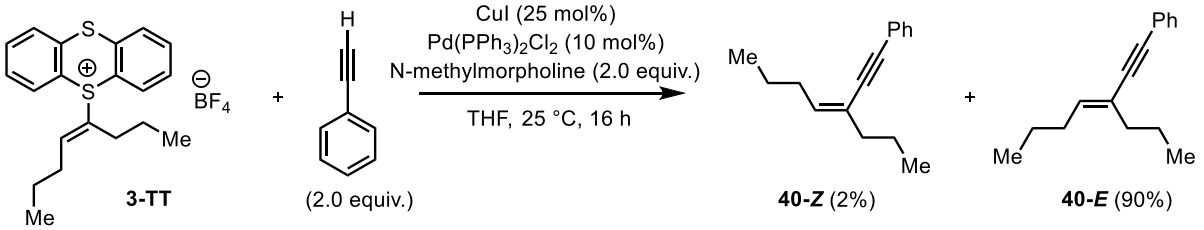

3-TT (2.0 equiv.) **40-*Z*** (2%) **40-*E*** (90%)

To a 4-mL borosilicate vial equipped with a stir bar was added $Pd(PPh_3)_2Cl_2$ (14 mg, 20 µmol, 10 mol%), CuI (9.6 mg, 50 µmol, 25 mol%), and alkenyl thianthrenium salt **3-TT** (82.8 mg, 0.200 mmol, 1.00 equiv.). The vial was transferred into a N_2-filled glovebox. After addition of THF (2.0 mL, c = 0.10 M), phenylacetylene (43.9 µL, 40.9 mg, 0.400mmol, 2.00 equiv.), and N-methylmorpholine (44.0 µL, 40.5 mg, 0.400 mmol, 2.00 equiv.), the vial was

capped, transferred out of the glovebox, and placed on a stirring plate. After being stirred at 25 °C for 16 h, the reaction mixture was diluted with CH_2Cl_2 (2 mL), and the resulting mixture was filtered through a short pad of Celite® using CH_2Cl_2 (5 mL) as eluent. The filtrate was collected and concentrated by rotary evaporation. The residue was purified by chromatography on silica gel eluting with pentane to afford **40-*Z*** (0.7 mg, 3.3 µmol, 2%) as a colorless oil and **40-*E*** (38.0 mg, 0.179 mmol, 90%) as a colorless oil.

40-*Z*

R_f = 0.76 (hexanes).

NMR Spectroscopy:

^{1}H NMR (500 MHz, $CDCl_3$, 298 K, δ): 7.37 – 7.31 (m, 2H), 7.25 – 7.14 (m, 3H), 5.90 (tt, *J* = 7.5, 1.1 Hz, 1H), 2.12 (t, *J* = 7.4, 1.0 Hz, 2H), 2.05 (q, *J* = 7.4 Hz, 2H), 1.59 – 1.47 (m, 2H), 1.41 – 1.29 (m, 2H), 0.88 (t, *J* = 7.4 Hz, 3H), 0.86 (t, *J* = 7.4 Hz, 3H).

^{13}C NMR {^{1}H} (126 MHz, $CDCl_3$, 298 K, δ): 138.5, 131.4, 128.2, 127.6, 123.9, 123.1, 91.9, 86.5, 32.7, 30.5, 22.6, 21.7, 13.9, 13.8.

GCMS-EI (m/z) calc'd. for $C_{16}H_{20}$ [M], 212.15595; found, 212.15579; deviation: +0.76 ppm.

40-*E*

R_f = 0.70 (hexanes).

NMR Spectroscopy:

^{1}H NMR (500 MHz, $CDCl_3$, 298 K, δ): 7.49 – 7.41 (m, 2H), 7.32 (tdt, *J* = 7.0, 5.4, 1.7 Hz, 3H), 5.75 (tt, *J* = 7.4, 1.3 Hz, 1H), 2.35 (q, *J* = 7.3 Hz, 2H), 2.23 – 2.15 (m, 2H), 1.68 – 1.57 (m, 2H), 1.53 – 1.43 (m, 2H), 0.97 (t, *J* = 7.4 Hz, 3H), 0.95 (t, *J* = 7.4 Hz,3H).

^{13}C NMR {^{1}H} (126 MHz, $CDCl_3$, 298 K, δ): 138.0, 131.4, 128.3, 127.8, 124.0, 123.1, 93.2, 88.5, 39.2, 32.7, 22.5, 21.8, 13.9, 13.5.

GCMS-EI (m/z) calc'd. for $C_{16}H_{20}$ [M], 212.15595; found, 212.15577; deviation: +0.85 ppm.

III.3. Experimental data for fluorination of aryl thianthrenium salts

Parts of this chapter are taken, with permission, from our published work in Nature Chemistry.[188] *The experimental data for fluorination was collected by the author with help from Dr. Jiakun Li. Fluorescence quench experiments were executed by Dr. Matthew B. Plutschack and the author. The CV experiments were conducted and analyzed by the author with help from Dr. Wonseok Ham.*

III.3.1. General procedure for fluorination of aryl thianthrenium salts

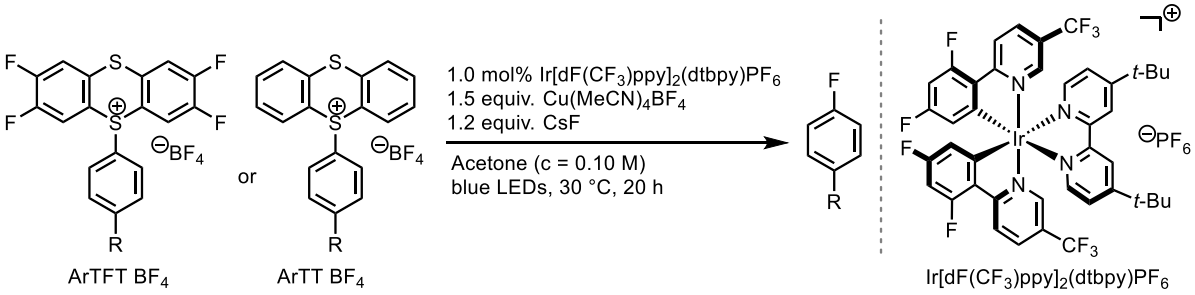

To a 4-mL borosilicate vial, equipped with a stir bar, was added $Ir[dF(CF_3)ppy]_2(dtbpy)PF_6$ (2.4 mg, 2.1 μmol, 1.0 mol%) and an aryl (tetrafluoro)thianthrenium salt (0.200 mmol, 1.00 equiv.). Under N_2 atmosphere, $Cu(MeCN)_4BF_4$ (94.4 mg, 0.300 mmol, 1.50 equiv.), anhydrous CsF (36.4 mg, 0.240 mmol, 1.20 equiv), and anhydrous acetone (2.0 mL, c = 0.10 M) was added into the reaction vial. Subsequently, the vial was capped and placed 5 cm away from two 34 W blue LEDs. The temperature was kept at approximately 30 °C through cooling with a fan. After being stirred for 20 h, the reaction mixture was diluted with CH_2Cl_2 (2 mL), and the resulting mixture was filtered through a short pad of Celite® using CH_2Cl_2 (5 mL) as eluent. The filtrate was collected and concentrated by rotary evaporation. The residue was purified by chromatography on silica gel to afford the fluorinated product.

NOTE: For optimal results, the use of anhydrous CsF is important for the reaction. When CsF was weighed under ambient atmosphere, the yield of the fluorinated product is lower and the yield of the hydrodefunctionalized product is higher. Schlenk techniques can be used to avoid moisture. For convenience, we have stored and weighed the CsF in a N_2-filled glovebox; the reactions can be performed outside of a glovebox.

Synthetic examples for fluorination of aryl thianthrenium salts

III.3.1.1 Fluorosalicin pentaacetate (**57**)

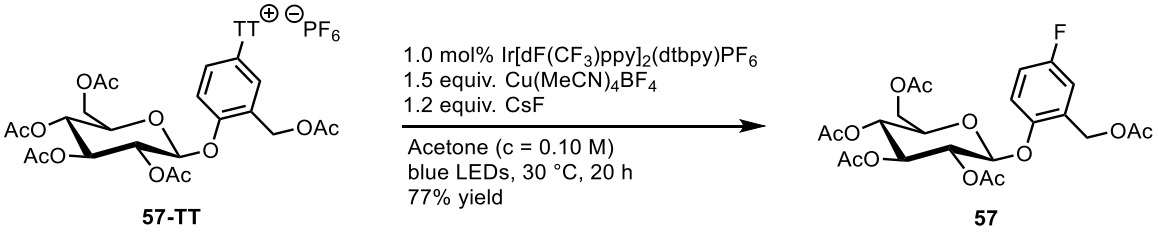

To a 4-mL borosilicate vial equipped with a stir bar was added Ir[dF(CF$_3$)ppy]$_2$(dtbpy)PF$_6$ (2.4 mg, 2.1 µmol, 1.0 mol%) and salicin pentaacetate-derived thianthrenium salt **57-TT** (171 mg, 0.200 mmol, 1.00 equiv.). The vial was transferred into a N_2-filled glovebox. After addition of Cu(MeCN)$_4$BF$_4$ (94.4 mg, 0.300 mmol, 1.50 equiv.), CsF (36.4 mg, 0.240 mmol, 1.20 equiv.) and acetone (2.0 mL, c = 0.10 M), the vial was capped, transferred out of the glovebox and placed 5 cm away from two 34 W blue LEDs. The temperature was kept at approximately 30 °C through cooling with a fan. After being stirred for 20 h, the reaction mixture was diluted with CH_2Cl_2 (2 mL), and the resulting mixture was filtered through a short pad of Celite® using CH_2Cl_2 (5 mL) as eluent. The filtrate was collected and concentrated by rotary evaporation. The residue was purified by chromatography on silica gel eluting with hexanes/ethyl acetate (40:1, v/v) to afford **57** (79.4 mg, 154 µmol, 77%) as a colorless solid.

R_f = 0.35 (hexanes/ethyl acetate 3:2, v/v).

NMR Spectroscopy:

^{1}H NMR (500 MHz, $CDCl_3$, 298 K, δ): 7.02 (td, *J* = 8.8, 8.4, 3.8 Hz, 2H), 6.90 (td, *J* = 8.5, 3.2 Hz, 1H), 5.27–5.21 (m, 2H), 5.12 (ddd, *J* = 9.4, 6.3, 3.1 Hz, 1H), 5.06 (d, *J* = 13.5 Hz, 1H), 4.96 (d, *J* = 13.2 Hz, 1H), 4.95 (dd, *J* = 5.4, 2.3 Hz, 1H), 4.23 (dd, *J* = 12.3, 5.3 Hz, 1H), 4.14 (dd, *J* = 12.3, 2.5 Hz, 1H), 3.79 (ddd, *J* = 10.0, 5.3, 2.5 Hz, 1H), 2.08 (s, 3H), 2.07 (s, 3H), 2.03 (s, 3H), 2.00 (s, 3H), 1.99 (s, 3H) ppm.

^{13}C NMR (126 MHz, $CDCl_3$, 298 K, δ): 170.5, 170.2, 169.4, 169.3, 158.8 (d, *J* = 242.4 Hz), 150.3 (d, *J* = 2.5 Hz), 128.7 (d, *J* = 7.7 Hz), 118.2 (d, *J* = 8.3 Hz), 115.6 (d, *J* = 24.2 Hz), 115.4 (d, *J* = 23.2 Hz), 100.1, 72.6, 72.1, 71.0, 68.3,

61.9, 60.5, 20.9, 20.7, 20.6 ppm.

^{19}F NMR (471 MHz, $CDCl_3$, 298 K, δ): –118.94 (td, *J* = 8.4, 4.4 Hz) ppm.

HRMS-ESI (m/z) calculated for $C_{23}H_{27}F_1O_{12}Na^+$ $[M+Na]^+$, 537.137878; found, 537.137930, deviation: –0.10 ppm.

III.3.1.2 Fluoroboscalid (**59**)

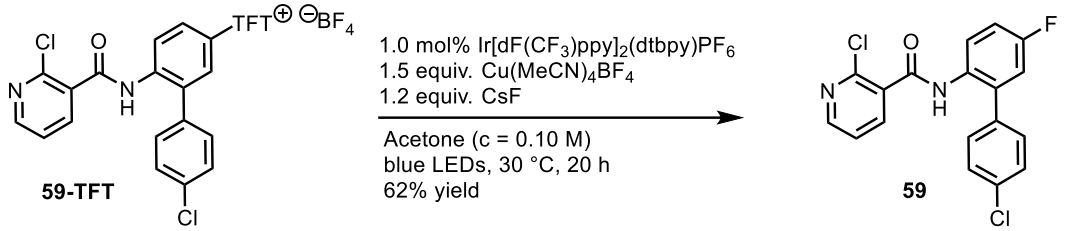

To a 4-mL borosilicate vial equipped with a stir bar was added $Ir[dF(CF_3)ppy]_2(dtbpy)PF_6$ (1.2 mg, 1.0 µmol, 1.0 mol%) and boscalid-derived tetrafluorothianthrenium salt **59-TFT** (71.7 mg, 0.100 mmol, 1.00 equiv.). The vial was transferred into a N_2-filled glovebox. After addition of $Cu(MeCN)_4BF_4$ (47.4 mg, 0.150 mmol, 1.50 equiv.), CsF (18.2 mg, 0.120 mmol, 1.20 equiv.) and acetone (1.0 mL, c = 0.10 M), the vial was capped, transferred out of the glovebox and placed 5 cm away from two 34 W blue LEDs. The temperature was kept at approximately 30 °C through cooling with a fan. After being stirred for 20 h, the reaction mixture was diluted with CH_2Cl_2 (2 mL), and the resulting mixture was filtered through a short pad of Celite® using CH_2Cl_2 (5 mL) as eluent. The filtrate was collected and concentrated by rotary evaporation. The residue was purified by chromatography on silica gel eluting with isohexane/ethyl acetate (5:1 to 3:1 + 1% CH_2Cl_2, v/v/v) to afford the title compound **59** (22.3 mg, 62.0 µmol, 62%) as a colorless solid.

R_f = 0.34 (hexanes/ethyl acetate 3:1, v/v).

NMR Spectroscopy:

^{1}H NMR (500 MHz, $CDCl_3$, 298 K, δ): 8.44 (dd, *J* = 4.7, 2.1 Hz, 1H), 8.32 (dd, *J* = 9.1, 5.3 Hz, 1H), 8.13 (dd, *J* = 7.7, 2.0 Hz, 1H), 8.09 (br, 1H), 7.44 (d, *J* = 8.4 Hz, 2H), 7.38–7.29 (m, 3H), 7.15 (td, *J* = 8.5, 3.0 Hz, 1H), 7.00 (dd, *J* = 8.7, 3.0 Hz, 1H) ppm.

^{13}C NMR (126 MHz, $CDCl_3$, 298 K, δ): 162.7, 159.8 (d, *J* = 246.6 Hz), 151.6,

146.8, 140.4, 135.4, 135.1, 134.7 (d, *J* = 7.8 Hz), 130.9, 130.7, 130.5 (d, *J* = 2.9 Hz), 129.6, 124.5 (d, *J* = 8.3 Hz), 123.1, 117.1 (d, *J* = 23.0 Hz), 115.6 (d, *J* = 21.8 Hz) ppm.

^{19}F NMR (471 MHz, $CDCl_3$, 298 K, δ): –116.19 (td, *J* = 8.3, 5.5 Hz) ppm.

HRMS-ESI (m/z) calculated for $C_{18}H_{11}Cl_2F_1N_2O_1Na^+$ $[M+Na]^+$, 383.012466; found, 383.012770, deviation: –0.79 ppm.

III.3.1.3 Fluoroamiodarone (**60**)

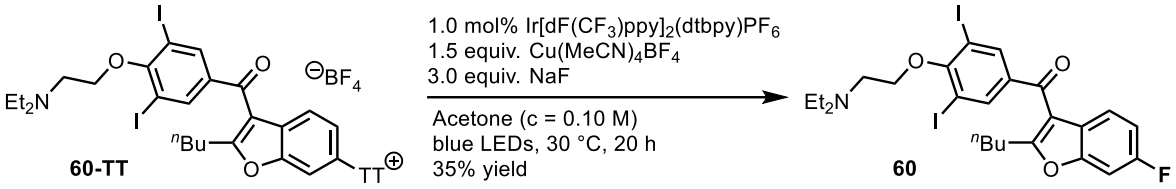

To a 4-mL borosilicate vial equipped with a stir bar was added $Ir[dF(CF_3)ppy]_2(dtbpy)PF_6$ (1.2 mg, 1.0 µmol, 1.0 mol%) and amiodarone-derived thianthrenium salt **60-TT** (102 mg, 0.100 mmol, 1.00 equiv.). The vial was transferred into a N_2-filled glovebox. After addition of $Cu(MeCN)_4BF_4$ (47.4 mg, 0.150 mmol, 1.50 equiv.), NaF (12.6 mg, 0.300 mmol, 3.00 equiv.) and acetone (1.0 mL, c = 0.10 M), the vial was capped, transferred out of the glovebox and placed 5 cm away from two 34 W blue LEDs. The temperature was kept at approximately 30 °C through cooling with a fan. After being stirred for 20 h, the reaction mixture was diluted with CH_2Cl_2 (2 mL), and the resulting mixture was filtered through a short pad of Celite® using CH_2Cl_2 (5 mL) as eluent. The filtrate was collected and concentrated by rotary evaporation. The residue was purified by chromatography on silica gel eluting with CH_2Cl_2/MeOH (100:1 to 20:1 + 2% Et_3N, v/v/v) to afford the title compound **29** with with minor impurities. Further purification of **60** by HPLC (YMC-Actus Triart C18 (30×150 mm: 5 µm), MeOH/20 mM NH_4HCO_3 = 98:2, flow rate = 42.5 mL/min, 25 °C, retention time; 10.6 min) provided **29** (23.1 mg, 35.0 µmol, 35% yield; >99% pure by HPLC).

R_f = 0.29 (CH_2Cl_2/MeOH 20:1, v/v).

NMR Spectroscopy:

^{1}H NMR (500 MHz, $CDCl_3$, 298 K, δ): 8.19 (s, 2H), 7.39 (dd, *J* = 8.7, 5.3 Hz, 1H), 7.21 (dd, *J* = 8.6, 2.3 Hz, 1H), 7.02 (ddd, *J* = 9.4, 8.6, 2.3 Hz, 1H), 4.18 (t, *J* = 6.5 Hz, 2H), 3.16 (t, *J* = 6.1 Hz, 2H), 2.80 (dd, *J* = 10.3, 5.2 Hz, 6H), 1.85–1.67 (m, 2H), 1.35 (h, *J* = 7.4 Hz, 2H), 1.16 (t, *J* = 7.1 Hz, 6H), 0.91 (t, *J* = 7.3 Hz, 3H) ppm.

^{13}C NMR (126 MHz, $CDCl_3$, 298 K, δ): 187.6, 166.7 (d, *J* = 3.6 Hz), 161.6, 161.0 (d, *J* = 243.9 Hz), 153.8 (d, *J* = 13.2 Hz), 140.8, 138.3, 122.9 (d, *J* = 1.8 Hz), 121.7 (d, *J* = 9.7 Hz), 115.8, 112.3 (d, *J* = 23.7 Hz), 99.2 (d, *J* = 26.5 Hz), 91.0, 52.1, 47.9, 30.1, 28.4, 22.7, 13.9, 11.8 ppm.

^{19}F NMR (471 MHz, $CDCl_3$, 298 K, δ): –116.32 (m) ppm.

HRMS-ESI (m/z) calculated for $C_{25}H_{29}F_1I_2N_1O_3^+$ $[M+H]^+$, 664.021542; found, 664.022040, deviation: –0.75 ppm.

III.3.1.4 Fluoropyriproxyfen (**61**)

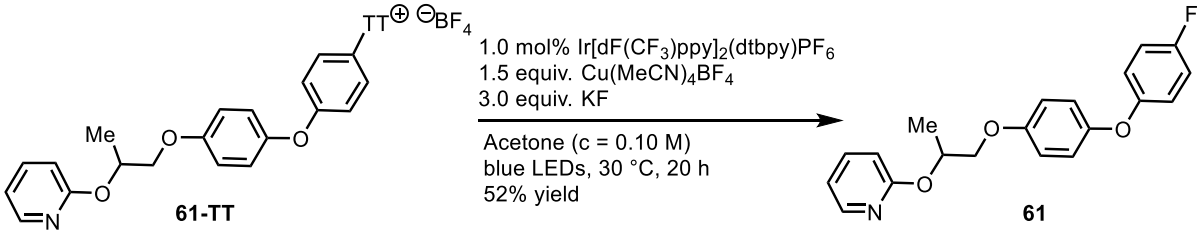

To a 4-mL borosilicate vial equipped with a stir bar was added $Ir[dF(CF_3)ppy]_2(dtbpy)PF_6$ (1.2 mg, 1.0 µmol, 1.0 mol%) and pyriproxyfen-derived thianthrenium salt **61-TT** (62.3 mg, 0.100 mmol, 1.00 equiv.). The vial was transferred into a N_2-filled glovebox. After addition of $Cu(MeCN)_4BF_4$ (47.2 mg, 0.150 mmol, 1.50 equiv.), KF (18.2 mg, 0.300 mmol, 3.00 equiv.) and acetone (1.0 mL, c = 0.10 M), the vial was capped, transferred out of the glovebox and placed 5 cm away from two 34 W blue LEDs. The temperature was kept at approximately 30 °C through cooling with a fan. After being stirred for 20 h, the reaction mixture was diluted with CH_2Cl_2 (2 mL), and the resulting mixture was filtered through a short pad of Celite® using CH_2Cl_2 (5 mL) as eluent. The filtrate was collected and concentrated by rotary evaporation. The residue was purified by chromatography on silica gel eluting with pentane/ethyl acetate (40:1 to 25:1, v/v) to afford the title compound with minor impurities. Further purification by chromatography on silica

gel eluting with toluene/CH_2Cl_2 (3:1, v/v) provided the title compound **61** (17.6 mg, 52.0 µmol, 52%) as a colorless liquid.

R_f = 0.30 (pentane/ethyl acetate 20:1, v/v).

NMR Spectroscopy:

^{1}H NMR (500 MHz, $CDCl_3$, 298 K, δ): 8.16–8.14 (m, 1H), 7.63–7.52 (m, 1H), 6.98 (t, *J* = 8.6 Hz, 2H), 6.94–6.88 (s, 6H), 6.88–6.84 (m, 1H), 6.74 (d, *J* = 8.3 Hz, 1H), 5.58 (h, *J* = 6.3, 5.7 Hz, 1H), 4.18 (dd, *J* = 9.8, 5.3 Hz, 1H), 4.07 (dd, *J* = 9.8, 4.8 Hz, 1H), 1.48 (d, *J* = 6.4 Hz, 3H) ppm.

^{13}C NMR (126 MHz, $CDCl_3$, 298 K, δ): 163.3, 158.5 (d, *J* = 240.7 Hz), 155.3, 154.4 (d, *J* = 2.7 Hz), 150.9, 146.9, 138.8, 120.3, 119.3 (d, *J* = 8.42 Hz), 116.2 (d, *J* = 23.36 Hz), 116.1, 116.0, 111.8, 71.2, 69.4, 17.2 ppm.

^{19}F NMR (471 MHz, $CDCl_3$, 298 K, δ): –121.37 (m) ppm.

HRMS-ESI (m/z) calculated for $C_{20}H_{19}F_1N_1O_3^+$ $[M+H]^+$, 340.134347; found, 340.134380, deviation: –0.10 ppm.

III.3.2. Representative procedure for thianthrenation of arenes

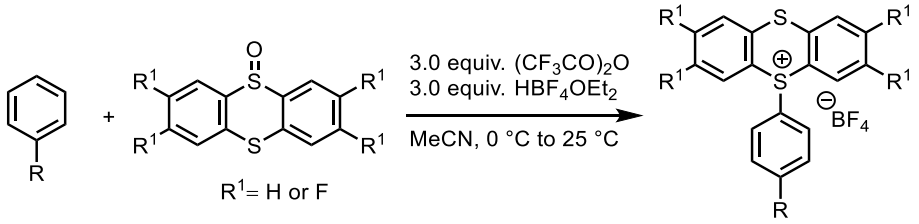

Under ambient atmosphere, a 20 mL glass-vial was charged with arene (0.500 mmol, 1.00 equiv.), (tetrafluoro)thianthrene-*S*-oxide (0.500 mmol, 1.00 equiv.) and dry MeCN (2.0 mL, c = 0.25 M). After cooling to 0 °C, trifluoroacetic anhydride (0.21 mL, 0.32 g, 1.5 mmol, 3.0 equiv.) was added in one portion at 0 °C, resulting in a color change to deep purple. Subsequently, $HBF_4{\cdot}OEt_2$ (1.2 equiv. + 1.0 equiv. per basic functional group) was added to the vial while stirring the reaction mixture. Other acids may be used instead of $HBF_4{\cdot}OEt_2$ like triflic acid (TfOH). For acid sensitive substrates $BF_3{\cdot}OEt_2$ or trimethylsilyltriflate (TMSOTf) can be used. The vial was sealed with a screw-cap. The mixture was stirred at 0 °C for 1 h and then at 25 °C until the intensity of the purple color decreased. The solution was concentrated, and the resulting residue

was diluted with 5 mL CH_2Cl_2 and poured onto a mixture of 30 mL CH_2Cl_2, 20 mL saturated aqueous $NaHCO_3$ solution. After shaking for 1 min at 25 °C, the mixture was poured into a separatory funnel, and the layers were separated. The CH_2Cl_2 layer was collected, and the aqueous layer was further extracted with CH_2Cl_2 (2 × ca. 10 mL). The combined CH_2Cl_2 solution was washed with aqueous $NaBF_4$ solution (2 × ca. 20 mL, 5 % w/w) and with water (2 × ca. 20 mL). The CH_2Cl_2 layer was dried over Na_2SO_4, filtered, and the solvent was removed under reduced pressure. In order to obtain analytically pure samples of thiantrhenium salts, the residue was purified by chromatography on silica gel eluting with CH_2Cl_2/*i*-PrOH, subsequently, the product was dissolved in 2 mL CH_2Cl_2 and precipitated with 20 mL Et_2O. The solid was dried in vacuo to afford the (tetrafluoro)thianthrenium salt.

Synthetic example for thianthrenation of arenes

III.3.2.1 Bromobenzene-derived thianthrenium salt **42-TFT**

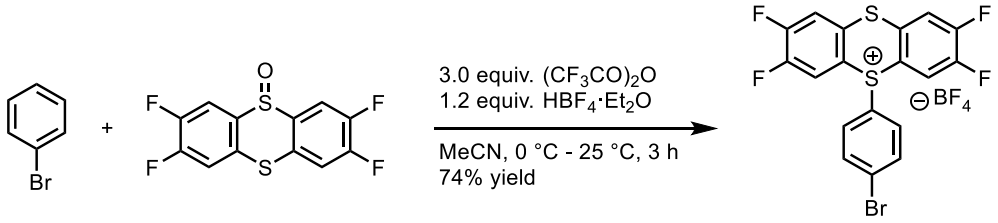

42-TFT

Under ambient atmosphere, a 20 mL borosilicate vial was charged with bromobenzene (105 µL, 157 mg, 1.00 mmol, 1.00 equiv.), tetrafluorothianthrene-*S*-oxide (314 mg, purity w.t. 97%, 1.00 mmol, 1.00 equiv.) and dry MeCN (4.0 mL, c = 0.25 M). After cooling to 0 °C, trifluoroacetic anhydride (0.42 mL, 0.64 mg, 3.0 mmol, 3.0 equiv.) addition at 0 °C in one portion, followed by HBF_4•OEt_2 (174 µL, 1.20 mmol, 1.20 equiv.) was added in one portion at 0 C. The vial was sealed with a screw-cap, and the deep purple mixture was allowed to stand at 0 °C for 1 h, followed by warming the reaction mixture to 25 °C over a period of 1 h. After stirring at 25 °C for 1 h further, the reaction mixture was concentrated under reduced pressure, and diluted with 10 mL CH_2Cl_2. The CH_2Cl_2 solution was poured onto a saturated aqueous $NaHCO_3$ solution (ca. 10 mL). The mixture was poured into a separatory funnel, and the layers were separated. The CH_2Cl_2 layer was collected, and the aqueous layer was further extracted with CH_2Cl_2 (2 × ca.

10 mL). The combined CH_2Cl_2 solution was washed with aqueous $NaBF_4$ solution (2 × ca. 10 mL, 5 % w/w). The organic layer was dried over Na_2SO_4, filtered, and the solvent was removed under reduced pressure. The residue was purified by chromatography on silica gel eluting with CH_2Cl_2/*i*-PrOH (50:1, v/v). The product was dissolved in 2 mL CH_2Cl_2, and precipitated with 10 mL Et_2O. The suspension was decanted, and the solid was dried in vacuo to afford **42-TFT** (395 mg, 743 µmol, 74 %) as a colorless solid.

R_f = 0.35 (CH_2Cl_2/MeOH, 15:1, v/v).

NMR Spectroscopy:

^{1}H NMR (600 MHz, CD_2Cl_2, 298 K, δ): 8.58 (dd, *J* = 8.4, 7.1 Hz, 2H), 7.77 (dd, *J* = 9.1, 6.7 Hz, 2H), 7.67 (d, *J* = 9.1 Hz, 2H), 7.08 (d, *J* = 9.1 Hz, 2H) ppm.

^{13}C NMR (151 MHz, CD_2Cl_2, 298 K, δ): 154.5 (dd, *J* = 266.1, 13.1 Hz), 151.4 (dd, *J* = 260.5, 13.4 Hz), 134.5, 134.4 (dd, *J* = 8.0, 4.2 Hz), 129.7, 129.4, 125.5 (dd, *J* = 21.8, 2.6 Hz), 122.0, 120.3 (d, *J* = 21.3 Hz), 114.7 (dd, *J* = 6.8, 3.6 Hz) ppm.

^{19}F NMR (376 MHz, CD_2Cl_2, 298 K, δ): –121.66 (d, *J* = 20.7 Hz), –129.58 (d, *J* = 20.8 Hz), –149.34 (bs), –149.40 (bs) ppm.

HRMS-ESI (m/z) calculated for $C_{18}H_8Br_1F_4S_2^+$ $[M\text{-}BF_4]^+$, 442.918160; found, 442.918460; deviation: –0.68 ppm.

III.3.2.2 3,3-Diphenylpropan-1-ol-derived thianthrenium salt **50**

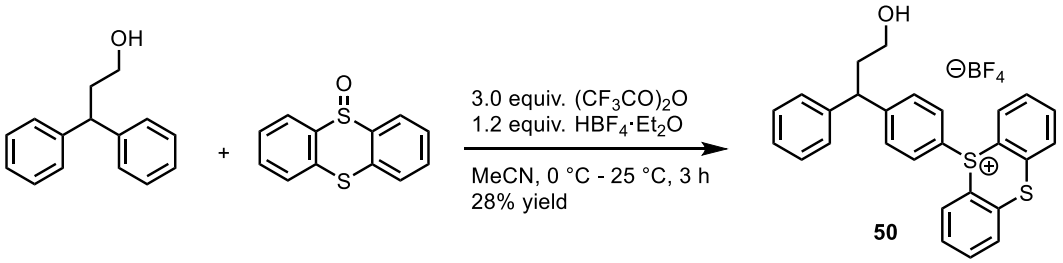

Under ambient atmosphere, a 50 mL round-bottom flask was charged with 3,3-diphenylpropan-1-ol (1.15 g, 5.40 mmol, 1.00 equiv.), thianthrene-*S*-oxide (1.26 g, 5.40 mmol, 1.00 equiv.) and dry MeCN (22 mL, c = 0.25 M). After cooling to 0 °C, trifluoroacetic anhydride (2.24 mL, 3.44 g, 16.2 mmol, 3.00 equiv.) was added in one portion at 0 °C, followed by HBF_4•OEt_2 (886 µL, 6.48 mmol,

1.20 equiv.) addition at 0 °C in one portion. The flask was sealed with a septum, which was equipped with a balloon. The mixture was allowed to stir at 0 °C for 1 h, followed by warming the reaction mixture to 25 °C over a period of 1 h. After stirring at 25 °C for 1 h further, the reaction mixture was concentrated under reduced pressure, and diluted with 20 mL CH_2Cl_2. The CH_2Cl_2 solution was poured onto a saturated aqueous $NaHCO_3$ solution (ca. 20 mL). After stirring at 25 °C for 2 h, the mixture was poured into a separatory funnel, and the layers were separated. The CH_2Cl_2 layer was collected, and the aqueous layer was further extracted with CH_2Cl_2 (2 × ca. 10 mL). The combined CH_2Cl_2 solution was washed with aqueous $NaBF_4$ solution (2 × ca. 20 mL, 5 % w/w). The CH_2Cl_2 layer was dried over Na_2SO_4, filtered, and the solvent was removed under reduced pressure. The residue was purified by chromatography on silica gel eluting with CH_2Cl_2/*i*-PrOH (50:1 to 30:1, v/v). The product was collected and dried in vacuo to afford **50** (790 mg, 1.54 mmol, 28 %) as a colorless foam.

$\mathbf{R_f}$ = 0.28 (CH_2Cl_2/MeOH, 15:1, v/v).

NMR Spectroscopy:

^{1}H NMR (500 MHz, CD_3CN, 298 K, δ): 8.32 (d, *J* = 7.9 Hz, 2H), 7.94 (d, *J* = 7.9 Hz, 2H), 7.87 (t, *J* = 7.7 Hz, 2H), 7.80 (t, *J* = 7.3 Hz, 2H), 7.41 (d, *J* = 8.7 Hz, 2H), 7.31–7.25 (m, 2H), 7.22 (d, *J* = 6.9 Hz, 2H), 7.18 (t, *J* = 7.1 Hz, 1H), 7.05 (d, *J* = 8.8 Hz, 2H), 4.18 (t, *J* = 7.8 Hz, 1H), 3.33 (t, *J* = 5.8 Hz, 2H), 2.24–2.15 (m, 3H) ppm.

^{13}C NMR (126 MHz, CD_3CN, 298 K, δ): 152.2, 144.4, 137.5, 136.1, 135.9, 131.7, 131.0, 130.9, 129.7, 129.2, 128.7, 127.7, 122.1, 119.52, 119.50, 60.1, 47.6, 38.3 ppm.

^{19}F NMR (471 MHz, CD_3CN, 298 K, δ): –151.73 (bs), –151.79 (bs) ppm.

HRMS-ESI (m/z) calculated for $C_{27}H_{23}O_1S_2^+$ $[M\text{-}BF_4]^+$, 427.118485; found, 427.118620; deviation: –0.32 ppm.

III.3.2.3 2,2,2-Trifluoro-*N*-phenylacetamide-derived thianthrenium salt **52-TT**

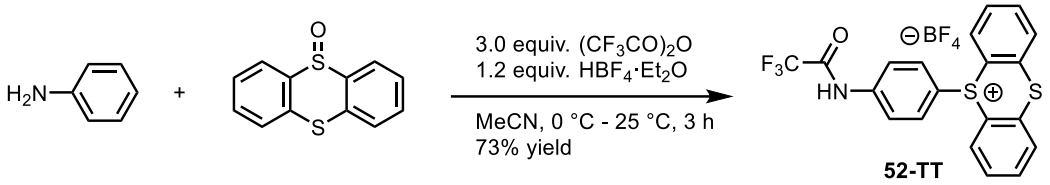

Under ambient atmosphere, a 50 mL round-bottom flask was charged with aniline (493 µL, 503 mg, 5.40 mmol, 1.00 equiv.), thianthrene-*S*-oxide (1.26 g, 5.40 mmol, 1.00 equiv.) and dry MeCN (22 mL, c = 0.25 M). After cooling to 0 °C, trifluoroacetic anhydride (2.24 mL, 3.44 g, 16.2 mmol, 3.00 equiv.) was added in one portion at 0 °C, followed by HBF_4•OEt_2 (886 µL, 6.48 mmol, 1.20 equiv.) addition at 0 °C in one portion. The flask was sealed by a septum which was equipped with a balloon, and the mixture was allowed to stand at 0 °C for 1 h, followed by warming the reaction mixture to 25 °C over a period of 1 h. After stirring at 25 °C for 1 h further, the reaction mixture was concentrated under reduced pressure, and diluted with 20 mL CH_2Cl_2. The CH_2Cl_2 phase was poured onto a saturated aqueous $NaHCO_3$ solution (ca. 20 mL). The mixture was poured into a separatory funnel, and the layers were separated. The CH_2Cl_2 layer was collected, and the aqueous layer was further extracted with CH_2Cl_2 (2 × ca. 10 mL). The combined CH_2Cl_2 solution was washed with aqueous $NaBF_4$ solution (2 × ca. 10 mL, 5 % w/w). The CH_2Cl_2 layer was dried over Na_2SO_4, filtered, and the solvent was removed under reduced pressure. The residue was purified by chromatography on silica gel eluting with CH_2Cl_2/*i*-PrOH (50:1, v/v). The product was dissolved in 5 mL CH_2Cl_2, and precipitated with 20 mL Et_2O. The suspension was decanted, and the solid was dried in vacuo to afford **52-TT** (1.94 g, 3.95 mmol, 73 %) as a colorless solid.

R_f = 0.35 (CH_2Cl_2/MeOH, 15:1, v/v).

NMR Spectroscopy:

^{1}H NMR (500 MHz, DMSO-d_6, 298 K, δ): 11.64 (br, 1H), 8.56 (dd, *J* = 8.0, 1.4 Hz, 2H), 8.07 (dd, *J* = 7.9, 1.3 Hz, 2H), 7.93 (td, *J* = 7.7, 1.4 Hz, 2H), 7.86 (td, *J* = 7.7, 1.3 Hz, 2H), 7.81 (d, *J* = 9.2 Hz, 2H), 7.28 (d, *J* = 9.2 Hz, 2H) ppm.

^{13}C NMR (126 MHz, DMSO-d_6, 298 K, δ): 155.0 (q, *J* = 37.4 Hz), 140.8, 135.5, 135.3, 134.8, 130.3, 129.6, 129.3, 122.4, 119.9, 119.5, 115.5 (q, *J* = 288.7 Hz)

ppm.

^{19}F NMR (471 MHz, DMSO-d_6, 298 K, δ): –73.95 (s), –148.21 (bs), –148.26 (bs) ppm.

HRMS-ESI (m/z) calculated for $C_{20}H_{13}F_3N_1O_1S_2^+$ $[M\text{-}BF_4]^+$, 404.038520; found, 404.038810; deviation: –0.72 ppm.

III.3.2.4 Salicin pentaacetate-derived thianthrenium salt **57-TT**

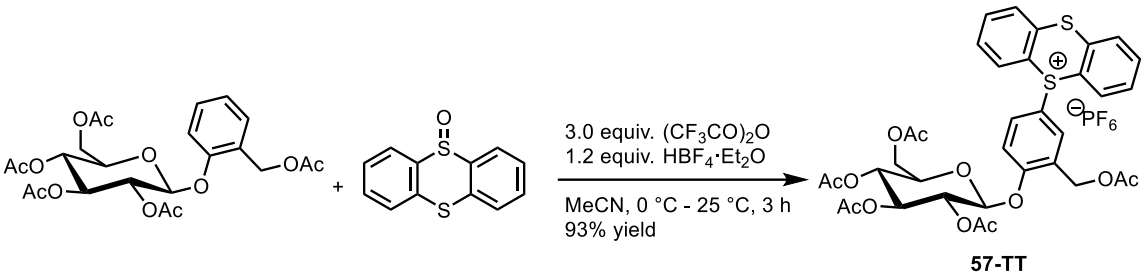

57-TT

Under ambient atmosphere, a 20 mL borosilicate vial was charged with salicin pentaacetat[1] (248 mg, 0.500 mmol, 1.00 equiv.), thianthrene-*S*-oxide (116 mg, 0.500 mmol, 1.00 equiv.) and dry MeCN (2.0 mL, c = 0.25 M). After cooling to 0 °C, trifluoroacetic anhydride (0.21 mL, 0.32 g, 1.5 mmol, 3.0 equiv.) addition at 0 °C in one portion, followed by HBF_4•OEt_2 (87 µL, 0.60 mmol, 1.2 equiv.) was added in one portion at 0 °C. The vial was sealed with a screw-cap, and the mixture was stirred at 0 °C for 1 h, followed by warming the reaction mixture to 25 °C over a period of 1 h. After stirring at 25 °C for 1 h further, the reaction mixture was concentrated under reduced pressure, and diluted with 10 mL CH_2Cl_2. The CH_2Cl_2 phase was poured onto a saturated aqueous $NaHCO_3$ solution (ca. 10 mL). The mixture was poured into a separatory funnel, and the layers were separated. The CH_2Cl_2 layer was collected, and the aqueous layer was further extracted with CH_2Cl_2 (2 × ca. 10 mL). The combined CH_2Cl_2 solution was washed with aqueous $NaPF_6$ solution (2 × ca. 10 mL, 5 % w/w). The organic layer was dried over Na_2SO_4, filtered, and the solvent was removed under reduced pressure. The residue was purified by chromatography on silica gel eluting with CH_2Cl_2/*i*-PrOH (50:1, v/v). The product was collected and dried in vacuo to afford **57-TT** (400 mg, 467 µmol, 93 %) as a colorless solid.

$\mathbf{R_f}$ = 0.35 (CH_2Cl_2/MeOH, 15:1, v/v).

NMR Spectroscopy:

^{1}H NMR (500 MHz, CD_2Cl_2, 298 K, δ): 8.34 (dt, *J* = 7.8, 1.5 Hz, 2H), 7.97 (dt, *J* = 7.9, 1.8 Hz, 2H), 7.91 (tt, *J* = 7.9, 1.4 Hz, 2H), 7.84 (td, *J* = 7.7, 1.5 Hz, 2H), 7.25 (d, *J* = 1.3 Hz, 2H), 7.13 (s, 1H), 5.37–5.28 (m, 2H), 5.24 (d, *J* = 7.2 Hz, 1H), 5.17 (t, *J* = 9.4 Hz, 1H), 4.96 (d, *J* = 2.1 Hz, 2H), 4.28 (dd, *J* = 12.5, 4.9 Hz, 1H), 4.15 (dd, *J* = 12.5, 2.4 Hz, 1H), 3.98 (ddd, *J* = 10.1, 4.9, 2.5 Hz, 1H), 2.06 (s, 3H), 2.05 (s, 3H), 2.03 (s, 3H), 2.02 (s, 3H), 2.01 (s, 3H) ppm.

^{13}C NMR (126 MHz, CD_2Cl_2, 298 K, δ): 170.6, 170.4, 170.1, 169.7, 169.6, 158.0, 137.0 (d, *J* = 2.5 Hz), 135.6, 134.6 (d, *J* = 4.5 Hz), 131.0 (d, *J* = 3.9 Hz), 130.7, 130.3, 129.7, 128.7, 118.8, 117.1, 116.3, 98.4, 72.6, 72.4, 70.9, 68.2, 61.9, 20.8, 20.74, 20.72 ppm.

^{19}F NMR (471 MHz, CD_2Cl_2, 298 K, δ): –72.30 (d, *J* = 711.2 Hz) ppm.

HRMS-ESI (m/z) calculated for $C_{35}H_{35}O_{12}S_2^+$ $[M\text{-}PF_6]^+$, 711.156450; found, 711.157400; deviation: –1.34 ppm.

III.3.2.5 Radical-clock SM thianthrenium salt **64**

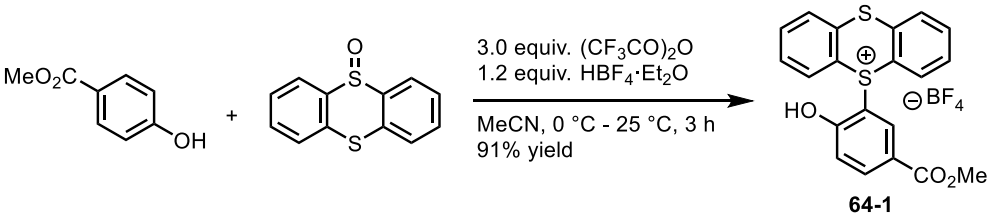

64-1

Under ambient atmosphere, a 20 mL borosilicate vial was charged with methyl 4-hydroxybenzoate (152 mg, 1.00 mmol, 1.00 equiv.), thianthrene-*S*-oxide (232 mg, 1.00 mmol, 1.00 equiv.) and dry MeCN (4.0 mL, c = 0.25 M). After cooling to 0 °C, HBF_4•OEt_2 (174 µL, 1.20 mmol, 1.20 equiv.) was added in one portion at 0 °C, followed by trifluoroacetic anhydride (0.42 mL, 0.64 g, 3.0 mmol, 3.0 equiv.) addition at 0 °C in one portion. The vial was sealed with a screw-cap, and the resulting orange mixture was allowed to stand at 0 °C for 1 h, followed by warming the reaction mixture to 25 °C over a period of 1 h. After stirring at 25 °C for 1 h further, the resulting beige reaction mixture was concentrated under reduced pressure, and diluted with 10 mL CH_2Cl_2. The CH_2Cl_2 solution was poured onto a saturated aqueous $NaHCO_3$ solution (ca. 10 mL). The mixture was poured into a separatory funnel, and the layers were separated. The CH_2Cl_2 layer was collected, and the aqueous layer was further extracted with CH_2Cl_2 (2 × ca. 10 mL). The combined CH_2Cl_2 solution was washed with aqueous $NaBF_4$ solution

(2 × ca. 10 mL, 5 % w/w). The CH_2Cl_2 layer was dried over Na_2SO_4, filtered, and the solvent was removed under reduced pressure. The residue was rinsed with 2 mL CH_2Cl_2, and the resulting colorless solid was filtered off, collected and dried in vacuo to afford **64-1** (415 mg, 914 µmol, 91 %) as a colorless solid. The solid was used for the next step without further purification.

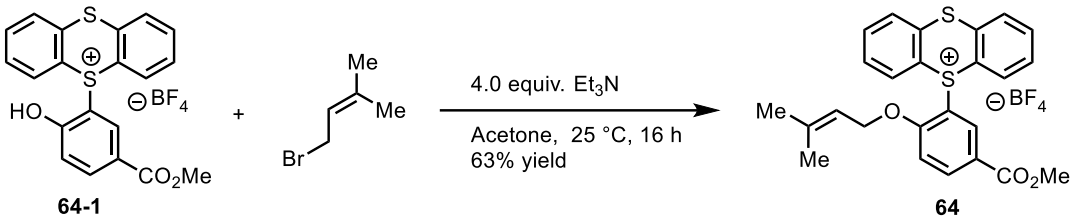

Under ambient atmosphere, a 20 mL borosilicate vial was charged with **64-1** (136 mg, 0.300 mmol, 1.00 equiv.) and acetone (3.0 mL, c = 0.30 M). After addition of triethylamine (167 µL, 121 mg, 1.20 mmol, 4.00 equiv.) at 25 °C, the reaction mixture turned into a clear solution. Prenylbromide (139 µL, 179 mg, 1.20 mmol, 4.00 equiv.) was subsequently added into the clear solution at 25 °C. After stirring at 25 °C for 30 min, colorless precipitates formed in the reaction mixture. After the resulting mixture was stirred at 25 °C for 15 h further, the reaction mixture was concentrated under reduced pressure, and the residue was dissolved in 10 mL CH_2Cl_2. The resulting mixture was poured into a separatory funnel, which was pre-charged with 10 mL of water. The CH_2Cl_2 layer was collected, and the aqueous layer was further extracted with CH_2Cl_2 (2 × ca. 10 mL). The combined CH_2Cl_2 solution was washed with aqueous $NaBF_4$ solution (2 × ca. 10 mL, 5 % w/w). The organic layer was dried over Na_2SO_4, filtered, and the solvent was removed under reduced pressure. The residue was purified by chromatography on silica gel eluting with CH_2Cl_2/*i*-PrOH (50:1 to 30:1). The product was collected and dried in vacuo to afford **64** (98.0 mg, 188 µmol, 63 %) as a colorless solid.

$\mathbf{R_f}$ = 0.35 (CH_2Cl_2/MeOH, 15:1, v/v).

NMR Spectroscopy:

^{1}H NMR (500 MHz, CD_2Cl_2, 298 K, δ): 8.29 (d, *J* = 7.9 Hz, 2H), 8.22 (dd, *J* = 8.7, 1.6 Hz, 1H), 7.94 (d, *J* = 7.8 Hz, 2H), 7.86 (t, *J* = 7.6 Hz, 2H), 7.76 (t, *J* = 7.6 Hz, 2H), 7.23 (d, *J* = 1.6 Hz, 1H), 7.18 (d, *J* = 8.7 Hz, 1H), 5.48 (t, *J* = 7.0

Hz, 1H), 4.76 (d, *J* = 7.2 Hz, 2H), 3.78 (s, 3H), 1.90 (s, 3H), 1.77 (s, 3H) ppm.

^{13}C NMR (126 MHz, CD_2Cl_2, 298 K, δ): 164.8, 161.0, 142.8, 138.1, 137.4, 135.6, 135.4, 131.0, 130.8, 130.3, 124.1, 117.1, 116.9, 114.7, 68.1, 52.9, 26.0, 18.5 ppm.

^{19}F NMR (471 MHz, CD_2Cl_2, 298 K, δ): –152.31 (bs), –152.37 (bs) ppm.

HRMS-ESI (m/z) calculated for $C_{25}H_{23}O_3S_2^+$ $[M\text{-}BF_4]^+$, 435.108315; found, 435.108800; deviation: –1.11 ppm.

III.3.2.6 Biphenyl-derived thianthrenium salt **69-TT**

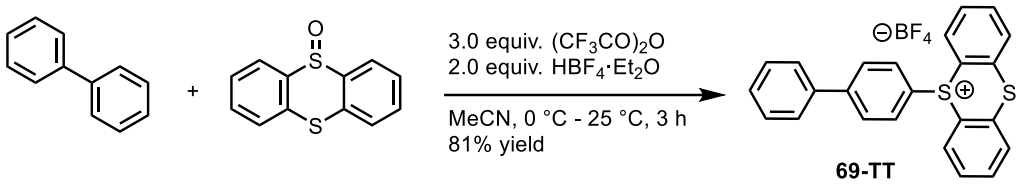

69-TT

Under ambient atmosphere, a 50 mL round-bottom flask was charged with biphenyl (832 mg, 5.40 mmol, 1.00 equiv), thianthrene-*S*-oxide (1.26 g, 5.40 mmol, 1.00 equiv.) and dry MeCN (22 mL, c = 0.25 M). After cooling to 0 °C, trifluoroacetic anhydride (2.24 mL, 3.44 g, 16.2 mmol, 3.00 equiv.) was added in one portion at 0 °C, followed by HBF_4•OEt_2 (886 µL, 6.48 mmol, 1.20 equiv.) addition at 0 °C in one portion. The flask was sealed with a rubber septum, which was equipped with a balloon. The mixture was allowed to stir at 0 °C for 1 h, followed by warming the reaction mixture to 25 °C over a period of 1 h. After stirring at 25 °C for 1 h further, the reaction mixture was concentrated under reduced pressure, and diluted with 20 mL CH_2Cl_2. The CH_2Cl_2 solution was poured onto a saturated aqueous $NaHCO_3$ solution (ca. 20 mL). The mixture was poured into a separatory funnel, and the layers were separated. The mixture was poured into a separatory funnel, and the layers were separated. The CH_2Cl_2 layer was collected, and the aqueous layer was further extracted with CH_2Cl_2 (2 × ca. 10 mL). The combined CH_2Cl_2 solution was washed with aqueous $NaBF_4$ solution (2 × ca. 20 mL, 5 % w/w). The CH_2Cl_2 layer was dried over Na_2SO_4, filtered, and the solvent was removed under reduced pressure. The residue was purified by chromatography on silica gel eluting with CH_2Cl_2/*i*-PrOH (50:1, v/v). The product was dissolved in 5 mL CH_2Cl_2, and precipitated with 20 mL Et_2O. The suspension

was decanted, and the solid was dried in vacuo to afford **69-TT** (2.01 g, 4.40 mmol, 81 %) as a colorless solid.

Alternatively, crystalline **69-TT** was obtained by the following procedure. Under an ambient atmosphere, a 20 ml glass-vial was charged with biphenyl (617 mg, 4.00 mmol, 1.00 equiv), thianthrene-*S*-oxide (929 mg, 4.00 mmol, 1.00 equiv), and MeCN (4.0 ml, c = 1.0 M). After cooling to 0 °C, $HBF_4{\cdot}OEt_2$ (1.09 mL, 1.30 g, 8.00 mmol, 2.00 equiv.) was added, followed by trifluoroacetic anhydride (1.67 mL, 2.51 g, 12.0 mmol, 3.00 equiv.). The vial was sealed with a screw-cap, and the mixture was stirred at 0 °C for 1 h, followed by stirring at 25 °C for 2 h. The reaction mixture was concentrated under reduced pressure, and subsequently, diluted with water (5 mL) and methanol (15 mL). The solution was removed from the resulting crystals, and then the crystals were washed with water. The suspended crystals were centrifuged at 3000 rpm for 5 min and the water was removed. The colorless crystals were dried under high vacuum providing the biphenyl-derived thianthrenium salt **69-TT** (0.637 g, 1.40 mmol, 35 %).

$\mathbf{R_f}$ = 0.35 (CH_2Cl_2/MeOH, 15:1, v/v).

NMR Spectroscopy:

^{1}H NMR (500 MHz, CD_3CN, 298 K, δ): 8.40 (dd, *J* = 7.9, 1.3 Hz, 2H), 7.97 (dd, *J* = 7.9, 1.3 Hz, 2H), 7.90 (td, *J* = 7.7, 1.4 Hz, 2H), 7.84 (td, *J* = 7.7, 1.4 Hz, 2H), 7.74–7.69 (m, 2H), 7.61–7.56 (m, 2H), 7.48–7.40 (m, 3H), 7.22–7.16 (m, 2H) ppm.

^{13}C NMR (126 MHz, $CDCl_3$, 298 K, δ): 144.7, 137.1, 135.8, 134.3, 134.2, 129.9, 129.1, 128.3, 128.1, 128.0, 127.7, 126.4, 121.5, 117.7 ppm.

^{19}F NMR (471 MHz, CD_3CN, 298 K, δ): –152.4 (bs), –152.5 (bs) ppm.

HRMS-ESI (m/z) calculated for $C_{24}H_{17}S_2^+$ $[M\text{-}BF_4]^+$, 369.076620; found, 369.076740; deviation: –0.32 ppm.

III.3.2.7 Acetophenone-derived thianthrenium salt **71-TT**

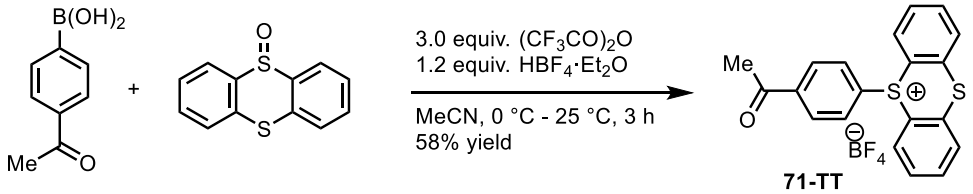

71-TT

Under ambient atmosphere, a 20 mL borosilicate vial was charged with 4-acetylphenylboronic acid (164 mg, 1.00 mmol, 1.00 equiv.), thianthrene-*S*-oxide (232 mg, 1.00 mmol, 1.00 equiv.) and dry MeCN (4.0 mL, c = 0.25 M). After cooling to 0 °C, trifluoroacetic anhydride (0.42 mL, 0.64 g, 3.0 mmol, 3.0 equiv.) addition at 0 °C in one portion, followed by HBF_4•OEt_2 (174 µL, 1.20 mmol, 1.20 equiv.) was added in one portion at 0 C. The vial was sealed with a screw-cap, and the deep purple mixture was allowed to stand at 0 °C for 1 h, followed by warming the reaction mixture to 25 °C over a period of 1 h. After stirring at 25 °C for 1 h further, the reaction mixture was concentrated under reduced pressure, and diluted with 10 mL CH_2Cl_2. The CH_2Cl_2 solution was poured onto a saturated aqueous $NaHCO_3$ solution (ca. 10 mL). The mixture was poured into a separatory funnel, and the layers were separated. The CH_2Cl_2 layer was collected, and the aqueous layer was further extracted with CH_2Cl_2 (2 × ca. 10 mL). The combined CH_2Cl_2 solution was washed with aqueous $NaBF_4$ solution (2 × ca. 10 mL, 5 % w/w). The organic layer was dried over Na_2SO_4, filtered, and the solvent was removed under reduced pressure. The residue was purified by chromatography on silica gel eluting with CH_2Cl_2/*i*-PrOH (50:1, v/v). The product was collected and dried in vacuo to afford **71-TT** (244 mg, 0.578 mmol, 58 %) as beige solid.

R_f = 0.35 (CH_2Cl_2/MeOH, 15:1, v/v).

NMR Spectroscopy:

^{1}H NMR (500 MHz, CD_2Cl_2, 298 K, δ): δ 8.52 (dd, *J* = 7.9, 1.4 Hz, 2H), 7.96 (d, *J* = 8.8 Hz, 2H), 7.94 – 7.87 (m, 4H), 7.84 (td, *J* = 7.6, 1.7 Hz, 2H), 7.21 (d, *J* = 8.8 Hz, 2H), 2.54 (s, 3H) ppm.

^{13}C NMR (126 MHz, CD_2Cl_2, 298 K, δ): 196.8, 140.8, 137.6, 136.0, 135.8, 131.3, 130.9, 130.4, 128.7, 128.6, 118.6, 27.2 ppm.

^{19}F NMR (471 MHz, CD_2Cl_2, 298 K, δ): –150.26 (bs), –150.32 (bs) ppm.

HRMS-ESI (m/z) calculated for $C_{20}H_{15}OS_2^+$ $[M\text{-}BF_4]^+$, 335.055885; found, 335.055820; deviation: +0.19 ppm.

III.3.2.8 Nitrobenzene-derived thianthrenium salt **72-TT**

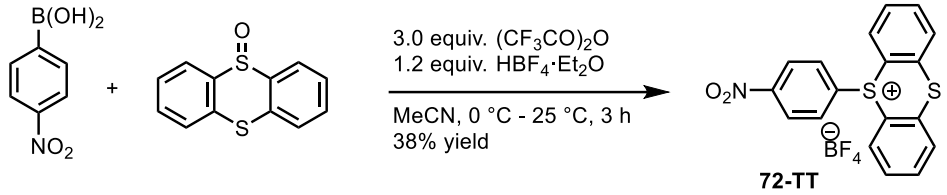

72-TT

Under ambient atmosphere, a 20 mL borosilicate vial was charged with 4-nitrophenylboronic acid (167 mg, 1.00 mmol, 1.00 equiv.), thianthrene-*S*-oxide (232 mg, 1.00 mmol, 1.00 equiv.) and dry MeCN (4.0 mL, c = 0.25 M). After cooling to 0 °C, trifluoroacetic anhydride (0.42 mL, 0.64 g, 3.0 mmol, 3.0 equiv.) addition at 0 °C in one portion, followed by HBF_4•OEt_2 (174 µL, 1.20 mmol, 1.20 equiv.) was added in one portion at 0 C. The vial was sealed with a screw-cap, and the deep purple mixture was allowed to stand at 0 °C for 1 h, followed by warming the reaction mixture to 25 °C over a period of 1 h. After stirring at 25 °C for 1 h further, the reaction mixture was concentrated under reduced pressure, and the residue was diluted with 10 mL CH_2Cl_2. The CH_2Cl_2 solution was poured onto a saturated aqueous $NaHCO_3$ solution (ca. 10 mL). The mixture was poured into a separatory funnel, and the layers were separated. The CH_2Cl_2 layer was collected, and the aqueous layer was further extracted with CH_2Cl_2 (2 × ca. 10 mL). The combined CH_2Cl_2 solution was washed with aqueous $NaBF_4$ solution (2 × ca. 10 mL, 5 % w/w). The organic layer was dried over Na_2SO_4, filtered, and the solvent was removed under reduced pressure. The residue was purified by chromatography on silica gel eluting with CH_2Cl_2/*i*-PrOH (50:1, v/v). The product was collected and dried in vacuo to afford **72-TT** (160 mg 0.376 mmol, 38 %) as beige solid.

R_f = 0.35 (CH_2Cl_2/MeOH, 15:1, v/v).

NMR Spectroscopy:

^{1}H NMR (500 MHz, CD_2Cl_2, 298 K, δ): 8.56 (dd, *J* = 7.8, 1.4 Hz, 2H), 8.20 (d, *J* = 9.1 Hz, 2H), 7.95–7.87 (m, 4H), 7.87–7.81 (m, 2H), 7.30 (d, *J* = 9.2 Hz, 2H).ppm.

^{13}C NMR (126 MHz, CD_2Cl_2, 298 K, δ): 150.7, 137.7, 136.2, 136.1, 131.5, 131.4, 131.1, 129.8, 125.6, 118.4.ppm.

^{19}F NMR (471 MHz, CD_2Cl_2, 298 K, δ): –150.26 (bs), –150.32 (bs) ppm.

HRMS-ESI (m/z) calculated for $C_{18}H_{12}NO_2S_2^+$ $[M\text{-}BF_4]^+$, 338.030399; found, 338.030270; deviation: –0.38 ppm.

III.3.2.9 Isopropoxylbenzene-derived thianthrenium salt **73-TT**

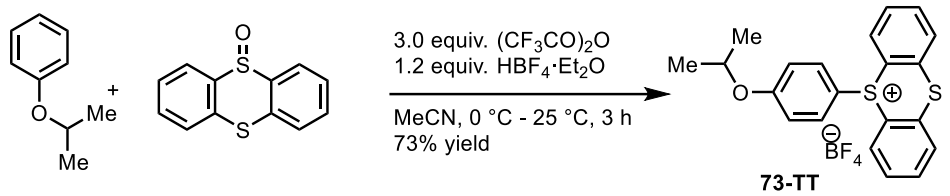

73-TT

Under ambient atmosphere, a 20 mL borosilicate vial was charged with isopropoxylbenzene (136 mg, 1.00 mmol, 1.00 equiv.), thianthrene-*S*-oxide (232 mg, 1.00 mmol, 1.00 equiv.) and dry MeCN (4.0 mL, c = 0.25 M). After cooling to 0 °C, trifluoroacetic anhydride (0.42 mL, 0.64 g, 3.0 mmol, 3.0 equiv.) addition at 0 °C in one portion, followed by HBF_4•OEt_2 (174 µL, 1.20 mmol, 1.20 equiv.) was added in one portion at 0 C. The vial was sealed with a screw-cap, and the deep purple mixture was allowed to stand at 0 °C for 1 h, followed by warming the reaction mixture to 25 °C over a period of 1 h. After stirring at 25 °C for 1 h further, the reaction mixture was concentrated under reduced pressure, and diluted with 10 mL CH_2Cl_2. The CH_2Cl_2 solution was poured onto a saturated aqueous $NaHCO_3$ solution (ca. 10 mL). The mixture was poured into a separatory funnel, and the layers were separated. The CH_2Cl_2 layer was collected, and the aqueous layer was further extracted with CH_2Cl_2 (2 × ca. 10 mL). The combined CH_2Cl_2 solution was washed with aqueous $NaBF_4$ solution (2 × ca. 10 mL, 5 % w/w). The organic layer was dried over Na_2SO_4, filtered, and the solvent was removed under reduced pressure. The residue was purified by chromatography on silica gel eluting with CH_2Cl_2/*i*-PrOH (50:1, v/v). The product was collected and dried in vacuo to afford **72-TT** (320 mg, 0.730 mmol, 73 %) as beige solid.

R_f = 0.35 (CH_2Cl_2/MeOH, 15:1, v/v).

NMR Spectroscopy:

^{1}H NMR (500 MHz, CD_2Cl_2, 298 K, δ): δ 8.28 (dd, *J* = 8.0, 1.4 Hz, 2H), 7.93 –

7.88 (m, 2H), 7.83 (tt, *J* = 7.8, 1.1 Hz, 2H), 7.76 (td, *J* = 7.7, 1.4 Hz, 2H), 7.24 – 7.18 (m, 2H), 6.96 (d, *J* = 9.1 Hz, 2H), 4.58 (pd, *J* = 6.1, 1.1 Hz, 1H), 1.30 (dd, *J* = 6.0, 1.1 Hz, 6H) ppm.

^{13}C NMR (126 MHz, CD_2Cl_2, 298 K, δ): 163.1, 136.8, 135.3, 134.4, 131.2, 131.0, 130.7, 120.0, 118.3, 112.4, 71.8, 21.9 ppm.

^{19}F NMR (471 MHz, CD_2Cl_2, 298 K, δ): –151.69 (bs), –151.76 (bs) ppm.

HRMS-ESI (m/z) calculated for $C_{21}H_{19}OS_2^+$ $[M\text{-}BF_4]^+$, 351.087185; found, 351.086900; deviation: +0.81 ppm.

III.3.3. Reaction optimization for fluorination

III.3.3.1 Control reactions

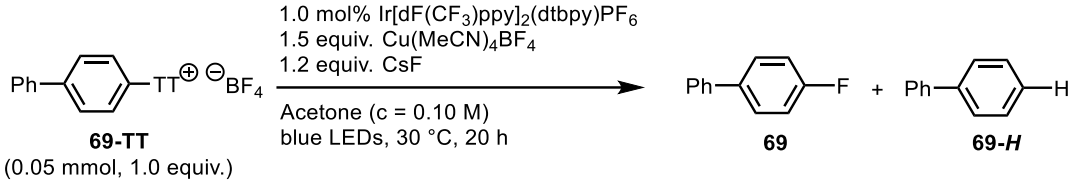

69-TT (0.05 mmol, 1.0 equiv.) → **69** + **69-*H***

change of reaction conditions	Yield of **69**[a]	Ratio of **69**/**69-*H***[b]
none	84%	43:1
no $Ir[dF(CF_3)ppy]_2(dtbpy)PF_6$	8%	2.7:1
no $Cu(MeCN)_4BF_4$	0%	--
no CsF	14%	0.9:1
no light	0%	--

Table III.1. Control experiments. [a]Yield was determined by ^{19}F NMR using 4-fluorobenzotrifluoride as an internal standard. [b]Ratios was determined by GC-FID.

In the absence of photocatalyst, the C–S bond of aryl thianthreniums fragments with visible light, albeit very slowly (11% conversion over 20 h). The fact that fluorination was observed without photocatalyst can be rationalized by a light induced homolysis of aryl thianthreniums to yield an aryl radical and thianthrene

radical cation (Figure III.5). These two intermediates can participate in the copper cycle proposed in the manuscript.

Product formation in the absence of CsF can be rationalized by a Balz-Schiemann type reaction where fluoride is abstracted from the tetrafluoroborate counterion.

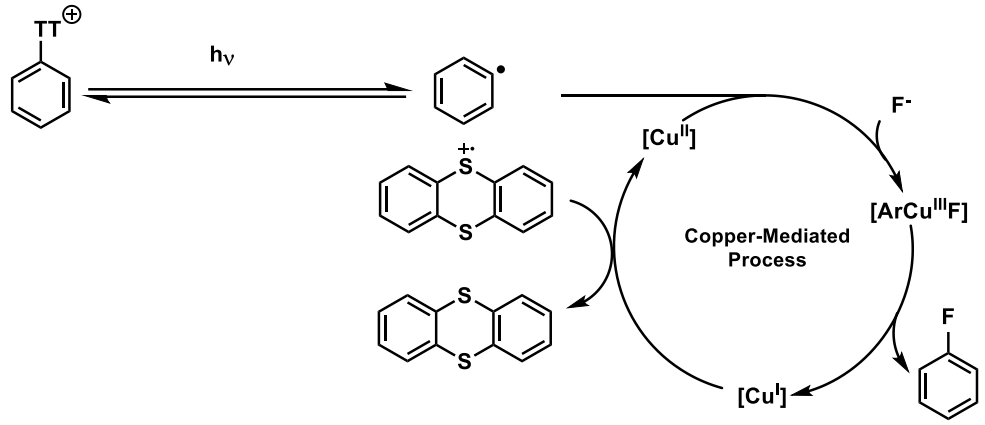

Figure III.5. Proposed mechanism for product formation in the absence of photocatalyst.

III.3.3.2 Comparison of the fluorination of TT and TFT salts

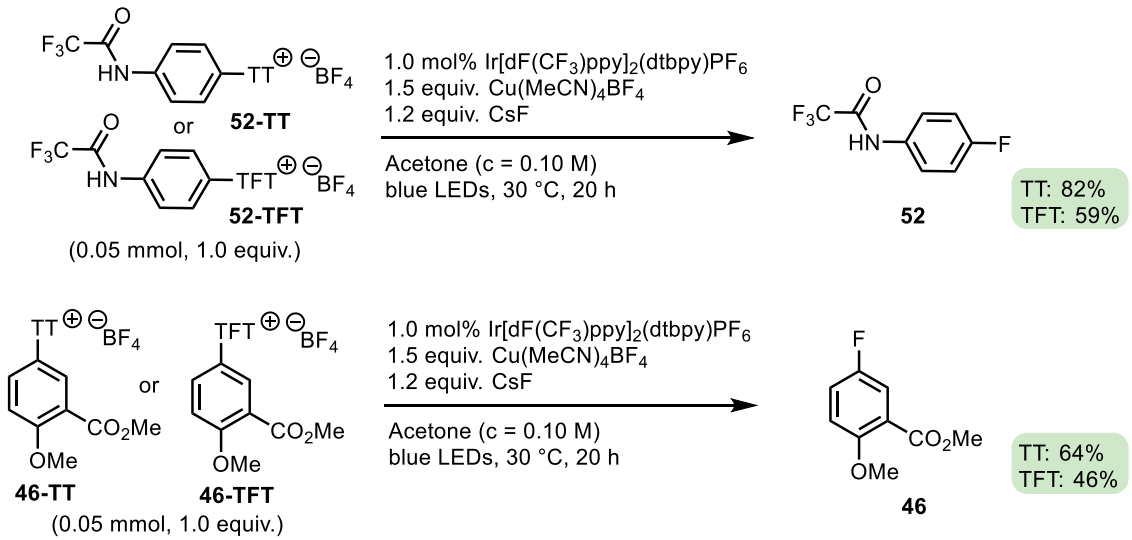

Figure III.6. Experiments for different aryl TT and TFT salts under standard reaction conditions.

III.3.3.3 $Cu(MeCN)_4BF_4$/CsF ratio optimization

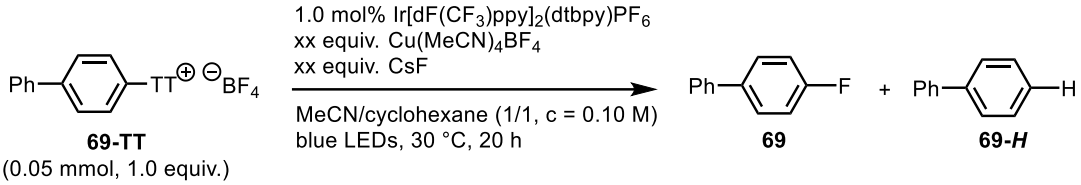

69-TT
(0.05 mmol, 1.0 equiv.)

69 + **69-*H***

$Cu(MeCN)_4BF_4$ (equiv.)	CsF (equiv.)	Yield of **69**[a]	Ratio of **69**/**69-*H***[b]
1.0	10.0	18%	0.5:1
1.0	1.5	66%	3.7:1
1.0	1.0	46%	1.5:1
2.0	1.5	72%	4.0:1
3.0	1.5	76%	6.3:1
3.0	1.5	84%	15.0:1[c]
1.5	1.2	81%	14.0:1[c]

Table III.2. Optimization of copper and fluoride ratio for fluorination of **69-TT**. [a]Yield was determined by ^{19}F NMR using 4-fluorobenzotrifluoride as an internal standard. [b]Ratios was determined by GC-FID. [c]MeCN as the solvent.

III.3.3.4 Solvent optimization

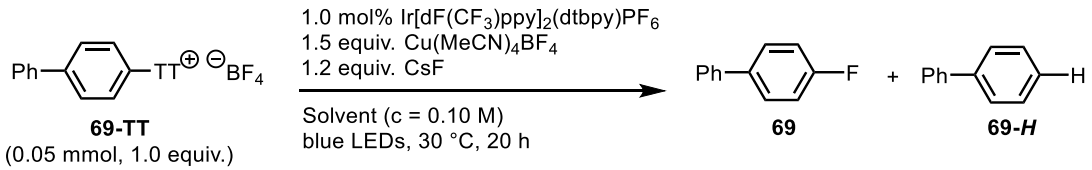

69-TT
(0.05 mmol, 1.0 equiv.)

69 + **69-*H***

Solvent	Yield of **69**[a]	Ratio of **69**/**69-*H***[b]
MeCN	81%	14.0:1
DMF	0%	--
DMSO	0%	--

$MeNO_2$	4%	1:2.8
Dioxane	1%	1:24
CH_2Cl_2	0%	--
DME	5%	1:11
	18%	1:2.1
	4%	1:30
	84%	43:1
MeCN/acetone(1/1)	51%	1.3:1

Table III.3. Solvent effects on fluorination of **69-TT**. [a]Yield was determined by ^{19}F NMR using 4-fluorobenzotrifluoride as an internal standard. [b]Ratios was determined by GC-FID.

III.3.3.5 Fluoride nucleophile comparison

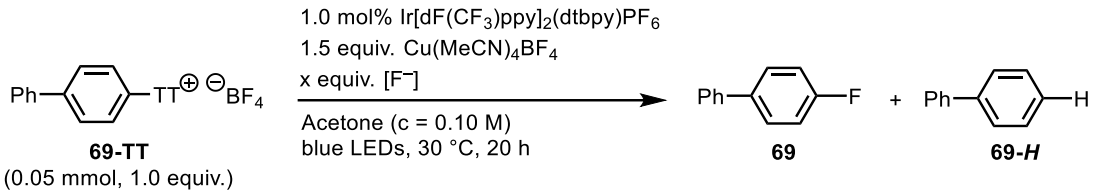

[F^-]	Yield of **69**[a]	Ratio of **69**/**69-*H***[b]
CsF (1.2 equiv)	84%	43:1
KF (1.2 equiv)	70%	21:1
NaF (3.0 equiv)	87%	24:1
TBAT (1.2 equiv)	26%	1.8:1

TMAF (1.2 equiv)	0%	--

Table III.4. Fluoride effects on fluorination of **69-TT**. [a]Yield was determined by ^{19}F NMR using 4-fluorobenzotrifluoride as an internal standard. [b]Ratios was determined by GC-FID.

III.3.3.6 Cu source optimization

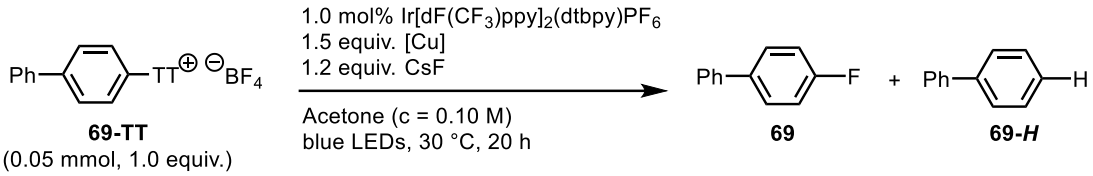

[Cu]	Yield of **69**[a]	Ratio of **69**/**69-*H***[b]
CuCl	0%	--
CuI	0%	--
Cu_2O	0%	--
IPrCuCl	0%	--
$Cu(MeCN)_4PF_6$	67%	28:1
$Cu(MeCN)_4OTf$	54%	29:1
$Cu(^tBuCN)_2OTf$	66%	39:1
$Cu(^tBuCN)_2BF_4$	87%	32:1
$Cu(MeCN)_4BF_4$	84%	43:1
$Cu(BF_4)_2$	0%	--

Table III.5. Copper salt effects on fluorination of **69-TT**. [a]Yield was determined by ^{19}F NMR using 4-fluorobenzotrifluoride as an internal standard. [b]Ratios was determined by GC-FID.

III.3.3.7 Comparison of various photocatalysts

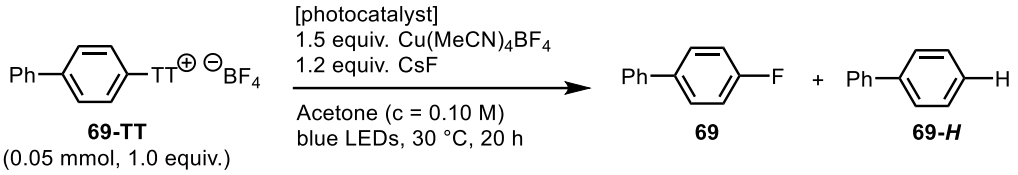

photocatalyst	Yield of **69**[a]	Ratio of **69**/**69-*H***[b]
$[Ir(dtbbpy)(ppy)_2][PF_6]$	25%	1.6:1
$Ir[dFFppy]_2$-(4,4'-dCF_3bpy)PF_6	1%	1:1.3
$Ir[dFMeppy]_2$-(4,4'-dCF_3bpy)PF_6	0%	--
C1	0%	--
C2	76%	24:1
$Ir[dF(CF_3)ppy]_2(dtbpy)PF_6$	84%	43:1
$Ru(bpm)_3Cl_2$	0%	--

Table III.6. Photocatalysts effecs on fluorination of **69-TT**. [a]Yield was determined by ^{19}F NMR using 4-fluorobenzotrifluoride as an internal standard. [b]Ratios was determined by GC-FID.

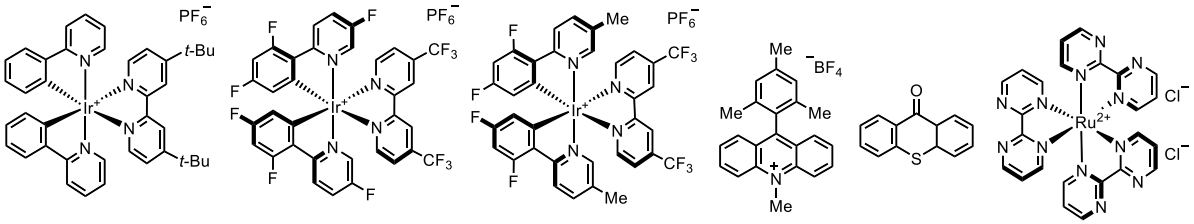

III.3.3.8 Effects of concentration on the yield and the ratio of **69**/**69-H**

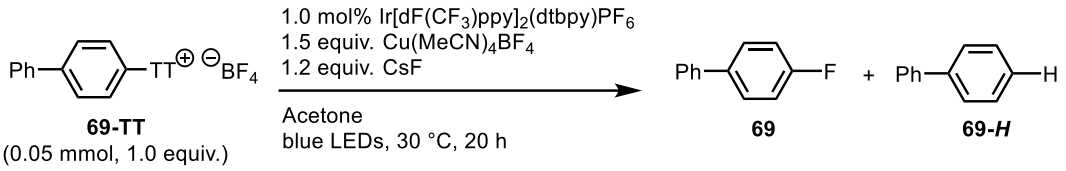

[c]	Yield of **69**[a]	Ratio of **69**/**69-*H***[b]
0.05 M	81%	19:1
0.1 M	84%	43:1
0.2 M	89%	35:1
0.3 M	86%	31:1
0.4 M	87%	23:1
0.5 M	85%	21:1

Table III.7. Concentration studies for fluorination of **69-TT**. [a]Yield was determined by ^{19}F NMR using 4-fluorobenzotrifluoride as an internal standard. [b]Ratios was determined by GC-FID.

III.3.4. Catalytic fluorination of aryl tetrafluorothianthrenium salts

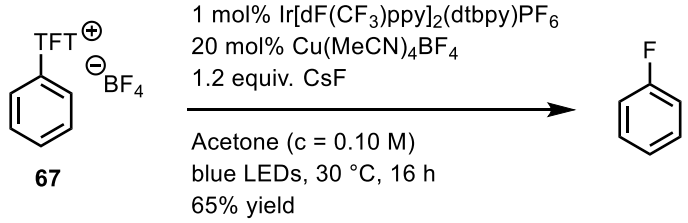

To a 4-mL borosilicate vial equipped with a stir bar was added Ir[dF(CF$_3$)ppy]$_2$(dtbpy)PF$_6$ (0.6 mg, 0.5 µmol, 1 mol%) and benzene-derived tetrafluorothianthrenium salt **67** (22.6 mg, 50.0 µmol, 1.00 equiv.). The vial was transferred into a N_2-filled glovebox. After addition of Cu(MeCN)$_4$BF$_4$ (3.2 mg, 10 µmol, 20 mol%), CsF (9.1 mg, 60 µmol, 1.2 equiv.) and acetone (0.50 mL, c = 0.10 M), the vial was capped, transferred out of the glovebox and placed 5 cm away from two 34 W blue LEDs. The temperature was kept at approximately 30 °C through cooling with a fan. After being stirred for 16 h, 4-fluorobenzotrifluoride (8.2

mg, 6.3 µL, 50 µmol, 1.0 equiv.) was added as an internal standard. The reaction mixture was diluted with $CDCl_3$, and the yield was determined by ^{19}F NMR integration relative to the internal standard (65% yield, standard: δ –108.40 ppm, and fluorobenzene: δ –114.10 (m) ppm). The ^{19}F NMR spectral data for fluorobenzene matched that of an authentic sample (TCI®,–114.10 (m) ppm).

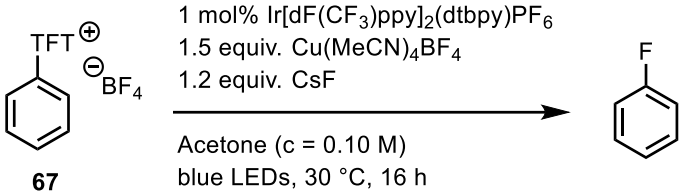

To a 4-mL borosilicate vial equipped with a stir bar was added $Ir[dF(CF_3)ppy]_2(dtbpy)PF_6$ (0.6 mg, 0.5 µmol, 1 mol%) and benzene-derived tetrafluorothianthrenium salt **67** (22.6 mg, 50.0 µmol, 1.00 equiv.). The vial was transferred into a N_2-filled glovebox. After addition of $Cu(MeCN)_4BF_4$ (23.6 mg, 75.0 µmol, 1.50 equiv.), CsF (9.2 mg, 60 µmol, 1.2 equiv.) and acetone (0.50 mL, c = 0.10 M), the vial was capped, transferred out of the glovebox and placed 5 cm away from two 34 W blue LEDs. The temperature was kept at approximately 30 °C through cooling with a fan. After being stirred for more 10 h, 4-fluorobenzotrifluoride (8.2 mg, 6.3 µL, 50 µmol, 1.0 equiv.) was added as an internal standard. The reaction mixture was diluted with $CDCl_3$, and the yield was determined by ^{19}F NMR integration relative to the internal standard (88% yield, standard: δ –108.40 ppm, and fluorobenzene: δ –114.10 (m) ppm).

III.3.5. Photocatalyzed fluorination of diazonium slat and iodonium salt

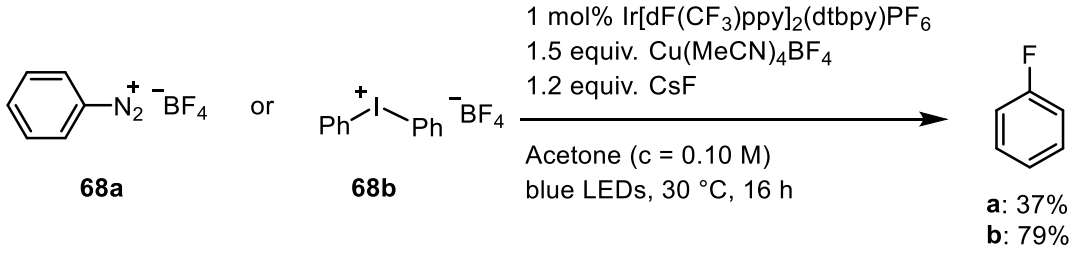

To a 4-mL borosilicate vial equipped with a stir bar was added $Ir[dF(CF_3)ppy]_2(dtbpy)PF_6$ (1.2 mg, 1.0 µmol, 1.0 mol%) and benzenediazonium tetrafluoroborate **68a** (19.2 mg, 0.100 mmol, 1.00 equiv.) or iodonium **68b** (36.8 mg, 0.100 mmol, 1.00 equiv.). The vial was transferred into a N_2-filled glovebox.

After addition of $Cu(MeCN)_4BF_4$ (47.2 mg, 0.150 mmol, 1.50 equiv.), CsF (18.4 mg, 0.120 mmol, 1.20 equiv.) and acetone (1.0 mL, c = 0.10 M), the vial was capped, transferred out of the glovebox and placed 5 cm away from two 34 W blue LEDs. The temperature was kept at approximately 30 °C through cooling with a fan. After being stirred for more 10 h, 4-fluorobenzotrifluoride (8.2 mg, 6.3 µL, 50 µmol, 1.0 equiv.) was added as an internal standard. The reaction mixture was diluted with $CDCl_3$, and the yield was determined by ^{19}F NMR integration relative to the internal standard (37% yield for **a** and 79% yield for **b**; standard: δ –108.4 ppm, and fluorobenzene: δ –114.1 (m) ppm).

III.3.6. Mechanistic experiments

III.3.6.1 Radical clock experiments

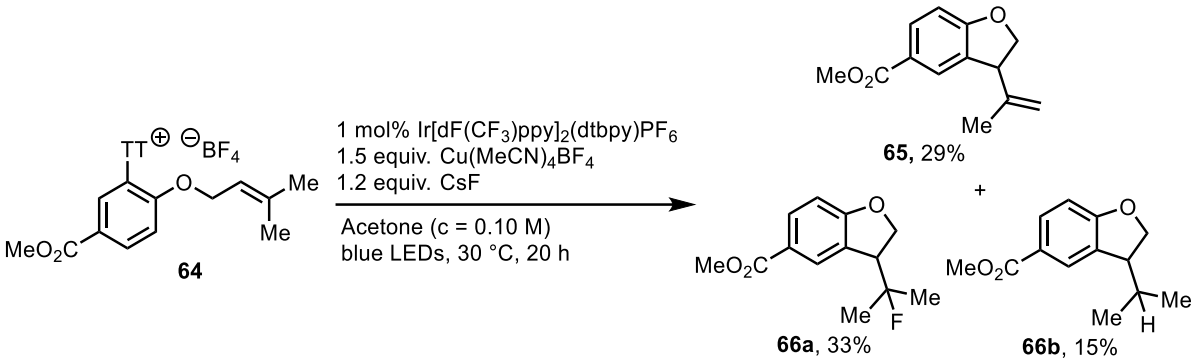

To a 4-mL borosilicate vial equipped with a stir bar was added $Ir[dF(CF_3)ppy]_2(dtbpy)PF_6$ (0.4 mg, 0.4 µmol, 1 mol%) and methyl gemfibrozil-derived thianthrenium salt **65** (16.5 mg, 31.6 µmol, 1.00 equiv.). The vial was transferred into a N_2-filled glovebox. After addition of $Cu(MeCN)_4BF_4$ (14.9 mg, 47.4 µmol, 1.50 equiv.), CsF (5.8 mg, 38 µmol, 1.2 equiv.) and acetone (0.30 mL, c = 0.10 M), the vial was capped, transferred out of the glovebox and placed 5 cm away from two 34 W blue LEDs. The temperature was kept at approximately 30 °C through cooling with a fan. After being stirred for 20 h, the reaction mixture was diluted with CH_2Cl_2 (2 mL), and the resulting mixture was filtered through a short pad of Celite® using CH_2Cl_2 (5 mL) as eluent. The filtrate was collected and concentrated by rotary evaporation. The residue was purified by chromatography on silica gel eluting with hexanes/ethyl acetate (50:1 to 30:1, v/v) to afford **66a** (2.5 mg, 11 µmol, 33%) as a colorless liquid, and mixture of **66b** and **65** (3.0 mg, **66b**/**65** = 1:2, **66b**: 15%, and **65**: 30%).

Methyl 3-(2-fluoropropan-2-yl)-2,3-dihydro-1-benzofuran-5-carboxylate (**66a**):

R_f = 0.30 (hexanes/ethyl acetate 5:1, v/v).

NMR Spectroscopy:

^{1}H NMR (400 MHz, $CDCl_3$, 298 K, δ): 7.96 (p, *J* = 1.0 Hz, 1H), 7.93 (ddd, *J* = 8.4, 1.9, 0.6 Hz, 1H), 6.84 – 6.79 (m, 1H), 4.63 (d, *J* = 1.3 Hz, 1H), 4.62 (s, 1H), 3.88 (s, 3H), 3.74 – 3.66 (m, 1H), 1.45 – 1.35 (m, 4H), 1.28 (d, *J* = 21.4 Hz, 4H) ppm.

^{13}C NMR (101 MHz, $CDCl_3$, 298 K, δ): 167.0, 164.9, 132.2, 127.9 (d, *J* = 1.6 Hz), 127.0 (d, *J* = 6.6 Hz), 123.0, 109.7, 96.4 (d, *J* = 170.2 Hz), 74.0 (d, *J* = 7.3 Hz), 52.1, 51.3 (d, *J* = 24.8 Hz), 24.5 (d, *J* = 24.0 Hz), 23.6 (d, *J* = 24.1 Hz) ppm.

^{19}F NMR (471 MHz, $CDCl_3$, 298 K, δ): –138.15 (pd, *J* = 21.7, 9.5 Hz) ppm.

HRMS-GC-EI (m/z) calculated for $C_{13}H_{15}O_3F_1^+$ $[M]^+$, 238.099973; found, 238.100210, deviation: –0.99 ppm.

The following data were obtained for the mixture:

Methyl 3-isopropyl-2,3-dihydro-1-benzofuran-5-carboxylate (**66b**):

NMR Spectroscopy:

^{1}H NMR (500 MHz, $CDCl_3$, 298 K, δ): 7.90 (d, *J* = 8.6 Hz, 1H), 7.84 (d, *J* = 36.0 Hz, 2H), 4.92 (s, 1H), 4.90–4.85 (m, 1H), 4.74 (t, *J* = 9.4 Hz, 1H), 4.46–4.38 (m, 1H), 4.22–4.14 (m, 1H), 3.87 (s, 3H), 1.64 (s, 3H) ppm.

HRMS-GC-EI (m/z) calculated for $C_{13}H_{16}O_3^+$ $[M]^+$, 220.109395; found, 220.109620, deviation: –1.02 ppm.

Methyl 3-(propen-2-yl)-2,3-dihydro-1-benzofuran-5-carboxylate (**65**):

NMR Spectroscopy:

^{1}H NMR (500 MHz, $CDCl_3$, 298 K, δ): 6.81 (d, *J* = 8.3 Hz, 2H), 6.77 (d, *J* = 8.2 Hz, 1H), 4.60 (t, *J* = 9.2 Hz, 1H), 4.48–4.45 (m, 1H), 3.88 (s, 3H), 3.37 (dt, *J* = 9.8, 5.1 Hz, 1H), 2.00 (dq, *J* = 12.9, 6.7 Hz, 1H), 0.96 (d, *J* = 6.9 Hz, 3H), 0.87

(d, *J* = 6.8 Hz, 3H) ppm.

HRMS-GC-EI (m/z) calculated for $C_{13}H_{14}O_3^+$ $[M]^+$, 218.093745; found, 218.094030, deviation: –1.31 ppm.

III.3.6.2 TEMPO trapping experiments

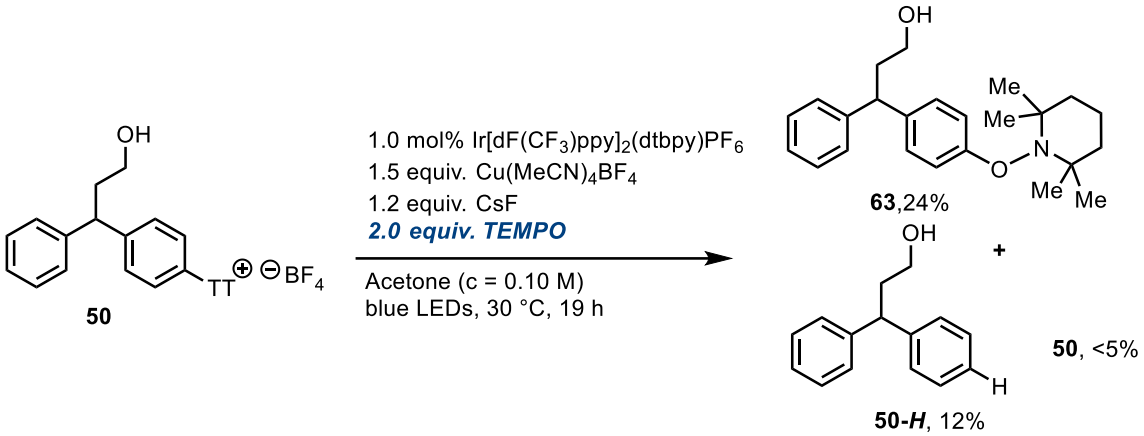

To a 4-mL borosilicate vial equipped with a stir bar was added $Ir[dF(CF_3)ppy]_2(dtbpy)PF_6$ (1.2 mg, 1.0 µmol, 1.0 mol%) 3,3-diphenylpropan-1-ol-derived thianthrenium salt **50** (51.4 mg, 0.100 mmol, 1.00 equiv.) and TEMPO(31.2 mg, 0.200 mmol, 2.00 equiv.). The vial was transferred into a N_2-filled glovebox. After addition of $Cu(MeCN)_4BF_4$ (47.2 mg, 0.150 mmol, 1.50 equiv.), CsF (18.2 mg, 0.120 mmol, 1.20 equiv.) and acetone (1.0 mL, c = 0.10 M), the vial was capped, transferred out of the glovebox and placed 5 cm away from two 34 W blue LEDs. The temperature was kept at approximately 30 °C through cooling with a fan. After being stirred for 19 h, the reaction mixture was diluted with CH_2Cl_2 (2 mL), and the resulting mixture was filtered through a short pad of Celite® using CH_2Cl_2 (5 mL) as eluent. The filtrate was collected and concentrated by rotary evaporation. The residue was purified by chromatography on silica gel eluting with pentane/ethyl acetate (10:1 to 6:1, v/v) to afford **63** (8.8 mg, 24 µmol, 24%) as a yellow liquid, and **50-*H*** (2.5 mg, 12 µmol, 12%) as a yellow liquid.

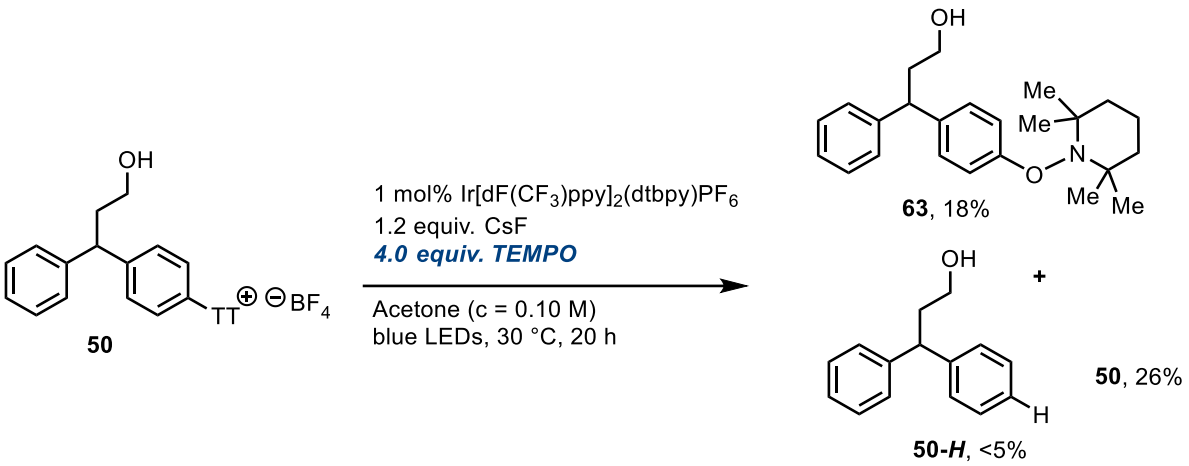

To a 4-mL borosilicate vial equipped with a stir bar was added Ir[dF(CF$_3$)ppy]$_2$(dtbpy)PF$_6$ (0.6 mg, 0.5 µmol, 1 mol%) 3,3-diphenylpropan-1-ol-derived thianthrenium salt **50** (25.7 mg, 50.0 µmol, 1.00 equiv.) and TEMPO(31.2 mg, 0.200 mmol, 4.00 equiv.). The vial was transferred into a N_2-filled glovebox. After addition of CsF (9.2 mg, 60 µmol, 1.2 equiv.) and acetone (0.50 mL, c = 0.10 M), the vial was capped, transferred out of the glovebox and placed 5 cm away from two 34 W blue LEDs. The temperature was kept at approximately 30 °C through cooling with a fan. After being stirred for 19 h, the reaction mixture was diluted with CH_2Cl_2 (2 mL), and the resulting mixture was filtered through a short pad of Celite® using CH_2Cl_2 (5 mL) as eluent. The filtrate was collected and concentrated by rotary evaporation. The residue was purified by chromatography on silica gel eluting with pentane/ethyl acetate (10:1 to 6:1, v/v) to afford **6** (3.4 mg, 9.2 µmol, 18%) as a yellow liquid, and eluting with CH_2Cl_2/MeOH (20:1 to 10:1, v/v) to afford **65** (6.8 mg, 13 µmol, 26%) as a colorless solid.

ArTEMPO product (**63**):

R_f = 0.47 (pentane/ethyl acetate 4:1, v/v).

NMR Spectroscopy:

^{1}H NMR (500 MHz, $CDCl_3$, 298 K, δ): 7.23–7.15 (m, 4H), 7.13–7.07 (m, 1H), 6.99 (br, 4H), 3.96 (t, *J* = 7.9 Hz, 1H), 3.53 (t, *J* = 6.3 Hz, 2H), 2.20 (ddt, *J* = 9.9, 6.5, 3.5 Hz, 2H), 1.54–1.43 (m, 6H), 1.35–1.30 (m, 1H), 1.13 (s, 6H), 0.91 (s, 3H), 0.90 (s, 3H) ppm.

^{13}C NMR (126 MHz, CD_2Cl_2, 298 K, δ): 162.4, 145.7, 136.3, 128.7, 128.1,

128.0, 126.3, 114.1, 61.3, 60.6, 47.0, 40.0, 38.9, 32.7, 20.4, 17.3 ppm.

HRMS-ESI (m/z) calculated for $C_{24}H_{34}N_1O_3^+$ $[M+H]^+$, 368.258404; found, 368.258440, deviation: –0.10 ppm.

III.3.6.3 Stern-Volmer luminescence quench studies

Visible light luminescence intensities were recorded using an Edinburgh Instruments FS5 spectrofluorometer. All luminescence measurements were recorded using a screw-top quartz cuvette (Hellma fluorescence quartz cuvette, 10 x 10 mm, 3.5 mL). All solutions of $[Ir\{dF(CF_3)ppy\}_2(dtbbpy)]PF_6$, anisole-derived thianthrenium tetrafluoroborate **62**, tetrakis(acetonitrile)copper tetrafluoroborate, and thianthrene were prepared in acetone in a nitrogen-filled glovebox. The solutions were transferred to the screw-top cuvette inside the glovebox, the cuvette was sealed, and then brought out of the glovebox for visible light luminescence measurements.

In a typical procedure, anisole-derived thianthrenium tetrafluoroborate **62** (0.329 g, 0.802 mmol) was dissolved and diluted to a final volume of 10 mL (c = 0.080 M arylthianthrenium salt) with a stock solution of $[Ir\{dF(CF_3)ppy\}_2(dtbbpy)]PF_6$ in acetone (c = 18 µM). Serial dilution of this 0.08 M arylthianthrenium salt solution was carried out by dilution of 7 mL of the 0.080 M arylthianthrenium salt solution to 10 mL (0.056 M) with the 18 µM stock solution of $[Ir\{dF(CF_3)ppy\}_2(dtbbpy)]PF_6$. All subsequent solutions were prepared by dilution of 7 mL of the preceding solution to a final volume of 10 mL. The final solution with a concentration of 0.011 M was prepared by dilution of 2 mL of the 0.027 M arylthianthrenium salt solution to a final volume of 5 mL. All solutions were excited at 450 nm and the emission was measured from 455 to 600 nm.

Quenching was analyzed by plotting I_0/I according to the Stern-Volmer relationship:

$$I_0/I = k_q\tau_0[Q]+1$$

where I_0 represents the integral of the luminescence over the range of 455 to 600 nm in the absence of a quencher, I is the integral of luminescence over the range of 455 to 600 nm in the presence of a quencher, k_q represents the

quenching rate constant, [Q] is the concentration of a given quencher, and τ_0 is the excited state lifetime of the emissive photocatalyst in the absence of quencher. The excited state lifetime of Ir[dF(CF$_3$)ppy]$_2$(dtbpy)PF$_6$ in MeCN is 2300 ns.[276]

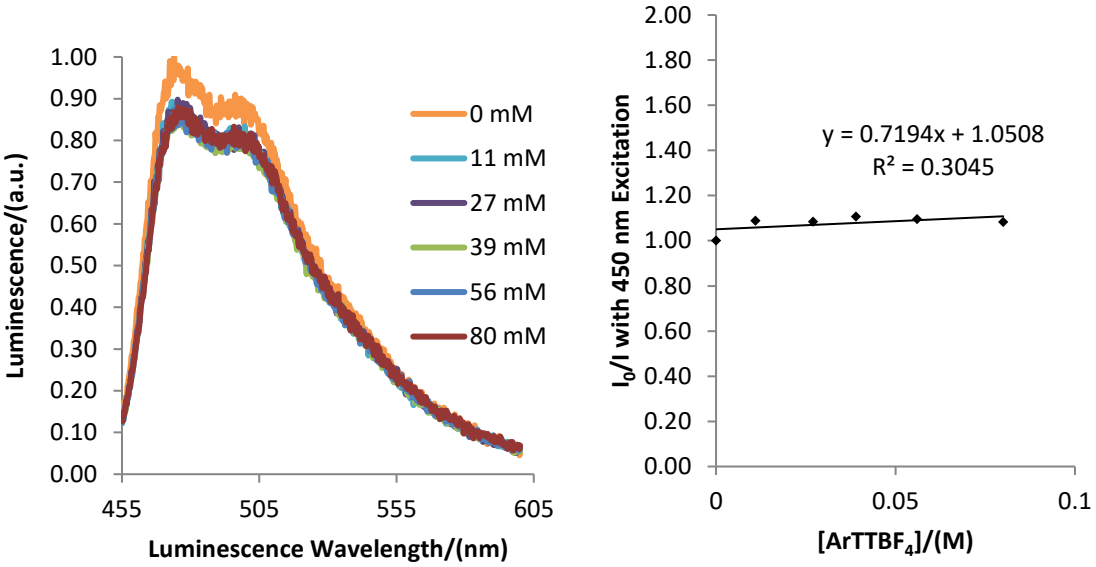

Figure III.7. Emission spectra for Ir(dF(CF$_3$)ppy)$_2$(dtbbpy)PF$_6$ luminescence quenching by anisole-derived thianthrenium BF$_4$ 4 (left) and Stern-Volmer plot (right). (Dr. Dr. Matthew B. Plutschack and the author collected the data; Dr. Dr. Matthew B. Plutschack drafted the figures)

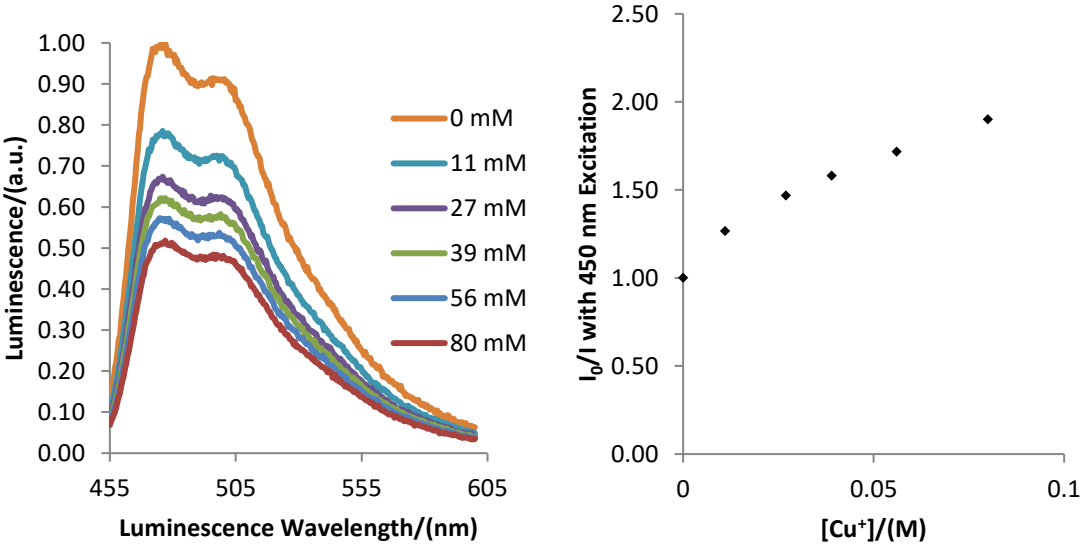

Figure III.8. Emission spectra for Ir(dF(CF$_3$)ppy)$_2$(dtbbpy)PF$_6$ luminescence quenching by tetrakis(acetonitrile)copper BF$_4$ (left) and Stern-Volmer plot (right).

(Dr. Dr. Matthew B. Plutschack and the author collected the data; Dr. Dr. Matthew B. Plutschack drafted the figures)

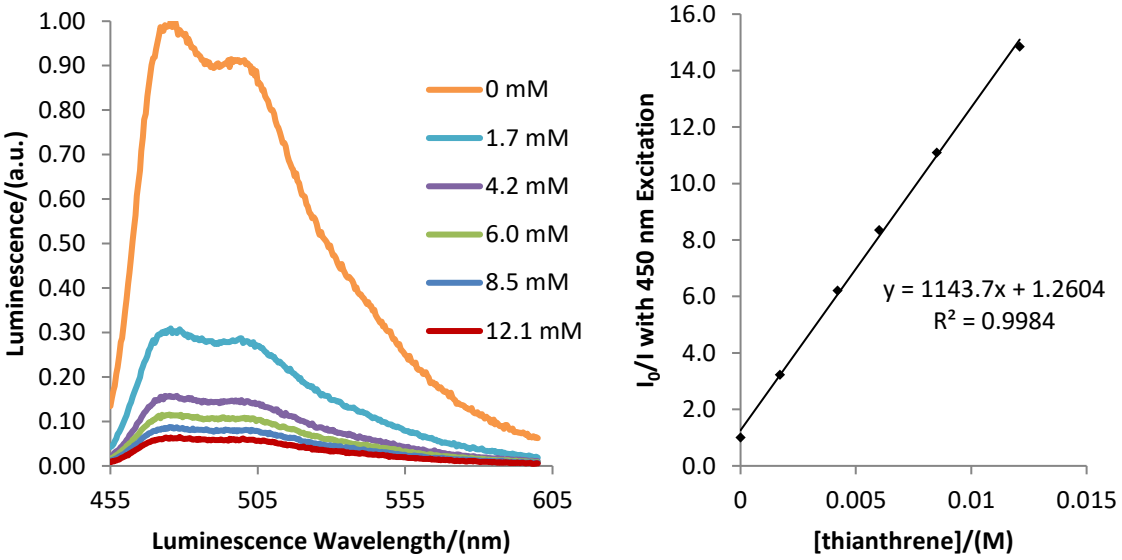

Figure III.9. Emission spectra for Ir(dF(CF_3)ppy)$_2$(dtbbpy)PF_6 luminescence quenching by thianthrene (left) and Stern-Volmer plot (right). (Dr. Dr. Matthew B. Plutschack and the author collected the data; Dr. Dr. Matthew B. Plutschack drafted the figures)

UV/Vis absorbance spectra were recorded using a Shimadzu UV/Visible Spectrophotometer UV-2600 with temperature controller. All spectral measurements were recorded using a quartz SUPRASIL cuvette (Hellma absorption quartz cuvette, 10 mm optical path length, 3.5 mL total volume). All solutions of tetrakis(acetonitrile)copper tetrafluoroborate were prepared in acetone in a nitrogen-filled glovebox. The solutions were transferred to quartz cuvette inside the glovebox, the cuvette was closed with a PTFE stopper, and then brought out of the glovebox for UV/Vis absorbance measurements at 25 °C.

UV/Vis absorbance was measured for tetrakis(acetonitrile)copper BF_4 in acetone at various concentrations to account for an inner filter effect (Figure III.10). Even at the highest concentration (80 mM) the absorbance is less than 0.02 at 450 nm (the excitation wavelength). This excludes an inner filter effect as a possible cause of non-linearity in the Stern-Volmer analysis of tetrakis(acetonitrile)copper BF_4 and Ir(dF(CF_3)ppy)$_2$(dtbbpy)PF_6.

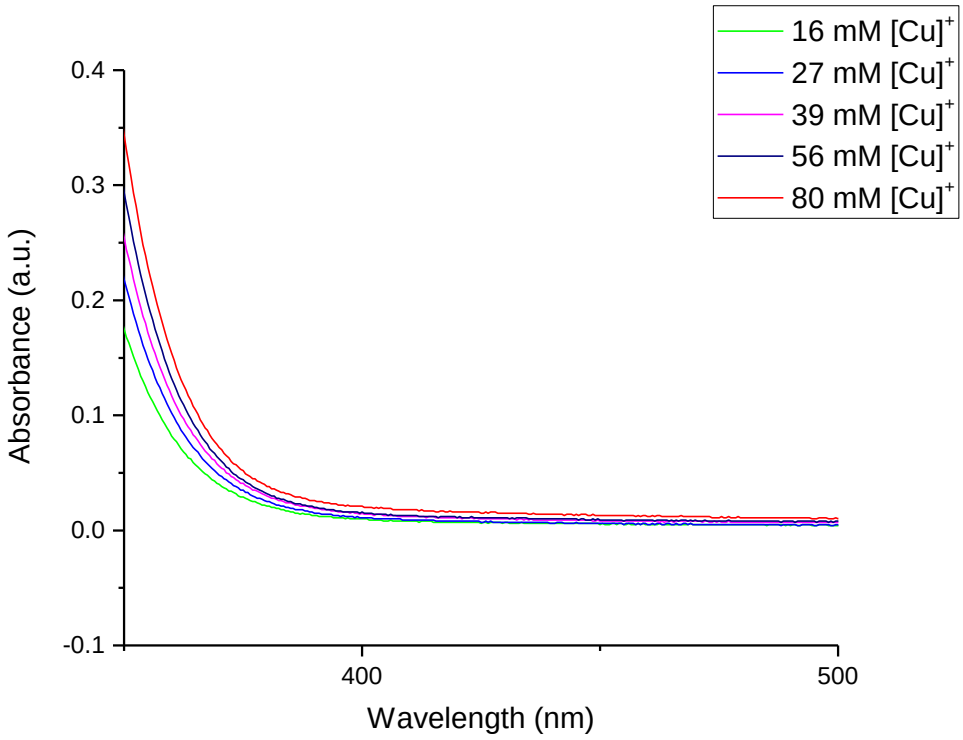

Figure III.10. UV/Vis absorbance of 16 mM (green), 27 mM (blue), 39 mM (magenta), 56 mM (navy), and 80 mM (red) solutions of tetrakis(acetonitrile)copper BF_4 in acetone. (Dr. Dr. Matthew B. Plutschack and the author collected the data; Dr. Dr. Matthew B. Plutschack drafted the figures)

Excitation inner filter effect correction factors, η, were calculated using the equation:[278]

$$\eta = \frac{A_{xo}(1 - 10^{-A_{xi}})}{A_{xi}(1 - 10^{-A_{xo}})}$$

Where Axo is the fluorophore absorbance (0.06 a.u.) at the excitation wavelength (450 nm), and Axi is the quencher absorbance at a given concentration. The corrected I_0/I values do not change significantly. An ion-pairing effect[279] is a more likely explanation. Knowles and co-workers[280] have observed this non-linearity in Stern-Volmer analysis for a photocatalyst with a PF_6^- counterion and quenching experiments with phosphates. Our iridium photocatalyst has a PF_6^-counterion and our copper(I) catalyst a BF_4^- counterion.

[Cu^{I}]/(mM)	Uncorrected I_0/I	Abs. Cu^{I} at 450 nm	Correction Factor, η	Corrected I_0/I
0	1	0	1	1
16	1.3	0.005	0.99	1.3
27	1.5	0.006	0.99	1.5
39	1.6	0.008	0.99	1.6
56	1.7	0.009	0.99	1.7
80	1.9	0.013	0.99	1.9

Table III.8. Calculated correction factors and corrected I_0/I values for tetrakis(acetonitrile)copper BF_4. (Dr. Dr. Matthew B. Plutschack and the author collected the data; Dr. Dr. Matthew B. Plutschack drafted the table)

In order to estimate an upper limit for the photocatalyst quenching rate by tetrakis(acetonitrile)copper BF_4, luminescence quenching measurements were performed twice more (Figure III.11, left), and a linear regression fit was performed for I_0 and I_0/I for the three lowest concentrations of tetrakis(acetonitrile)copper BF_4 (Figure III.11, right).

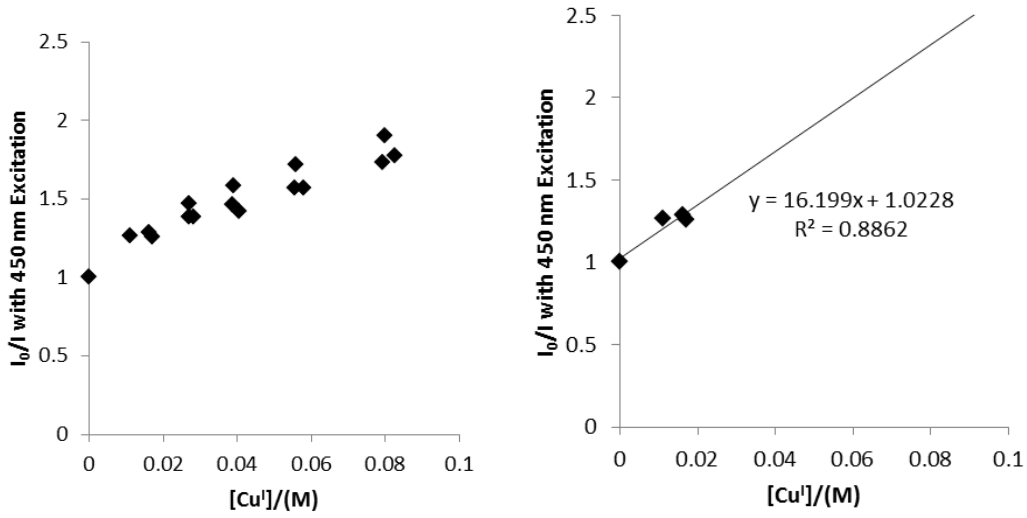

Figure III.11. Stern-Volmer plot for Ir(dF(CF_3)ppy)$_2$(dtbbpy)PF_6 luminescence quenching by tetrakis(acetonitrile)copper BF_4 measured in triplicate (left). Linear regression fit for the three lowest concentrations to estimate an upper limit for the

quenching rate constant k_q. (Dr. Dr. Matthew B. Plutschack and the author collected the data; Dr. Dr. Matthew B. Plutschack drafted the figures)

Quencher	**k_q/($M^{-1}s^{-1}$)**
4	$3.1*10^5$
$Cu(MeCN)_4BF_4$	$7.0*10^6$
thianthrene	$5.00*10^8$

Table III.9. Quencher rate coefficients. (Dr. Dr. Matthew B. Plutschack and the author collected the data; Dr. Dr. Matthew B. Plutschack drafted the table)

III.3.6.4 Cyclic voltammetry

Cyclic voltammetry (CV) is one of the most frequently used techniques for analyzing electrochemical reactions. It provides convenient access to redox potentials, thermodynamic and kinetic information about electron-transfer processes. Typical features of such measurements consist of a cell fitted with three electrodes (working, reference and counter electrodes), intended compounds, solvents with electrolyte, and cyclic wave currents supplied by a potentiostat. The resulting cyclic voltammograms depict peak positions/potentials (E_p), peak currents (I_p), and can be reversible, quasi-reversible or irreversible depending on electrochemical processes. Characteristic data based on scan rate and the peak current implies whether a reaction is electrochemically reversible or electrochemically irreversible. A reversible cyclic voltammogram represents a reversible reaction, for which peak potentials remain constant, while the peak currents change proportionally with the applied scan rate. Totally irreversible cyclic voltammograms imply electrochemical reactions with a rate-determining electron transfer step followed by other fast chemical reactions. The quasi-irreversible case is more complicated regarding to chemical reactions, which can be either reversible or irreversible depending on scan rate. Higher scan rates will render greater reaction irreversibility.

In the case of an electrochemically reversible reaction, where the electron transfer is fast, and the formal potential (E_f^o) can be easily calculated based on the voltammogram comprising both reduction (E_p^{re}) and oxidation (E_p^{ox}) peaks:

$$E_f^o = (E_p^{ox} - E_p^{re})/2 \qquad \text{(III-1)}$$

For a completely irreversible system, quantitative characterization of formal potential can be generated from scan rates and peak potentials:

$$E_p = E_f^o - \frac{RT}{\alpha n' F}\left[0.78 + ln\left(\frac{k_S^{el}}{\sqrt{\alpha F n' \upsilon D / RT}}\right)\right] \qquad \text{(III-2)}$$

where R is the universal gas constant (8.314 J•K^{-1}•mol^{-1}), T is the temperature (often 298 K), F is Faraday constant (96,485.33 C•mol^{-1}), α is the cathodic transfer coefficient ($\alpha = -\frac{RT}{n'F} * \frac{dln|I_c|}{dE}$, I_c is the cathodic current), k_S^{el} is the forward heterogeneous electron transfer constant, υ is scan rate, n' is the number of electrons transferred per mole before the hypothetical rate-determining step. Practically, the transfer coefficient α may be derived from the slope of the E_p vs. logυ diagram or from the peak width. For the case we are going to discuss late on, approximation results $\alpha = \frac{1.86\,RT}{F\,(E_{p/2} - E_p)}$ (III-3), where $(E_{p/2} - E_p)$ is peak width).[271] In such case, the Randles-Sěvćik equation is:

$$I_p = 0.496(\alpha n')^{0.5} nFAc(FD\upsilon/RT)^{0.5} \qquad \text{(III-4)}$$

where n is the total number of electrons transferred, A is the geometric area of the electrode (cm^2), c is substrate concentration, D is diffusion constant (cm^2•s^{-1}). The competition parameter (γ_C) between electron transfer and a follow-up first-order homogeneous chemical reaction can be derived with the dimensionless variables:[271]

$$\gamma_C = k_S^{el}\, k_c^{-\alpha/2}\, D^{-1/2} \left(\frac{RT}{F\upsilon}\right)^{(1-\alpha)/2} \qquad \text{(III-5)}$$

where k_c is the rate for the follow-up reaction. When γ_C is small, it suggests a rate determining electron transfer (together with diffusion), while the opposite is true when γ_C is large. When reactions are under mixed kinetic control, a characteristic linear variation of the transfer coefficient α versus scan rate can be diagnosed. By treatment of the newly derived dimensionless expression of current-potential curves with approximation (variation on α) for experimental data, two parameters

C_1 and C_2 can be defined.[281] When α equals 0.5, proposed theoretical curves often fit well with experimental data. The corresponding derived formulations are:

$$C_1 = log\left(\frac{Fk_cD^2}{2RTk_{s,el}^4}\right) \qquad \text{(III-6)}$$

$$C_2 = E_f^o + \left(\frac{RT}{F} ln\, 10\right) log\left(\frac{k_cD}{k_{s,el}^2}\right) \qquad \text{(III-7)}$$

Conceptual Idea Constructed by Dr. Wonseok Ham

The peak potential linearly shifts to more negative values as the sweep rate increases, with a slope of 65 mV. The coefficient α_{app} is approximately constant over the range of sweep rates, with the average value of 0.43 (lower than 0.5, but not significantly), indicating that the reductive cleavage occurs through a stepwise mechanism, and the electrochemical cleavage process is under kinetic control by the initial electrode electron transfer.[269] In such a situation, α_{app} is a true transfer coefficient α (0.43), and the following relationship[267,269] between the standard reduction potential (E^0) and the peak potential (E_p) holds:

$$E_p = E^0 - 0.78\,\frac{RT}{\alpha F} + \frac{RT}{\alpha F}\ln\left(\frac{k_S^{el}}{\sqrt{\alpha F \upsilon D\,/\,RT}}\right)$$

where k_S^{el} is the forward heterogeneous electron transfer rate constant.

The diffusion coefficient D was approximated as 1.5×10^{-5} cm^2/s, which is a reasonable estimate for the molecular size[267] of simple arylthianthrenium salts.

The value of k_S^{el} may be approximated from known k_S^{el} values of related molecules.[268,282]

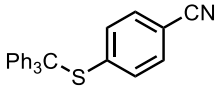

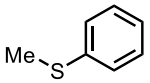

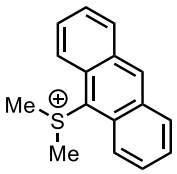

k_s^{el} =	0.18 $cm \cdot s^{-1}$ (reduction)	1.0 $cm \cdot s^{-1}$ (oxidation)	3.0 $cm \cdot s^{-1}$ (reduction)

The k_S^{el} value primarily depends on the extent of charge delocalization upon electron transfer. The LUMO of arylthianthrenium salts is computationally predicted to be spread over the thianthrene moiety.[188] Therefore, the k_S^{el} values of arylthianthrenium salt are expected to be between those of triphenylmethyl *p*-cyanophenyl sulfide (in which the charge acceptor would be the cyanophenyl moiety) and anthracen-9-yldimethylsulfonium (in which the charge acceptor would be anthracenyl moiety). We approximate the k_S^{el} value of arylthianthrenium salt compounds to be 0.5 cm/s, which is a conservative guess.

An equation for the competition parameter γ_C, which determines the kinetic competition between the electrode electron transfer and the follow-up chemical process, is given as following:[270]

$$\gamma_C = k_S^{el}\, k_c^{-\alpha/2}\, D^{-1/2} \left(\frac{RT}{F\upsilon}\right)^{(1-\alpha)/2}$$

When γ_C is small, the reductive cleavage is kinetically controlled by the electron transfer, and the opposite is true when γ_C is large. We estimate the lower limit of the cleavage rate constant (k_c) by setting the high limit of γ_C as 0.1, using the smallest sweep rate for which the kinetic control by the electron transfer is observed.

General Procedure Designed by Dr. Wonseok Ham

In a glovebox, a 100 mL round-bottom flask was charged with arylthianthrenium salt (0.100 mmol, 1.00 equiv), $TBAPF_6$ (2.91 g, 7.50 mmol, 75.0 equiv), and phenol (18.8 mg, 0.200 mmol, 2.00 equiv). Dry acetonitrile (50.0 mL, c = 2.00 mM) was added via syringe, and the flask was swirled to ensure homogeneity. The resulting solution (1.5 mL) was added via syringe to a quartz cuvette equipped with a magnetic stirring bar. A glassy-carbon working electrode (2 mm diameter), a platinum-mesh counter electrode, and a silver-wire quasi-reference electrode were immersed in the solution while not touching the stirring bar. The solution was stirred for 10 sec, then a cyclic voltammogram was obtained at 298 K with an Autolab PGSTAT204 potentiostat.

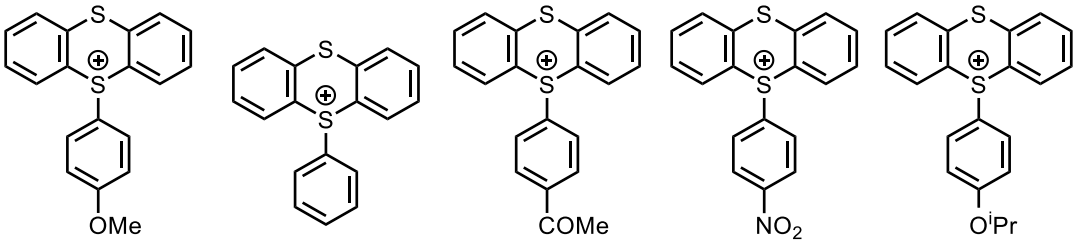

62 **70** **71** **72** **73**

For acetophenone-derived thianthrenium BF_4 **71**, severe nonlinearity in the plot of E_p (peak potential) versus log υ (potential sweep rate) was observed. Such phenomenon was minimized by examining the cyclic voltammetry without phenol additive.

For each arylthianthrenium salt compound, multiple cyclic voltammograms with varied potential sweep rates (ranging from 10 mV/s to 10 V/s) were obtained. After each measurement, the working electrode was taken out of the glovebox, and then carefully polished and ultrasonically rinsed in distilled water before use. A fresh solution of arylthianthrenium salt, $TBAPF_6$, and phenol was used for each measurement.

The quasi-reference electrode potential was calibrated by obtaining a cyclic voltammogram of a solution of ferrocene (2.00 mM) and $TBAPF_6$ (150 mM) in acetonitrile with 1 V/s potential sweep rate. The standard redox potential of Fc/Fc^+ couple was taken as 310 mV vs. SCE.[283]

Cyclic Voltammograms

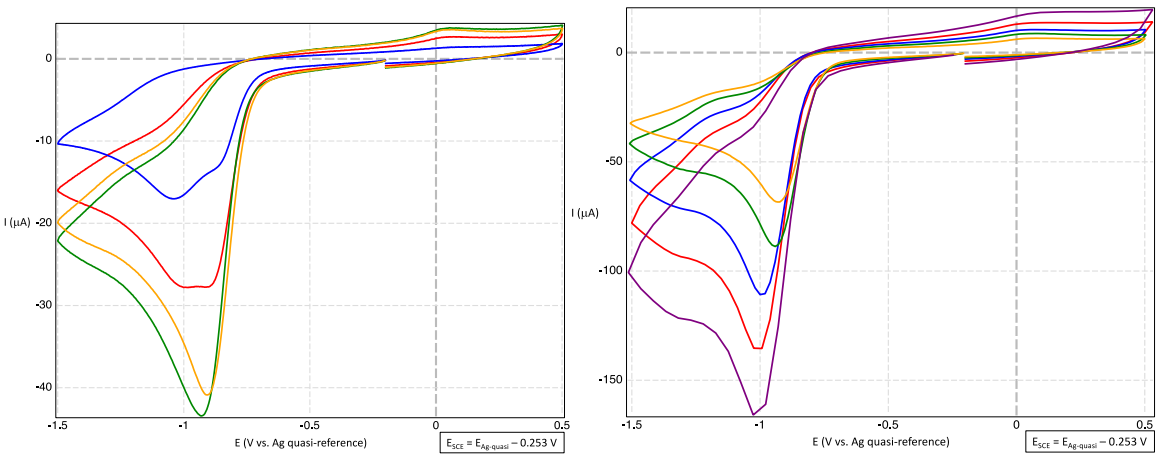

Figure III.12. CV of acetophenone-derived thianthrenium BF_4 **71** (without phenol additive). Potential sweep rates are as following. (Left) blue: 398 mV/s, red: 1000

mV/s, yellow: 1585 mV/s, green: 1890 mV/s. (Right) yellow: 3981 mV/s, green: 6309 mV/s, blue: 10000 mV/s, red: 15000 mV/s, purple: 25000 mV/s.

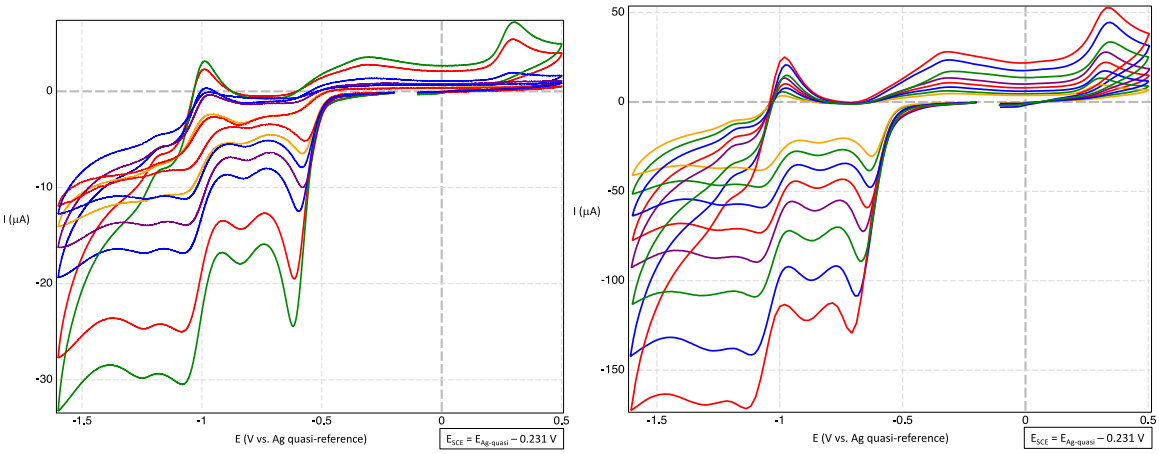

Figure III.13. CV of nitrobenzene-derived thianthrenium BF_4 **72**. Potential sweep rates are as following. (Left) 10 mV/s, 16 mV/s, 25 mV/s, 40 mV/s, 63 mV/s, 158 mV/s, 251 mV/s, from red to green. (Right) 398 mV/s, 631 mV/s, 1000 mV/s, 1585 mV/s, 2512 mV/s, 3981 mV/s, 6309 mV/s, 10000 mV/s, from yellow to red.

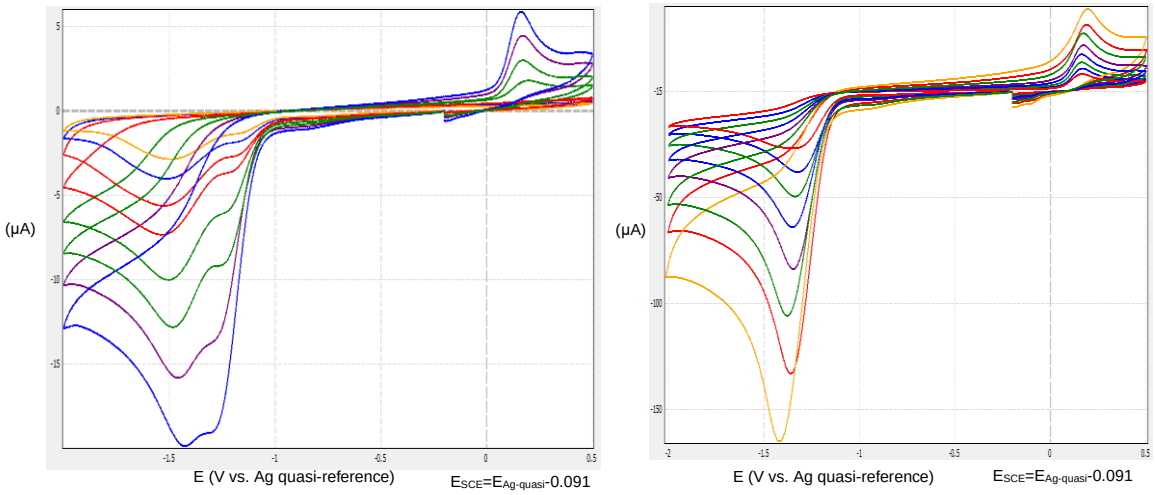

Figure III.14. CV of isopropoxylbenzene-derived thianthrenium BF_4 **73**. Potential sweep rates are as following. (Left) 10 mV/s, 16 mV/s, 25 mV/s, 40 mV/s, 63 mV/s, 158 mV/s, 251 mV/s, from yellow to blue. (Right) 398 mV/s. 631 mV/s, 1000 mV/s, 1585 mV/s, 2512 mV/s, 3981 mV/s, 6309 mV/s, 10000 mV/s, from red to yellow.

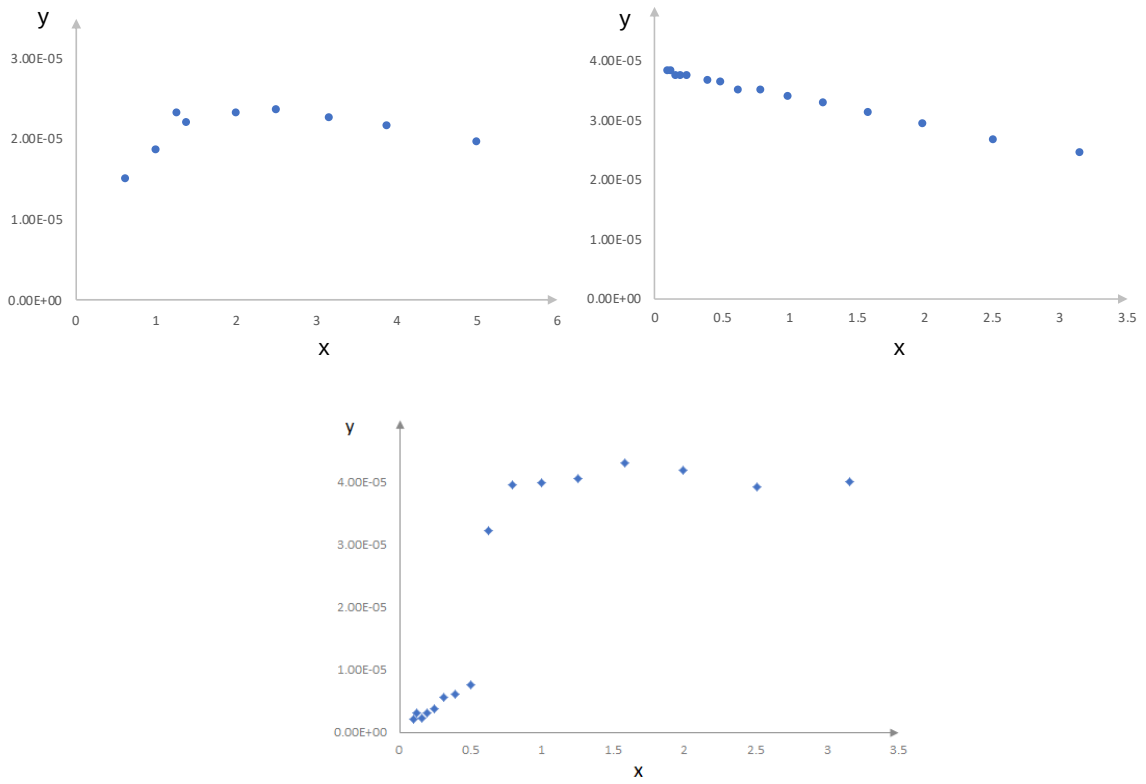

Figure III.15. Plot of $y = I_p/\upsilon^{1/2}$ ($A \cdot s^{1/2} \cdot V^{-1/2}$) versus $x = \upsilon^{1/2}$ ($V^{1/2} \cdot s^{-1/2}$) for arylthianthrenium salt compounds. Top left: acetophenone-derived thianthrenium BF_4. Top right: nitrobenzene-derived thianthrenium BF_4. Bottom: isopropoxylbenzene-derived thainthrenium BF_4.

Analysis of E^0 and k_c for 71

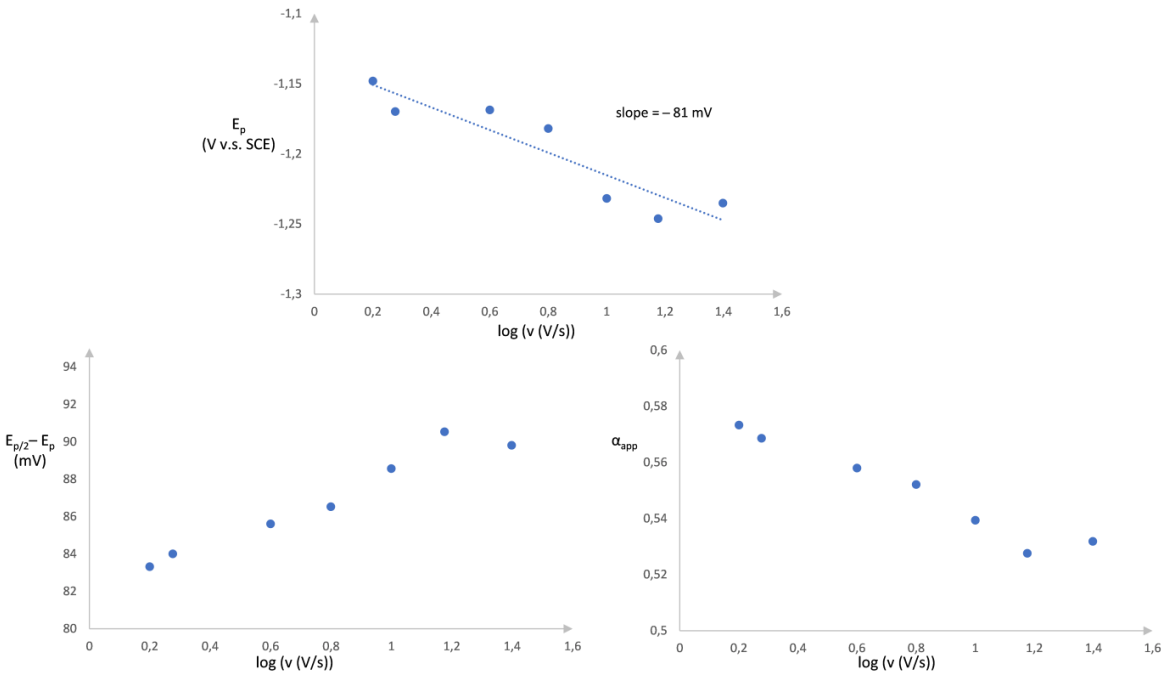

Figure III.16. Plots of peak potentials, peak widths, and apparent transfer coefficients versus log υ (υ between 1585 mV/s and 25 V/s) for **71**.

While the correlation between the peak potential and log υ appears roughly linear, the peak width increases (and thus the apparent transfer coefficient decreases) as the sweep rate increases. The obtained apparent transfer coefficients are between 0.5 and 0.6. Such CV behavior indicates mixed kinetic control between the initial electron transfer and the subsequent fragmentation reaction.[281,282] The decrease of α_{app} indicates a transition from mixed kinetic control by eletron transfer and the subsequent chemical fragmentation to mainly kinetic control by electron transfer. In such a situation of mixed-kinetic control, the variations of $E_p - C_2$ and $E_{p/2} - E_p$ with log υ + C_1 (α = 0.5), where

$$C_1 = \log\left(\frac{Fk_cD^2}{2RTk_{s,el}^4}\right), C_2 = E^0 + \left(\frac{RT}{F}\ln 10\right)\log\left(\frac{k_cD}{k_{s,el}^2}\right)$$

(F is the Faraday constant, k_S^{el} = forward heterogeneous electron transfer constant, k_c = cleavage rate constant, D is the diffusion coefficient of arylthianthrenium salt, R is gas constant, and T is temperature), should follow a universal trend regardless of the specific electrochemical reaction. Such a universal trend has been derived by numerical solution of differential equations based on electron transfer theory.[281] The corresponding theoretical curves are shown below (We thank Prof. Cyrille Costentin (Université Paris VII) for providing the theoretical curves):

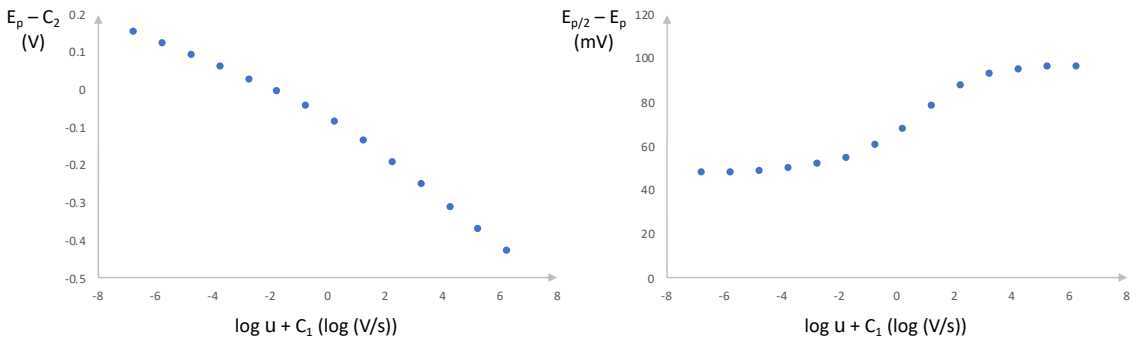

Figure III.17. Mixed kinetic control between electron transfer and subsequent chemical step (fragmentation). Theoretical variations of $E_p - C_2$ and $E_{p/2} - E_p$ with $\log \upsilon + C_1$ ($\alpha = 0.5$).

We fitted our data onto the theoretical plots and adjusted C_1 and C_2 so that the experimental data points adhere to the working curves.

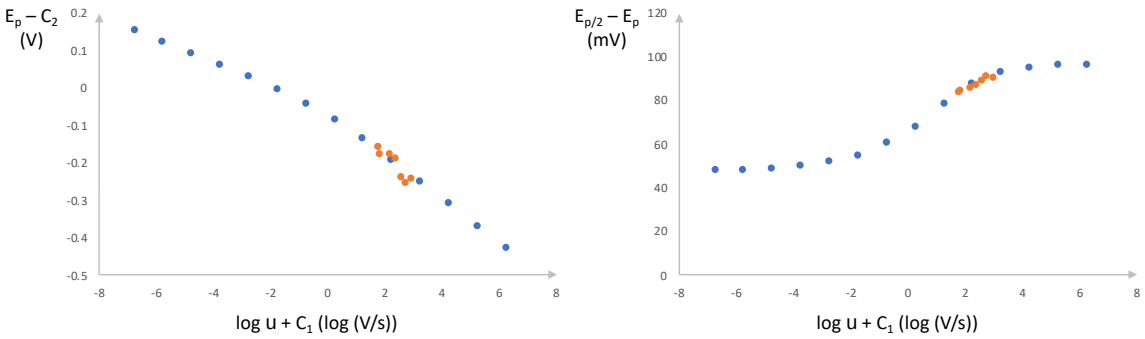

Figure III.18. Test of consistency between the peak potential/width data (orange) and the theoretical working curve (blue). (resulting: $C_1 = 1.6$, $C_2 = -0.99$).

The standard reduction potential E^0 and the fragmentation rate constant k_c were determined by solving the following equations, where $D = 2 \times 10^{-5}$ cm^2/s (approx.) and $k_S^{el} = 0.5$ cm/s (approx.):

$$C_1 = \log\left(\frac{F k_c D^2}{2RT k_{s,el}^4}\right) = 1.6$$

$$C_2 = E^0 + \left(\frac{RT}{F}\ln 10\right)\log\left(\frac{k_c D}{k_{s,el}^2}\right) = -0.99$$

$$E^0 = -1.25\ V\ vs.SCE$$

$$k_c = 3.2 \times 10^8\ s^{-1}$$

Analysis of E^0 and k_c for 72

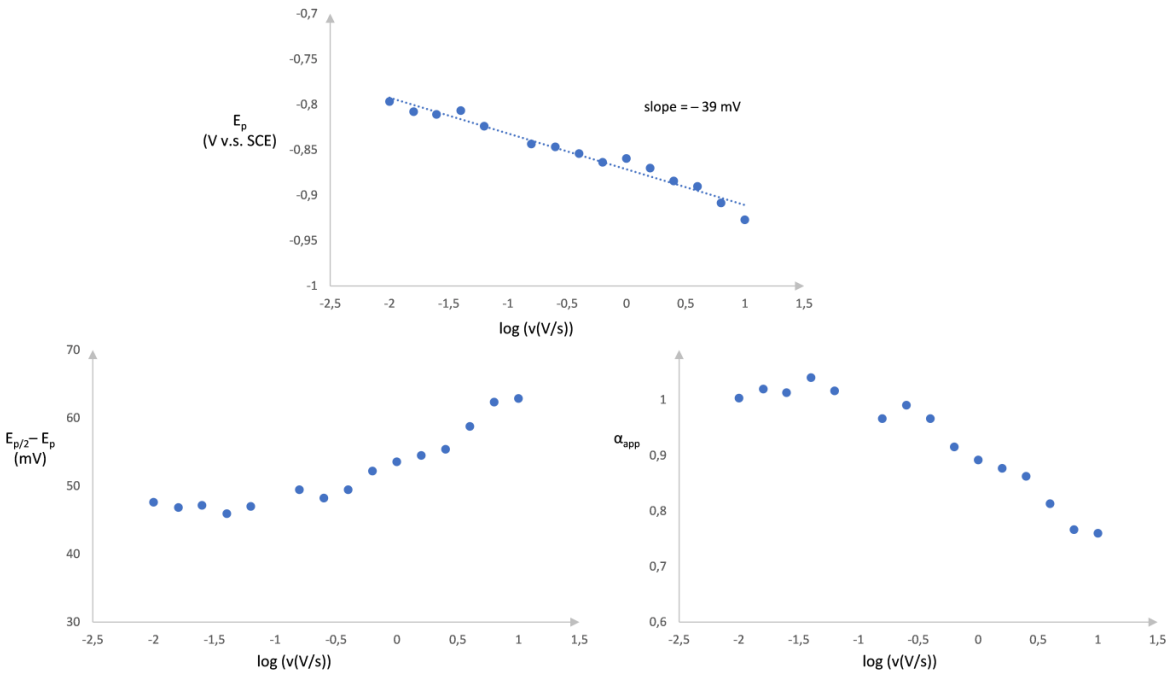

Figure III.19. Plots of peak potentials, peak widths, and apparent transfer coefficients versus log υ (υ between 10 mV/s and 10 V/s) for **72**.

The mechanistic assignment and the methods for analysis are analogous to those for acetophone-derived thianthrenium compound **71**, except that the decrease of the apparent transfer coefficient (ranging from 1 to 0.75), which represents the transition from the kinetic control by the follow-up cleavage step to the mixed control by electron transfer and subsequent chemical fragmentation.

The consistency between the peak potential/width data and the theoretical working curves was checked by adjusting C_1 and C_2 values, so that the experimental data points adhere to the theoretical variations of $E_p - C_2$ and $E_{p/2} - E_p$ with log υ + C_1 (α = 0.5).

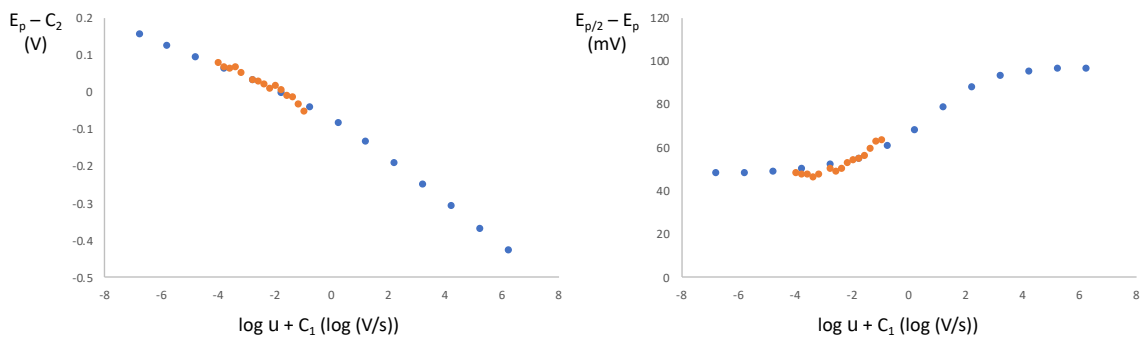

Figure III.20. Test of consistency between the peak potential/width data (orange) and theoretical working curve (blue). (resulting: C_1 = –1.9, C_2 = –0.87).

The k_S^{el} value of **71** should be approximated in an alternative manner, due to the tendency of charge localization within the nitro moiety in reduced nitroaromatic compounds. Reported k_S^{el} values of 4-nitrobenzyl chloride and nitrobenzene are 1.0 and 2.2 cm/s, respectively.[272, 284] Given that nitrobenzene-derived thianthrenium BF_4 contains the electron-withdrawing thianthrenium group in addition to the nitro group, approximation of its k_S^{el} value as 1.0 cm/s would be a conservative guess.

The standard reduction potential E^0 and the fragmentation rate constant k_c were determined by solving the following equations, where D = 2 × 10^{-5} cm^2/s (approx.) and k_S^{el} = 1.0 cm/s (approx.):

$$C_1 = \log\left(\frac{F k_c D^2}{2RT k_{s,el}^4}\right) = -1.9$$

$$C_2 = E^0 + \left(\frac{RT}{F}\ln 10\right)\log\left(\frac{k_c D}{k_{s,el}^2}\right) = -0.87$$

$$E^0 = -0.96\ V\ vs.SCE$$

$$k_c = 1.6 \times 10^6\ s^{-1}$$

Analysis of E^0 and k_c for 73

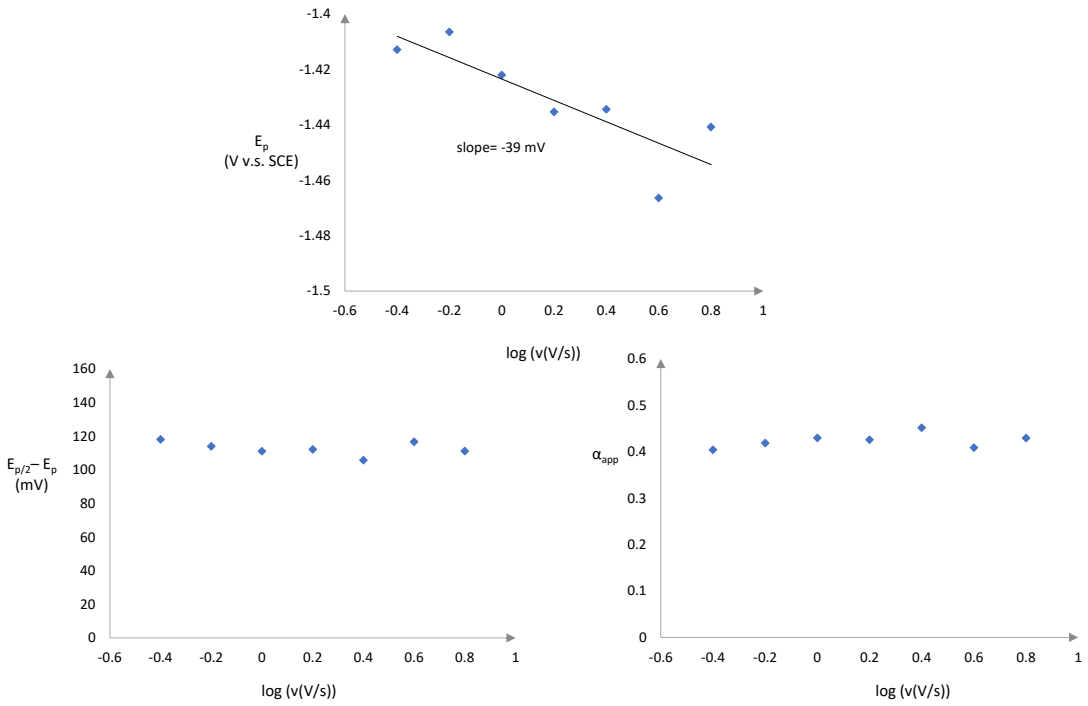

Figure III.21. Plots of peak potentials, peak widths, and apparent transfer coefficients versus log υ (υ between 398 mV/s and 6.309 V/s) for **73**.

The mechanistic assignment and the methods for analysis are analogous to those for anisole-derived thianthrenium compound **62**. α_{app} is approximately constant over the range of sweep rates, with the average value of 0.42 (lower than 0.5, but not significantly), indicating that the reductive cleavage occurs through a stepwise mechanism, and the electrochemical cleavage process is under kinetic control by the initial electrode electron transfer. In such a situation, α_{app} is a true transfer coefficient α (0.42).

$$E_p = E^0 - 0.78\,\frac{RT}{\alpha F} + \frac{RT}{\alpha F}\ln\left(\frac{k_S^{el}}{\sqrt{\alpha F \upsilon D\,/\,RT}}\right)\ (for\ \upsilon\ \geq 0.398\,V/s)$$

$$\gamma_C = \ k_S^{el}\ k_c^{-\alpha/2}\ D^{-1/2}\left(\frac{RT}{F\upsilon}\right)^{(1-\alpha)/2} \leq 0.1\ (for\ \upsilon\ \geq 0.398\,V/s)$$

From the above equations, where D = 2 × 10^{-5} cm^2/s (approx.) and k_S^{el} = 0.5 cm/s (approx.), the standard reduction potential and the lower limit of the fragmentation rate constant are obtained as follows:

$$E^0 = \ -1.57\,V\ vs.SCE$$

$$k_c \geq 5.7 \times 10^{12}\ s^{-1}$$

υ (mV/s)	E_p (V vs. SCE)	E^0 (V vs. SCE)
398	–1.503	**–1.594**
631	–1.483	**–1.574**
1000	–1.484	**–1.575**
1585	–1.483	**–1.575**
2512	–1.469	**–1.560**
3981	–1.487	**–1.578**
6309	–1.447	**–1.538**
average		**–1.571**

Table III.10. Estimation of E^0 of **73**.

We approximate the k_c as the low-limit value.

III.3.6.5 Differential Pulse Voltammetry

General Procedure Designed by Dr. Wonseok Ham

In a glovebox, a 20 mL vial was charged with arylthanthrenium salt (20.0 μmol, 1.00 equiv) and $TBAPF_6$ (581 mg, 1.50 mmol, 75.0 equiv). Dry acetonitrile (10.0 mL, c = 2.00 mM) was added via syringe, and the vial was swirled to ensure homogeneity. The resulting solution (1.5 mL) was added via syringe to a quartz cuvette equipped with a magnetic stirring bar. A glassy-carbon working electrode (2 mm diameter), a platinum-mesh counter electrode, and a silver-wire quasi-reference electrode were immersed in the solution while not touching the stirring bar. The solution was stirred for 10 sec, then a differential pulse voltammogram was obtained at 298 K with an Autolab PGSTAT204 potentiostat using the following parameters: Step = 0.001 V, Modulation amplitude = 0.005 V, Modulation time = 0.05 sec, Interval time = 0.5 sec. Onset reduction potentials are estimated

based on the intersection of the baseline and tangent at the inflection point.[285,286]

The quasi-reference electrode potential was calibrated by obtaining a cyclic voltammogram of a solution of ferrocene (2.00 mM) and $TBAPF_6$ (150 mM) in acetonitrile with 1 V/s potential sweep rate. The standard redox potential of Fc/Fc^+ couple was taken as 310 mV vs. SCE.[283]

Estimation of Onset Reduction Potentials

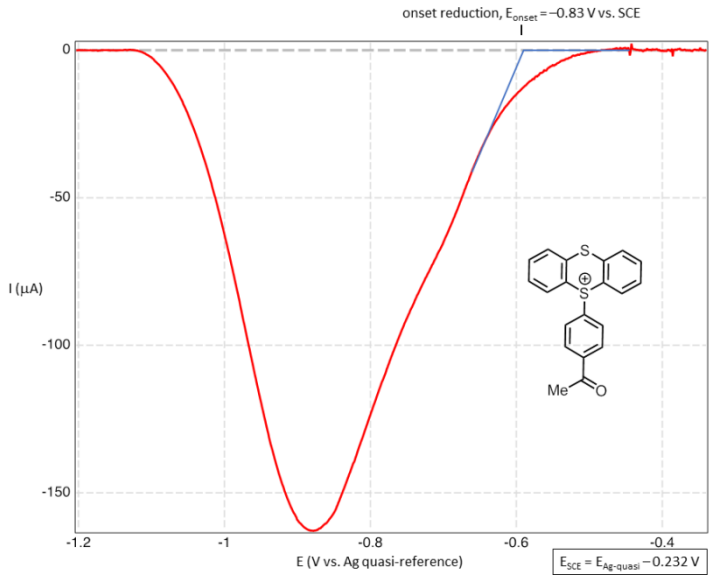

Figure III.22. DPV of **71**. Onset is observed at –0.83 V vs. SCE.

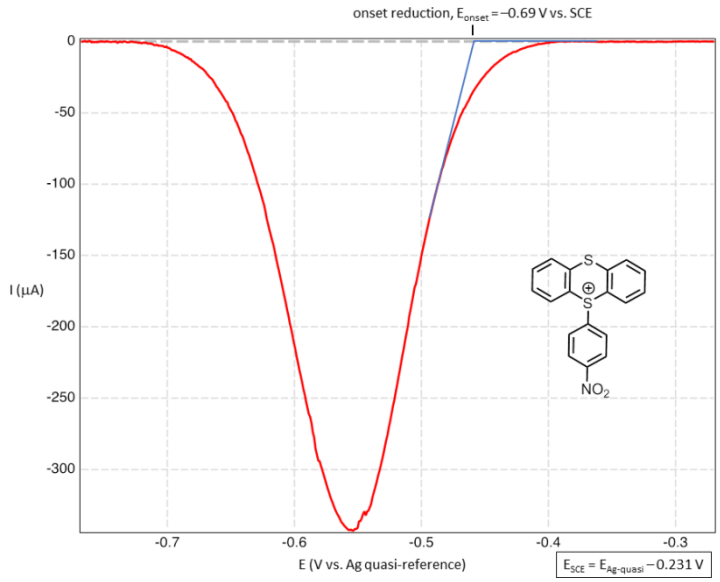

Figure III.23. DPV of **72**. Onset is observed at –0.69 V vs. SCE.

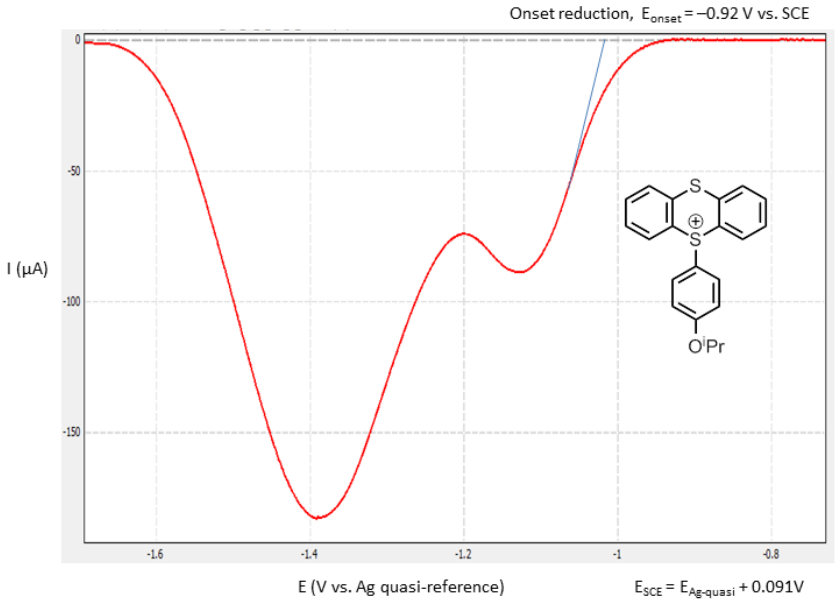

Figure III.24. DPV of **73**. Onset is observed at –0.92 V vs. SCE.

III.3.6.6 Hammett Plot

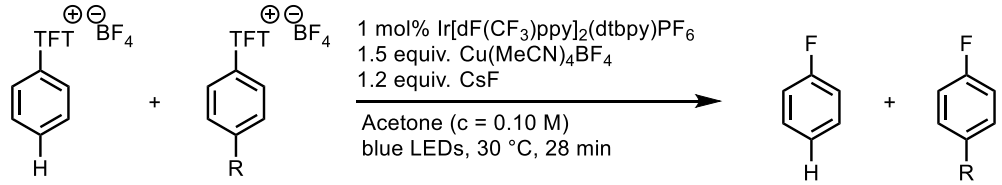

To a 4-mL borosilicate vial equipped with a stir bar was added Ir[dF(CF$_3$)ppy]$_2$(dtbpy)PF$_6$ (0.6 mg, 0.5 µmol, 1 mol%), benzene-derived tetrafluorothianthrenium salt (11.3 mg, 25.0 µmol, 0.500 equiv.) and para substituted benzene-derived tetrafluorothianthrenium salt (25.0 µmol, 0.500 equiv.). The vial was transferred into a N_2-filled glovebox. After addition of Cu(MeCN)$_4$BF$_4$ (23.6 mg, 75.0 µmol, 1.50 equiv.), CsF (9.2 mg, 60 µmol, 1.2 equiv.) and acetone (0.50 mL, c = 0.10 M), the vial was capped, transferred out of the glovebox and placed 5 cm away from two 34 W blue LEDs. The temperature was kept at approximately 30 °C through cooling with a fan. After being stirred for 28 min, 4-fluorobenzotrifluoride (8.2 mg, 6.3 µL, 50 µmol, 1.0 equiv.) was added as an internal standard. The reaction mixture was diluted with ethyl acetate, and the yield was determined by ^{19}F NMR integration relative to the internal standard.

Based on Hammett equation ($\log \frac{k}{k_0} = \sigma\rho$, k_0 is the reference reaction rate of the unsubstituted reactant, and k that of a para-substituted reactant), two reactions

with two aromatic reactants which only differs in the type of substituents, will have different reaction rates.

para-substituent (X)	yield ratio for X/H (%/%)			
	entry 1	entry 2	entry 3	entry 4
CF_3	5.00/2.85	5.00/2.40		
I		12.00/9.00	12.00/8.00	10.25/7.07
Cl	8.72/7.80		13.00/11.00	
F	9.54/11.07		8.88/11.53	8.41/11.11
H	1			
Ph			28.87/8.96	30.00/11.00
Me	10.68/13.88	9.01/14.31	13.72/18.11	16.00/23.00
PhO	2.01/3.12		5.00/6.00	3.00/5.00
^{i}PrO	4.07/10.31	5.77/11.85		

Table III.11. ^{19}F-NMR yields for competition reactions. (X: yield for para-substituted aryl thianthrenium salts; H: yield for benzene-derived thianthrenium salt).

para-substituent (X)	para-effect	k/k_0				k/k_0 average	$\log(k/k_0)$
		entry 1	entry 2	entry 3	entry 4		
CF_3	0.540	1.75	2.08			1.92	0.3
I	0.276		1.33	1.50	1.45	1.43	0.2
Cl	0.227	1.12		1.18		1.15	0.1

F	0.062	0.86		0.77	0.76	0.80	–0.1
H	0.000	1.00				1.00	0.0
Ph	-0.010			3.22	2.73	2.98	0.5
Me	-0.170	0.77	0.63	0.76	0.70	0.72	–0.1
PhO	-0.320	0.64		0.83	0.60	0.69	–0.2
^{i}PrO	-0.450	0.39	0.49			0.44	–0.4

Table III.12. Reaction rate ratio for competition reactions (k: reaction rate for para-substitute aryl tetrafluorothianthrenium salts; k_0: reaction rate for benzene-derived tetrafluorothianthrenium salt).

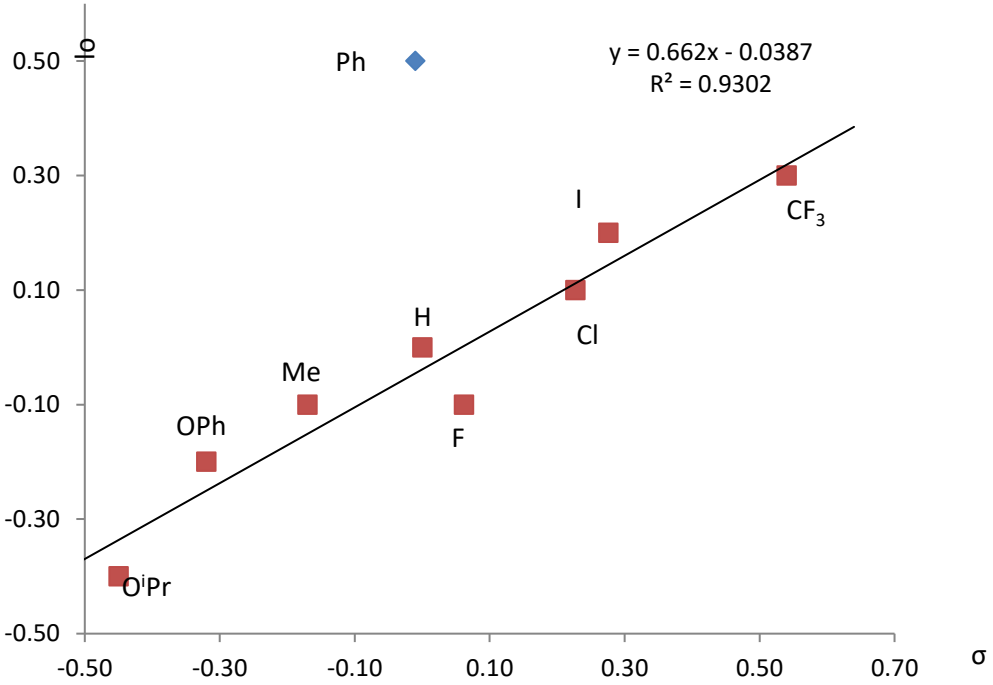

Figure III.25. Hammett-plot for the fluorination of aryltetrafluorothenthrenium salts.

III.3.6.7 Quantum Yield Measurement

Determination of the light intensity of the blue LED

The radiant flux of blue LED was determined by standard ferrioxalate actinometry.[287,288,289] A 0.15 M solution of ferrioxalate was prepared by dissolving

potassium ferrioxalate hydrate (328 mg, 0.750 mmol) in 5.0 mL of 0.20 M aqueous sulfuric acid. A 0.15 M buffered solution of 1,10-phenanthroline was prepared by dissolving 1,10-phenanthroline (541 mg, 3.00 mmol) and sodium acetate (1.23 g, 15.0 mmol) in 20 mL of 0.20 M aqueous sulfuric acid.

To a 4-mL borosilicate vial equipped with a stir bar was added 0.50 mL of the ferrioxalate solution. The vial was sealed and placed 5 cm away from two 34 W blue LEDs. After irradiation for 7 seconds, 1.5 mL of the aqueous sulfuric acid and 2.0 mL of the buffered solution was added to the vial. The solution was then allowed to rest for 1 hour to allow the resultant ferrous ions to react completely with 1,10-phenanthroline. 50 µL of the resulting solution was taken as an aliquot and diluted with 3.0 mL of 0.20 M aqueous sulfuric acid. The absorbance of the resulting solution in a cuvette (l = 1.0 cm) at 510 nm was measured by UV-Vis spectrometer. A non-irradiated sample and other samples with different irradiation time were also prepared and the absorbance at 510 nm was measured.

The amount of ferrous ion formed was calculated as follows:

$$n_{Fe^{2+}} = \frac{V \times \Delta A}{l \times \epsilon}$$

where V is the total volume (0.24 L) of the solution that was analyzed, ΔA is the difference in absorbance at 510 nm between the irradiated and non-irradiated samples, l is the path length (1.00 cm), and ε is the molar absorptivity at 510 nm, which is 11,100 L/(mol•cm).[290]

The radiant flux δ was calculated as follows:

$$\delta = \frac{n_{Fe^{2+}}}{\Phi \times t \times f}$$

where Φ is the quantum yield for the ferrioxalate actinometer (approximated as 0.845, which was reported for a 0.15 M solution at λ = 457.9 nm),[290] t is the irradiation time, and f is the fraction of light absorbed at 450 nm (0.9896).

The fraction of light absorbed was determined by the following equation:

$f = 1 - 10^{-A} = 0.9896$

where A is the measured absorbance (1.985) of the 0.15 M solution of potassium ferrioxalate at 450 nm.

irradiation time (s)	absorbance	ΔA	mol Fe^{2+} (mol)	radiant flux (Einstein/s)
non-irradiation	0.015	—	—	—
7	0.141	0.126	2.72432E-06	4.65E-07
10	0.189	0.174	3.76216E-06	4.50E-07
15	0.293	0.278	6.01081E-06	4.79E-07
30	0.360	0.345	7.45946E-06	2.97E-07
45	0.466	0.451	9.75135E-06	2.59E-07

Table III.13. Calculation of radiant flux.

The radiant flux is **3.9×10^{-7}** Einstein/s.

Determination of quantum yield

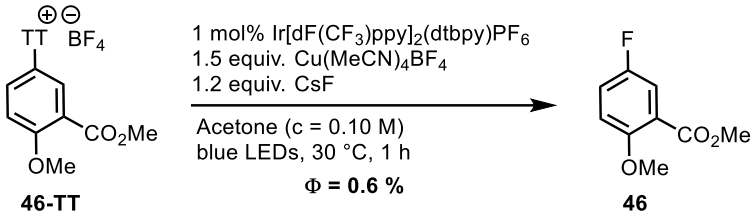

To a 4-mL borosilicate vial equipped with a stir bar was added $Ir[dF(CF_3)ppy]_2(dtbpy)PF_6$ (0.6 mg, 0.5 µmol, 1 mol%) and methyl-2-methoxybenzoate-derived thianthrenium salt **46-TT** (23.4 mg, 50.0 µmol, 1.00 equiv.). The vial was transferred into a N_2-filled glovebox. After addition of $Cu(MeCN)_4BF_4$ (23.6 mg, 75.0 µmol, 1.50 equiv.), CsF (9.2 mg, 60 µmol, 1.2 equiv.) and acetone (0.50 mL, c = 0.10 M), the vial was capped, transferred out of the glovebox and placed 5 cm away from two 34 W blue LEDs. The temperature was kept at approximately 30 °C through cooling with a fan. After being stirred for 1 h, 4-fluorobenzotrifluoride (6.3 µL, 8.2 mg, 50 µmol, 1.0 equiv.) was added as an internal standard. The reaction mixture was diluted with $CDCl_3$, and comparison of

the integration of the Csp^2–F of the internal standard (−108.42 ppm, m) with that of the formed product (−124.84 ppm, m) revealed 8% yield of **46** (4×10^{-6} mol).

The quantum yield was calculated as follows:

$$\Phi = \frac{n_{product}}{\sigma \times \mathrm{t} \times \mathrm{f}}$$

where flux is the photon flux determined by ferrioxalate actinometry (3.9×10^{-7} Einstein/s), t is the time (3600 s), and f is the fraction of light absorbed by $Ir[dF(CF_3)ppy]_2(dtbpy)PF_6$ at 450 nm.

A 1.0×10^{-3} M solution of $Ir[dF(CF_3)ppy]_2(dtbpy)PF_6$ in acetone was prepared, and the absorbance of the solution at 450 nm was 0.252. The fraction of light absorbed at 450 nm was calculated: $f = 1 - 10^{-A} = 1 - 10^{-0.252} = 0.4402$.

$$\Phi = \frac{4 \times 10^{-6}\ mol}{3.9 \times 10^{-7}\mathrm{Einstein}/s \times 3600\mathrm{s} \times 0.440} = 0.006$$

The quantum yield is 0.6%.

IV. ABBREVIATIONS

°C	degree Celsius
18-cr-6	1,4,7,10,13,16-hexaoxacyclooctadecane
Ac	acetyl
acac	acetylacetonate
Ac-Ala-OH	*N*-Acetyl-L-alanine
aq	aqueous
BDE	bond dissociation energy
bipy	2,2-bi-pyridine
Bn	benzyl
Boc	tert-butyloxycarbonyl
Bpin	bis-pinacolate
bpy	2,2'-bipyridine
BQ	1,4-benzoquinone
ca.	circa, approximately
cat.	catalytic
catBCl	B-chloro-catecholborane
CCDC	the Cambridge Crystallographic Data Centre
CFL	compact fluorescent lamp
CMD	concerted metalation-deprotonation
COD	1,5-cyclooctadiene
COE	cyclooctene
conv.	conversion
CPCM	conductor-like polarizable continuum model
CV	cyclic voltammetry
Cy	cyclohexyl

CYPs	cytochrome P450 enzyme
d.r.	diastereomeric ratio
DCE	1,2-dichloroethane
DCM	dichloromethane
dFppy	2-(2,4-difluorophenyl)pyridyl
DFT	density functional theory
DG	directing group
DMA	*N,N*-dimethylacetamide
DMAP	4-dimethylaminopyridine
DMF	*N,N*-dimethylformamide
DMSO	dimethylsulfoxide
DPV	differential pulse voltammetry
Dr.	doctor
dtbbpy/dtbpy	4,4’-di-tert-butyl-2,2'-bipyridine
E	electrophile
ED_{50}	half maximal effective dose
EDG	electron donating group
EDTA	ethylenediaminetetraacetic acid
ee	enatiomeric excess
EI	electron impact ionization
E_p	peak potential
$E_{p/2}–E_p$	half peak width
EPR	electron paramagnetic resonance spectroscopy
equiv/eq	equivalent(s)
ESI	electrospray ionization
Et	ethyl
Fc	ferrocene

FDA	food and drug administration
FG	functional group
FID	flame-ionization detection
GC	gas chromatography
h	hour(s)
HAT	hydrogen atom transfer
HFIP	1,1,1,3,3,3-hexafluoro-2-propanol
HMDS	hexamethyldisilazide
HOMO	highest occupied molecular orbital
HOTf	trifluoromethylsulfonic acid
LC	liquid chromatography
HRMS	high resolution mass spectrometry
hv	photon energy
I_p	peak current
^{i}Pr	iso-propyl
IPr	bis(2,6-diisopropylphenyl)-imidazolium
ISC	intersystem crossing
KIE	kinetic isotope effect
LDA	lithium diisopropylamide
LED	light-emitting diode
LUMO	lowest unoccupied molecular orbital
M	molar concentration
M.O.	molecular orbital
Me	methyl
MeCN	acetonitrile
Mes	mesityl

Mes-Acr$^+$	9-mesityl-10-methylacridinium
min	minute(s)
MOM	methoxymethyl ethers
Ms	methanesulfonyl
n/o	not observed
NBO	natural bond orbital
NBS	*N*-bromosuccinimide
NCS	*N*-chlorosuccinimide
nep	neopentyl
NHS	succinimide
NMP	*N*-Methyl-2-pyrrolidone
NMR	nuclear magnetic resonance spectroscopy
Ns	2-nitrobenzenesulfonyl
Nu	nucleophile
OX	oxidant
PC	photocatalyst
PDI	*N,N*-bis(2,6-diisopropylphenyl)perylene3,4,9,10-bis(dicarboximide
PET	positron emission tomography
Ph	phenyl
PhIO	iodosobenzene
Piv	pivolate
pK_a	acid dissociation constant
PMP	p-methoxylphenyl
ppm	part per million
Py	pyridine
r.s.m.	recovery of starting material

RCC	radio chemical conversion
RCY	radio chemical yield
RE	reductant
r.t.	room temperature
S.A.	specific activity
SCE	saturated calomel electrode
SET	single electron transfer
S_NAr	nucleophilic aromatic substitution
S_NAr	concerted nucleophilic aromatic substitution
solv.	solvent
SOMO	singly occupied molecular orbital
TBAF	tetra-n-butyl ammonium fluoride
^{t}Bu	tert-butyl
TEDA	triethylenediamine
TEMPO	(2,2,6,6-tetramethylpiperidin-1-yl)oxyl
terpy	2,2';6',2''-terpyridine
Tf	trifluoromethyl sulfonyl
TFA	trifluoroacetyl
TFAA	trifluoroacetic anhydride
TFT	2,3,6,7-tetrafluorothianthrene
THF	tetrahydrofurane
TLC	thin-layer chromatography
TMP	5,10,15,20-tetrakismesityl porphyrin
TMS	tetramethylsilyl
TT	thianthrene
UV/Vis	ultraviolet-visible spectroscopy

v/v	volume/volume ratio
vs.	versus
µwave	microwave

V. REFERENCES

[1]. Wade, L.G., *Organic Chemistry.* 6th Ed., Pearson Prentice Hall, New Jersey, 2006, pp 279.

[2]. https://www.researchandmarkets.com/research/2xl4dr/the_ethylene.

[3]. https://www.chemicals-technology.com/news/newsworldwide-demand-for-propylene-to-rise-to-130-million-tonnes-by-2023-says-ihs-4356137/.

[4]. https://www.ceresana.com/en/market-studies/chemicals/butadiene/ceresana-market-study-butadiene.html.

[5]. Fleming, I., *Molecular Orbitals and Organic Chemical Reactions.* Reference Ed., John Wiley & Son Ltd, West Sussex, 2010, pp 1–20.

[6]. Rylander, P. N., "Hydrogenation and Dehydrogenation" in *Ullmann's Encyclopedia of Industrial Chemistry.* Wiley-VCH, Weinheim, 2005.

[7]. Kolb, H. C.; Van Nieuwenhze, M. S.; Sharpless, K. B., Catalytic Asymmetric Dihydroxylation. *Chem. Rev.* **1994**, *94*, 2483–2547.

[8]. Roberts, I.; Kimball, G. E., The Halogenation of Ethylenes. *J. Am. Chem. Soc.* **1937***, 59,* 947–948*.*

[9]. Veysoglu, T.; Mitscher, L. A.; Swayze, J. K., A Convenient Method for the Control of Selective Ozonizations of Olefins. *Synthesis* **1980**, *10*, 807–810.

[10]. Kropp, P. J.; Daus, K. A.; Crawford, S. D.; Tubergen, M. W.; Kepler, K. D.; Craig, S. L.; Wilson, V. P., Surface-mediated reactions. 1. Hydrohalogenation of Alkenes and Alkynes. *J. Am. Chem. Soc.* **1990**, *112*, 7433–7434.

[11]. Dewar, M. J.; Olivella, S.; Stewart, J. J., Mechanism of the Diels-Alder reaction: Reactions of Butadiene with Ethylene and Cyanoethylenes. *J. Am. Chem. Soc.* **1986**, *108*, 5771–5779.

[12]. Galli, M.; Fletcher, C. J.; del Pozo, M.; Goldup, S. M., Scalable anti-Markovnikov Hydrobromination of Aliphatic and Aromatic Olefins. *Org. Biomol. Chem.* **2016**, *14*, 5622–5626

[13]. Bartlett, P. D., Recent Work on the Mechanisms of Peroxide Reactions. *Record of Chemical Progress*. **1950**, *11*, 47–51.

[14]. Reznichenko, A. L.; Hultszch, K. C., Hydroamination of Alkenes. *Org. React.* **2015**, *88*, 1–554.

[15]. Furukawa, J.; Kawabata, N.; Nishimura, J., Synthesis of Cyclopropanes by the Reaction of Olefins with Dialkylzinc and Methylene iodide. *Tetrahedron* **1968**, *24*, 53–58.

[16]. Franke, R.; Selent, D.; Börner, A., Applied Hydroformylation. *Chem. Rev.* **2012**, *112*, 5675–5732.

[17]. Calderon, N.; Ofstead, E. A.; Ward, J. P.; Judy, W. A..; Scott, K. W., Olefin Metathesis. I. Acyclic Vinylenic Hydrocarbons. *J. Am. Chem. Soc.* **1968**, *90*, 4133–4140.

[18]. Jenkins, A. D.; Kratochvíl, P.; Stepto, R. F. T.; Suter, U. W., Glossary of Basic Terms in Polymer Science (IUPAC Recommendations 1996). *Pure and Applied Chemistry* **1996**, *68*, 2287–2311.

[19]. Smidt, J.; Hafner, W.; Jira, R.; Sedlmeier, J.; Sieber, R.; Rüttinger, R.; Kojer, H., Katalytische Umsetzungen von Olefinen an Platinmetall-Verbindungen Das Consortium-Verfahren zur Herstellung von Acetaldehyd. *Angew. Chem.* **1959**, *71*, 176–182.

[20]. Rittle, J.; Green, M. T., Cytochrome P450 Compound I: Capture, Characterization, and C-H Bond Activation Kinetics. *Science* **2010**, *330*, 933–937.

[21]. Gonzalez, F. J.; Gelboin, H. V., Human Cytochromes P450: Evolution and cDNA-directed Expression. *Environmental Health Perspectives.* **1992**, *98*, 81–85.

[22]. Fenton, H. J. H., Oxidation of Tartaric Acid in Presence of Iron. *J. Chem. Soc., Trans.* **1894**, *65*, 899−911.

[23]. Shilov, A. E.; Shul'pin, G. B., Activation of C–H Bonds by Metal Complexes. *Chem. Rev.* **1997**, *97*, 2879−2932.

[24]. Stahl, S. S.; Labinger, J. A.; Bercaw, J. E., Homogeneous Oxidation of Alkanes by Electrophilic Late Transition Metals. *Angew. Chem. Int. Ed.* **1998**, *37*, 2180−2192.

[25]. Shilov, A. E.; Shul'pin, G. B., Activation Catalytic Reactions of Saturated Hydrocarbons in the Presence of Metal Complexes–Processes of C–H Bond Activation. Springer, 2002, pp 8–20.

[26]. Wencel-Delord, J.; Glorius, F., C–H Bond Activation Enables the Rapid Construction and Late-stage Diversification of Functional Molecules. *Nat. Chem.* **2013**, *5*, 369–375.

[27]. Abrams, D. J.; Provencher, P. A.; Sorensen, E. J., Recent Applications of C–H Functionalization in Complex Natural Product Synthesis. *Chem. Soc. Rev.* **2018,** *47*, 8925–8967.

[28]. Dai, H.-X.; Stepan, A. F.; Plummer, M. S.; Zhang, Y.-H.; Yu, J.-Q. J., Divergent C–H Functionalizations Directed by Sulfonamide Pharmacophores: Late-Stage Diversification as a Tool for Drug Discovery. *J. Am. Chem. Soc.* **2011**, *133*, 7222–7228.

[29]. Meyer, C.; Schepmann, D.; Yanagisawa, S.; Yamaguchi, J.; Itami, K.; Wünsch, B., Late–Stage C–H Bond Arylation of Spirocyclic σ1 Ligands for Analysis of Complementary σ1 Receptor Surface. *Eur. J. Org. Chem.* **2012**, 5972–5979.

[30]. Shintani, R.; Otomo, H.; Ota, K.; Hayashi, T., Palladium-Catalyzed Asymmetric Synthesis of Silicon-Stereogenic Dibenzosiloles via Enantioselective C–H Bond Functionalization. *J. Am. Chem. Soc.* **2012**, *134*, 7305–7308.

[31]. Tang, X.; Jia, X.; Huang, Z., Challenges and Opportunities for Alkane Functionalisation Using Molecular Catalysts. *Chem. Sci.* **2018**, *9*, 288–299.

[32]. Janowicz, Andrew H.; Bergman, Robert G., Carbon–Hydrogen Activation in Saturated Hydrocarbons: Direct Observation of M + R−H → M(R)(H). *J. Am. Chem. Soc.* **1982**, *104, 352–354.*

[33]. Arndtsen, B. A.; Bergman, R. G.; Mobley, T. A.; Peterson, T. H., Selective Intermolecular Carbon-Hydrogen Bond Activation by Synthetic Metal Complexes in Homogeneous Solution. *Acc. Chem. Res.* **1995**, *28*, 154–162.

[34]. Lersch, M.; Tilset, M., Mechanistic Aspects of C−H Activation by Pt Complexes. *Chem. Rev.* **2005**, *105*, 2471–2526.

[35]. Lyons, T. W.; Sanford, M. S., Palladium-Catalyzed Ligand-Directed C−H Functionalization Reactions. *Chem. Rev.* **2010**, *110*, 1147–1169.

[36]. Labinger, J. A., Platinum-Catalyzed C–H Functionalization. *Chem. Rev.* **2016**, *117*, 8483–8496.

[37]. Watson, P. L., Methane Exchange Reactions of Lanthanide and Early-Transition-Metal Methyl Complexes. *J. Am. Chem. Soc.* **1983**, *105*, 6491–6493.

[38]. Thompson, M. E.; Baxter, S. M.; Bulls, A. R.; Burger, B. J.; Nolan, M. C.; Santarsiero, B. D.; Schaefer, W. P.; Bercaw, J. E., "σ Bond metathesis" for C–H bonds of Hydrocarbons and Sc–R (R= H, Alkyl, Aryl) Bonds of Permethylscandocene Derivatives. Evidence for Noninvolvement of the π System in Electrophilic Activation of Aromatic and Vinylic C–H Bonds. *J. Am. Chem. Soc.* **1987**, *109*, 203–219.

[39]. Perutz, R. N.; Sabo-Etienne, S. J., The σ-CAM Mechanism: σ Complexes as the Basis of σ-Bond Metathesis at Late-Transition-Metal Centers. *Angew. Chem. Int. Ed.* **2007**, *46*, 2578–2592.

[40]. Hoshi, K.; Tahara, A.; Sunada, Y.; Tsutsumi, H.; Inoue, R.; Tanaka, H.; Shiota, Y.; Yoshizawa, K.; Nagashima, H., σ-CAM Mechanisms for the Hydrogenation of Alkenes by *cis*-and *trans*-Disilametallacyclic Carbonyl Complexes (M= Fe, Ru, Os): Experimental and Theoretical Studies. *Bull. Chem. Soc. Jpn.* **2017**, *90*, 613–626.

[41]. Balcells, D.; Clot, E.; Eisenstein, O., C–H Bond Activation in Transition Metal Species from a Computational Perspective. *Chem. Rev.* **2010**, *110*, 749–823.

[42]. Ackermann, L., Carboxylate-Assisted Transition-Metal-Catalyzed C−H Bond Functionalizations: Mechanism and Scope. *Chem. Rev.* **2011**, *111*, 1315–1345.

[43]. Scott, L. T.; DeCicco, G. J., Intermolecular Carbon-Hydrogen Insertion of Copper Carbenoids. *J. Am. Chem. Soc.* **1974**, *96*, 322–323.

[44]. Díaz-Requejo, M. M.; Pérez, P. J., Coinage Metal Catalyzed C−H Bond Functionalization of Hydrocarbons. *Chem. Rev.* **2008**, *108*, 3379–3394.

[45]. Doyle, M. P.; Duffy, R.; Ratnikov, M.; Zhou, L., Catalytic Carbene Insertion into C−H Bonds. *Chem. Rev.* **2009**, *110*, 704–724.

[46]. Sakakura, T.; Tanaka, M., Efficient Catalytic C–H Activation of Alkanes: Regioselective Carbonylation of the Terminal Methyl Group of n-Pentane by $RhCl(CO)(PMe_3)_2$. *J. Chem. Soc., Chem. Commun.* **1987**, *10*, 758–759.

[47]. Waltz, K. M.; Hartwig, J. F., Selective Functionalization of Alkanes by Transition-Metal Boryl Complexes. *Science* **1997**, *277*, 211–213.

[48]. Mkhalid, I. A. I.; Barnard, J. H.; Marder, T. B.; Murphy, J. M.; Hartwig, J. F., C−H Activation for the Construction of C−B Bonds. *Chem. Rev.* **2010**, *110*, 890–931.

[49]. Hartwig, J. F., Regioselectivity of the Borylation of Alkanes and Arenes. *Chem. Soc. Rev.* **2011**, *40*, 1992–2002.

[50]. Astruc, D., C–H Activation and Functionalization of Alkanes and Arenes. *Organometallic Chemistry and Catalysis*, Springer Berlin Heidelberg: Berlin, Heidelberg, 2007, pp 409–429.

[51]. Chen, H.; Schlecht, S.; Semple, T. C.; Hartwig, J. F., Thermal, Catalytic, Regiospecific Functionalization of Alkanes. *Science* **2000**, *287*, 1995–1997.

[52]. Lellmann, E., Ueber die Coniceïne. *Ber. Dtsch. Chem. Ges*. **1890**, *23*, 2141–2142.

[53]. Majetich, G.; Wheless, K., Remote Intramolecular Free Radical Functionalizations: An Update". *Tetrahedron* **1995**, *51*, 7095–7129.

[54]. Thullen, S. M.; Treacy, S. M.; Rovis, T., Regioselective Alkylative Cross-Coupling of Remote Unactivated C(sp3)–H Bonds. *J. Am. Chem. Soc.* **2019**, *141*, 14062−14067.

[55]. Liu, W.; Huang, X.; Cheng, M.-J.; Nielsen, R. J.; Goddard, W. A.; Groves, J. T., Oxidative Aliphatic CH Fluorination with Fluoride Ion Catalyzed by a Manganese Porphyrin. *Science* **2012**, *337*, 1322−1325.

[56]. Liu, W.; Huang, X.; Groves, J. T., Oxidative Aliphatic C–H Fluorination with Manganese Catalysts and Fluoride Ion. *Nat. Protoc.* **2013**, *8*, 2348–2354.

[57]. Xia, G.; Weng, J.; Liu, L.; Verma, P.; Li, Z.; Yu, J.-Q., Reversing Conventional Site-Selectivity in C(sp3)–H Bond Activation. *Nat. Chem.* **2019**, *11*, 571–577.

[58]. Baudoin, O., Ring Construction by Palladium(0)-Catalyzed C(sp^3)–H Activation. *Acc. Chem. Res.* **2017**, *50*, 1114–1123.

[59]. He, J.; Wasa, M.; Chan, K. S. L.; Shao, Q.; Yu, J.-Q., Palladium-Catalyzed Transformations of Alkyl C–H Bonds. *Chem. Rev.* **2017**, *117*, 8754–8786.

[60]. Chen, M. S.; White, M. C., A Predictably Selective Aliphatic C–H Oxidation Reaction for Complex Molecule Synthesis. *Science* **2007**, *318*, 783–787.

[61]. Stang, E. M.; White, M. C., Total synthesis and study of 6-deoxyerythronolide B by late-stage C–H oxidation. *Nat. Chem.* **2009**, *1*, 547–551.

[62]. Chen, M. S.; White, M. C., Combined Effects on Selectivity in Fe-Catalyzed Methylene Oxidation. *Science* **2010**, *327*, 566–571.

[63]. Gormisky, P. E.; White, M. C., Catalyst-Controlled Aliphatic C–H Oxidations with a Predictive Model for Site-Selectivity. *J. Am. Chem. Soc.* **2013**, *135*, 14052–14055.

[64]. Osberger, T. J.; Rogness, D. C.; Kohrt, J. T.; Stepan, A. F.; White, M. C., Oxidative Diversification of Amino Acids and Peptides by Small-Molecule Iron Catalysis. *Nature* **2016**, *537*, 214–219.

[65]. Shono, T.; Kosaka, T., Organic Synthesis by Electrolysis III Anodic Allylic Substitution. *Tetrahedron Lett.* **1968**, *9*, 6207–6208.

[66]. Shono, T.; Ikeda, A., Electroorganic Chemistry X Anodic Allylic Substitution. *J. Am. Chem. Soc.* **1972**, 94, 7892–7898.

[67]. Horn, E. J.; Rosen, B. R.; Chen, Y.; Tang, J.; Chen, K.; Eastgate, M. D.; Baran, P. S., Scalable and Sustainable Electrochemical Allylic C–H Oxidation. *Nature* **2016**, *533*, 77–81.

[68]. Sequeira, C. A. C.; Santos, D. M. F., Electrochemical Routes for Industrial Synthesis. *J. Braz. Chem. Soc.* **2009**, *20*, 387–406.

[69]. Friedel, C.; Crafts, J. M., Sur une nouvelle méthode générale de synthèse d'hydrocarbures, d'acétones, etc. *Compt. Rend.* **1877**, *84*, 1392 & 1450.

[70]. Groves, J. K., The Friedel–Crafts Acylation of Alkenes. *Chem. Soc. Rev.* **1972**, *1*, 73–97.

[71]. Rueping, M.; Nachtsheim, B. J., A Review of New Developments in the Friedel–Crafts Alkylation–From Green Chemistry to Asymmetric Catalysis. *Beilstein J. Org. Chem.* **2010**, *6*, No. 6.

[72]. Fier, P. S.; Hartwig, J. F., Selective C–H Fluorination of Pyridines and Diazines Inspired by a Classic Amination Reaction. *Science* **2013**, *342*, 956–960.

[73]. Murakami, K.; Yamada, S.; Kaneda, T.; Itami, K., C–H Functionalization of Azines. *Chem. Rev.* **2017**, *117*, 9302–9332.

[74]. Charushin, V. N.; Chupakhin, O. N., Nucleophilic C–H Functionalization of Arenes: a Contribution to Green Chemistry. *Russian Chemical Bulletin* **2019**, *68*, 453–471.

[75]. O'Hara, F.; Blackmond, D. G.; Baran, P. S., Radical-Based Regioselective C-H Functionalization of Electron-Deficient Heteroarenes: Scope, Tunability, and Predictability. *J. Am. Chem. Soc.* **2013**, *135*, 12122–12134.

[76]. Yu, J.-T.; Pan, C., Radical C–H Functionalization to Construct Heterocyclic Compounds. *Chem. Commun.* **2016**, *52*, 2220–2236.

[77]. Yi, H.; Zhang, G.; Wang, H.; Huang, Z.; Wang, J.; Singh, A. K.; Lei, A., Recent Advances in Radical C–H Activation/Radical Cross-Coupling. *Chem. Rev.* **2017**, *117*, 9016–9085.

[78]. Kunin, A. J.; Eisenberg, R., Photochemical Carbonylation of Benzene by Iridium(I) and Rhodium(I) Square-Planar Complexes. *Organometallics* **1988**, *7*, 2124–2129.

[79]. Murai, S.; Kakiuchi, F.; Sekine, S.; Tanaka, Y.; Kamatani, A.; Sonoda, M.; Chatani, N., Efficient Catalytic Addition of Aromatic Carbon–Hydrogen Bonds to Olefins. *Nature* **1993**, *366*, 529–531.

[80]. Jiang, Y.-Y.; Man, X.; Bi, S., Advances in Theoretical Study on Transition-Metal-Catalyzed C−H Activation. *Sci. China Chem.* **2016**, *59*, 1448–1466.

[81]. Snieckus, V., Directed Ortho Metalation. Tertiary Amide and O-Carbamate Directors in Synthetic Strategies for Polysubstituted Aromatics. *Chem. Rev.* **1990**, *90*, 879–933.

[82]. Clayden, J., Directed Metallization of Aromatic Compounds. PATAI'S Chemistry of Functional Groups. 2009, John Wiley & Sons, Ltd.

[83]. El-Hiti, G. A.; Smith, K.; Hegazy, A. S.; Masmali, A. M.; Alshammari, M. B., Directed Lithiation of Simple Aromatics and Heterocycles for Synthesis of Substituted Derivatives. *ARKIVOC* **2015**, *4,* 19–47.

[84]. Grzybowski, M.; Skonieczny, K.; Butenschön, H.; Gryko, D. T., Comparison of Oxidative Aromatic Coupling and the Scholl Reaction. *Angew. Chem. Int. Ed.* **2013**, *52*, 9900–9930.

[85]. Zhang, M.; Zhang, Y.; Jie, X.; Zhao, H.; Li, G.; Su, W., Recent Advances in Directed C–H Functionalizations Using Monodentate Nitrogen-Based Directing Groups. *Org. Chem. Front.* **2014**, *1*, 843–895.

[86]. Sambiagio, C.; Schönbauer, D.; Blieck, R.; Dao-Huy, T.; Pototschnig, G.; Schaaf, P.; Wiesinger, T.; Zia, M. F.; Wencel-Delord, J.; Besset, T.; Maes, B. U. W.; Schnürch, M., A Comprehensive Overview of Directing Groups Applied in Metal-Catalysed C–H Functionalisation Chemistry. *Chem. Soc. Rev.* **2018**, *47*, 6603–6743.

[87]. Prakash, G. S.; Mathew, T.; Hoole, D.; Esteves, P. M.; Wang, Q.; Rasul, G.; Olah, G. A., N-Halosuccinimide/BF_3−H_2O, Efficient Electrophilic Halogenating Systems for Aromatics. *J. Am. Chem. Soc.* **2004**, *126*, 15770–15776.

[88]. Börgel, J.; Tanwar, L.; Berger, F.; Ritter, T., Late-Stage Aromatic C–H Oxygenation. *J. Am. Chem. Soc.* **2018**, *140*, 16026–16031.

[89]. Boursalian, G. B.; Ham, W. S.; Mazzotti, A. R.; Ritter, T., Charge-Transfer-Directed Radical Substitution Enables Para-Selective C–H Functionalization. *Nat. Chem.* **2016**, *8*, 810–815.

[90]. Ishiyama, T.; Takagi, J.; Ishida, K.; Miyaura, N.; Anastasi, N. R.; Hartwig, J. F., Mild Iridium-Catalyzed Borylation of Arenes. High Turnover Numbers, Room Temperature Reactions, and Isolation of a Potential Intermediate. *J. Am. Chem. Soc.* **2002**, *124*, 390–391.

[91]. Simmons, E. M.; Hartwig, J. F., On the Interpretation of Deuterium Kinetic Isotope Effects in C–H Bond Functionalizations by Transition-Metal Complexes. *Angew. Chem. Int. Ed.* **2012**, *51*, 3066–3072.

[92]. Larsen, M. A.; Hartwig, J. F., Iridium-Catalyzed C–H Borylation of Heteroarenes: Scope, Regioselectivity, Application to Late-Stage Functionalization, and Mechanism. *J. Am. Chem. Soc.* **2014**, *136*, 4287–4299.

[93]. Wang, X.; Truesdale, L.; Yu, J.-Q., Pd(II)-Catalyzed ortho-Trifluoromethylation of Arenes Using TFA as a Promoter. *J. Am. Chem. Soc.* **2010**, *132*, 3648–3649.

[94]. Nakao, Y.; Yamada, Y.; Kashihara, N.; Hiyama, T., Selective C-4 Alkylation of Pyridine by Nickel/Lewis Acid Catalysis. *J. Am. Chem. Soc.* **2010**, *132*, 13666–13668.

[95]. Zhao, D.; Xu, P.; Ritter, T., Palladium-Catalyzed Late-Stage Direct Arene Cyanation. Chem **2019**, *5*, 97–107.

[96]. Romero, N. A.; Margrey, K. A.; Tay, N. E.; Nicewicz, D. A., Site-Selective Arene C–H Amination via Photoredox Catalysis. *Science* **2015**, *349*, 1326–1330.

[97]. Ham, W. S.; Hillenbrand, J.; Jacq, J.; Genicot, C.; Ritter, T., Divergent Late-Stage (Hetero)aryl C−H Amination by the Pyridinium Radical Cation. *Angew. Chem. Int. Ed.* **2019**, *58*, 532–536.

[98]. Ruffoni, A.; Juliá, F.; Svejstrup, T. D.; McMillan, A. J.; Douglas, J. J.; Leonori, D., Practical and Regioselective Amination of Arenes using Alkyl Amines. *Nat. Chem.* **2019**, *11*, 426–433.

[99]. Gulevich, A. V.; Melkonyan, F. S.; Sarkar, D.; Gevorgyan, V., Double-Fold C–H Oxygenation of Arenes Using PyrDipSi: a General and Efficient Traceless/Modifiable Silicon-Tethered Directing Group. *J. Am. Chem. Soc.* **2012**, *134*, 5528–5531.

[100]. Lian, Z.; Bhawal, B. N.; Yu, P.; Morandi, B., Palladium-Catalyzed Carbon-Sulfur or Carbon-Phosphorus Bond Metathesis by Reversible Arylation. *Science* **2017**, *356*, 1059−1063.

[101]. Yamamoto, K.; Li, J.; Garber, J. A. O.; Rolfes, J. D.; Boursalian, G. B.; Borghs, J. C.; Genicot, C.; Jacq, J.; van Gastel, M.; Neese, F.; Ritter, T., Palladium-Catalysed Electrophilic Aromatic C–H Fluorination. *Nature* **2018**, *554*, 511–514.

[102]. Murai, S.; Kakiuchi, F.; Sekine, S.; Tanaka, Y.; Kamatani, A.; Sonoda, M.; Chatani, N., Efficient Catalytic Addition of Aromatic Carbon-Hydrogen Bonds to Olefins. *Nature* **1993**, *366*, 529–531.

[103]. Matsubara, T.; Koga, N.; Musaev, D. G.; Morokuma, K., Density Functional Study on Activation of *ortho*-CH Bond in Aromatic Ketone by Ru Complex. Role of Unusual Five-Coordinated d^6 Metallacycle Intermediate with Agostic Interaction. *J. Am. Chem. Soc.* **1998**, *120*, 12692–12693.

[104]. Helmstedt, U.; Clot, E., Hydride Ligands make the Difference: Density Functional Study of the Mechanism of the Murai Reaction Catalyzed by $[Ru(H)_2(H_2)_2(PR_3)_2]$(R= cyclohexyl). *Chem. Eur. J.* **2012**, *18*, 11449–11458.

[105]. Guari, Y.; Sabo-Etienne, S.; Chaudret, B., Exchange Couplings between a Hydride and a Stretched Dihydrogen Ligand in Ruthenium Complexes. *J. Am. Chem. Soc.* **1998**, *120*, 4228–4229.

[106]. Kakiuchi, F.; Kochi, T.; Mizushima, E.; Murai, S., Room-Temperature Regioselective C−H/Olefin Coupling of Aromatic Ketones Using an Activated Ruthenium Catalyst with a Carbonyl Ligand and Structural Elucidation of Key Intermediates. *J. Am. Chem. Soc.* **2010**, *132*, 17741–17750.

[107]. Cho, J.-Y.; Tse, M. K.; Holmes, D.; Maleczka, R. E.; Smith, M. R., Remarkably Selective Iridium Catalysts for the Elaboration of Aromatic C–H Bonds. *Science* **2002**, *295*, 305–308.

[108]. Murphy, J. M.; Liao, X.; Hartwig, J. F., Meta Halogenation of 1,3-Disubstituted Arenes via Iridium-Catalyzed Arene Borylation. *J. Am. Chem. Soc.* **2007**, *129*, 15434–15435.

[109]. Phipps, R. J.; Gaunt, M. J., A Meta-Selective Copper-Catalyzed C–H Bond Arylation. *Science* **2009**, *323*, 1593–1597.

[110]. Chen, B.; Hou, X.-L.; Li, Y.-X.; Wu, Y.-D., Mechanistic Understanding of the Unexpected Meta Selectivity in Copper-Catalyzed Anilide C–H Bond Arylation. *J. Am. Chem. Soc.* **2011**, *133*, 7668–7671.

[111]. Leow, D.; Li, G.; Mei, T.-S.; Yu, J.-Q., Activation of Remote *meta*-C–H Bonds Assisted by an End-on Template. *Nature* **2012**, *486*, 518–522.

[112]. Yu, Q.; Hu, L. a.; Wang, Y.; Zheng, S.; Huang, J., Directed *meta*-Selective Bromination of Arenes with Ruthenium Catalysts. *Angew. Chem. Int. Ed.* **2015**, *54*, 15284–15288.

[113]. Teskey, C. J.; Lui, A. Y.; Greaney, M. F., Ruthenium-Catalyzed *meta*-Selective C–H Bromination. *Angew. Chem. Int. Ed.* **2015**, *54*, 11677–11680.

[114]. Dao, H. T.; Li, C.; Michaudel, Q.; Maxwell, B. D.; Baran, P. S., Hydromethylation of unactivated olefins. *J. Am. Chem. Soc.* **2015**, *137*, 8046–8049.

[115]. Chen, C.; Luo, Y.; Fu, L.; Chen, P.; Lan, Y.; Liu, G., Palladium-Catalyzed Intermolecular Ditrifluoromethoxylation of Unactivated Alkenes: CF_3O-Palladation Initiated by Pd(IV). *J. Am. Chem. Soc.* **2018**, *140*, 1207–1210.

[116]. Guo, S.; Cong, F.; Guo, R.; Wang, L.; Tang, P., Asymmetric Silver-Catalysed Intermolecular Bromotrifluoromethoxylation of Alkenes with a New Trifluoromethoxylation Reagent. *Nat. Chem.* **2017**, *9*, 546–551.

[117]. McDonald, R. I.; Liu, G.; Stahl, S. S., Palladium(II)-Catalyzed Alkene Functionalization via Nucleopalladation: Stereochemical Pathways and Enantioselective Catalytic Applications. *Chem. Rev.* **2011**, *111*, 2981–3019.

[118]. Robert, J. D.; Caserio, M. C., *Basic Principles of Organic Chemistry.* 2nd Ed., W. A. Benjamin, Inc.: Menlo Park, CA, 1977; Chapter 10; Chapter 22.

[119]. Bischler, A.; Napieralski, B., Zur Kenntniss einer neuen Isochinolinsynthese. *Ber.* **1893***, 26*, 1903–1908.

[120]. Schnider, O.; Hellerbach, J., Synthese von Morphinanen. (2. Mitteilung). *Helv. Chim. Acta* **1950**, *33***,** 1437–1448.

[121]. Sugasawa, S.; Ushioda, S., Extension of the Bischler-Napieralski reaction–II synthesis of pyrroline derivatives. *Tetrahedron* **1959**, *5*, 48–52

[122]. Huang, P.-Q.; Huang, Y.-H.; Geng, H.; Ye, J.-L., Metal-Free C–H Alkyliminylation and Acylation of Alkenes with Secondary Amides. *Sci. Rep.* **2016**, *6*, 1–10.

[123]. Maraswami, M.; Loh, T.-P., Transition-Metal-Catalyzed Alkenyl sp2 C–H Activation: A Short Account. *Synthesis* **2019,** *51*, 1049–1062.

[124]. Guan, Z.; Cotts, P. M.; McCord, E. F.; McLain, S. J., Chain Walking: A New Strategy to Control Polymer Topology. *Science* **1999**, *283*, 2059–2062.

[125]. Guo, L.; Dai, S.; Sui, X.; Chen, C., Palladium and Nickel Catalyzed Chain Walking Olefin Polymerization and Copolymerization. *ACS Catal.* **2016**, *6*, 428–441.

[126]. McAtee, J. R.; Martin, S. E. S.; Ahneman, D. T.; Johnson, K. A.; Watson, D. A., Preparation of Allyl and Vinyl Silanes by the Palladium-Catalyzed Silylation of Terminal Olefins: A Silyl-Heck Reaction. *Angew. Chem. Int. Ed.* **2012**, *51*, 3663–3667.

[127]. Martin, S. E. S.; Watson, D. A., Preparation of Vinyl Silyl Ethers and Disiloxanes via the Silyl-Heck Reaction of Silyl Ditriflates. *J. Am. Chem. Soc.* **2013**, *135*, 13330–13333.

[128]. Morimoto, M.; Miura, T.; Murakami, M., Rhodium-Catalyzed Dehydrogenative Borylation of Aliphatic Terminal Alkenes with Pinacolborane. *Angew. Chem. Int. Ed.* **2015**, *54*, 12659–12663.

[129]. Reid, W. B.; Spillane, J. J.; Krause, S. B.; Watson, D. A., Direct Synthesis of Alkenyl Boronic Esters From Unfunctionalized Alkenes: A Boryl-Heck Reaction. *J. Am. Chem. Soc.* **2016**, *138*, 5539–5542.

[130]. Teruaki, M.; Eiichiro, H.; Tohru, Y., Convenient and Simple Preparation of Nitroolefins Nitration of Olefins with Nitric Oxide. *Chem. Lett.* **1995**, *24*, 505–506.

[131]. Maity, S.; Manna, S.; Rana, S.; Naveen, T.; Mallick, A.; Maiti, D., Efficient and Stereoselective Nitration of Mono- and Disubstituted Olefins with $AgNO_2$ and TEMPO. *J. Am. Chem. Soc.* **2013**, *135*, 3355–3358.

[132]. Gao, D.-W.; Vinogradova, E. V.; Nimmagadda, S. K.; Medina, J. M.; Xiao, Y.; Suciu, R. M.; Cravatt, B. F.; Engle, K. M., Direct Access to Versatile Electrophiles via Catalytic Oxidative Cyanation of Alkenes. *J. Am. Chem. Soc.* **2018**, *140*, 8069–8073.

[133]. Aukland, M. H.; Talbot, F. J. T.; Fernández-Salas, J. A.; Ball, M.; Pulis, A. P.; Procter, D. J., An Interrupted Pummerer/Nickel-Catalysed Cross-Coupling Sequence. *Angew. Chem. Int. Ed.* **2018**, *57*, 9785–9789.

[134]. Schreib, B. S.; Carreira, E. M., Palladium-Catalyzed Regioselective C–H Iodination of Unactivated Alkenes. *J. Am. Chem. Soc.* **2019**, *141*, 8758–8763.

[135]. Yu, D.-G.; Li, B.-J.; Shi, Z.-J., Exploration of New C−O Electrophiles in Cross-Coupling Reactions. *Acc. Chem. Res.* **2010**, *43*, 1486–1495.

[136]. Amal Joseph, P. J.; Priyadarshini, S., Copper-Mediated C–X Functionalization of Aryl Halides. *Org. Process Res. Dev.* **2017**, *21*, 1889–1924.

[137]. Hayashi, S.; Yorimitsu, H.; Oshima, K., Synthesis of Aziridines by Palladium-Catalyzed Reactions of Allylamines with Aryl and Alkenyl Halides: Evidence of a syn–Carboamination Pathway. *Angew. Chem. Int. Ed.* **2009**, *48*, 7224–7226.

[138]. Rosen, B. R.; Ney, J. E.; Wolfe, J. P., Use of Aryl Chlorides as Electrophiles in Pd-Catalyzed Alkene Difunctionalization Reactions. *J. Org. Chem.* **2010**, *75*, 2756–2759.

[139]. Green, R. A.; Hartwig, J. F., Nickel‐Catalyzed Amination of Aryl Chlorides with Ammonia or Ammonium Salts. *Angew. Chem. Int. Ed.* **2015**, *54*, 3768–3772.

[140]. Liu, X.-W.; Echavarren, J.; Zarate, C.; Martin, R., Ni-Catalyzed Borylation of Aryl Fluorides via C–F Cleavage. *J. Am. Chem. Soc.* **2015**, *137*, 12470–12473.

[141]. Niwa, T.; Ochiai, H.; Watanabe, Y.; Hosoya, T., Ni/Cu-Catalyzed Defluoroborylation of Fluoroarenes for Diverse C–F Bond Functionalizations. *J. Am. Chem. Soc.* **2015**, *137*, 14313–14318.

[142]. Lim, S.; Song, D.; Jeon, S.; Kim, Y.; Kim, H.; Lee, S.; Cho, H.; Lee, B. C.; Kim, S. E.; Kim, K.; Lee, E., Cobalt-Catalyzed C–F Bond Borylation of Aryl Fluorides. *Org. Lett.* **2018**, *20*, 7249–7252.

[143]. van der Boom, M. E.; Liou, S.-Y.; Ben-David, Y.; Shimon, L. J. W.; Milstein, D., Alkyl− and Aryl−Oxygen Bond Activation in Solution by Rhodium(I), Palladium(II), and Nickel(II). Transition-Metal-Based Selectivity. *J. Am. Chem. Soc.* **1998**, *120*, 6531–6541.

[144]. Sergeev, A. G.; Hartwig, J. F., Selective, Nickel-Catalyzed Hydrogenolysis of Aryl Ethers. *Science* **2011**, *332*, 439−443.

[145]. Wang, L.; Chen, H.; Duan, Z., Synthetic Applications of Transition-Metal-Catalyzed C−P Bond Cleavage. *Chem. Asian J.* **2018**, *13*, 2164−2173.

[146]. Fujimoto, H.; Kusano, M.; Kodama, T.; Tobisu, M., Cyclization of Bisphosphines to Phosphacycles via the Cleavage of Two Carbon–Phosphorus Bonds by Nickel Catalysis. *Org. Lett.* **2019**, *21*, 4177−4181

[147]. Lüdersdorf, R.; Khait, I.; Muszkat, K. A.; Praefcke, K.; Margaretha, P., Photochemica CS Bond Cleavage in Methyl Aryl Sulfides and Sulfoxides. A CIDNP Studey of Reactivity Enhancement by Methylthio Gr. *Phosphorus and Sulfur* **1981**, *12*, 37−54.

[148]. Luo, Y-R., Handbook of Bond Dissociation Energy in Organic Compounds. CRC Press, Taylor & Francis group, 2002.

[149]. Serpier, F.; Pan, F.; Ham, W. S.; Jacq, J.; Genicot, C.; Ritter, T., Selective Methylation of Arenes: A Radical C−H Functionalization/Cross-Coupling Sequence. *Angew. Chem. Int. Ed.* **2018**, *130*, 10857−10861.

[150]. Berger, F.; Plutschack, M. B.; Riegger, J.; Yu, W.; Speicher, S.; Ho, M.; Frank, N.; Ritter, T., Site-Selective and Versatile Aromatic C−H Functionalization by Thianthrenation. *Nature* **2019**, *567*, 223–228.

[151]. Sambiagio, C.; Schönbauer, D.; Blieck, R.; Dao-Huy, T.; Pototschnig, G.; Schaaf, P.; Wiesinger, T.; Zia, M. F.; Wencel-Delord, J.; Besset, T.; Maes, B. U. W.; Schnürch, M., A Comprehensive Overview of Directing Groups Applied in Metal-Catalysed C–H Functionalisation Chemistry. *Chem. Soc. Rev.* **2018**, *47*, 6603–6743.

[152]. Truong, T.; Klimovica, K.; Daugulis, O., Copper-Catalyzed, Directing Group-Assisted Fluorination of Arene and Heteroarene C–H Bonds. *J. Am. Chem. Soc.* **2013**, *135*, 9342–9345.

[153]. Sun, X.; Shan, G.; Sun, Y.; Rao, Y., Regio- and Chemoselective C–H Chlorination/Bromination of Electron-Deficient Arenes by Weak Coordination and Study of Relative Directing-Group Abilities. *Angew. Chem. Int. Ed.* **2013**, *52*, 4440–4444.

[154]. Mfuh, A. M.; Doyle, J. D.; Chhetri, B.; Arman, H. D.; Larionov, O. V., Scalable, Metal- and Additive-Free, Photoinduced Borylation of Haloarenes and Quaternary Arylammonium Salts. *J. Am. Chem. Soc.* **2016**, *138*, 2985–2988.

[155]. Roglans, A.; Pla-Quintana, A.; Moreno-Mañas, M., Diazonium Salts as Substrates in Palladium-Catalyzed Cross-Coupling Reactions. *Chem. Rev.* **2006**, *106*, 4622–4643.

[156]. Dreher, E. L.; Torkelson, T. R.; Beutel, K. K., "Chlorethanes and Chloroethylenes" in Ullmann's Encyclopedia of Industrial Chemistry. Wiley-VCH, Weinheim. 2011.

[157]. Morrison, R. T; Boyd R. N. *Organic Chemistry*; 6th Ed.; Prentice Hall, Inc.: Englewood Cliffs, NJ, 1992, pp 287–310.

[158]. Morrill, C.; Grubbs, R. H., Synthesis of Functionalized Vinyl Boronates via Ruthenium-Catalyzed Olefin Cross-Metathesis and Subsequent Conversion to Vinyl Halides. *J. Org. Chem.* **2003**, *68*, 6031–6034.

[159]. Pawluć, P.; Hreczycho, G.; Szudkowska, J.; Kubicki, M.; Marciniec, B., New One-Pot Synthesis of (*E*)-β-Aryl Vinyl Halides from Styrenes. *Org. Lett.* **2009**, *11*, 3390–3393.

[160]. Takai, K.; Nitta, K.; Utimoto, K., Simple and Selective Method for RCHO→RCH=CHX Conversion by Means of a CHX_3–$CrCl_2$ System. *J. Am. Chem. Soc.* **1986**, *108*, 7408–7410.

[161]. Stork, G.; Zhao, K., A Stereoselective Synthesis of (*Z*)-1-Iodo-1-Alkenes. *Tetrahedron Lett.* **1989**, *30*, 2173–2174.

[162]. Lebrun, M.-E.; Le Marquand, P.; Berthelette, C., Stereoselective Synthesis of *Z* Alkenyl Halides via Julia Olefination. *J. Org. Chem.* **2006**, *71*, 2009–2013.

[163]. Bertleff, W.; Roeper, M. and Sava, X., Carbonylation. in *Ullmann's Encyclopedia of Industrial Chemistry*, 2003, Wiley-VCH: Weinheim.

[164]. Ratcliffe, R. W., Oxidation with the Chromium Trioxide-Pyridine Complex Prepared in situ: 1-Decanal. *Organic Syntheses* **1988**, *6*, pp 373.

[165]. Gao, F.; Hoveyda, A. H., α-Selective Ni-Catalyzed Hydroalumination of Aryl- and Alkyl-Substituted Terminal Alkynes: Practical Syntheses of Internal Vinyl Aluminums, Halides, or Boronates. *J. Am. Chem. Soc.* **2010**, *132*, 10961–10963.

[166]. Suess, A. M.; Lalic, G., Copper-Catalyzed Hydrofunctionalization of Alkynes. *Synlett* **2016**, *27*, 1165–1174.

[167]. Keitz, B. K.; Endo, K.; Herbert, M. B.; Grubbs, R. H., Z-Selective Homodimerization of Terminal Olefins with a Tuthenium Metathesis Catalyst. *J. Am. Chem. Soc.* **2011**, *133*, 9686–9688.

[168]. Ogba, O. M.; Warner, N. C.; O'Leary, D. J.; Grubbs, R. H., Recent Advances in Ruthenium-Based Olefin Metathesis. *Chem. Soc. Rev.* **2018**, *47*, 4510–4544.

[169]. Schrock, R. R., High-Oxidation-State Molybdenum and Tungsten Alkylidyne Complexes. *Acc. Chem. Res.* **1986**, *19*, 342–348.

[170]. Schrock, R. R.; Hoveyda, A. H., Molybdenum and Tungsten Imido Alkylidene Complexes as Efficient Olefin-Metathesis Catalysts. *Angew. Chem. Int. Ed.* **2003**, *42*, 4592–4633.

[171]. Ibrahem, I.; Yu, M.; Schrock, R. R.; Hoveyda, A. H., Highly Z- and Enantioselective Ring-Opening/Cross-Metathesis Reactions Catalyzed by Stereogenic-at-Mo Adamantylimido Complexes. *J. Am. Chem. Soc.* **2009**, *131*, 3844–3845.

[172]. Koh, M. J.; Nguyen, T. T.; Zhang, H.; Schrock, R. R.; Hoveyda, A. H., Direct Synthesis of Z-Alkenyl Halides through Catalytic Cross-Metathesis. *Nature* **2016**, *531*, 459–465.

[173]. Nguyen, T. T.; Koh, M. J.; Shen, X.; Romiti, F.; Schrock, R. R.; Hoveyda, A. H., Kinetically Controlled *E*-Selective Catalytic Olefin Metathesis. *Science* **2016**, *352*, 569–575.

[174]. Tamura, M.; Kochi, J. K., Vinylation of Grignard Reagents. Catalysis by Iron. *J. Am. Chem. Soc.* **1971**, *93*, 1487–1489.

[175]. Molander, G. A.; Rahn, B. J.; Shubert, D. C.; Bonde, S. E., Iron Catalyzed Cross-Coupling Reactions. Synthesis of Arylethenes. *Tetrahedron Lett.* **1983**, *24*, 5449–5452.

[176]. Gärtner, D.; Stein, A. L.; Grupe, S.; Arp, J.; Jacobi von Wangelin, A., Iron-Catalyzed Cross-Coupling of Alkenyl Acetates. *Angew. Chem. Int. Ed.* **2015**, *54*, 10545–10549.

[177]. Hansen, A. L.; Ebran, J. P.; Ahlquist, M.; Norrby, P. O.; Skrydstrup, T. J., Heck Coupling with Nonactivated Alkenyl Tosylates and Phosphates: Examples of Effective 1, 2-Migrations of the Alkenyl Palladium (II) Intermediates. *Angew. Chem. Int. Ed.* **2006,** *45*, 3349–3353.

[178]. Hansen, A. L.; Ebran, J.-P.; Gøgsig, T. M.; Skrydstrup, T., Investigations on the Suzuki−Miyaura and Negishi Couplings with Alkenyl Phosphates: Application to the Synthesis of 1,1-Disubstituted Alkenes. *J. Org. Chem.* **2007**, *72*, 6464–6472.

[179]. Xu, L.; Li, B.-J.; Wu, Z.-H.; Lu, X.-Y.; Guan, B.-T.; Wang, B.-Q.; Zhao, K.-Q.; Shi, Z.-J., Nickel-Catalyzed Efficient and Practical Suzuki-Miyaura Coupling of Alkenyl and Aryl Carbamates with Aryl Boroxines. *Org. Lett*. **2010**, *12*, 884–887.

[180]. Iwasaki, T.; Miyata, Y.; Akimoto, R.; Fujii, Y.; Kuniyasu, H.; Kambe, N., Diarylrhodates as Promising Active Catalysts for the Arylation of Vinyl Ethers with Grignard Reagents. *J. Am. Chem. Soc.* **2014**, *136*, 9260–9263.

[181]. Yu, D.-G.; Li, B.-J.; Shi, Z.-J., Exploration of New C−O Electrophiles in Cross-Coupling Reactions. *Acc. Chem. Res.* **2010**, *43*, 1486–1495.

[182]. Itami, K.; Higashi, S.; Mineno, M.; Yoshida, J.-i., Iron-Catalyzed Cross-Coupling of Alkenyl Sulfides with Grignard Reagents. *Org. Lett.* **2005**, *7*, 1219–1222.

[183]. Chen, J.; Chen, S.; Xu, X.; Tang, Z.; Au, C.-T.; Qiu, R. Nickel-Catalyzed Regioselective Cleavage of Csp^2−S Bonds: Method for the Synthesis of Tri- and Tetrasubstituted Alkenes. *J. Org. Chem.* **2016**, 81, 3246−3255.

[184]. Dubbaka, S. R.; Vogel, P., Organosulfur Compounds: Electrophilic Reagents in Transition-Metal-Catalyzed Carbon–Carbon Bond-Forming Reactions. *Angew. Chem. Int. Ed.* **2005**, *44*, 7674–7684.

[185]. Dominguez, E.; Guo, D.; Mader, M. M.; Nguyen, A.-Q. H.; Del Prado, M. F.; Richett, M. E.; Rodriguez, M. J.; Yip, Y. Y. M.; Yu, K.-L. Preparation of 1,2-

Dihydropyridinylmethyl-6,7-dihydrothieno[3,2-c]pyridin-4(5*H*)-one Compounds as EZH2 Inhibitors for Treatment of Cancer. WO2017035060A1, **2017**.

[186]. Ishitobi, K.; Muto, K.; Yamaguchi, J., Pd-Catalyzed Alkenyl Thioether Synthesis from Thioesters and N-Tosylhydrazones. *ACS Catalysis* **2019**, *9*, 11685–11690.

[187]. Kondoh, A.; Takami, K.; Yorimitsu, H.; Oshima, K., Stereoselective Hydrothiolation of Alkynes Catalyzed by Cesium Base: Facile Access to (Z)-1-Alkenyl Sulfides. *J. Org. Chem.* **2005**, *70*, 6468−6473.

[188]. Li, J.; Chen, J.; Sang, R.; Ham, W.-S.; Plutschack, M. B.; Berger, F.; Chabbra, S.; Schnegg, A.; Genicot, C.; Ritter, T., Photoredox Catalysis with Aryl Sulfonium Salts enables Site-Selective Late-Stage Fluorination. *Nat. Chem.* **2019**, *12*, 56–62.

[189]. Engl, P. S.; Häring, A. P.; Berger, F.; Berger, G.; Pérez-Bitrián, A.; Ritter, T., C–N Cross-Couplings for Site-Selective Late-Stage Diversification via Aryl Sulfonium Salts. *J. Am. Chem. Soc.* **2019**, *141*, 13346–13351.

[190]. Sang, R.; Korkis, S. E.; Su, W.; Ye, F.; Engl, P. S.; Berger, F.; Ritter, T., *Angew. Chem. Int. Ed.* **2019**, *58*, 16161–16166.

[191]. Ye, F.; Berger, F.; Jia, H.; Ford, J.; Wortman, A.; Börgel, J.; Genicot, C.; Ritter, T., Aryl Sulfonium Salts for Site-Selective Late-Stage Trifluoromethylation. *Angew. Chem. Int. Ed.* **2019**, *58*, 14615–14619.

[192]. Chen, J.; Li, J.; Plutschack, M. B.; Berger, F.; Ritter, T., Regio- and Stereoselective Thianthrenation of Olefins to Access Versatile Alkenyl Electrophiles. *Angew. Chem. Int. Ed.* **2020**, *132*, 5665–5669.

[193]. Alunni, S.; De Angelis, F.; Ottavi, L.; Papavasileiou, M.; Tarantelli, F., Evidence of a Borderline Region between E1cb and E2 Elimination Reaction Mechanisms: A Combined Experimental and Theoretical Study of Systems Activated by the Pyridine Ring. *J. Am. Chem. Soc.* **2005**, *127*, 15151–15160.

[194]. Smith, M., *March's Advanced Organic Chemistry Reactions, Mechanisms, and Structure* 6th Ed., Hoboken, N.J.: Wiley-Interscience, 2007, pp 1488–1493.

[195]. Pluta, R.; Nikolaienko, P.; Rueping, M., Direct Catalytic Trifluoromethylthiolation of Boronic Acids and Alkynes Employing Electrophilic

Shelf-Stable N-(trifluoromethylthio)phthalimide. *Angew. Chem. Int. Ed.* **2014**, *53*, 1650–1653.

[196]. Murahashi, S.; Yamamura, M.; Yanagisawa, K.; Mita, N.; Kondo, K., Stereoselective Synthesis of Alkenes and Alkenyl Sulfides from Alkenyl Halides using Palladium and Ruthenium Catalysts. *J. Org. Chem.* **1979**, *44*, 2408–2417.

[197]. Hansen, S. V. F.; Christiansen, E.; Urban, C.; Hudson, B. D.; Stocker, C. J.; Due-Hansen, M. E.; Wargent, E. T.; Shimpukade, B.; Almeida, R.; Ejsing, C. S.; Cawthorne, M. A.; Kassack, M. U.; Milligan, G.; Ulven, T., Discovery of a Potent Free Fatty Acid 1 Receptor Agonist with Low Lipophilicity, Low Polar Surface Area, and Robust in Vivo Efficacy. *J. Med. Chem.* **2016**, *59*, 2841–2846.

[198]. Goumans, T. P. M.; van Alem, K.; Lodder, G., Photochemical Generation and Structure of Vinyl Radicals. *Eur. J. Org. Chem.* **2008**, *2008*, 435–443.

[199]. Haufe, G.; Leroux, F., *Fluorine in Life Sciences: Pharmaceuticals, Medicinal Diagnostics, and Agrochemicals: Progress in Fluorine Science Series*. Academic Press, 2018.

[200]. Gouverneur, V., *Fluorine in Pharmaceutical and Medicinal Chemistry: from biophysical aspects to clinical applications. 1st ed*., Imperial College Press, London: 2012.

[201]. Meanwell, N. A., Fluorine and Fluorinated Motifs in the Design and Application of Bioisosteres for Drug Design. *J. Med. Chem.* **2018**, *61*, 5822–5880.

[202]. Jagodzinska, M.; Huguenot, F.; Candiani, G.; Zanda, M., Assessing the Bioisosterism of the Trifluoromethyl Group with a Protease Probe. *ChemMedChem* **2009**, *4*, 49–51.

[203]. Agrawal, A.; Romero‐Perez, D.; Jacobsen, J. A.; Villarreal, F. J.; Cohen, S. M., Zinc-Binding Groups Modulate Selective Inhibition of MMPs. *ChemMedChem* **2008**, *3*, 812–820.

[204]. van Heek, M.; France, C. F.; Compton, D. S.; Mcleod, R. L.; Yumibe, N. P.; Alton, K. B.; Sybertz, E. J.; Davis, H. R.; Therapeutics, E., In Vivo Metabolism-Based Discovery of a Potent Cholesterol Absorption Inhibitor, SCH58235, in the

Rat and Rhesus Monkey through the Identification of the Active Metabolites of SCH48461. *J. Pharmacol. Exp. Ther*. **1997**, *283*, 157–163.

[205]. Clader, J. W., The Discovery of Ezetimibe: A View from Outside the Receptor. *J. Med. Chem.* **2004**, *47*, 1–9.

[206]. Mei, H.; Han, J.; Fustero, S.; Medio-Simon, M.; Sedgwick, D. M.; Santi, C.; Ruzziconi, R.; Soloshonok, V. A., Fluorine-Containing Drugs Approved by the FDA in 2018. *Chem. Eur.J.* **2019**, *25*, 11797–11819.

[207]. Fowler J. S.; Wolf A. P., The Synthesis of Carbon-11, Fluorine-18 and Nitrogen-13 Labeled Radiotracers for Biomedical Applications. Nucl. Sci. Ser. Natl Acad. Sci. Natl Res. Council Monogr. 1982.

[208]. Ametamey, S. M.; Honer, M.; Schubiger, P. A., Molecular Imaging with PET. *Chem. Rev.* **2008**, *108*, 1501–1516.

[209]. Sandford, G., Elemental Fluorine in Organic Chemistry (1997–2006). *J. Fluor. Chem.* **2007**, *128*, 90–104.

[210]. Balz, G.; Schiemann, G., Ueber aromatische fluorverbindungen, I.: Ein neues verfahren zu ihrer darstellung. *Ber. Dtsch. Chem. Ges.* **1927**, *60*, 1186–1190.

[211]. Finger, G. C.; Kruse, C. W., Aromatic Fluorine Compounds. VII. Replacement of Aromatic–Cl and –NO_2 groups by –F. *J. Am. Chem. Soc.* **1956**, *78*, 6034–6037.

[212]. Subramanian, M. A.; Manzer, L. E., A "Greener" Synthetic Route for Fluoroaromatics via Copper(II) Fluoride. *Science* **2002**, *297*, 1665–1665.

[213]. Coenen, H., Fluorine-18 Labeling Methods: Features and Possibilities of Basic Reactions. In *PET chemistry*, Springer: 2007; pp 15–50.

[214]. Grushin, V. V., Palladium Fluoride Complexes: One More Step toward Metal-Mediated C−F Bond Formation. *Chem. Eur. J.* **2002**, *8*, 1006–1014.

[215]. Fraser, S. L.; Antipin, M. Y.; Khroustalyov, V. N.; Grushin, V. V., Molecular Fluoro Palladium Complexes. *J. Am. Chem. Soc.* **1997**, *119*, 4769–4770.

[216]. Hull, K. L.; Anani, W. Q.; Sanford, M. S., Palladium-Catalyzed Fluorination of Carbon−Hydrogen Bonds. *J. Am. Chem. Soc.* **2006**, *128*, 7134–7135.

[217]. Tang, P.; Furuya, T.; Ritter, T., Silver-Catalyzed Late-Stage Fluorination. *J. Am. Chem. Soc.* **2010**, *132*, 12150–12154.

[218]. Watson, D. A.; Su, M.; Teverovskiy, G.; Zhang, Y.; Garcia-Fortanet, J.; Kinzel, T.; Buchwald, S. L., Formation of ArF from LPdAr(F): Catalytic Conversion of Aryl Triflates to Aryl Fluorides. *Science* **2009**, *325*, 1661–1664.

[219]. Hartwig, J. F., Carbon−Heteroatom Bond-Forming Reductive Eliminations of Amines, Ethers, and Sulfides. *Acc. Chem. Res.* **1998**, *31*, 852–860.

[220]. Furuya, T.; Kamlet, A. S.; Ritter, T., Catalysis for Fluorination and Trifluoromethylation. *Nature* **2011**, *473*, 470–477.

[221]. Hartwig, J. F., Electronic Effects on Reductive Elimination To Form Carbon−Carbon and Carbon−Heteroatom Bonds from Palladium(II) Complexes. *Inorg. Chem.* **2007**, *46*, 1936−1947.

[222]. Clark, J. H., Fluoride Ion as a Base in Organic Synthesis. *Chem. Rev.* **1980**, *80*, 429–452.

[223]. Maimone, T. J.; Milner, P. J.; Kinzel, T.; Zhang, Y.; Takase, M. K.; Buchwald, S. L., Evidence for in situ Catalyst Modification during the Pd-Catalyzed Conversion of Aryl Triflates to Aryl Fluorides. *J. Am. Chem. Soc.* **2011**, *133*, 18106–18109.

[224]. Sather, A. C.; Lee, H. G.; De La Rosa, V. Y.; Yang, Y.; Muller, P.; Buchwald, S. L., A Fluorinated Ligand Enables Room-Temperature and Regioselective Pd-Catalyzed Fluorination of Aryl Triflates and Bromides. *J. Am. Chem. Soc.* **2015**, *137*, 13433–13438.

[225]. Furuya, T.; Kaiser, H. M.; Ritter, T., Palladium-Mediated Fluorination of Arylboronic Acids. *Angew. Chem. Int. Ed.* **2008**, *47*, 5993–5996.

[226]. Furuya, T.; Ritter, T., Fluorination of Boronic Acids Mediated by Silver(I) Triflate. *Org. Lett.* **2009**, *11*, 2860–2863.

[227]. Ye, Y.; Sanford, M. S., Mild Copper-Mediated Fluorination of Aryl Stannanes and Aryl Trifluoroborates. *J. Am. Chem. Soc.* **2013**, *135*, 4648–4651.

[228]. Ye, Y.; Schimler, S. D.; Hanley, P. S.; Sanford, M. S., $Cu(OTf)_2$-Mediated Fluorination of Aryltrifluoroborates with Potassium Fluoride. *J. Am. Chem. Soc.* **2013**, *135*, 16292–16295.

[229]. Matthew, T.; M., P. S.; J., T. N.; Stefan, G.; Mickael, H.; Jan, P.; Joël, M.; Christophe, G.; Véronique, G., A General Copper-Mediated Nucleophilic ^{18}F Fluorination of Arenes. *Angew. Chem. Int. Ed.* **2014**, *126*, 7885–7889.

[230]. Mazzotti, A. R.; Campbell, M. G.; Tang, P.; Murphy, J. M.; Ritter, T., Palladium(III)-Catalyzed Fluorination of Arylboronic Acid Derivatives. *J. Am. Chem. Soc.* **2013**, *135*, 14012–14015.

[231]. Lee, E.; Kamlet, A. S.; Powers, D. C.; Neumann, C. N.; Boursalian, G. B.; Furuya, T.; Choi, D. C.; Hooker, J. M.; Ritter, T., A Fluoride-Derived Electrophilic Late-Stage Fluorination Reagent for PET Imaging. *Science* **2011**, *334*, 639–642.

[232]. Lee, E.; Hooker, J. M.; Ritter, T., Nickel-Mediated Oxidative Fluorination for PET with Aqueous [^{18}F] Fluoride. *J. Am. Chem. Soc.* **2012**, *134*, 17456–17458.

[233]. Hoover, A. J.; Lazari, M.; Ren, H.; Narayanam, M. K.; Murphy, J. M.; van Dam, R. M.; Hooker, J. M.; Ritter, T., A Transmetalation Reaction Enables the Synthesis of [^{18}F]5-Fluorouracil from [^{18}F]Fluoride for Human PET Imaging. *Organometallics* **2016**, *35*, 1008–1014.

[234]. Tang, P.; Wang, W.; Ritter, T., Deoxyfluorination of Phenols. *J. Am. Chem. Soc.* **2011**, *133*, 11482–11484.

[235]. Sladojevich, F.; Arlow, S. I.; Tang, P.; Ritter, T., Late-Stage Deoxyfluorination of Alcohols with PhenoFluor. *J. Am. Chem. Soc.* **2013**, *135*, 2470–2473.

[236]. Fujimoto, T.; Ritter, T., PhenoFluorMix: Practical Chemoselective Deoxyfluorination of Phenols. *Org. Lett.* **2015**, *17*, 544–547.

[237]. Goldberg, N. W.; Shen, X.; Li, J.; Ritter, T., AlkylFluor: Deoxyfluorination of Alcohols. *Org. Lett.* **2016**, *18*, 6102–6104.

[238]. Neumann, C. N.; Hooker, J. M.; Ritter, T., Concerted Nucleophilic Aromatic Substitution with $^{19}F^-$ and $^{18}F^-$. *Nature* **2016**, *534*, 369–373.

[239]. Schimler, S. D.; Cismesia, M. A.; Hanley, P. S.; Froese, R. D. J.; Jansma, M. J.; Bland, D. C.; Sanford, M. S., Nucleophilic Deoxyfluorination of Phenols via Aryl Fluorosulfonate Intermediates. *J. Am. Chem. Soc.* **2017**, *139*, 1452–1455.

[240]. Fier, P. S.; Hartwig, J. F., Selective C–H Fluorination of Pyridines and Diazines Inspired by a Classic Amination Reaction. *Science* **2013**, *342*, 956–960.

[241]. Yoon, T. P.; Ischay, M. A.; Du, J., Visible Light Photocatalysis as a Greener Approach to Photochemical Synthesis. *Nat. Chem.* **2010**, *2*, 527–532.

[242]. Prier, C. K.; Rankic, D. A.; MacMillan, D. W., Visible Light Photoredox Catalysis with Transition Metal Complexes: Applications in Organic Synthesis. *Chem. Rev.* **2013**, *113*, 5322–5363.

[243]. Marzo, L.; Pagire, S. K.; Reiser, O.; König, B., Visible-Light Photocatalysis: Does It Make a Difference in Organic Synthesis? *Angew. Chem. Int. Ed.* **2018**, *57*, 10034–10072.

[244]. Alexander, E., Action of Light on Pigments I. *Chem-ZTG.* **1991**, *35*, 753–755.

[245]. Bogdos, M. K.; Pinard, E.; Murphy, J. A., Applications of Organocatalysed Visible-Light Photoredox Reactions for Medicinal Chemistry. *Beilstein J. Org. Chem.* **2018**, *14*, 2035–2064.

[246]. Atkins, P. W.; Friedman, R. S. Molecular Quantum Mechanics. Oxford University Press, Oxford, 2001.

[247]. Gilbert, A.; Baggot, J. Essentials of Molecular Photochemistry. Blackwell Science, Oxford, 1991.

[248]. Zhao, Q.; Liu, S.; Shi, M.; Wang, C.; Yu, M.; Li, L.; Li, F.; Yi, T.; Huang, C., Series of New Cationic Iridium(III) Complexes with Tunable Emission Wavelength and Excited State Properties: Structures, Theoretical Calculations, and Photophysical and Electrochemical Properties. *Inorg. Chem.* **2006**, *45*, 6152–6160.

[249]. Wu, S.-H.; Ling, J.-W.; Lai, S.-H.; Huang, M.-J.; Cheng, C. H.; Chen, I.-C., Dynamics of the Excited States of $[Ir(ppy)_2bpy]^+$ with Triple Phosphorescence. *J. Phys. Chem. A* **2010**, *114*, 10339–10344.

[250]. Wang, C.; Lystrom, L.; Yin, H.; Hetu, M.; Kilina, S.; McFarland, S. A.; Sun, W., Increasing the Triplet Lifetime and Extending the Ground-State Absorption of Biscyclometalated Ir(III) Complexes for Reverse Saturable Absorption and Photodynamic Therapy Applications. *Dalton Trans.* **2016**, *45*, 16366–16378.

[251]. Pac, C.; Ihama, M.; Yasuda, M.; Miyauchi, Y.; Sakurai, H., Tris (2, 2'-bipyridine) ruthenium (2+)-mediated photoreduction of olefins with 1-benzyl-1, 4-dihydronicotinamide: a mechanistic probe for electron-transfer reactions of NAD (P) H-model compounds. *J. Am. Chem. Soc.* **1981**, *103*, 6495–6497.

[252]. Cano-Yelo, H.; Deronzier, A., Photo-Oxidation of Some Carbinols by the Ru(II) Polypyridyl Complex-Aryl Diazonium Salt System. *Tetrahderon Lett.* **1984**, *25*, 5517–5520.

[253]. Fukuzumi, S.; Mochizuki, S.; Tanaka, T., Photocatalytic Reduction of Phenacyl Halides by 9, 10-Dihydro-10-methylacridine: Control between the Reductive and Oxidative Quenching Pathways of Tris(bipyridine) Ruthenium Complex Utilizing an Acid Catalysis. *J. Phys. Chem.* **1990**, *94*, 722–726.

[254]. Nicewicz, D. A.; MacMillan, D. W., Merging Photoredox Catalysis with Organocatalysis: the Direct Asymmetric Alkylation of Aldehydes. *Science* **2008**, *322*, 77–80.

[255]. Ischay, M. A.; Anzovino, M. E.; Du, J.; Yoon, T. P., Efficient Visible Light Photocatalysis of [2+2] Enone Cycloadditions. *J. Am. Chem. Soc.* **2008**, *130*, 12886–12887.

[256]. Narayanam, J. M. R.; Tucker, J. W.; Stephenson, C. R. J., Electron-Transfer Photoredox Catalysis: Development of a Tin-Free Reductive Dehalogenation Reaction. *J. Am. Chem. Soc.* **2009**, *131*, 8756–8757.

[257]. Ghosh, I.; Ghosh, T.; Bardagi, J. I.; König, B., Reduction of Aryl Halides by Consecutive Visible Light-Induced Electron Transfer Processes. *Science* **2014**, *346*, 725–728.

[258]. Twilton, J.; Le, C.; Zhang, P.; Shaw, M. H.; Evans, R. W.; MacMillan, D. W. C., The Merger of Transition Metal and Photocatalysis. *Nat. Rev. Chem.* **2017**, *1*, 1–19.

[259]. Kalyani, D.; McMurtrey, K. B.; Neufeldt, S. R.; Sanford, M. S., Room-Temperature C–H Arylation: Merger of Pd-Catalyzed C–H Functionalization and Visible-Light Photocatalysis. *J. Am. Chem. Soc.* **2011**, *133*, 18566–19569.

[260]. Ye, Y.; Sanford, M. S., Merging Visible-Light Photocatalysis and Transition-Metal Catalysis in the Copper-Catalyzed Trifluoromethylation of Boronic Acids with CF_3I. *J. Am. Chem. Soc.* **2012**, *134*, 9034–9037.

[261]. Zuo, Z.; Ahneman, D. T.; Chu, L.; Terrett, J. A.; Doyle, A. G.; MacMillan, D. W., Merging Photoredox with Nickel Catalysis: Coupling of α-Carboxyl sp^3-Carbons with Aryl Halides. *Science* **2014**, *345*, 437–440.

[262]. Le, C.; Chen, T. Q.; Liang, T.; Zhang, P.; MacMillan, D. W. C., A Radical Approach to the Copper Oxidative Addition Problem: Trifluoromethylation of Bromoarenes. *Science* **2018**, *360*, 1010–1014.

[263]. Ghosh, I.; Marzo, L.; Das, A.; Shaikh, R.; König, B., Visible Light Mediated Photoredox Catalytic Arylation Reactions. *Acc. Chem. Res.* **2016**, *49*, 1566–1577.

[264]. Natarajan, P.; Bala, A.; Mehta, S. K.; Bhasin, K. K., Visible-Light Photocatalyzed Synthesis of 2-Aryl *N*-Methylpyrroles, Furans and Thiophenes utilizing Arylsulfonyl Chlorides as a Coupling Partner. *Tetrahedron* **2016**, *72*, 2521–2526.

[265]. Deng, G. B.; Wang, Z. Q.; Xia, J. D.; Qian, P. C.; Song, R. J.; Hu, M.; Gong, L. B.; Li, J. H., Tandem Cyclizations of 1,6-Enynes with Arylsulfonyl Chlorides by Using Visible-Light Photoredox Catalysis. *Angew. Chem. Int. Ed.* **2013**, *52*, 1535–1538

[266]. Ghosh, I.; König, B., Chromoselective Photocatalysis: Controlled Bond Activation through Light-Color Regulation of Redox Potentials. *Angew. Chem. Int. Ed.* **2016**, *55*, 7676–7679.

[267]. Savéant, J. M., Coupling of Electrode Electron Transfers with Homogeneous Chemical Reactions. In *Elements of Molecular and Biomolecular Electrochemistry,* John Wiley & Sons, Hoboken, NJ, 2006, pp 78–181.

[268]. Costentin, C.; Robert, M.; Saveant, J. M., Fragmentation of Aryl Halide π anion radicals. Bending of the Cleaving Bond and Activation vs Driving Force Relationships. *J. Am. Chem. Soc.* **2004**, *126*, 16051–16057.

[269]. Andrieux, C. P., Savéant, J.-M., Tallec, A., Tardivel, R. & Tardy, C. Concerted and Stepwise Dissociative Electron Transfer. Oxidability of the Leaving Group and Strength of the Breaking Bond as Mechansim and Reactivity Governing Factors Illustrated by the Electrochemical Reduction of α-Substituted Acetophenones, *J. Am. Chem. Soc.* **1997**, *119*, 2420–2429.

[270]. Monk, P. M. S., *Fundamentals of Electroanalytical Chemistry*, John Wiley & Sons, Chicester, 2001.

[271]. Kojima, H.; Bard, A. J., Determination of Rate Constants for the Electroreduction of Aromatic Compounds and Their Correlation with Homogeneous Electron Transfer Rates, *J. Am. Chem. Soc.* **1975**, *97*, 6317–6324.

[272]. Compton, R. G., Dryfe, R. A. W., Fisher, A. G., Photoelectrochemical Dehalogenation of *p*-Halo-Nitrobenzenes. *J. Electronal. Chem*. **1993**, *361*, 275–278.

[273]. Severin, M. G.; Arévalo, M. C.; Maran, F.; Vianello, E., Electron-Transfer Bond-Breaking Processes. An Example of Nonlinear Activation–Driving Force Relationship in the Reductive Cleavage of the Carbon–Sulfur Bond, *J. Phys. Chem.* **1993**, *97*, 150–157.

[274]. Sutin, N., Nuclear, Electronic, and Frequency Factors in Electron-Transfer Reactions *Acc. Chem. Res.* **1982**, *15*, 275–282.

[275]. Hammerich, O.; Parker, V. D., The Reversible Oxidation of Aromatic Cation Radicals to Dications. Solvents of Low Nucleophilicity. *Electrochim. Acta.* **1973**, *18*, 537–541.

[276]. Lowry, M. S.; Goldsmith, J. I.; Slinker, J. D.; Rohl, R.; Pascal, R. A.; Malliaras, G. G.; Bernhard, S., Single-Layer Electroluminescent Devices and Photoinduced Hydrogen Production from an Ionic Iridium(III) Complex. *Chem. Mater.* **2005**, *17*, 5712–5719.

[277]. Laage, D.; Burghardt, I.; Sommerfeld, T.; Hynes, J. T., On the Dissociation of Aromatic Radical Anions in Solution. *ChemPhysChem* **2003**, *4*, 61−66.

[278]. Borissevitch, I. E., More about the Inner Filter Effect: Corrections of Stern-Volmer Fluorescence Quenching Constants are Necessary at Very Low Optical Absorption of the Quencher. *Journal of Luminescence* **1999**, *81*, 219–214.

[279]. Ward, W. M.; Farnum, B. H.; Siegler, M.; Meyer, G. J., Chloride Ion-Pairing with Ru(II) Polypyridyl Compounds in Dichloromethane. *J. Phys. Chem. A* **2013**, *117*, 8883–8894.

[280]. Valencia, D. P.; González, F., Understanding the Linear Correlation Between Diffusion Coefficient and Molecular Weight. A Model to Estimate Diffusion Coefficients in Acetonitrile Solutions. *Electrochemistry Communications* **2011**, *13*, 129–132.

[281]. Choi, G. J.; Zhu, Q.; Miller, D. C.; Gu, C. J.; Knowles, R. R., Catalytic Alkylation of Remote C–H Bonds Enabled by Proton-Coupled Electron Transfer. *Nature* **2016**, *539*, 268–271.

[282]. Bard, A. J.; Faulkner, L. R., *Electrochemical Methods: Fundamentals and Applications*, John Wiley & Sons, New York, NY, 2001.

[283]. Andrieux, C. P.; Robert, M.; Saeva, F. D.; Savéant, J. M., Passage from Concerted to Stepwise Dissociative Electron Transfer as a Function of the Molecular Structure and of the Energy of the Incoming Electron. Electrochemical Reduction of Aryldialkyl Sulfonium Cations. *J. Am. Chem. Soc.* **1994**, *116*, 7864–7871.

[284]. Andrieux, C. P.; Le Gorande, A.; Savéant, J. M., Electron Transfer and Bond Breaking. Example of Passage from a Sequential to a Concerted Mechanism in the Electrochemical Reductive Cleavage of Arylmethyl Halides. *J. Am. Chem. Soc.* **1992**, *114*, 6892–6904.

[285]. Willems, R. E. M.; Weijtens, C. H. L.; de Vries, X.; Coehoorn, R.; Janssen, R. A. J., Relating Frontier Orbital Energies from Voltammetry and Photoelectron Spectroscopy to the Open-Circuit Voltage of Organic Solar Cells. *Adv. Energy Mater.* **2019**, *9*, 1803677.

[286]. Beatty, J. W.; Douglas, J. J.; Miller, R.; McAtee, R. C.; Cole, K. P.; Stephenson, C. R. J., Photochemical Perfluoroalkylation with Pyridine N-Oxides:

Mechanistic Insights and Performance on a Kilogram Scale. *Chem* **2016**, *1*, 456–472.

[287]. Kuhn, H. J.; Braslavsky, S. E.; Schmidt, R., Chemical actinometry (IUPAC Technical Report). *Pure Appl. Chem.* **2004**, *76*, 2105–2146.

[288]. Montalti, M.; Credi, A.; Prodi L.; Gandolfi, M. T., *Chemical Actinometry. Handbook of Photochemistry*, 3rd Ed., Taylor & Francis Group, Boca Raton, 2016, pp 601–616.

[289]. Cismesia, M. A.; Yoon, T. P., Characterizing Chain Processes in Visible Light Photoredox Catalysis. *Chem. Sci.* **2015**, *6*, 5426–5434.

[290]. Hatchard, C. G.; Parker, C. A., A New Sensitive Chemical Actinometer. II. Potassium Ferrioxalate as a Standard Chemical Actinometer, *Proc. Roy. Soc. (London)* **1956**, *A235*, 518–536.

VI. APPENDIX

VI.1. List of publications

7. **Chen, J.**; Li, J.; Plutschack, M. B.; Berger, F.; Ritter, T.* *Angew. Chem. Int. Ed.* **2020**, *132*, 5665–5669. “Regio- and Stereoselective Thianthrenation of Olefins to Access Versatile Alkenyl Electrophiles” (featured as *VIP paper*)
6. Li, J.; **Chen, J.**; Sang, R.; Ham, W.; Plutschack, M. B.; Berger, F.; Chabbra, S.; Schnegg, A.; Genicot, C.; Ritter, T.* *Nat. Chem.* **2020**, *12*, 56–62. “Photoredox Catalysis with Aryl Sulfonium Salts Enables Site-Selective Late-Stage Fluorination
5. **Chen, J.**; Ritter, T.* *Org. Synth.* **2019**, *96*, 16–35. “Late-stage Deoxyfluorination of Phenols with PhenoFluorMix”
4. Sun, X.; **Chen, J.**; Ritter, T.* *Nat. Chem.* **2018**, *10*, 1229–1233. “Catalytic Dehydrogenative Decarboxyolefination of Carboxylic Acids”
3. Guo, S.;* **Chen, J.** *RSC Adv.* **2018**, 8, 17110–17120. “Recent advances in the synthesis of fluorinated hydrazones”
2. Ye, F.; **Chen, J.**; Ritter, T.* *J. Am. Chem. Soc.* **2017**, *139*, 7184–7187. “Rh-Catalyzed Anti-Markovnikov Hydrocyanation of Terminal Alkynes”
1. Beyzavi, M. H.; Mandal; D.; Strebl, M. G.; Neumann, C. N.; D’Amato, E. M.; **Chen, J.**; Hooker, J. M.; Ritter, T.* *ACS Cent. Sci.* **2017**, *3*, 944–948. “^{18}F–Deoxyfluorination of Phenols via Ru π–Complexes”

VI.2. Curricular Vitae

Personal Details

Last name: Chen First name: Junting

Date of birth: July 27th, 1994 Place of birth: Hunan, P.R. China

Languages: Native Chinese, fluent English, basic German (B1).

Education & Scientific Experiences

Ph.D. in Chemistry Sept/2016–Sept/2020(Expected)

Aachen University (Aachen, Germany)

Max-Planck-Institut für Kohlenforschung (Mülheim an der Ruhr, Germany)

Organic synthesis chemistry

^{18}F-fluorination labelling protocol development and selective C–H functionalization.

(*Supervisor*: Prof. Tobias Ritter)

Teaching assistant Sept/2019

Catalysis for Modern Organic Synthesis, master course (Aachen, Germany)

Poster presentation Jul/2018

22nd International Symposium in Fluorine Chemistry (Oxford, UK)

B.Sc. degree Sept/2012–Jul/2016

Nankai University (Tianjin, China)

Chemistry, GPA: 88.0/100.0 (Top 5%)

Natural product synthesis.

(*Supervisor*: Prof. Pingping Tang)

Internship Mar/2015–Feb/2016

Harvard University (Boston, USA), Chemistry

New methodology development for fluorination.

(*Supervisor*: Prof. Tobias Ritter)

Honors & Awards

National Inspirational Scholarship (*first-class*) Dec/2015

National Inspirational Scholarship (*first-class*) Dec/2014

Merit Student Nov/2014

First-class Scholarship for Undergraduate Dec/2013